**THÈSE DE DOCTORAT**
DE l'UNIVERSITÉ PIERRE ET MARIE CURIE

École doctorale Sciences Mécaniques, Acoustique, Électronique et Robotique de Paris

Spécialité

**Robotique**

Présentée par

**Pauline MAURICE**

Pour obtenir le grade de
**DOCTEUR de l'UNIVERSITÉ PIERRE ET MARIE CURIE**

# Virtual ergonomics for the design of collaborative robots

*Soutenance prévue le 16 Juin 2015*

**Devant le jury composé de :**

| | | |
|---|---|---|
| M. Franck MULTON | Professeur à l'Université de Rennes 2 | Rapporteur |
| M. Philippe SOUÈRES | Directeur de Recherche au LAAS-CNRS | Rapporteur |
| M. Ambarish GOSWAMI | Principal Scientist at Honda Research Institute | Examinateur |
| M. Guillaume MOREL | Professeur à l'Université Pierre et Marie Curie | Examinateur |
| M. Thomas ROBERT | Chargé de Recherche à l'IFSTTAR | Examinateur |
| M. Yvan MEASSON | Ingénieur de recherche au CEA-LIST | Co-encadrant |
| M. Vincent PADOIS | Maître de Conférences à l'Université Pierre et Marie Curie | Co-encadrant |
| M. Philippe BIDAUD | Professeur à l'Université Pierre et Marie Curie | Directeur de thèse |

# Abstract

The growing number of musculoskeletal disorders in industry could be addressed by the use of collaborative robots, which allow the joint manipulation of objects by both a robot and a person. However the efficiency of a collaborative robot regarding the reduction of musculoskeletal disorders risks is highly task-dependent. Yet, even when designing dedicated systems, the ergonomic benefit provided by the robot is hardly ever quantitatively evaluated, because of the lack of relevant assessment tools.

This work aims at developing a generic tool for performing accurate ergonomic assessments of dynamic situations with very little input data. More specifically, it focuses on the development of a methodology to quantitatively compare the ergonomic benefit provided by different collaborative robots, when performing a given task. The word *ergonomy* refers here to biomechanical factors only. The proposed methodology relies on an evaluation carried out within a digital world, using a virtual manikin to simulate the worker. Indeed, the simulation with a virtual manikin enables easy access to many detailed biomechanical quantities, for different kinds of human morphologies. Besides in the case of collaborative robotics, a virtual - instead of a physical - mock-up of the robot is used, which can be more easily modified. Therefore ergonomic assessments of the robot-worker system can be performed throughout the design process.

Ergonomic indicators which match the requirements of collaborative robotics are defined. Such indicators account for the different biomechanical solicitations which occur during manual activities, performed with or without the assistance of a collaborative robot.

The measurement of the proposed ergonomic indicators requires the simulation of the activity with a virtual manikin. To this purpose, a framework for the dynamic simulation of co-manipulation activities is implemented. A strength amplification control law is used for the co-manipulation robot, and the virtual manikin is animated through a LQP optimization technique.

The reliability of the proposed measurement framework is then validated. Motion capture based experiments are carried out in order to estimate the realism of the manikin model, and the consistency of the proposed ergonomic indicators. A fully automatic simulation is implemented in order to ensure the usefulness of the manikin-robot simulation, regarding the ergonomic comparison of collaborative robots.

The proposed simulation framework allows to estimate a variety of ergonomic indicators while performing a given task. However the high number of indicators makes any kind of conclusion difficult for the user. Hence, a methodology for

analyzing the sensitivity of the various indicators to the robot and task parameters is proposed. The goal of such an analysis is to reduce the number of ergonomic indicators which are considered in an evaluation, while sufficiently accounting for the global ergonomic level of the considered activity. The proposed method is validated on various simple tasks, and is applied to an industrial drilling job.

Finally, an application of the proposed methodology to the optimization of a cobot morphology is presented. The collaborative robots evaluation framework is linked to a multi-objective genetic algorithm software for the optimization. The genetic algorithm is used for providing robot candidates to be evaluated. The simulation tool is used for numerically estimating the various objectives for each robot candidate. The optimization framework is applied to optimize a cobot for a drilling job.

# Résumé

Parce qu'elle permet d'associer les capacités physiques d'un robot aux capacités perceptives et cognitives de l'Homme, la robotique collaborative - ou de co-manipulation - peut être une solution pour répondre au problème des troubles musculo-squelettiques (TMS) dans l'industrie. L'efficacité d'un robot collaboratif vis-à-vis de la réduction des TMS dépend toutefois fortement de la tâche pour laquelle il est utilisé. Pour autant, même lorsqu'un robot est conçu pour une application bien spécifique, le gain en terme d'ergonomie qu'apporte son utilisation est rarement évalué quantitativement, à cause du manque d'outils adéquats.

Ce travail vise à développer un outil générique permettant d'effectuer des évaluation ergonomiques précises, à partir de très peu de données d'entrée. Un tel outil doit en particulier permettre de comparer, de manière quantitative, le gain d'ergonomie lié à l'utilisation de différents robots collaboratifs. Il est question ici d'ergonomie dans un sens exclusivement biomécanique. L'outil développé s'appuie sur une évaluation de l'ergonomie en simulation, à l'aide d'un mannequin virtuel. En effet, la simulation permet de mesurer facilement et à moindre coût de nombreuses grandeurs biomécaniques, pour différentes morphologies d'ouvriers. De plus, dans le contexte de la robotique collaborative, la simulation permet de s'affranchir du besoin d'un prototype physique du robot, en le remplaçant par un modèle virtuel, plus simple et moins coûteux à modifier. Le gain d'ergonomie apporté par un robot peut ainsi être évalué tout au long du processus de conception.

Dans un premier temps, des indicateurs d'ergonomie qui satisfont aux exigences de la robotique collaboratives sont définis. Ces indicateurs permettent de quantifier les différentes sollicitations biomécaniques auxquelles sont exposés les ouvriers lorsqu'ils réalisent des tâches manuelles.

Afin de pouvoir mesurer ces indicateurs, il est nécessaire de simuler l'activité considérée avec un mannequin virtuel. Une méthode générique permettant de simuler des activités de co-manipulation est donc mise en œuvre. Le mannequin virtuel est animé grâce à une technique d'optimisation LQP, et le robot est contrôlé par une loi de commande en amplification d'effort.

La fiabilité des mesures effectuées avec l'outil mis en place est ensuite évaluée. Dans ce but, des expériences basées sur la capture de mouvement sont réalisées, afin d'évaluer le réalisme du mannequin et la cohérence biomécanique des indicateurs d'ergonomie. Une activité de co-manipulation est ensuite simulée, avec un mannequin virtuel autonome, afin d'estimer l'apport d'une telle simulation pour la comparaison de l'ergonomie de différents robots collaboratifs.

L'outil développé permet de mesurer de nombreux indicateurs d'ergonomie pendant des activités de co-manipulation. Toutefois, le choix d'un robot plutôt que d'un

autre est rendu difficile par le nombre élevé d'indicateurs à prendre en compte. Une méthode pour analyser la sensibilité des indicateurs aux différents paramètres du robot et de la tâche considérée est donc développée. Une telle analyse permet de réduire le nombre d'indicateurs à prendre en compte pour comparer différents robots, tout en rendant suffisamment compte de l'ergonomie de chaque situation. Cette méthode est validée sur différentes tâches élémentaires, puis appliquée à une tâche de perçage.

Enfin, l'outil développé est utilisé pour optimiser la cinématique d'un robot collaboratif. L'outil de simulation mis en place est couplé à un logiciel d'optimisation multi-objectif basée sur des algorithmes génétiques. L'algorithme génétique est utilisé pour explorer l'espace des cinématiques possibles et ainsi générer des robots à tester. L'outil de simulation permet d'évaluer les performances de chacun de ces robots. La méthode d'optimisation proposée est mise en œuvre pour optimiser la cinématique d'un robot collaboratif pour une tâche de perçage.

**Mots clés :** Analyse ergonomique, humain virtuel, robotique collaborative, simulation dynamique.

# Contents

# List of Figures

# List of Tables

# Chapter 1

# Introduction

## Contents

Among the features that characterize the human-being, one of the most distinctive is the use of tools, intended for increasing human abilities. Physical abilities can be improved, for instance, by a lever for amplifying forces, a wheelbarrow for carrying heavy loads, or a steam engine for generating thrust. Tools are also used for improving cognitive abilities (*e.g.* an abacus for performing mathematical operations) or perceptive abilities (*e.g.* a telescope or a microscope for observing objects which can otherwise not be seen).

Robots are a kind of tool that have initially been thought for replacing humans at work. Indeed the word *robot* comes from the Czech words *robota*, meaning *work*, and *robotník* meaning *worker*. Since the second half of the twentieth century, robots have been increasingly used in industrial applications. For instance, pick and place robots allow fast and accurate positioning of various objects, such as electronic components on a circuit board. Palletizers are another example of widely used industrial robots. They have been developed for automatically placing products onto pallets, an activity which is tiring and time-consuming for a human-being.

Such industrial robots are fully automated and programmed to do repetitive tasks with very limited human intervention.

In some situations however, the human cognitive and perceptive abilities are needed to carry out the task. Tele-operated robots address this problem with a master-slave system. The slave robot copies the movement of the master system controlled by a human operator. This is particularly useful for situations in which the operator cannot enter the work environment, such as maintenance operations in nuclear core facilities. More recently co-manipulated systems have been developed, in which the robot and the operator physically interact for carrying out the task. Such systems combine the physical abilities of the robot with the reasoning abilities of the operator. Hence they are increasingly used for providing assistance to the operator in physically demanding and complex tasks. As such, co-manipulated systems are a potential solution to the growing problem of work-related musculoskeletal disorders.

## 1.1   Work-related musculoskeletal disorders

Musculoskeletal disorders (MSDs) are injuries or pain that affect the body's muscles, joints, tendons, ligaments or nerves. Examples of common MSDs are tendinitis, bursitis, carpal tunnel syndrome, and back pains (Fig. 1.1). They occur when biomechanical solicitations at work exceed the worker's physical capacity, both in terms of intensity and frequency [Luttmann 2003, Aptel 2011], and result in pain, but also in joint stiffness, clumsiness and loss of force.



**Neck**
*Tension neck syndrome*

**Shoulder**
*Rotator cuff tendinitis*

**Elbow**
*Epicondylitis*

**Back**
*Low back pain*

**Wrist, Hand**
*Carpal tunnel syndrome*

**Knee**
*Bursitis*

**Ankle**
*Achilles tendinitis*
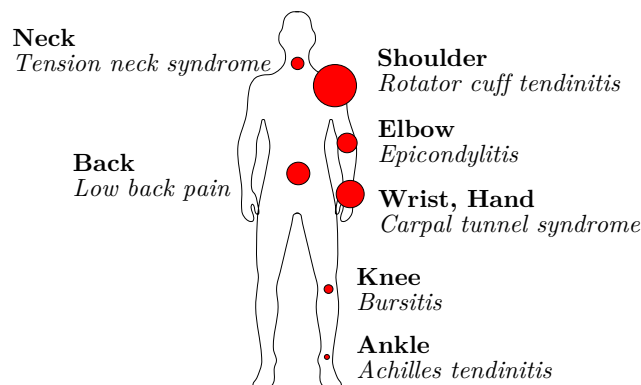
Figure 1.1: Most frequent work-related MSDs. Circle size qualitatively represents the global cost of the corresponding MSD, *i.e.* average unit cost multiplied by the number of reported cases (adapted from ARACT Ile de France[1]).

---

[1] http://www.aractidf.org/les-troubles-musculo-squelettiques-cest-quoi

### 1.1.1   Cost of work-related MSDs

Though working conditions have improved in developed countries, work-related MDSs remain a major health problem. They account for the majority of reported occupational diseases (59 % in Europe, 75 % in France in 2005) and affect almost 50 % of industrial workers [Schneider 2010]. In France, according to the CNAMTS (Caisse Nationale d'Assurance Maladie des Travailleurs Salariés), MSDs caused 8.4 M lost workdays in 2013, which represent a direct cost of 1.5 B€ (medical expenses and workers' compensation covered by companies contributions), plus productiveness loss due to turnover and hiring difficulties. In the US, the Bureau of Labor Statistics estimated the direct cost of MSDs at 20 B\$ per year, and the total cost between 45 and 54 B\$ per year [NRC 2001]. Hence reducing MSD is a high-stakes socio-economic issue.

Besides, the number of reported MSDs has been significantly growing in the last decades. In Europe, they increased by 32 % from 2002 to 2005. In France, despite a recent slowdown in the progression, the yearly number of reported MSDs has been multiplied by ten between 1993 and 2013 (Fig. 1.2). The exact underlying causes of this significant increase are not well established. However, besides a better recognition of these diseases, a possible explanation can be found in the changes in work organization. On one hand, just-in-time, tight flow or zero inventory production systems require a rather constant workload. On the other end, due to partially automated productions and high economic stress, companies tend to demand increasing work rate and productiveness, therefore pushing their employees to their physical limits.
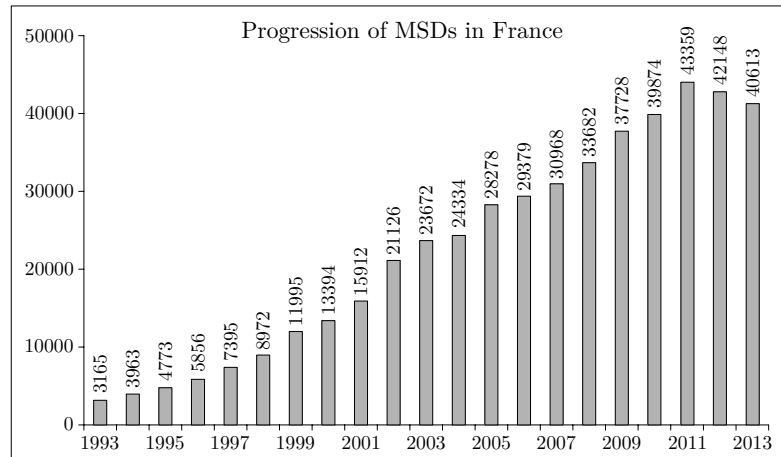


Figure 1.2: Yearly number of reported occupational diseases corresponding to the French health insurance table 57 "Periarticular illness caused by work postures and movements"[2].

---

[2]http://www.risquesprofessionnels.ameli.fr/statistiques-et-analyse/
sinistralite-atmp/dossier/nos-statistiques-sur-les-maladies-professionnelles-par-ctn

### 1.1.2 Risk factors for MSDs

The causes of MSDs are often multi-factorial and include different kinds of factors:

- personal: age, gender...;

- organizational: working time, frequency and duration of breaks...;

- psychosocial: job decision latitude, social support from co-workers...;

- biomechanical (see examples on Fig. 1.3): awkward postures, high forces, static postures, repetitive work (and to a lesser extent: vibration, temperature, contact stress and gloves wearing).

The biomechanical factors represent the physical solicitations to which the worker is exposed. They are the major risk factors, especially when they are combined together. However their combination with other kinds of factors increases the risk of developing MSDs, since personal, organisational, and psychosocial factors affect a person's physical capacity.



Figure 1.3: Examples of work situations that could cause MSDs (pictures from the INRS website[3]). Left: awkward posture associated with significant force. Right: static work.

## 1.2 Collaborative robotics

Since MSDs result from strenuous biomechanical solicitations, replacing men by robots to accomplish hard tasks might be considered an option in order to decrease the number of MSDs. Thanks to the significant development of automation in industry during the last century, some human related limits have been overcome. However as of today, many hard tasks cannot be fully automatized (at all or at reasonable costs): because of their unpredictability and/or technicality, they still require human expertise (*e.g.* high standing and job lot automotive production, mass customization).

---

[3]http://www.inrs.fr/risques/tms-troubles-musculosquelettiques

### 1.2.1 Definition

A solution to decrease MSDs in complex tasks is to assist the worker with a collaborative robot, rather than replacing him. A collaborative robot enables the joint manipulation of objects with the worker (co-manipulation) and can thereby be used to alleviate the worker's physical load. This new approach combines the qualities of both humans and robots: the worker brings his job expertise and decision-making skills whereas the robot brings its positioning accuracy and capacity to generate high forces.

Though the generic term for such devices is *Intelligent Assist Devices* (IADs) [Colgate 2003], they are often called *cobots* (portmanteau of collaborative robots). The word *cobots* was proposed by Colgate and Peshkin in 1996 to refer to wheeled robots using computer-controlled steering of wheels to guide motion in shared manipulation [Colgate 1996]. Despite its very specific initial meaning, the word *cobot* is now often used to refer to any robot for direct physical interaction with a human operator, within a shared workspace.

Collaborative robots can be classified into three families: parallel, serial and orthotic co-manipulation. When the human manipulates the robot by its end-effector, the human-robot system forms a parallel kinematics system, therefore the co-manipulation is said to be parallel. When the human-robot interaction is distributed in multiple points, the co-manipulation is orthotic. Orthotic co-manipulators are also called exoskeletons. Finally serial co-manipulation refers to hand-held devices, since the human-robot system then forms a serial kinematic chain.

### 1.2.2 Functions of collaborative robots

Collaborative robots provide a variety of benefits such as weight compensation, inertia masking, strength amplification, and guidance via virtual surfaces and paths [Colgate 2003]. These functions aim at reducing two of the main biomechanical risk factors for MSDs:

- High forces: Part of the forces resulting from the interaction with the tool or environment are supported by the robot, therefore reducing the worker effort in power tasks. Moreover, by reducing or eliminating some external force disturbances, the robot decreases the control effort required from the worker in high precision tasks.

- Awkward postures: Posture improvement can be a consequence of reduced effort. The posture can also be modified by setting the user-robot interaction port away from the tool, thus requiring smaller gestures from the worker to reach the work area.

Others functions, such as amplification of force feedback and tremor filtering, can be provided to facilitate fine manipulation [Erden 2011]. However they do not directly address the problem of MSDs, and therefore will not be considered in this work.

**Weight compensation:** Weight compensation is used in manual handling jobs. It consists in cancelling the vertical component of the load gravity wrench, and was first proposed by Powell in 1969 with the *Tool Balancer* [Powell 1969]. The load is hung up to a variable-length cable, and in current systems its vertical manipulation is power-assisted thanks to a force sensor set on the user handle (Fig. 1.4).



Figure 1.4: Weight compensation systems enabling manual handling of heavy loads. Left: *Free Standing Easy Arm™*, Gorbel. Right: *iLift™*, Stanley Assembly Technologies.

**Inertia masking:** Inertia masking consists in reducing the starting, stopping, and turning forces when manipulating a load, and ensuring that motions in all directions respond equally to human input. This function is used for manual shifting of heavy objects. Inertia masking can be achieved by the computer-controlled steering of wheeled robots (based on virtual surfaces). The load is set on a trolley, which wheels orientation is automatically adapted depending on the force applied by the user. The inertia effects experienced by the user during speed or direction changes are therefore reduced. This function was proposed by Colgate and Peshkin in the *Scooter* cobot (Fig. 1.5) [Peshkin 2001]. The *iTrolley* (Stanley Assembly Technologies), which is an addition to the *iLift* weight compensation system, is another example of inertia masking system. The inertial effects of the load are compensated by a servo-controlled trolley and a measure of the cable deviation from vertical.

**Strength amplification:** Strength amplification consists in controlling the robot so that the force it exerts on the manipulated tool (or environment) is an amplified image of the force applied by the worker onto the robot. This function was first implemented during the *Hardiman* project (General Electrics) [Groshaw 1969]. The system was based on force feedback tele-operation: it consisted of two interlocked anthropomorphic manipulators, one (master) physically attached to the

Figure 1.5: *Scooter* cobot: virtual paths are implemented thanks to the computer-controlled steering of the three wheels, in order to reduce inertia effects in direction changes.

user, the other (slave) following the user motions while exerting amplified efforts on the environment. This concept was later modified in the *Extender* project by removing the master robot, the user thus directly interacting with the slave robot [Kazerooni 1993].

Today, exoskeletons probably are the most famous strength amplification systems [Bogue 2009], *e.g.* *HULC (Human Universal Load Carrier)* (Ekso Bionics), or *Hercule* (RB3D, CEA-LIST). These two systems are designed to help the user carry heavy loads without limiting his/her displacements. However non-orthotic strength amplification systems also exist. For instance, the *HookAssist* (Kinea Design) designed for beef boning (Fig. 1.6 left) [Santos-Munne 2010], or the *Cobot 7A.15* (RB3D, CEA-LIST, CETIM) which was first designed for tire retreading, but has now been adapted for various machining jobs (Fig. 1.6 right). Strength amplification has also been implemented on generic industrial manipulators [Lee 2006, Lamy 2011].



Figure 1.6: Collaborative robots providing strength amplification. Left: *HookAssist* (Kinea Design) for beef boning. Right: *Cobot 7A.15* (RB3D, CEA-LIST, CETIM) for tire retreading or machining.

**Guidance via virtual surfaces and paths:** Motion guidance consists in limiting the end-effector degrees of freedom by hardware or software means, so that the tool can only perform specific motions [Book 1996]. The human technical gesture thus gains in speed and accuracy, while requiring less co-contraction effort. The cognitive load associated with the task is also reduced.

## 1.3 Human-oriented evaluation of collaborative robots

The afore-mentioned functions cover a wide range of applications, therefore more and more sectors are interested in collaborative robotics - or *cobotics* - to address the MSDs problem: automotive and aeronautics industries, food-processing industry... Each application, even within the same sector, involves specific features (gesture, force range, workspace organization...), which are as many constraints for both the worker and the cobot. Therefore the efficiency of a cobot regarding the reduction of MSDs risks is highly task-dependent. Yet, even when designing dedicated systems, the ergonomic benefit provided by the cobot is hardly ever quantitatively evaluated, because of the lack of relevant assessment tools.

### 1.3.1 Problematic

The purpose of this work is to develop a methodology to quantitatively compare the ergonomic benefit provided by different collaborative robots when performing a given task. The word *ergonomy* refers here to biomechanical factors only. Other factors (see section 1.1.2) are not considered, even if they can be affected by the use of a cobot (*e.g.* worker's perception of his work).

The proposed methodology relies on an evaluation carried out within a digital world, using a virtual manikin to simulate the worker. Indeed, the digital evaluation presents several major advantages over a physical evaluation. Firstly, the simulation enables easy access, through the manikin, to detailed biomechanical quantities, which cannot be measured on real humans, or only with heavy instrumentation (*e.g.* muscle or joint forces). Secondly, thanks to the simulation, the collaborative robot can easily and quickly be tested with many different morphologies of workers, without the need for a wide variety of real workers. Thirdly, a virtual - instead of a physical - mock-up of the robot is used for digital ergonomic assessments. Assessments of the cobot-worker system can thus easily be performed very early, and then all along, the design process. The cost of building a new prototype every time a parameter of the robot is tuned is removed: a virtual mock-up can be more easily modified. Therefore, when integrated in a design process, the simulation potentially decreases the overall development time and cost of a collaborative robot.

The methodology presented in this work focuses on collaborative robots dedicated to power tasks, *i.e.* tasks requiring significant effort. Precision tasks are not addressed. More specifically, only parallel co-manipulation robots which provide strength amplification are considered. Among the functions that can be used to

reduce MSDs risk in power tasks, strength amplification is particularly interesting, because it addresses a wide range of applications, and in particular jobs requiring hand-held tools (*e.g.* machining, boning...). On the contrary, weight compensation and inertia masking are limited to material handling jobs. Due to this focus on power tasks, serial co-manipulation are excluded from this work. Serial co-manipulation devices for MSDs reduction do exist (*e.g.* electric power screwdrivers), however these hand-held devices are not adapted to power tasks. When significant forces are involved, the cobot need powerful actuators which are usually heavy, hence a heavy structure. So if the worker is carrying the cobot, this one becomes a cause of MSDs because of its weight. The same criticism applies to entirely wearable orthotic robots. Nevertheless, most parts of the methodology proposed in this work can still be extended to other kinds of collaborative robots (functions and/or structure).

### 1.3.2 Thesis contents

In this work, a novel approach for evaluating collaborative robots through simulation is proposed. This approach is based on the association of a framework for exhaustive measurement of biomechanical solicitations, with an analysis method for selecting relevant comparison criteria. The whole methodology is summarized in Fig. 1.7. The organization of this thesis is detailed hereafter.

Chapter 2 first presents the requirements of an ergonomic evaluation for co-manipulation activities. Given these requirements, the various evaluation methods and digital human model (DHM) software tools that are currently used for ergonomic evaluations are reviewed. However none of them fully match the expected requirements. The tools used for workstation design provide a few ergonomic indicators that are very rough and/or do not cover all kinds of manual activities. The tools used for biomechanical studies provide a high number of measurements which interpretation - both in terms of reliability and task-related relevance - requires specific biomechanical knowledge. Therefore, a novel approach situated in between the existing ones is proposed. This approach combines a framework for measuring numerous detailed ergonomic indicators, with an analysis method to identify the most relevant indicators for a given task.

The framework developed for measuring biomechanical solicitations during co-manipulation activities is presented in chapter 3. This measurement framework is based on a high level representation of the human body (no muscles), and consists of two components: a list of ergonomic indicators, and a simulation tool. Ergonomic indicators which match the requirements of collaborative robotics are defined. Such indicators account for the different biomechanical solicitations which occur during manual activities, performed with or without the assistance of a collaborative robot. The proposed list contains sufficiently diverse indicators so as
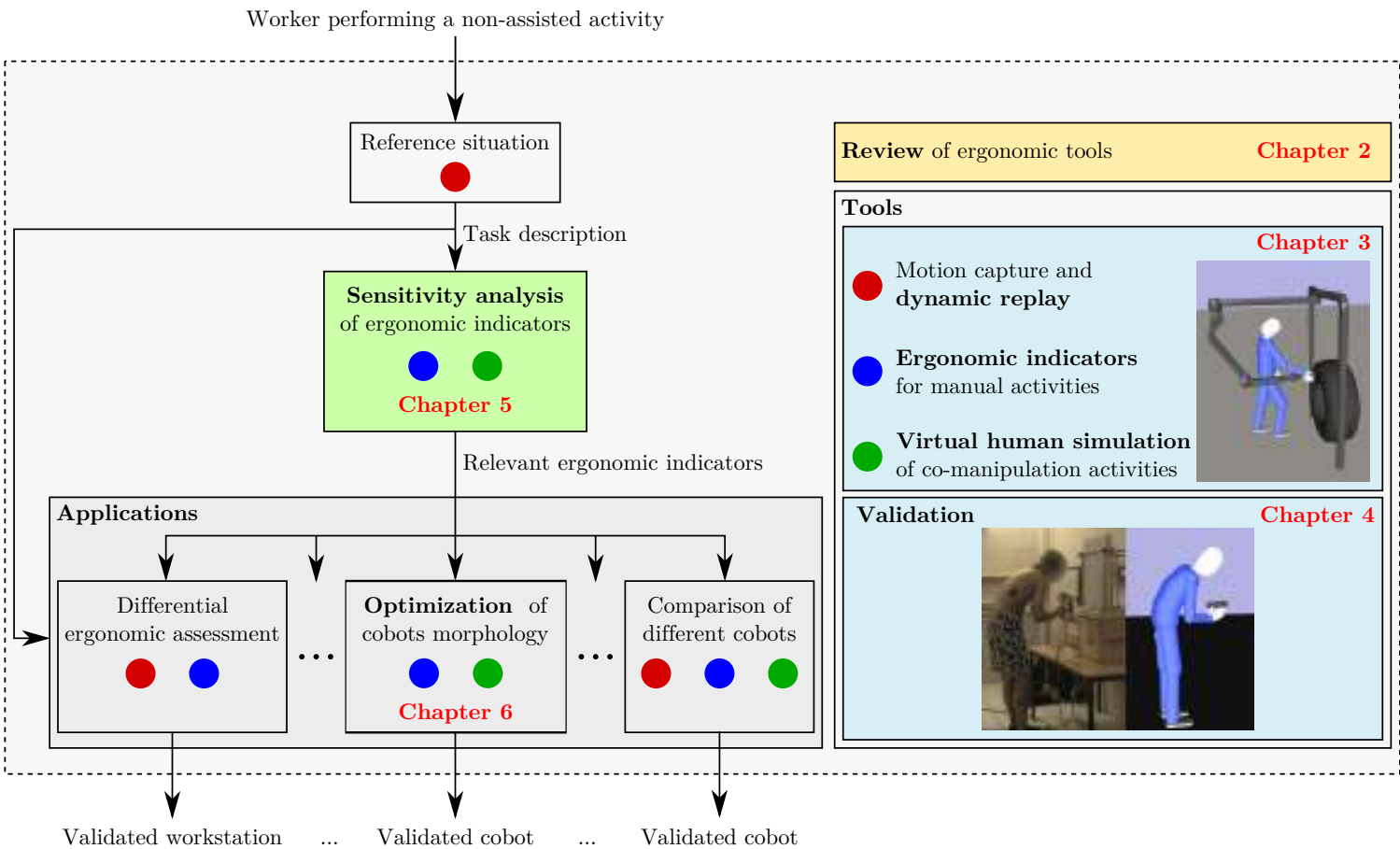
Figure 1.7: Overview of the methodology developed for performing ergonomic assessments of collaborative robots. Though this work focuses on collaborative robots evaluation, the tools and methods that are developed can also be used – with slight modifications – for a wider range of applications, such as the evaluation of workstations, or other kinds of assistive devices.

to cover all kinds of manual activities as exhaustively as possible (excluding precision tasks). The measurement of the proposed ergonomic indicators requires the simulation of the activity with a virtual manikin. Therefore a framework for the dynamic simulation of co-manipulation activities is implemented. A virtual manikin is animated through standard optimization techniques in order to automatically perform all kinds of manual activities with the assistance of a collaborative robot. Any parallel co-manipulation robot for strength amplification can be used in the simulation. Finally a method for dynamically replaying pre-recorded motions with the virtual manikin is proposed. This method is developed mainly for validation purposes, detailed in the next chapter.

Chapter 4 presents a validation of the measurement framework presented in the previous chapter. Two motion capture based experiments are carried out in order to estimate the realism of the manikin model, and the consistency of the proposed ergonomic indicators. Then a fully automatic simulation is implemented on a simple task in order to validate the reliability and usefulness of the manikin-robot simulation. The results obtained in all three experiments are mostly satisfying, and validate the methodology proposed for biomechanical measurements during co-manipulation activities. However, the results also highlight several limitations which may affect the validity of the measurements. These limitations, mostly related to the manikin model and control, are discussed.

Chapter 5 presents a method for selecting relevant comparison criteria for a given task, among all the proposed ergonomic indicators. In order to facilitate the interpretation of the results when comparing different collaborative robots, the number of ergonomic indicators that are considered must be limited. Yet the remaining indicators must sufficiently account for the global ergonomic level of the task. The proposed method is based on the analysis of the sensitivity of the ergonomic indicators to the robot and task parameters. In order to conduct such an analysis, the indicators must be measured, for each new task, in many different conditions, *i.e.* with the assistance of many different cobots. Therefore a framework for such an evaluation is implemented. It is based on the simulation tool described in chapter 3, associated with a dedicated representation of collaborative robots, and standard methods for the design of experiments. The proposed method is validated on various simple tasks, and applied to an industrial drilling job.

Finally, chapter 6 presents an application of the proposed methodology to the optimization of the cobot morphology. The ergonomic indicators analysis method presented in chapter 5 is used to select relevant optimization criteria (objectives). Then the simulation framework presented in chapter 3 is linked to a multi-objective genetic algorithm software for the optimization. The genetic algorithm is used for exploring the space of robot morphologies, *i.e.* providing robot candidates to be evaluated. The simulation tool is used for numerically estimating the various ob-

jectives for each robot candidate. The proposed optimization framework is applied to optimize a cobot for a drilling job.

### 1.3.3 Publications

Beyond the specific application to the evaluation of collaborative robots, this work has a wider ambition. It aims at developing a generic tool for performing accurate ergonomic assessments of dynamic situations with very little input data, contrarily to existing tools which generally require much input data in order to perform accurate evaluations. The development of such a tool requires three main components:

1. Accurate and generic measurements of the biomechanical solicitations experienced by the manikin/worker.

2. A physically consistent dynamic simulation with an autonomous virtual manikin, in which scenarii can easily be created and automatically simulated.

3. A tool for automatically evaluating the relevance of the ergonomic measurements, in regard to each specific situation.

All these components are presented in this thesis, and have been published in three international conferences, listed hereafter:

P. Maurice, Y. Measson, V. Padois, and P. Bidaud. *Experimental assessment of the quality of ergonomic indicators for collaborative robotics computed using a digital human model.* 3rd Digital Human Modeling Symposium, 2014 (component 1, chapters 3 and 4)[4].

P. Maurice, Y. Measson, V. Padois, and P. Bidaud. *Assessment of physical exposure to musculoskeletal risks in collaborative robotics using dynamic simulation.* CISM International Centre for Mechanical Sciences, Romansy 19 - Robot Design, Dynamics and Control. Vol 544 Pages 325-332, 2013 (component 2, chapter 4)[5].

P. Maurice, P. Schlehuber, V. and Padois, P. Bidaud, and Y. Measson. *Automatic selection of ergonomic indicators for the design of collaborative robots: a virtual-human in the loop approach.* IEEE-RAS International Conference on Humanoid Robots, 2014 (component 3, chapter 5)[6].

---

[4]https://hal.archives-ouvertes.fr/hal-00971319/document
[5]https://hal.archives-ouvertes.fr/hal-00720750/document
[6]https://hal.archives-ouvertes.fr/hal-01072228/document

# Chapter 2

# Review of ergonomic tools

## Contents

The work presented in this thesis aims at developing a tool which enables the comparison, through simulation, of the ergonomic benefit provided by various collaborative robots. Such a tool must match the specific requirements of collaborative robots evaluation. These requirements can be divided in two families: those related to the evaluation metric, and those related to the simulation tool. The requirements related to the evaluation metric are the following:

- The activities that can be addressed by collaborative robotics are diverse, so the evaluation criteria must cover all kinds of manual activities.

- The evaluation of a collaborative robot must take the whole task execution into account, and not only the phases in which the robot is expected to assist the worker. Indeed, an ill-adapted robot can cause new MSDs, thus not improving (and possibly worsening) the overall ergonomic situation. The dynamic phases are especially important since the negative effects of the robot are likely to be more significant in those phases.

- All parts of the human body must be considered in the evaluation, and not only those initially affected by MSDs. An ill-adapted cobot may delocalized the MSDs risk to other body parts, instead of reducing the overall risk.

- The interpretation of the results must be straightforward, because the tool developed in this work is intended for robot designers rather than for biomechanics specialists.

The goal of the simulation tool is to enable the estimation of the measurements included in the evaluation metric. Therefore the requirements related to the simulation tool are closely linked to those related to the evaluation metric:

- The simulation framework must ensure the physical consistency of all measurements, especially the dynamic ones.

- The motion of the manikin must be realistic, otherwise the results of the ergonomic assessment are not reliable.

- The motion of the manikin must be automatically generated, otherwise the development of each simulation is much more time consuming.

- The simulation tool must enable the simulation of co-manipulation activities, *i.e.* of a virtual manikin physically interacting with a collaborative robot.

This chapter therefore reviews the existing ergonomic tools (evaluation methods and simulation software), in order to check whether or not they match the requirements cited above. Then, the approach proposed in this work is detailed.

## 2.1  Ergonomic assessment methods for workplace evaluation

Due to the growing number of MSDs, and in order to improve the design of workplaces, various methods have been developed to assess the biomechanical risks associated with an activity. These methods can be classified into two families: posture-based methods for risk evaluation, and physical limit recommendations [Li 1999, David 2005].

### 2.1.1 Observation-based methods

The first family of methods consists of posture-based methods, which require the observation of a worker performing the task. They are often grids or check-lists that assign a score to the activity for each one of the main MSDs factors: posture, effort, duration and frequency of the task, and sometimes for additional factors such as vibrations, temperature, or gloves-wearing. They result in a estimation of an absolute level of risk (*e.g.* acceptable, not recommended, unacceptable) indicating whether changes in the workplace organization should be investigated.

The most widely known methods are the Owako Working Posture Analysis System (OWAS) [Karhu 1981], the Rapid Upper Limb Assessment (RULA, Fig. 2.1) [McAtamney 1993], the Rapid Entire Body Assessment (REBA) [Hignett 2000], the Occupational Repetitive Action index (OCRA) [Occhipinti 1998], the OSHA checklist [OSHA 1999], and the Strain Index [Moore 1995].

### 2.1.2 Physical limit recommendations

The second family of methods consists of equations or tables that give physical limits not to exceed in order to minimize the MSDs risk during manual handling operations. The most widely used are the NIOSH (National Institute for Occupational Safety and Health) equation [Waters 1993], and the Liberty Mutual Manual Material Handling tables (or Snook and Ciriello tables) [Snook 1991].

The NIOSH equation provides a recommended weight limit for lifting tasks, based on the height and distance of the load to the body, the vertical displacement of the load, the upper body twisting angle, the frequency and duration of lifts, and the quality of grasp. The Liberty Mutual tables consider approximately the same factors, but they provide the population percentage able to perform lifting/lowering/pushing/pulling/carrying tasks, for various load weights.

### 2.1.3 Standard

Given the number of ergonomic assessment methods, the French standardization agency issued a document in order to guide designers. The french standard EN NF 1005 "Safety of machinery - Human physical performance" relies on several methods to provide recommendations about MSDs risks evaluation for various manual activities [AFNOR 2008a]:

- 1005-2: manual handling of objects weighting more than $3\,\text{kg}$, displaced less than $2\,\text{m}$ (NIOSH lifting equation),

- 1005-3: static pushing and pulling jobs,

- 1005-4: postural evaluation for tasks with no external load,

- 1005-5: highly repetitive manipulation of light objects (OCRA index).

Figure 2.1: Form used to estimate the level of MSDs risk according to the Rapid Upper Limb Assessment method.

### 2.1.4 Limitations

Despite this wide variety of ergonomic assessment methods, all have some features which make them unsuitable for the evaluation of a job performed with a collaborative robot. Their limitations are detailed hereafter.

# RULA  Employee Assessment Worksheet

Complete this worksheet following the step-by-step procedure below.  Keep a copy in the employee's personnel folder for future reference.

## A. Arm & Wrist Analysis

**Step 1: Locate Upper Arm Position**

+1   +2   +2   +3   +4

-20° to +20°   > -20°   +20° to 45°   +45° to 90°   90°+

**Step 1a: Adjust…**
If shoulder is raised: +1;
If upper arm is abducted: +1;
If arm is supported or person is leaning: -1

*Final Upper Arm Score =*

**Step 2: Locate LowerArm Position**

+1   +2   +2   +1   +1

-60° to 100°   0-60°   100°+

**Step 2a: Adjust…**
If arm is working across midline of the body: +1;
If arm out to side of body: +1

*Final Lower Arm Score =*

**Step 3: Locate Wrist Position**

+1   +3   +2   +1   +1
0°   0° to 15°   15°+

15°+
+2
0° to 15°
+3
15°+

**Step 3a: Adjust…**
If wrist is bent from the midline: +1

*Final Wrist Score =*

**Step 4: Wrist Twist**
If wrist is twisted mainly in mid-range =1;
If twist at or near end of twisting range = 2

*Wrist Twist  Score =*

**Step 5: Look-up Posture Score in Table A**
Use values from steps 1,2,3 & 4 to locate Posture Score in table A

*Posture Score A =*

**Step 6: Add Muscle Use Score**
If posture mainly static (i.e. held for longer than 1 minute) or;
If action repeatedly occurs 4 times per minute or more: +1

*Muscle Use  Score =*

**Step 7: Add Force/load Score**
If load less than 2 kg (intermittent): +0;
If 2 kg to 10 kg (intermittent): +1;
If 2 kg to 10 kg (static or repeated): +2;
If more than 10 kg load or repeated or shocks: +3

*Force/load  Score =*

**Step 8: Find Row in Table C**
The completed score from the Arm/wrist analysis is used to find the row on Table C

*Final Wrist & Arm  Score =*

## SCORES

### Table A

| Upper Arm | Lower Arm | Wrist 1 Wrist Twist 1 | 1 Wrist Twist 2 | 2 Wrist Twist 1 | 2 Wrist Twist 2 | 3 Wrist Twist 1 | 3 Wrist Twist 2 | 4 Wrist Twist 1 | 4 Wrist Twist 2 |
|---|---|---|---|---|---|---|---|---|---|
| 1 | 1 | 1 | 2 | 2 | 2 | 2 | 3 | 3 | 3 |
|   | 2 | 2 | 2 | 2 | 2 | 3 | 3 | 3 | 3 |
|   | 3 | 2 | 3 | 3 | 3 | 3 | 4 | 4 | 4 |
| 2 | 1 | 2 | 3 | 3 | 3 | 3 | 4 | 4 | 4 |
|   | 2 | 3 | 3 | 3 | 3 | 3 | 4 | 4 | 4 |
|   | 3 | 3 | 4 | 4 | 4 | 4 | 5 | 5 | 5 |
| 3 | 1 | 3 | 3 | 4 | 4 | 4 | 4 | 5 | 5 |
|   | 2 | 3 | 4 | 4 | 4 | 4 | 5 | 5 | 5 |
|   | 3 | 4 | 4 | 4 | 4 | 5 | 5 | 5 | 5 |
| 4 | 1 | 4 | 4 | 4 | 4 | 5 | 5 | 5 | 5 |
|   | 2 | 4 | 4 | 4 | 4 | 5 | 5 | 5 | 5 |
|   | 3 | 4 | 4 | 4 | 5 | 5 | 5 | 6 | 6 |
| 5 | 1 | 5 | 5 | 5 | 5 | 5 | 6 | 6 | 7 |
|   | 2 | 5 | 6 | 6 | 6 | 6 | 7 | 7 | 7 |
|   | 3 | 6 | 6 | 6 | 7 | 7 | 7 | 7 | 8 |
| 6 | 1 | 7 | 7 | 7 | 7 | 7 | 8 | 8 | 9 |
|   | 2 | 8 | 8 | 8 | 8 | 9 | 9 | 9 | 9 |
|   | 3 | 9 | 9 | 9 | 9 | 9 | 9 | 9 | 9 |

### Table C

|   | 1 | 2 | 3 | 4 | 5 | 6 | 7+ |
|---|---|---|---|---|---|---|---|
| 1 | 1 | 2 | 3 | 3 | 4 | 5 | 5 |
| 2 | 2 | 2 | 3 | 4 | 4 | 5 | 5 |
| 3 | 3 | 3 | 3 | 4 | 4 | 5 | 6 |
| 4 | 3 | 3 | 3 | 4 | 5 | 6 | 6 |
| 5 | 4 | 4 | 4 | 5 | 6 | 7 | 7 |
| 6 | 4 | 4 | 5 | 6 | 6 | 7 | 7 |
| 7 | 5 | 5 | 6 | 6 | 7 | 7 | 7 |
| 8+ | 5 | 5 | 6 | 7 | 7 | 7 | 7 |

**+**

**+**

**=**

**Final Score=**

## B. Neck, Trunk & Leg Analysis

**Step 9: Locate Neck Position**

0° to 10°   10° to 20°   20°+   in extension
+1   +2   +3   +4

**Step 9a: Adjust…**
If neck is twisted: +1; If neck is side-bending: +1

*=Final Neck Score*

**Step 10: Locate Trunk Position**

1 also if trunk is well sup-ported while seated 2 if not

0° to 10°   standing erect   seated - 20°   +1
0° to 20°   +2
-20° to 60°   +3
60°+   +4

**Step 10a: Adjust…**
If trunk is twisted: +1; If trunk is side-bending: +1

*= Final Trunk Score*

**Step 11: Legs**
If legs & feet supported and balanced: +1;
If not: +2

*= Final LegScore*

### Table B

Trunk Posture Score

|      | 1 Legs |   | 2 Legs |   | 3 Legs |   | 4 Legs |   | 5 Legs |   | 6 Legs |   |
|------|---|---|---|---|---|---|---|---|---|---|---|---|
| Neck | 1 | 2 | 1 | 2 | 1 | 2 | 1 | 2 | 1 | 2 | 1 | 2 |
| 1 | 1 | 3 | 2 | 3 | 3 | 4 | 5 | 5 | 6 | 6 | 7 | 7 |
| 2 | 2 | 3 | 2 | 3 | 4 | 5 | 5 | 5 | 6 | 7 | 7 | 7 |
| 3 | 3 | 3 | 3 | 4 | 4 | 5 | 5 | 6 | 6 | 7 | 7 | 7 |
| 4 | 5 | 5 | 5 | 6 | 6 | 7 | 7 | 7 | 7 | 7 | 8 | 8 |
| 5 | 7 | 7 | 7 | 7 | 7 | 8 | 8 | 8 | 8 | 8 | 8 | 8 |
| 6 | 8 | 8 | 8 | 8 | 8 | 8 | 8 | 9 | 9 | 9 | 9 | 9 |

**Step 12: Look-up Posture Score in Table B**
Use values from steps 8,9,& 10 to locate Posture Score in Table B

*= Posture B Score*

**Step 13: Add Muscle Use Score**
If posture mainly static or;
If action 4/minute or more: +1

*= Muscle Use Score*

**Step 14: Add Force/load Score**
If load less than 2 kg (intermittent): +0;
If 2 kg to 10 kg (intermittent): +1;
If 2 kg to 10 kg (static or repeated): +2;
If more than 10 kg load or repeated or shocks: +3

*= Force/load  Score*

**Step 15: Find Column in Table C**
The completed score from the Neck/Trunk & Leg analysis is used to find the column on Chart C

*= Final Neck, Trunk & Leg  Score*

Subject: _____
Company: _____   Department: _____
Date: __ / __ / __
Scorer: _____

**FINAL SCORE: 1 or 2 = Acceptable; 3 or 4 investigate further; 5 or 6 investigate further and change soon; 7 investigate and change immediately**

*Source: McAtamney, L. & Corlett, E.N. (1993) RULA: a survey method for the investigation of work-related upper limb disorders, Applied Ergonomics, 24(2) 91-99.*

© *Professor Alan Hedge, Cornell University. Feb. 2001*

**Lack of precision regarding force consideration:** Several methods, particularly the posture-based ones, are not very accurate regarding the force factor. It is calculated based on the magnitude (and possibly direction) of the external force, but it is not affected by the posture (*e.g.* RULA assessment form step 7 or 14 in Fig. 2.1). However, in order to accurately evaluate the effect of an external force on the musculoskeletal system, the repartition of the effort among joints - which depends on the posture - must be considered.

**Specificity regarding applications:** Among the afore-mentioned methods, most of them are not generic: they are specific either to a type of activity and/or to a body part (see Table 2.1, and section 2.1.3). But the activities which may be addressed by collaborative robots are various and often complex, consisting of a mix and/or succession of several elementary tasks. Therefore the evaluation of the entire activity is very likely to require the use of several methods together. This raises two problems:

- The choice of the appropriate method to evaluate an elementary task is not always straightforward. There might be no method corresponding exactly to the features of the considered task. In that case, even if a closely-related method is used, this could lead to wrong results.

- The results of the afore-mentioned assessment methods are mostly not homogeneous. Even when considering only posture-based methods, output scores cannot be compared from one method to another [Li 1999]. Therefore, if different methods are used to evaluate different phases of the activity, no global score (*i.e.* for the whole activity) can be computed.

| Posture-based risk assessment | | |
|---|---|---|
| Method | Body part considered | Jobs considered |
| OWAS | Whole body | Non-specific |
| RULA | Upper limb | Sedentary jobs |
| REBA | Whole body | Non-sedentary jobs |
| OCRA | Upper limb | Repetitive jobs |
| Strain Index | Distal upper extremity | Non-specific |
| OSHA Check-list | Upper limb | Non-specific |

| Physiological limits recommendations | | |
|---|---|---|
| Method | Posture considerations | Jobs considered |
| NIOSH Lifting equation | Hands height | Lifting jobs |
| Liberty Mutual tables | Hands height | Manual handling jobs |

Table 2.1: Specificities of standard methods for ergonomic assessment, regarding the body parts and the jobs considered.

**Lack of dynamic consideration:**  The other, and the major, drawback of the existing observational methods is that they are static, meaning that dynamic phenomena are not taken into account. Posture-based methods usually only evaluate a static pose and just add a frequency and duration factor. Even in methods where motions are taken into account (*e.g.* in material handling evaluations), this consideration is strictly geometric (lifting/lowering... distance). The only methods considering dynamic phenomena are REBA and the Strain Index. However, though REBA is said to be for "dynamic postures evaluation", the dynamic factor is quite rough: it consists in modifying the final score if the "action causes rapid large changes in posture or an unstable base". The Strain Index qualitatively considers the speed of work, but it only applies to hands motions evaluation.

Yet it has been established that fast motions increase the risk of developing MSDs because of the efforts they generate in biological tissues [Marras 1993]. Besides, in collaborative robotics, evaluating the dynamic phases of the activity is even more important because the robot is never perfectly backdrivable. Some phenomena, especially inertial effects, can be hard to compensate, even with a dedicated control law. In such cases, manipulating the robot requires extra efforts from the worker. If too important, these efforts can cause new MSDs, and worsen the overall ergonomic situation of the worker. For instance, collaborative robots providing strength amplification are generally powerful thus heavy: they are highly inertial so leaving dynamic stages out of the assessment can lead to an underestimation of the risk.

In order to overcome these limitations, some techniques rely on more advanced instrumentation, *e.g.* goniometers, accelerometers, and motion capture techniques to accurately measure continuous dynamic motions, force sensors and electromyography for effort measurement [Li 1999, David 2005]. However, these techniques require heavy instrumentation from the worker, and can hinder his gestures. Besides, as for basic observational methods, they require a physical prototype of the workplace, and can therefore not be used at an early stage of the design process.

## 2.2   Virtual manikins for workplace design

An alternative to physical evaluation is to carry out the evaluation within a digital world. Digital evaluation has been enabled by the development of digital modeling tools, which improved workstation design methods in the last twenty years [Claudon 2008]. Today several software providing digital human modeling and animation tools can be interfaced with computer-aided design (CAD) software, thereby enabling the simulation of a human operator in a virtual environment (the virtual operator is also called virtual manikin). Despite the initial additional cost of the simulation due to the development time of the animation, the use of digital human model (DHM) software is widening. Indeed, the final design costs decrease when using the simulation, because modifications are easier and cheaper on the simulated

workstation [Chaffin 2007]. Such tools are now common enough, so that specific standards have been established [AFNOR 2008b].

### 2.2.1 General features

Digital human model software for workplace evaluation can be described as "external" macroscopic models: the human body is a rigid-body model, and each joint is controlled by a sole actuator (*i.e.* they do not include muscle models). Initially, they mainly aimed at checking geometric dimensions of the workspace [Chedmail 2002, Regazzoni 2014]. Now, they have been enriched with further features so that they can be used for ergonomic assessment [Feyen 2000, Bossomaier 2010]:

- **Anthropometric database:** The human model is scalable in order to represent the workers diversity (size, mass, male or female...).

- **Geometric assessment:** The collisions between the human model and the environment are detected. The operator's field of vision and reach envelope are displayed.

- **Ergonomic assessment:** Several standard assessment methods are usually included, such as RULA, OWAS, the NIOSH lifting equation, the Liberty Mutual tables... Besides, some software include more detailed analysis, such as computation of joints static effort, energy expenditure, low-back load analysis, fatigue analysis. Though these analyses are biomechanically more meaningful than the standard assessment methods, they still do not consider dynamic phenomena in their computation, or only for very specific tasks.

### 2.2.2 Common DHM software

The main DHM software can be classified into two families: those for generic applications, and those dedicated to specific applications.

#### 2.2.2.1 DHM for generic applications

The most common DHM software for generic applications are listed below, and their main features are summarized in Table 2.2.

- **Jack:** The development of Jack started in the mid 80s at the Centre for Human Modelling and Simulation of the University of Pennsylvania, and was funded by NASA and the US Army [Blanchonette 2010, Raschke 2004]. It is now distributed by Siemens PLM Software (Plano, TX, USA).

- **DELMIA:** DELMIA is an evolution of the Safework Pro DHM software, which was first developed at Ecole Polytechnique de Montreal in the 80s. It is now distributed by Dassault Systèmes (Vélizy-Villacoublay, France).

- **Process Engineer:** Ergoman - Process Engineer was developed in the 90s by DELTA Industrie Informatik GmbH (Fellbach, Germany), in collaboration with the Technische Universität Darmstadt [Schaub 1997]. It is now distributed by Dassault Systèmes.

- **SAMMIE:** SAMMIE (System for Aiding Man-Machine Interactive Evaluation) was first developed by the Universities of Nottingham and Loughborough at the end of the 70s [Porter 2004]. It is currently distributed by SAMMIE CAD Ltd (Loughborough, UK).

- **HumanCAD:** HumanCAD was initially developed as MANNEQUINPRO, and is currently distributed by NexGen Ergonomics Inc (Pointe Claire, Québec, Canada).

### 2.2.2.2 DHM for specific applications

The most common DHM software for specific applications are listed below, and their main features are summarized in Table 2.3

- **3DSSPP:** The development of 3DSSPP (3D Static Strength Prediction Program) started in the 90s at the Center for Ergonomics of the University of Michigan [Chaffin 1997]. It is not exactly a DHM software for workplace design, in the sense that no virtual environment is simulated. However it predicts static strength requirements for manual handling tasks such as lifts, presses, pushes, and pulls.

- **RAMSIS:** The development of RAMSIS (Realistic Anthropological Mathematical System for Interior comfort Simulation) started in 1987 at the Technische Universität München, in collaboration with the Techmach company, and was funded by a consortium of automotive designers [Seidl 2004]. It is now distributed by Human Solutions GmbH (Kaiserslautern, Germany). It is dedicated to vehicle interior design (cars, trucks, planes...).

- **BHMS:** BHMS (Boeing Human Modeling System) has been developed by the Boeing company for aeronautic applications [Rice 2004]. It was initially dedicated to cockpit design, but can now be used for plane assembly and maintenance tasks.

- **MAN3D:** MAN3D was developed at the Laboratoire de Biomécanique et de Modélisation Humaine de l'IFSTTAR (Lyon, France), in collaboration with Renault, and aims at simulating vehicle ingress motions and driving postures.

- **IMMA:** IMMA (Intelligently Moving Manikins) is a project of the Fraunhofer-Chalmers Research Centre for Industrial Mathematics (Chalmers, Sweden) that started in 2009, carried out in collaboration with the vehicle industry in

| | | Jack | Delmia | Process Eng. | Sammie | HumanCAD |
|---|---|---|---|---|---|---|
| **Manikin animation** | **Forward kinematics** | ✓ | ✓ | ✓ | ✓ | ✓ |
| | **Inverse kinematics** | ✓ | ✓ | - | ✓ | ✓ |
| | **Predefined behaviors** | ✓ | ✓ | - | ✓ | ✓ |
| | **Motion capture** | ✓ | ✓ | - | under development | - |
| | **Others** | Force-influenced posture prediction | - | - | - | - |
| **General features** | **Reach envelope** | ✓ | ✓ | ✓ | ✓ | ✓ |
| | **Collision detection** | ✓ | ✓ | - | ✓ | ✓ |
| | **Field of vision** | ✓ | ✓ | ✓ | ✓ | ✓ |
| | **Static force calculation** | ✓ | ✓ | - | - | ✓ |
| | **Others** | - | Center of mass / Base of support | - | - | - |
| **Ergonomic assessment** | **RULA** | ✓ | ✓ | - | ✓ | - |
| | **OWAS** | ✓ | - | - | - | - |
| | **NIOSH lifting equation** | ✓ | ✓ | ✓ | ✓ | ✓ |
| | **Liberty Mutual tables** | ✓ | ✓ | - | - | - |
| | **Others** | Fatigue analysis Low-back analysis Energy expenditure | - | - | - | - |

Table 2.2: Main features of common DHM software for generic applications. Some of these features are not included in the basic version of the software but can be purchased as extra toolboxes.

Sweden [Hanson 2011]. It is dedicated to automotive assembly jobs, and focuses on generating collision free motions for digital humans (as well as parts) in complex assembly situations.

### 2.2.3   Manikin animation

In order to perform geometric or ergonomic assessments, the posture and/or motions of the manikin must be determined, either manually by the user, or semi-automatically through various methods:

- **Forward kinematics:** The user directly sets the values of the joint angles. This method is highly subjective, and requires expert skills in human motion in order to come up with a realistic motion/posture. Besides it is highly time-consuming.

- **Inverse kinematics:** The user sets the trajectory or end point of the distal extremities (generally the hands), and the joints motions are automatically calculated. The human body being a redundant system, an infinity of solutions exists. However the selection of the solution rarely considers the inertial properties of the human body and never accounts for external forces, therefore the resulting motion lacks realism.

- **Pre-defined postures and behaviors:** Some behaviors such as *walk towards*, *reach towards*, *grasp*, *look at* are automatically calculated given a target point. This method results in much more realistic motions than the previous ones, since it relies on a pre-recorded motions database. However, only a few behaviors can be simulated, and they become unrealistic when external conditions are modified (*e.g.* adding a load in a reaching motion).

- **Motion capture:** The motions of a real person are recorded and mapped on the virtual manikin. This method results in human-like motions, provided that the digital model is scaled to match the person's morphology, and that the person experiences a similar environment. In particular, the interaction forces with the environment are needed since they affect the posture. Therefore it requires either a physical mock-up or heavy instrumentation (digital mock-up through virtual reality and force feedback devices). Besides, motion capture based animation is highly time consuming. On one hand, the motion capture process in itself is time consuming (set-up preparation, acquisition, data treatment). On the other hand, new acquisitions are required for each new activity.

- **Posture prediction:** A few software provide automatic posture generation which take into account the influence of external forces. This is an improvement compared to kinematic methods, however this is limited to static postures and forces.

|  | | 3DSSPP | Ramsis | BHMS | MAN3D | IMMA |
|---|---|---|---|---|---|---|
|  | Applications | Material handling | Vehicle interior design | Plane design, and assembly | Vehicle ingress Driving postures | Automotive assembly |
| Manikin animation | Forward kinematics | - | ✓ | ✓ | ✓ | - |
| | Inverse kinematics | - | ✓ | - | ✓ | ✓ |
| | Predefined behaviors | - | ✓ | - | - | - |
| | Motion capture | - | - | - | ✓ | - |
| | Others | Automatic posture generation | Driving posture prediction | - | - | Path planning with balance and comfort considerations |
| General features | Reach envelope | - | ✓ | ✓ | ✓ | - |
| | Collision detection | - | ✓ | ✓ | ✓ | ✓ |
| | Field of vision | - | ✓ | ✓ | ✓ | ✓ |
| | Static force calculation | ✓ | ✓ | - | ✓ | ✓ |
| | Others | - | Mirror vision | Handheld tools toolbox | - | - |
| Ergonomic assessment | NIOSH lifting equation | ✓ | - | - | - | - |
| | Liberty Mutual tables | ✓ | - | - | - | - |
| | Others | Low-back analysis | Seating comfort | - | Seating comfort | Company specific methods |

Table 2.3: Main features of common DHM software for specific applications.

- **Motion simulator:** The HUMOSIM Ergonomics Framework, developed at
  the University of Michigan, is a motion generation framework that mixes
  several of the afore-mentioned animation methods, in order to automatically
  generate complex motions [Reed 2006].

Apart from motion capture, none of these animation techniques takes into account
dynamic properties of the human body and load. Therefore the simulated motion
does not necessarily resembles the one a real human would do, causing errors in
geometric and postural evaluations. Furthermore, the human effort required to
perform the task may be underestimated because the inertial effects are not con-
sidered in the calculation. Eventually, the manikin balance is never considered in
posture/motion calculation (except in IMMA), which also affects the relevance of
the evaluation [Lämkull 2009].

### 2.2.4 Conclusion

The DHM software for workplace evaluation present two majors drawbacks. First,
as stated in section 2.2.3, the manikin motions and forces either lack realism, or
requires a real subject and heavy instrumentation (motion capture). Secondly,
concerning ergonomic assessment, the same criticism apply as those raised in sec-
tion 2.1.4 about observational ergonomic assessment methods (specificity, no dy-
namics, lack of precision). Even when more detailed measurements and/or analysis
are provided (*e.g.* joint force and moment), the fact that the simulation does not
consider dynamics is very limiting.

## 2.3 Detailed biomechanical models

Concurrently to the macroscopic DHM software presented in the previous section,
another kind of DHM software exists, which provide accurate biomechanical mod-
els of the human body and enable dynamics simulation. Contrarily to macroscopic
DHM software for workplace evaluation, these tools focus on biomechanical con-
sequences of the motion, rather than the posture. Therefore applications concern
ergonomic analysis, but also study of safety in transport (virtual "crash tests"),
human performance during sports activities, and orthopaedic purposes.

### 2.3.1 General features

The detailed biomechanical models are more complex than the macroscopic ones.
They include the skeleton (bones), possibly with deformable elements and joints,
muscle tissues, tendons, and ligaments. They provide the following functionalities:

- **Model scaling:** Similar to the macroscopic models, the biomechanical mod-
  els can be scaled according to anthropometric database. However, each seg-
  ment of the body can also be manually tuned, in order to adapt the model to
  specific morphologies.

- **Biomechanical measures:** These software provide classic macroscopic measurements (joint angles, joint force and moment), but also dynamic measurements such as joint velocities and accelerations. Besides, they enable access to quantities that more accurately account for the biomechanical solicitations of the human body, such as muscle force (including antagonistic muscle actions), tendon deformation, muscle fiber length. However the high number of outputs (one for each muscle/tendon/joint) makes it difficult for the user to interpret without specific biomechanical knowledge.

### 2.3.2 Common biomechanical models

The most common DHM software providing a biomechanical model of the human body are listed below, and their main features are summarized in Table 2.4.

- **OpenSim:** OpenSim is developed by Stanford University [Delp 2007]. It only aims at studying human motions: no virtual environment can be added to the simulation. Therefore it is mainly used for medical purposes (orthopaedics, sport performance).

- **AnyBody:** AnyBody Modeling System$^{\text{TM}}$ was developed by Aalborg University [Damsgaard 2006] and is distributed by the AnyBody Technology company (Aalborg, Danemark). It enables full body musculoskeletal simulations for activities of daily living, including physical interactions with virtual environments.

- **LifeMOD:** LifeMOD$^{\text{TM}}$ is distributed by LifeModeler Inc. (San Clemente, CA, USA). Like AnyBody, it enables the simulation of the human body within its environment, and can be interfaced with various CAD software.

- **Santos:** Santos is developed by the Virtual Soldier Research group at the University of Iowa since 2003 for US Army applications [Abdel-Malek 2006]. It is now also used in some automotive applications. It is distributed by SantosHuman$^{\text{TM}}$ Inc. It is probably the most advanced human simulation tool regarding both the animation of the manikin, and the physiological measurements provided. However it is not currently available to the public.

### 2.3.3 Model animation

The model can be animated directly by the user (forward kinematics), but most of the time motion capture techniques associated with inverse kinematics and/or dynamics are used in order to achieve human-like motions. Inverse kinematics computes the joint angles for a musculoskeletal model that best reproduce the motion of a subject. Inverse dynamics then uses joint angles, velocities, and accelerations of the model, to solve for the net reaction forces and net moments at each of the joints, or directly for muscle forces. Experimental measurements of ground (or

| | | OpenSim | AnyBody | LifeMOD | Santos |
|---|---|---|---|---|---|
| **Manikin animation** | **Inverse kinematics** | ✓ | ✓ | ✓ | ✓ |
| | **Forward dynamics** | ✓ | - | ✓ | - |
| | **Inverse dynamics** | ✓ | ✓ | ✓ | - |
| | **Motion capture** | ✓ | ✓ | ✓ | ✓ |
| | **Others** | - | Automatic calculation of contact forces | Automatic calculation of ground forces | Optimization based posture and motion prediction |
| **Biomechanical measurements** | **Joint angles velocities, accelerations** | ✓ | ✓ | ✓ | ✓ |
| | **Joint force and moment** | ✓ | ✓ | ✓ | ✓ |
| | **Muscle force** | ✓ | ✓ | ✓ | ✓ |
| | **Muscle-Tendon length** | ✓ | ✓ | ✓ | - |
| | **Others** | - | - | - | Metabolic energy expenditure, Physiological measures, NIOSH equation, Liberty Mutual tables |

Table 2.4: Main features of common DHM software based on detailed biomechanical models.

other environment) reaction forces and moments may also be needed for inverse dynamics calculation, *e.g.* in OpenSim. In AnyBody however, support forces are automatically computed so that the model maintains balance. Their measurement is not necessary except for validation purposes.

However, the human musculoskeletal system is highly redundant. Therefore estimating muscle forces with inverse dynamics raises the problem of muscle recruitment, *i.e.* which muscles should be activated among the infinity of possible activation patterns. The muscles are activated by the Central Nervous System by mechanisms that are currently not sufficiently understood for detailed modeling. So no general muscle recruitment criterion has been established yet [Damsgaard 2006, Chaffin 2006]. Usually some optimality criterion is used to determine muscle activation (*e.g.* minimize the sum, or the maximum of normalized muscles forces), but there is no consensus on the right criterion, and its choice might be left to the user.

Beyond the muscle recruitment problem, these motion capture based animation techniques require (as in macroscopic-DHM software) a human subject and heavy instrumentation, in order to obtain realistic motions. To address this limitation, Santos proposes a robotic approach based on optimization techniques which aims at predicting human posture and motions. Given some targets (*e.g.* hand position), the manikin motions are automatically computed in order to optimize several criteria such as joint effort, energy expenditure, joint comfort, balance [Xiang 2010a, Xiang 2010b]. These techniques seem promising, however Santos is not available to the public.

### 2.3.4 Conclusion

Though the detailed biomechanical models provide a dynamic simulation of the motion, and associated joint and muscle measurements, they still have two major drawbacks regarding the evaluation of collaborative robots. Firstly, the manikin animation presents the same drawbacks as in macroscopic DHM software. Animation techniques require motion capture data, hence heavy instrumentation. Otherwise, the realism of the manikin motion is not ensured. Secondly, detailed biomechanical software require biomechanical knowledge for model tuning and for results interpretation. In particular, because of the actuation redundancy of the human body, the computed muscle forces (as well as others muscles and tendons features) strongly depend on the criterion chosen to solve the muscle recruitment problem. Since no general criterion is established for the muscle recruitment problem, the realism of the resulting measurements is not ensured. Besides, validating the realism of such measurements on real subjects is hardly feasible given the considered quantities. In conclusion, biomechanical models provide measurements much more detailed than macroscopic models, but in the absence of ground truth, the reliability of such measurements is questionable.

## 2.4    Ergonomic assessment of robot-worker collaboration

Beyond the drawbacks of macroscopic and biomechanical DHM software, the main requirement when evaluating (through simulation) the ergonomic benefit provided by a collaborative robot, is to be able to include the robot into the simulation. Most macroscopic DHM and some biomechanical DHM software enable the simulation of a virtual environment. However it usually consists of static elements, whereas a robot moves. Furthermore, the motion of a collaborative robot depends on its physical interaction with the user, both through its control law and through physical interferences. The manikin-robot physical interaction and the robot response to it therefore need to be simulated.

### 2.4.1    State of the art

Simulation of industrial human-robot cooperation for ergonomic assessment purposes is rarely presented in the literature. Only two examples were found: Busch *et al.* [Busch 2013] and Ore *et al.* [Ore 2014].

The problem addressed by Busch *et al.* is the planning of a robot trajectory that minimizes physical stress on the human body. They consider an industrial robot that cooperates with a human worker in that they share the same workspace. They create a plug-in to import a basic human character in a robot path-planning software, so that they can try various trajectories for the robot, and set a feasible manikin posture (no collision, task visible and reachable). An OWAS analysis is then performed to choose the best robot trajectory regarding the manikin posture. However, there is no real cooperation between the human and the robot: the robot trajectory is pre-defined and cannot be modified by the worker (no co-manipulation). The robot is a "moving environment", but there is no voluntary physical interaction between the robot and the worker, no contact forces.

The problem addressed by Ore *et al.* is closer to a co-manipulation problem. They compare the operating time and biomechanical solicitations when an assembly task (including the manipulation of a heavy load) is performed by a worker alone, by an industrial robot alone, and jointly by the worker and the robot. In the collaborative scenario, the robot is used to carry the load, and its motion is controlled by the operator through force sensors in the robot joints. So there is a physical interaction between the robot and the human. However, it is unclear how this interaction is simulated, especially how it influences the robot motion, since the IMMA software they use is based on inverse kinematics [Bohlin 2014]. Moreover, dynamic phenomena such as the robot inertia are not considered. Besides, the biomechanical stress evaluation is based on RULA, which, as stated before, is quite limited.

## 2.4.2 Proposed approach

Despite many available tools for simulating human activity and performing an ergonomic evaluation of this activity, none of them meet the requirements of collaborative robots evaluation. On one hand, macroscopic DHM software for workplace evaluation provide simple human models and return a sole (or a few) indicator representing the global level of exposure. However, these indicators are very rough and/or task-specific, and do not take dynamic phenomena into account. On the other hand, biomechanical models software return detailed measurements for each joint or muscle and consider dynamic phenomena. But their use and interpretation require specific biomechanical knowledge, especially because of the complexity of the evaluation output. Besides none of these software (macroscopic or biomechanical models) enable automatic simulation of a virtual manikin interacting with a controlled collaborative robot.

This work proposes a novel approach situated in between the two existing ones. A macroscopic rigid body model is used for representing the human body. This model does not include any muscles. Instead, the manikin is actuated by a single actuator at each joint. The biomechanical quantities measured with such a model are therefore less detailed than what could be achieved with a biomechanical model. In particular, the actions of several muscles are summarized in a single actuator, which necessarily results in a loss of information (since a same joint torque can be produced by different combinations of muscle forces). However, as stated in section 2.3.4, the reliability of detailed biomechanical measurements can hardly be guaranteed. On the contrary, the macroscopic measurements provided by macroscopic DHM models can more easily be verified, for instance through motion capture validation. The questionable gain of information, associated with a much more important computational cost, reduces the interest of detailed biomechanical models. Therefore a macroscopic model is preferred.

The proposed approach aims at associating the advantages of both the macroscopic and the biomechanical DHM tools. The main interest of the biomechanical DHM software is that they provide measurements which accurately account for all kinds of biomechanical solicitations, without requiring any *a priori* hypotheses on the activity that is performed. On the contrary, the macroscopic DHM software usually require the user to select one assessment method in a catalog of methods. Even if the right method is chosen, it does not necessarily account for all the solicitations that occur during the activity. Therefore, similarly to biomechanical DHM software, this work proposes a list of biomeachanical measurements (or ergonomic indicators) which cover all kinds of solicitations that can occur during manual activities[1]. Such measurements are "raw", *i.e.* they directly represent the

---

[1]In this work, *manual activities* refer to physical activities which are at least partly performed with the hands, but most of the time such activities also require the use of other body parts. For instance, working with a portable tool (welding, drilling...) or manipulating loads (possibly while walking) are manual activities.

biomechanical solicitations without any task-related aggregation. The numerical evaluation of the proposed ergonomic indicators requires the simulation of the considered activity with a virtual manikin. However, the existing DHM simulation tools are ill-adapted for the automatic simulation of realistic human motions in general, and even more for co-manipulation activities. Therefore, a dedicated simulation framework is developed.

However, as in the biomechanical DHM software, an exhaustive list of ergonomic indicators has a major drawback: the user is provided with many measurements, and has to select which ones to consider by himself. Depending on the activity that is studied, not all measurements are equally informative, and besides, they can yield antagonistic results (one quantity is improved, whereas one is worsened). On the contrary, task-oriented assessment methods (included in macroscopic DHM software) have the advantage of providing a single output which interpretation is straightforward. Nevertheless, in both cases, the user has, at one point, to decide which method/measurement to use for the evaluation. To address this selection problem, this work proposes a method for automatically analyzing the relevance of each ergonomic indicator, depending on the activity that is considered. Thus, instead of choosing relevant indicators based on his/her potentially limited biomechanical knowledge, the user makes his/her choice according to the results of the analysis.

The different components of the proposed methodology are detailed in the following chapters. The framework for biomechanical measurements in co-manipulation activities, *i.e.* dedicated ergonomic indicators and simulation tool, is detailed in chapter 3, and validated in chapter 4. The method for analyzing the relevance of ergonomic indicators is detailed in chapter 5.

Chapter 3

# Ergonomic measurements for co-manipulation activities

## Contents

The work presented in this thesis addresses the problem of the ergonomic evaluation of collaborative robots. According to the literature review presented in the previous chapter, the existing ergonomic assessment tools are not adapted for evaluating co-manipulation activities. Therefore a dedicated assessment methodology must be developed. The base component of the proposed methodology is a framework enabling the measurement of biomechanical indicators for co-manipulation activities. Developing such a framework requires to address the two following problems: what needs to be measured, and how to measure it.

The first problem requires the definition of ergonomic indicators which match the requirements of collaborative robotics, and are adapted to the level of details of the chosen human body representation. Such indicators must account for the different biomechanical solicitations which occur during manual activities, performed with or without the assistance of a collaborative robot. The proposed indicators must be

sufficiently diverse to cover all kinds of manual activities as exhaustively as possible (the selection of relevant indicators for a specific activity is addressed in chapter 5).

The second problem is related to the measurement of ergonomic indicators. The proposed indicators must be numerically evaluated whenever a new task or cobot is considered. This evaluation requires the simulation of the task execution with a virtual manikin. In order to address co-manipulation activities, the simulation tool must enable the dynamic simulation of an autonomous virtual manikin physically interacting with a collaborative robot.

This chapter presents the tools that are developed to answer these two problems.

## 3.1 Definition of ergonomic indicators

Ergonomic indicators aim at characterizing the physical demand to which a worker is exposed when executing manual activities, with or without a collaborative robot. Such indicators must enable a quantitative comparison of the biomechanical solicitations experienced during a task performed with various collaborative robots, *i.e.* they must represent a relative level of solicitation. However, their purpose is not to assess an absolute level of risk of developing MSDs. Besides, though it belongs to the main risk factors, the repetitiveness factor is omitted in this work. Indeed, the target robots (strength amplification robots) are not supposed to significantly affect the work rate, hence the repetitiveness. The ergonomic comparison is therefore conducted on a single work cycle. The robot which most decreases the physical solicitations on one work cycle is assumed to the best overall.

Ergonomic indicators must represent the main MSDs risk factors (section 1.1.2) that are considered in classic ergonomic assessment methods (posture, force, and duration), but with higher accuracy and genericity (*i.e.* no task-specific formulation). Ergonomic indicators must also address phenomena that are usually left aside in ergonomic assessments, such as dynamic solicitations. In order to establish indicators matching these requirements, performance criteria in two domains are reviewed: robotic manipulators control and human motion control. Performance criteria for robotic manipulators design and control (see [Pholsiri 2004] for an exhaustive review) are used to quantify the physical solicitations on the robot joints, or the ability to perform certain tasks. Though the human body is not strictly a robotic mechanism, some of these criteria are transposable to the human body. Indeed, some robotic performance criteria are used as optimality criteria in digital human motion control. To solve the kinematic redundancy of the human body, automatic generation of human-like motion requires, besides the Cartesian target, an additional criterion. This criterion is generally formulated as an objective to optimize. There is no consensus on the proper criterion that is optimized by the central nervous system, however several formulations have been proposed and sometimes validated on specific motions. Since human-beings usually perform motions in a way that minimize (or at least limit) the biomechanical solicitations on their body, optimality criteria for human motion control could be used as ergonomic indicators.

The performance criteria which are selected and adapted to represent the biomechanical solicitations during manual activities are detailed hereafter. These ergonomic indicators can be classified into two families: *local* or *constraint oriented* indicators, and *global* or *goal oriented* indicators. Their mathematical formulation requires the definition of physical quantities related to the human motion, which are therefore presented beforehand.

## 3.1.1 Dynamic motion equation

As mentioned in section 2.4.2, the approach proposed in this work is based on a macroscopic human model. The human body is represented as a rigid-body tree structure. No muscle model is included. Instead, the model is actuated by revolute actuators localized in each joint. The actuation variables are therefore the joint torques. Given the chosen representation, the human body motion can be mathematically modeled using a robotic approach. The equations of motion are computed from the derivation of the Lagrangian of the system (difference between kinetic and potential energies, see [Murray 1994] for further details) and can be written:

$$M(\mathbf{q})\ddot{\mathbf{q}} + \mathbf{C}(\mathbf{q}, \dot{\mathbf{q}}) + \mathbf{g}(\mathbf{q}) = S\,\boldsymbol{\tau} - \sum_i J_{c_i}^T(\mathbf{q})\mathbf{w_{c_i}} \qquad (3.1)$$

with

- $\mathbf{q}$ the generalized coordinates of the system, and $\dot{\mathbf{q}}$ and $\ddot{\mathbf{q}}$ its first and second derivatives,

- $\boldsymbol{\tau}$ the vector of joint torques,

- $\mathbf{w_{c_i}}$ the *ith* contact wrench,

- $M$ the generalized inertia matrix of the system,

- $\mathbf{C}$ the vector of centrifugal and Coriolis forces,

- $\mathbf{g}$ the vector of gravity forces,

- $S$ the actuation selection matrix

- $J_{c_i}$ the Jacobian matrix of *ith* contact.

It should be noted that equation 3.1 is also valid for a human model including muscles. The only difference is that when muscles are used, the joint torques are not directly the actuation variables, but they are functions of muscle-related variables (*e.g.* muscle activation).

### 3.1.2 Constraint oriented indicators

Constraint oriented indicators correspond to local joint measurements, and evaluate the proximity of various quantities to their limits (one indicator per quantity): position, velocity, torque... In robotic performance, they measure the normalized solicitation for each joint, *i.e.* the distance between the joint current state $s_i$ and its maximal capacity $s_i^{max}$. Then a global indicator (representing the situation of the whole robot, $N$ joints) is obtained either by summing the squared contributions of every joint ($I_{square}$ eq. 3.2), or by taking the maximal contribution ($I_{max}$ eq. 3.3):

$$I_{square} = \frac{1}{N} \sum_{i=1}^{N} \left( \frac{s_i}{s_i^{max}} \right)^2, \tag{3.2}$$

$$I_{max} = \max_{i \in 1..N} \left| \frac{s_i}{s_i^{max}} \right|. \tag{3.3}$$

Since MSDs risks appear as soon as the biomechanical solicitations exceed the worker's physical capacity, such indicators are well adapted for ergonomic measurement. After the normalization by $s_i^{max}$, all joints are considered equivalent: there is no hypothesis on MSDs being more dangerous for one part of the body compared to another. For instance, a joint solicitation $s_i = 0.2\,s_i^{max}$ is as dangerous, whether localized in the wrist or in the back (*i.e.* back pains are not considered more dangerous than Carpal tunnel syndrome).

Grouping several joints in one indicator decreases the number of indicators, and thereby the complexity of the ergonomic analysis. However the different limbs of the human body can perform different tasks simultaneously. It is therefore preferable to keep an indicator per body part, in order to limit the loss of information. So, the legs, the right and left arms, and the torso (including the head) are considered in separate indicators. The $I_{square}$ indicator is preferred over the $I_{max}$ one, because it does not exclude any joints from the final formula (with the $I_{max}$ indicator, the indicator value is the same whether only one, or all the joints reach their maximal values).

One limitation of this kind of indicator however, is that the maximal capacity of the human joints are not as straightforward to obtain as those of robots joints. Firstly they are person-dependant, and secondly coupling between joints, and between several quantities (*e.g.* torque and position) occur because of the muscular actuation. So for some quantities limit values are not available in the literature and the normalization cannot be carried out. In such cases, $s_i^{max} = 1\,SI$ is used for all joints, as a first approximation.

#### 3.1.2.1 Joint position

The proximity to joint limit (in terms of range of motion) increases MSDs risk, because it causes tendons deformation, and potential compression of soft tissues thus decreasing their vascularization (*e.g.* compression of median nerve causes

carpal tunnel syndrome). This risk is evaluated in most posture-based ergonomic assessment methods, but as a discrete measure (joint range of motion is parted in several sub-ranges corresponding to different scores).

In this work, a continuous measure is chosen to evaluate proximity to joint limit:

$$I_q = \frac{1}{N} \sum_{i=1}^{N} \left( \frac{q_i - q_i^{neutral}}{q_i^{max} - q_i^{neutral}} \right)^2 \qquad (3.4)$$

where $N$ is the total number of joints in the considered body part, $q_i(t)$ the angle of joint $i$, $q_i^{max}$ is the joint limit, and $q_i^{neutral}$ the neutral position of the joint. The body neutral position $q^{neutral}$ is defined according to the REBA comfort zones, and is depicted on Fig. 3.1. The human joint limits are not symmetric, therefore the value of $q_i^{max}$ depends on the sign of $q_i - q_i^{neutral}$. A similar indicator is used by Yang *et al.* to quantify human joint stress for upper-body posture prediction, though the normalization value is not defined as the joint limit [Yang 2004]. They also propose a much more complex indicator for joint discomfort evaluation, however the additional relevance provided by this more complex formulation is not explicitly proven.
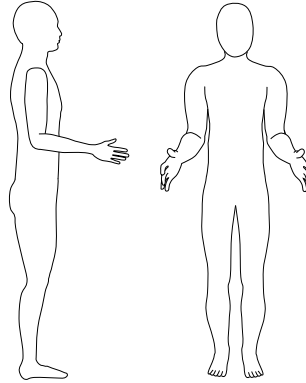


Figure 3.1: Neutral posture regarding joint positions. The elbow is flexed at 80°.

In this work, average values measured on a panel of young healthy males are used for the joint limits $q_i^{max}$ [Chaffin 2006] (see appendix A for numerical values). Indeed, the purpose here is not to evaluate the risk for a specific worker, but to compare collaborative robots that can be used by a variety of workers. So average values are well-adapted. Besides, though a joint limit is affected by the position of adjacent joints, this phenomenon is not taken into account here, due to the lack of mathematical formulations of such couplings for every joint.

### 3.1.2.2 Joint torque

In posture-based ergonomic assessment methods, the force solicitation is usually represented by two factors. One is included in the postural score and corresponds to the effort needed to maintain the posture because of gravity effect on the body

segments. The other is an additional score depending on the intensity of external forces. Despite their various origins, these phenomena both result in muscles solicitation.

In this work, the force solicitation is evaluated with the joint torques resulting from the inverse dynamical model of the human body (equation 3.1):

$$I_\tau = \frac{1}{N} \sum_{i=1}^{N} \left( \frac{\tau_i}{\tau_i^{max}} \right)^2 \tag{3.5}$$

where $\tau_i$ the torque of joint $i$, and $\tau_i^{max}$ the joint torque capacity. These torques have the advantage of including both static and dynamic forces associated with the motion. Besides, they accurately account for the repartition of the effort among the joints. Ma *et al.* use the same criterion to predict human posture in a manual drilling task [Ma 2009]. Leboeuf *et al.* use a time-integral version of this criterion for gymnastic movement synthesis [Leboeuf 2006], and Xiang *et al.* for human lifting motion synthesis [Xiang 2010a], though the normalization value is not defined as the torque limit. Khatib *et al.* propose a similar torque based optimality criterion for posture prediction, however only gravity torques are considered since they are interested in posture rather than motion [Khatib 2004].

As for the joint position indicator, average values are used in this work for torque capacities [Holzbaur 2005, Chaffin 2006] (see appendix A for numerical values). Though the torque capacity depends on the joint position and velocity and potentially on those of adjacent joints [Chaffin 2006], these couplings are not considered, because of the difficulty to find coupling models for all joints. However, contrarily to joint limit, the maximal torque capacity $\tau_i^{max}$ does not remain constant over time, but is strongly affected by fatigue. Several factors cause physical fatigue, *i.e.* a reduction in the maximal physical capacity. However, knowing that only one work cycle is evaluated, only the effect of previous solicitations during the task is considered here. Besides no recovery of the physical capacity is modeled. The evolution of torque capacity over time follows the model from Ma *et al.* [Ma 2009]:

$$\tau_i^{max}(t) = \tau_i^{max}(0) \, e^{-k \int_0^t \frac{\tau_i(u)}{\tau_i^{max}(0)} \, du} \tag{3.6}$$

where $k$ is a fatigue rate assigned to $1 \, min^{-1}$, $\tau_i^{max}(0)$ is the nominal torque capacity (before any effort), and $\tau_i^{max}(t)$ and $\tau_i(t)$ are respectively the torque capacity and the torque exerted by the joint at time $t$. This model of fatigue is chosen, because to the author knowledge, it is the only one that considers an articular actuation model, rather than a muscle model.

### 3.1.2.3  Joint velocity and acceleration

The speed of motion is never considered in standard ergonomic assessment methods (except in the Strain Index), however fast motions and especially strong accelerations induce sudden and significant efforts in the musculoskeletal tissues. For instance, fast arm motions can cause acute shoulder tendinitis.

Therefore a robotic performance criterion for joint velocity limits is applied here to the human body, in order to evaluate the biomechanical solicitations due to fast motions:

$$I_{\dot{q}} = \frac{1}{N} \sum_{i=1}^{N} \left( \frac{\dot{q}_i}{\dot{q}_i^{max}} \right)^2 \tag{3.7}$$

where $\dot{q}_i$ the joint velocity, and $\dot{q}_i^{max}$ the joint velocity limit. A similar indicator is used for the joint acceleration $\ddot{q}_i$:

$$I_{\ddot{q}} = \frac{1}{N} \sum_{i=1}^{N} \left( \frac{\ddot{q}_i}{\ddot{q}_i^{max}} \right)^2 \tag{3.8}$$

However, contrarily to joint position and torque, joint velocity and acceleration capacities are hardly available in the literature. Therefore, the normalization by the joint capacity is currently omitted for this two indicators ($\dot{q}_i^{max} = 1\,m.s^{-1}$ and $\ddot{q}_i^{max} = 1\,m.s^{-2}$ is used for all joints). The differences in the joints capacities from one joint to another are then not taken into account.

### 3.1.2.4 Joint jerk

The minimum jerk criterion has been proposed by Flash and Hogan (Cartesian jerk) and Rosenbaum *et al.* (joint jerk) to characterize human reaching motions [Flash 1985, Rosenbaum 1995]. Though this criterion has been validated, and is now widely used to generate or evaluate human motion, it is not considered in this work. Indeed the purpose is not to evaluate the human feature of a motion, but the solicitations on the biomechanical system. The solicitations associated with motion are already considered in the velocity and acceleration indicators.

### 3.1.2.5 Joint power

Several DHM software provide the computation of the metabolic energy expenditure [Garg 1978]. This measure can be used as a fatigue indicator. However its calculation requires a very detailed biomechanical model of the human body (except for specific activities where tables are available). Instead, a macroscopic energetic indicator is used in this work, based on joint power:

$$I_p = \frac{1}{N} \sum_{i=1}^{N} \mid \dot{q}_i\,\tau_i \mid . \tag{3.9}$$

A time-integral version of this indicator is used by Leboeuf *et al.* (along with the torque indicator) for gymnastic movement synthesis [Leboeuf 2006]. A close indicator (based on joint work) is also used by Kang *et al.* for reaching motions [Kang 2005].

### 3.1.3 Goal oriented indicators

Contrarily to constraint oriented indicators, goal oriented indicators are not directly associated with limits of the human body, but they quantify the ability to comfortably perform certain actions. They have the advantage of being very synthetic, since one global measure accounts for the whole body.

#### 3.1.3.1 Kinetic energy

The energetic indicator based on joint power proposed in section 3.1.2.5 enables to distinguish the solicitations on the various parts of the human body (legs, both arms and torso). On the contrary, the kinetic energy of the system forms a global energetic indicator:

$$K = \frac{1}{2}\dot{\mathbf{q}}^T M(\mathbf{q})\dot{\mathbf{q}}. \tag{3.10}$$

Kinetic energy is often used to characterize robots performance and solve kinematic redundancy, because it is directly associated with the power consumed by the system during operation. In [Abdel-Malek 2005], Abdel-Malek *et al.* propose to use it for measuring human performance.

#### 3.1.3.2 Manipulability

Manipulability measures have been introduced by Yoshikawa to quantify the ability of robotic mechanisms to generate velocities or forces [Yoshikawa 1985b]. The manipulability ellipsoid (resp. force manipulability ellipsoid) represents the set of end-effector Cartesian velocities (resp. forces) that can be reached from unit joint velocities (resp. torques). For the human body, manipulability measures are indirect but global images of the joint solicitations needed to perform a motion or exert a force. For instance, Jacquier-Bret *et al.* quantify the human motion capacities of the upper body with a manipulability measure [Jacquier-Bret 2012].

From the manipulability ellipsoid, several indices can be computed to represent different abilities.

**Dexterity:** Dexterity often refers to the ability to move (or exert force) equally well in every direction. This is quantified by the isotropy of the ellipsoid. The volume of the ellipsoid can also be used to characterize dexterity, though the isotropic feature is not evaluated. However, this work focuses on evaluating skilled technical gestures. The worker is supposed to be an expert, so he knows the trajectories to follow and the forces to exert. Therefore directional manipulability measures are preferred.

**Velocity transmission ratio:** The velocity transmission ratio (VTR) has been proposed by Chiu to evaluate the capacity to produce end-effector Cartesian velocity in a given direction [Chiu 1987]. It is the distance between the center and the boundary of the manipulability ellipsoid along the direction of interest. Instead of its

original version, the VTR used in this work is based on the dynamic manipulability ellipsoid, in order to account for the dynamic effects and the non-homogeneity of the human joints [Yoshikawa 1985a, Chiaacchio 1998]. Besides the inverse of the VTR is preferred, so that as for the other indicators, a good ergonomic situation corresponds to a small value of the indicator:

$$VTR_{inv} = \left[ \mathbf{u}^T (JM^{-1}L^2 M^{-1}J^T)^{-1}\mathbf{u} \right]^{\frac{1}{2}} \tag{3.11}$$

where $\mathbf{u}$ is the direction of interest, $J$ the Jacobian matrix of the considered end-effector, and $L = diag(\tau_i^{max})$ contains the joint torque capacities. This indicator is evaluated for both "human end-effectors" that are expected to produce Cartesian velocity in a manual job, *i.e.* both hands.

**Force transmission ratio:** The force transmission ratio (FTR, also proposed by Chiu) evaluates the capacity to produce an end-effector force in a given direction $\mathbf{u}$. Its formulation is dual to the VTR formulation (also inverse and different from the original one, for the same reasons), given the force-velocity duality:

$$FTR_{inv} = \left[ \mathbf{u}^T (JM^{-1}L^{-2}M^{-1}J^T)\mathbf{u} \right]^{\frac{1}{2}}. \tag{3.12}$$

As for the VTR, the FTR is evaluated for both hands.

The VTR/FTR must however be used carefully to evaluate the biomechanical solicitations. They represent the ease to produce a force/velocity in a given direction. Therefore when an external force is exerted in this direction, the FTR is a qualitative image of the joint torques. However it has no meaning when no force is exerted with the corresponding body part. Similarly the VTR cannot represent the current ergonomic situation when no motion is required in the considered direction. Therefore, their inclusion in the list of indicators, and the direction(s) along which they are evaluated must be chosen depending on the technical gesture that is studied.

**Precision:** The inverse of the VTR (resp. FTR) can be used to evaluate the displacement (resp. force) precision capacity [Chiu 1987]. Indeed a small VTR means that a big joint displacement causes a small Cartesian displacement, resulting in a better control of the positioning. However, precision tasks are not addressed in this work, therefore these indices are not included in the list of ergonomic indicators.

### 3.1.3.3 Vision

When performing manual activities, workers tend to look at what they are doing, since working blindly is tiring and often impossible. Therefore the posture is influenced by the task visibility. Some studies on posture prediction have thus considered criteria for estimating visual comfort, *e.g.* visual acuity, which is based on the angular distance between the fovea and the visual target [Marler 2006]. However, the

purpose of this work is not to predict human motion, but to evaluate biomechanical solicitations, so visual comfort is not considered.

Nevertheless, estimating the ability to easily move one's head in various directions gives an insight into whether following a visual target requires small or large postural changes. Thus it represents the biomechanical solicitations associated with this motion. Therefore the rotational dexterity of the head (isotropy of the head manipulability ellipsoid) is used as a "vision-related" indicator:

$$D_{head} = \frac{\sigma_{min}}{\sigma_{max}} \tag{3.13}$$

where $\sigma_{min}$ (resp. $\sigma_{max}$) is the smaller (resp. bigger) singular value of $J_{rot}M^{-1}L$, with $J_{rot}$ the rotational part of the head Jacobian matrix. $M$ and $L$ are added to take the body dynamic properties, and effort capacities into account.

### 3.1.3.4 Balance

Evaluating the balance quality gives an insight into the effort needed to maintain the posture. Unstable balance requires higher muscular effort because the posture must always be slightly adapted in order not to fall. Several indicators can be used for evaluating the stability of legged robots [Goswami 1999, Garcia 2002, Pratt 2006, Hoyet 2010]. In this work, two balance indicators are added to the list of ergonomic indicators, both based on the position of the Center of Pressure (CoP).

The CoP is the point of application of the ground reaction force vector. In order to evaluate the balance of humanoids, the Zero Moment Point (ZMP) is more commonly used [Vukobratović 2004]. The ZMP is defined as the point of the ground at which the resultant tangential moments of inertial and gravity forces are zero. The ZMP and the CoP are equivalent, when the only forces at play are the inertial forces, the gravity forces, and the ground reaction forces. However, if external forces (*e.g.* the weight of a load) are exerted on the humanoid, the ZMP and the CoP are not equivalent anymore. Indeed, the most common definition of the ZMP does not include external forces, whereas they are necessarily taken into account in the CoP. Since this work focuses on activities that could be assisted with a strength amplification collaborative robot, external forces are potentially significant. So their influence on balance stability must be considered, therefore the CoP is preferred to the ZMP (this is equivalent to considering a "modified ZMP" which includes external forces).

**Balance stability margin:** This indicator represents the capacity to withstand external disturbances. It is computed as the sum of the square distances between the CoP and the base of support boundaries:

$$COP_{margin} = \frac{1}{M} \sum_{i=1}^{M} d_i^2 \tag{3.14}$$

where $M$ is the number of base of support boundaries, and $d_i$ the distance between the CoP current position and the *ith* boundary of the base of support. A time-integral version of this indicator (however on the ZMP) is used by Xiang *et al.*, along with a joint torque criterion, to predict human lifting motion [Xiang 2010a].

**Dynamic balance:** This indicator evaluates the dynamic quality of the balance. It is computed as the time $T_{out}$ before the CoP reaches the base of support boundary, assuming its velocity remains the same. This is a simplified indicator in which the acceleration of the CoP is assumed to be null. For the sake of homogeneity, the inverse formulation $1/T_{out}$ is used, so that tending towards a better ergonomic situation corresponds to minimizing the indicator value:

$$COP_{dyn} = \frac{1}{T_{out}} = \frac{\parallel \mathbf{v_{CoP}} \parallel}{d} \tag{3.15}$$

where $\mathbf{v_{CoP}}$ is the CoP current velocity, and $d$ the distance between the CoP current position and the base of support boundary, along the direction of $\mathbf{v_{CoP}}$.

### 3.1.4 Conclusion

In standard ergonomic assessment methods, risk factors of different nature (posture, effort, frequency,...) are often combined together to form a single ergonomic score. Indeed, the combination of several MSD factors increases the risk. However, the way these various factors interact is not well-established [Li 1999]. Therefore it is preferred here to keep all the indicators presented above as distinct measurements, rather than trying to mix them together.

Table 3.1 summarizes all the indicators that have been proposed to evaluate biomechanical solicitations. This list includes indicators representing different kinds of solicitations, in order to cover a wide range of physically demanding manual activities.

However, all these indicators are instantaneous. In order to represent the whole activity with only one value (for each indicator), the instantaneous values are time-integrated, hence taking into account the duration factor. This is roughly similar to what is done in the OCRA index calculation [Occhipinti 1998], where the final score depends on the time spent in "dangerous zones". Here, the "danger coefficient" is the value of the instantaneous solicitation. Nevertheless, one limitation of this time-integral formulation, is that temporal variations of the indicator are lost. For instance, the same final value can result either from a medium solicitation all along the task, or from an alternation of strong and light solicitations. Yet both situations do not have the same biomechanical consequences. This problem is all the more important than the activity studied is complex, *i.e.* consists of several subtasks where the solicitations are very different. This suggests that more accurate evaluations could be achieved by first segmenting complex activities into several subtasks, then evaluating each subtask separately (see section 5.2.3 for further discussion on this topic).

| Indicator definition | | Indicator type | Ref. equation |
|---|---|---|---|
| Joint normalized position | - right arm<br>- left arm<br>- back<br>- legs | local | 3.4 |
| Joint normalized torque | - right arm<br>- left arm<br>- back<br>- legs | local | 3.5 |
| Joint velocity | - right arm<br>- left arm<br>- back<br>- legs | local | 3.7 |
| Joint acceleration | - right arm<br>- left arm<br>- back<br>- legs | local | 3.8 |
| Joint power | - right arm<br>- left arm<br>- back<br>- legs | local | 3.9 |
| Kinetic energy | | global | 3.10 |
| Velocity transmission ratio | - right hand<br>- left hand | global | 3.11 |
| Force transmission ratio | - right hand<br>- left hand | global | 3.12 |
| Head dexterity | | global | 3.13 |
| Balance stability margin | | global | 3.14 |
| Dynamic balance | | global | 3.15 |

Table 3.1: List of ergonomic indicators for the evaluation of biomechanical solicitation during manual activities.

## 3.2   Simulation of co-manipulation activities

In order to measure the ergonomic indicators defined in the previous section, a DHM simulation tool is required. This tool must enable the dynamic simulation of co-manipulation activities with an autonomous virtual manikin. As stated in chapter 2, commercial DHM software are not sufficient for accurate ergonomic evaluations, because they do not enable automatic and physically consistent simulation of a human-cobot activity.

To address the physical consistency problem, the simulation is run in a dynamic simulation framework based on a physics engine. The framework used in this work

is XDE[1], developed by CEA-LIST [Merlhiot 2012]. It enables the simulation and control of physically interacting mechanisms, for instance a robot and a virtual manikin. The XDE manikin is modeled by a robotic mechanism: it consists of 21 rigid bodies linked together by 20 joints with a total of 45 degrees of freedom (DoF), plus 6 DoFs for the free floating base. Each DoF is a revolute joint controlled by a sole actuator. Several human morphologies can easily be tested, since given a size and a mass, the manikin is automatically scaled according to average anthropometric coefficients (see appendix B for further details).

## 3.2.1 Virtual human control

In order to animate a virtual manikin, kinematic techniques or dynamic techniques can be used. However, kinematic techniques do not consider forces, therefore the computed motion is not physically consistent. This is particularly limiting for the ergonomic assessment of activities where significant forces can be at play. Therefore a dynamic technique is preferred here: it relies on the equation of motion 3.1.1, thus ensuring the consistency of the forces and motions.

Since the human body is kinematically redundant, a same Cartesian motion (*e.g.* hand trajectory) can be achieved by different combinations of joint motions. Human-beings usually use this redundancy to perform several tasks simultaneously, *e.g.* manipulation and postural tasks. However these tasks are often conflicting in some way. Two strategies exist to handle these conflicts: hierarchical and weighting strategies. In weighting strategies, the solution is a compromise between the tasks, based on their relative importance. This compromise is usually achieved through quadratic programming optimization techniques [Abe 2007, Collette 2007, Salini 2011, Liu 2012]. In strictly hierarchical strategies, higher-priority tasks are completely fulfilled, whereas lower-priority tasks are projected into the null-spaces of higher-priority tasks and therefore only partially fulfilled. This approach is associated either with analytical resolution techniques, *i.e.* null-space projector [Siciliano 1991, Khatib 2008, Sentis 2004], or with optimization techniques, *i.e.* hierarchical quadratic programming [Kanoun 2009, Saab 2011, Escande 2014].

When performing motions, human-beings do not only have to handle compromises between different tasks, but they are also subjected to equality and inequality constraints, such as actuation limits, or unilateral contacts. Contrarily to optimization techniques, analytical techniques cannot take inequality constraints properly into account. Therefore an optimization-based technique is preferred in this work. It should be noted that the current section does not present an original contribution: the structure of the controller that is used in this work and presented hereafter was already implemented in the XDE framework.

The motion of the manikin is computed according to a weighting strategy, with the linear quadratic programming (LQP) controller framework developed by Salini *et al.* [Salini 2011]. Linear quadratic programming handles the optimization of a

---

[1]www.kalisteo.fr/lsi/en/aucune/a-propos-de-xde

quadratic objective that depends on several variables, subjected to linear equality and inequality constraints. The variables here are the joint torques, the contact forces, and the joint accelerations (though the latter could be excluded from the optimization variable and computed with the equation of motion). The control problem is formulated as follows:

$$\underset{\mathbb{X}}{\operatorname{argmin}} \quad \sum_i \omega_i T_i(\mathbb{X})$$

$$\text{s.t.} \begin{cases} M(\mathbf{q})\ddot{\mathbf{q}} + \mathbf{C}(\mathbf{q}, \dot{\mathbf{q}}) + \mathbf{g}(\mathbf{q}) = S\,\boldsymbol{\tau} - \sum_k J_{c_k}^T(\mathbf{q})\mathbf{w}_{\mathbf{c_k}} \\ \\ G\mathbb{X} \preceq \mathbf{h} \end{cases} \qquad (3.16)$$

where $\mathbb{X} = (\boldsymbol{\tau}, \mathbf{w_c}, \ddot{\mathbf{q}})^T$. The equality constraint is the equation of motion 3.1.1. The inequality constraint includes the bounds on the joint positions, velocities, and torques (all formulated with $\boldsymbol{\tau}$ and $\ddot{\mathbf{q}}$), and the contact existence conditions for each contact point, according to the Coulomb friction model:

$$\begin{aligned} C_{c_j}\mathbf{w_{c_j}} &\leq 0 \quad \forall j \\ J_{c_j}(\mathbf{q})\ddot{\mathbf{q}} + \dot{J}_{c_j}(\ddot{\mathbf{q}}, \mathbf{q})\dot{\mathbf{q}} &= 0 \quad \forall j \end{aligned} \qquad (3.17)$$

where $c_j$ is the *jth* contact point, $C_{c_j}$ the corresponding linearized friction cone, and $\mathbf{w_{c_j}}$ the contact wrench.

The objective function is a weighted sum of tasks $T_i$ representing the squared error between a desired acceleration or wrench and the system acceleration/wrench ($\omega_i$ are the weighting coefficients). The following tasks are defined:

- Operational space acceleration $\quad \|J_i\ddot{\mathbf{q}} + \dot{J}_i\dot{\mathbf{q}} - \ddot{\mathbf{X}}_{\mathbf{i}}^*\|^2$
- Joint space acceleration $\quad \|\ddot{\mathbf{q}} - \ddot{\mathbf{q}}^*\|^2$
- Operational space wrench $\quad \|\mathbf{w_{c_i}} - \mathbf{w}_{\mathbf{c_i}}^*\|^2$
- Joint torque $\quad \|\boldsymbol{\tau} - \boldsymbol{\tau}^*\|^2$

where $\ddot{\mathbf{X}}_{\mathbf{i}}$ is the Cartesian acceleration of body $i$, and $\mathbf{w_{c_i}}$ the wrench associated with body $i$. The superscript * refers to the desired acceleration/force, which are defined by a proportional derivative control. For instance, the desired acceleration is:

$$\ddot{\mathbf{X}}^* = \ddot{\mathbf{X}}^{\mathbf{goal}} + K_d(\dot{\mathbf{X}}^{\mathbf{goal}} - \dot{\mathbf{X}}) + K_p(\mathbf{X}^{\mathbf{goal}} - \mathbf{X}) \qquad (3.18)$$

where $K_p$ and $K_d$ are the proportional and derivative gains. The superscript $^{goal}$ indicates the position, velocity and acceleration wanted for the body or joint.

### 3.2.2 Tasks for manual activities

The tasks $T_i$ which compose the objective function vary depending on the activity that is simulated. However some tasks are almost always needed for the simulation of manual activities, *e.g.* balance, manipulation, or gazing. These tasks are detailed hereafter, and summarized in Fig. 3.2.

**Balance:** The balance of the manikin is managed with a center of mass (CoM) task. Controlling only the CoM position is limited to very static activities. In particular it does not enable the simulation of walking motions. In order to ensure the balance during both standing and walking phases, a ZMP preview control method is used [Kajita 2003]. The reference CoM acceleration is obtained from the CoM jerk computed with the preview control, while the position and velocity are not controlled ($K_p = 0$ and $K_d = 0$).

The original ZMP preview control scheme is slightly modified in this work, so that it takes into account external forces which affect the manikin balance, such as a load weight. However, the force magnitude, direction and application point must be known in advance.

For walking motions, feet operational acceleration tasks are added in order to move the swing foot along a given trajectory. Both cyclic walking motion and stepping motion can be generated. However, the step length (or foot end position in stepping motions) and duration must be specified beforehand.

In all the standing activities that are simulated in this work, the balance task is always assigned the largest weight, since balancing is the first priority in most daily life situations.

**Manipulation:** When performing manual activities, one (or both) hand needs to reach a target or follow a defined trajectory, and possibly apply a desired force on the environment. The corresponding hand operational acceleration and force tasks are called manipulation tasks in this work.

When the purpose of the gesture is to reach a target with no further constraints on the trajectory, a position task could be used, *i.e.* only the reference position is specified, while the reference velocity and acceleration are set to zero. However, if the task proportional and derivative gains ($K_p$ and $K_d$ in eq. 3.18) are kept constant during the motion, this solution leads to a significant positioning error. Indeed, the value of the proportional gain is limited by the distance between the start and end points, otherwise causing very fast unrealistic motions. This problem is solved either by imposing a discretized trajectory rather than just an end point, or by varying the values of $K_p$ and $K_d$ in accordance with the position error. The first solution is preferred, because it forces the hand trajectory to follow a specific pattern. For technical gestures, the reference trajectory is an input specified by the user. For less specific gestures (especially reaching motions), the reference trajectory results from a polynomial interpolation between the start and end points, with initial and final conditions on the position, velocity and acceleration. Indeed it has been demonstrated that in reaching motions, humans tend to follow an approximately straight line, with a bell shape velocity profile [Morasso 1981, Flash 1985].

The hands operational acceleration and force tasks are given the second most important weights after the balance task, because they determine whether the job is correctly performed or not.
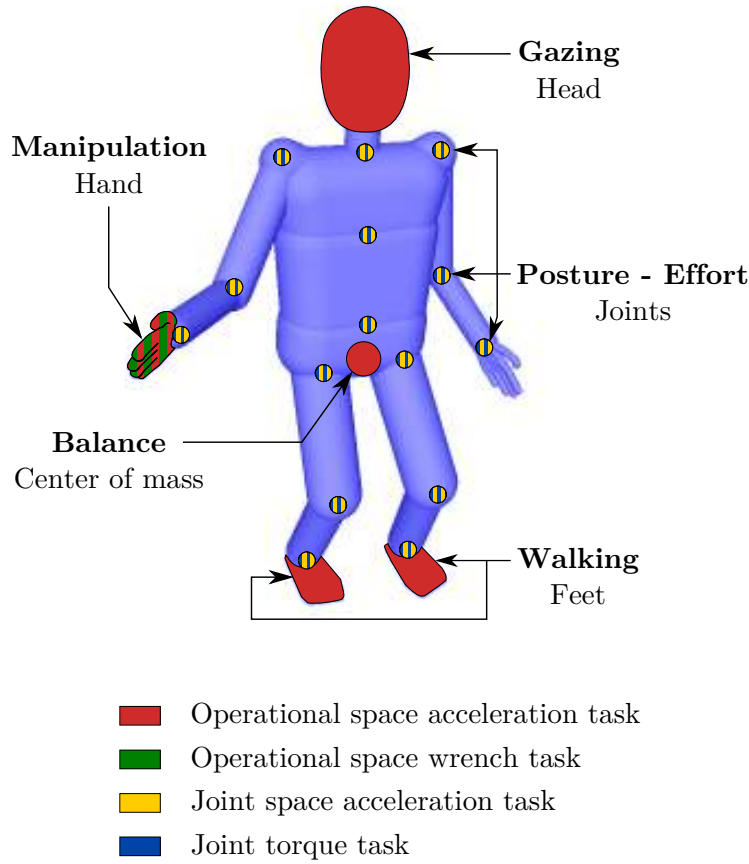
Figure 3.2: Joint space and operational space tasks used in the LQP controller for simulating manual activities with the virtual manikin.

**Gazing:** In order that the manikin looks at what it is doing, an orientation task is associated with the head. This task consists in aligning the head forward direction with the eye-to-target direction. However, this gazing task only partly constrains the manikin posture, because visual collisions are not detected and taken into account yet.

The gazing task is assigned a weight that is similar to those of manipulation tasks. Indeed, though the manipulation task is the final goal of the activity, it can hardly be performed blindly. Besides, manipulation and gazing tasks are associated with different limbs of the human tree structure, therefore they only slightly interfere with each other.

**Postural task:** Joint position tasks are used in the simulation to define a reference posture which should be adopted by the manikin when no specific activity is performed. The desired joint positions usually correspond to a standing posture, arms along the body (resting posture). Low weights are associated to these postural tasks, so that they do not hinder the balance task or the manipulation tasks.

The weights of the joint position tasks are not equal, but rather decrease when

nearing the distal members (hands and feet), in order to favor their motion compared to the body parts closer to the torso.

**Joint effort:**   For each joint, a joint torque task is added, which aims at minimizing the joint torque to prevent useless effort (the reference torque is zero). These torque tasks are also mathematically needed in order to ensure the uniqueness of the solution to the optimization problem. The weights of the joint torque tasks are the smallest since they must not hinder the other tasks.

### 3.2.3   Motion capture replay

The evaluation tool developed in this work aims at enabling the ergonomic comparison of collaborative robots, without the need for physical prototypes of the robots. As stated in chapter 2, due to the absence of physical prototype, motion capture data cannot be used for realistic animation of the manikin in co-manipulation activities. However, motion capture based animation is nevertheless needed for the following purposes:

- **Validation of the evaluation tool:** the comparison between recorded and simulated data is used for assessing the consistency of different components of the evaluation framework (see chapter 4 for the actual validation).

- **Acquisition of a reference situation:** in order to ensure that a collaborative robot does decrease MSDs risks - and does not create new MSDs - the execution of the activity with and without the cobot must be compared. The situation without assistance (reference situation) is recorded on real workers within their work environment. Thus the realism of the manikin behavior in the reference situation is improved, compared to automatically generated behaviors. Such a recording also enables the acquisition of a ground truth for the technical gesture (trajectories to follow and forces to exert).

- **Evaluation of existing cobots:** though this is not the main purpose of this work, the proposed framework can as well be used for evaluating already existing cobots. In such cases, motion capture data - recorded on a worker assisted by the robot - ensure better realism of the manikin behavior (see appendix C for an example).

Animation with pre-recorded data is therefore needed not only for validation purposes, but also for each new activity that is studied.

The main steps for animating the XDE manikin with motion capture data are detailed hereafter and summarized in Fig. 3.3. The method presented here is dedicated to optical motion capture techniques, in which markers are positioned on the body of the subject. The system specifically used in this work is the CodaMotion system[2]. However the whole method can easily be adapted to other motion capture

---

[2]`www.codamotion.com`

systems using a marker-based technology (*e.g.* Vicon[3]), and, to some extent, to systems using video information (*e.g.* Kinect sensors with the Microsoft SDK or OpenNI). The CodaMotion system is an optical motion capture system using active infra-red markers. Each marker emits a different signal, so there is no ambiguity on the identity of the marker. The Cartesian position of the markers are measured with infra-red cameras embedded in Coda sensor units. Each unit consists of three cameras, so the markers 3D position can be estimated with a single Coda sensor unit. However several units can be used together in order to minimize the position error, and the visual occlusions of the markers.

**Markers positioning:** The markers are positioned directly on the subject skin (preferably) or tight clothes. Both skin and clothes are deformable, so the distance between two markers varies during the motion. On the contrary, the manikin used for replaying the motion is a rigid body model. So the distance between two virtual markers on the manikin body is fixed all along the motion. This difference between fixed and varying inter-markers distance is a source of error for the motion replay. In order to minimize this error, the markers are positioned on little deformable zones of the human body, generally at the joints on protruding bones. Fig. 3.3 (top left) displays the markers placement used when recording whole body motions. If only a part of the body is to be captured (*e.g.* upper body), the useless markers can be moved to little equipped body parts, *e.g.* the back. Given the redundancy of the human body, markers are placed on most of the main joints in order to capture the human motion as exhaustively as possible. However the number of markers is limited by the CodaMotion system and the acquisition frequency (28 markers maximum when recording at 100 Hz).

**Calibration:** Since the manikin is not an exact model of the human body, a calibration step is necessary to determine the correspondence between the markers positions on the human body and on the manikin body. Indeed each marker is associated to a segment of the manikin body, but the exact position of the marker in the segment frame is not known. In order to estimate these position offsets, the fully equipped subject adopts a known posture, and the markers absolute positions are recorded. The offset calculation is detailed in the data treatment section. Two reference postures are used in this work: the resting position (standing, arms along the body and palms towards the body), and the T-position (standing, arms in a T position, palms towards the ground). The markers offsets are computed from both reference postures together, in order to minimize the error due to the deformation of the human skin (at least for the arms, which are the most important body parts in manual activities).

**Data acquisition:** The motion of interest is recorded. The acquisition rate used in this work is 100 Hz, which is highly sufficient for human motions. Three Coda

---

[3]http://www.vicon.com/
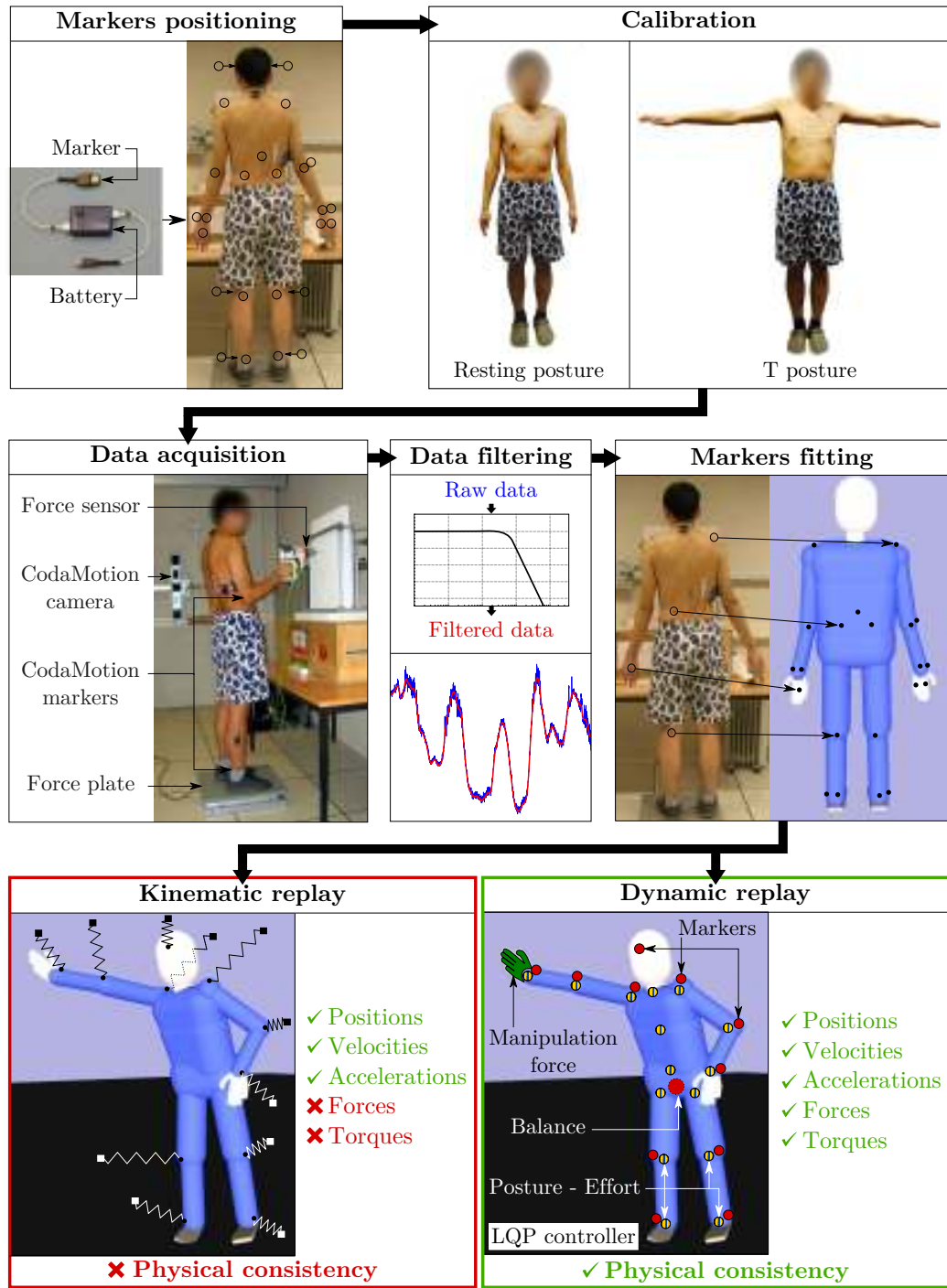
Figure 3.3: General method for motion capture replay. The black circles in the *Markers positioning* step represent the position of the CodaMotion markers on the human body. The circles with an arrow represent the markers that are hidden in the current position. The color code used for the tasks in the *Dynamic replay* step is the same as in Fig. 3.2.

sensor units are used, so that each marker is always seen by at least one unit. However, the motion alone is rarely sufficient for consistently replaying the task with the virtual manikin. Interaction forces are also needed, especially in the context of collaborative robotics. Indeed, collaborative robots (especially those providing strength amplification) are usually used for power tasks, *i.e.* tasks requiring significant interaction forces from the worker. The ground contact forces are not necessarily required for the replay, but can be recorded for validation purposes. An AMTI[4] force plate is used: it provides the six components of the ground contact wrench and the center of pressure position. The force plate is already integrated in the CodaMotion system, so both acquisitions are easily synchronized. For the forces specifically related to the activity of interest, a force sensor is embedded in the working tool[5]. The force components are then measured in the sensor frame. The sensor - or tool it is embedded in - is therefore equipped with CodaMotion markers, so that its position and orientation in a fixed frame are known. The acquisitions of the force sensor and CodaMotion data are synchronized thanks to an external trigger with an Arduino[6].

**Data treatment:**  The recorded CodaMotion and force sensors data are filtered with a zero-phase 10 Hz low pass 4th order Butterworth filter (no delay is introduced between the raw and the filtered data). The markers velocities and accelerations are then computed from the markers positions with finite differences.

The second step of the data treatment consists in positioning the markers on the manikin body. The manikin is firstly scaled according to the subject height and mass (if needed, the length of each segment can be scaled separately). The scaled manikin is then positioned in the reference posture adopted for the calibration. The calibration postures must be simple, and motionless, so that they can easily be manually reproduced on the manikin. The offset between each markers and the corresponding segment frame is measured for each time step of the recorded data, and for both reference postures. The offset values are then computed by the least squares method.

**Kinematic replay:**  The easiest way to reproduce the recorded motion is the kinematic replay. The manikin is animated like a puppet (no controller). For each marker, one extremity of a virtual spring-damper system is attached to the manikin body, according to the previously computed offset. The position of the other end of the spring-damper system is given by the recorded position of the marker. With the kinematic replay, all kinds of motions can be reproduced, including walking motions or unstable postures. Biomechanical quantities such as joint positions or velocities can be measured on the manikin, but not the driving forces (joint torques). The

---

[4]http://www.amti.biz/

[5]Different ATI force sensors are used in this work, depending on the force range required for the considered application.

[6]http://www.arduino.cc/

interest of kinematic replay is therefore very limited regarding ergonomic evaluation. Besides, if only a few markers are positioned on the human body, the inverse kinematic solution is not unique (the motion of some segments are not entirely constrained by the markers trajectories). The resulting motion is therefore not necessarily similar to the original motion.

Joint torques can nevertheless be *a posteriori* estimated from a kinematic replay, thanks to the dynamic motion equation (eq. 3.1). Indeed, the positions, velocities and accelerations are known, since measured beforehand in the replay. However, the dynamic motion equation also requires all interaction forces - including the ground contact forces - to be given as an input. Measuring ground contact forces requires heavy instrumentation, and is therefore generally avoided (except for validation purposes). For both this instrumentation reason, and the potential non uniqueness of the inverse kinematics solution, the two-step solution which combines kinematic replay and joint torques estimation is not used in the remaining of this work.

**Dynamic replay:** To ensure the physical consistency of the motion and forces without needing ground contact forces measurements, the manikin motion is rather calculated with the LQP controller described in section 3.2.1. The controller architecture is similar to the one used for generating autonomous motions, however the tasks included are different. An operational acceleration task is created for each marker on the manikin's body (position only, no orientation since only the markers 3D positions are recorded with the CodaMotion system). The reference trajectory (position, velocity and acceleration) corresponds to the recorded marker trajectory. Depending on the total number of markers and their respective placement on the subject, the problem can - and often is - over constrained: not all markers trajectories can be accurately followed. However the LQP controller is designed to deal with conflicting objectives. So redundancy in the markers is preferable because it minimizes the influence of measurement errors. Still, the weights of the different markers tasks must be wisely chosen, since they affect the resulting motion. The markers tasks are not all assigned the same weight: the markers associated with limbs extremities are given the biggest weight, then the weight decreases when the body on which the marker is set is further away from the extremities. This weight assignment process is in accordance with the recommendations of Demircan *et al.* [Demircan 2010], though they use hierarchical control instead of weighted control. Extremities are more affected by cumulative errors on the preceding joint positions. So assigning the biggest weights to the operational position tasks of the limb extremities tends to reduce this bias.

If a force is to be exerted on the environment by the manikin hand (possibly through a portable tool), an operational force task is created. The reference force is given by the corresponding force sensor measurement.

The low-weight postural task used for autonomous motions (section 3.2.2) is also used for dynamic motion replay, in case some bodies are not entirely constrained by the markers tasks. The joint torque minimization task is also added to ensure

the uniqueness of the solution.

Finally, a balance task is added, but its weight is reduced (compared to autonomous motions) so that is is less important than the distal extremities markers tasks. Indeed, the markers tracking tasks are not sufficient to maintain the balance of the manikin, especially in motions where the balance is strongly solicited. Without any balance task, the balance control is only an open-loop control, through the markers tracking tasks (the manikin is not instructed to keep its balance). Due to the imprecisions in the human model and markers positions measurements, the open-loop balance control generally results in the fall of the manikin. Therefore a balance task is needed to prevent the manikin from falling. However the balance task may (and generally does) alter the manikin posture. So the weight of the balance task results from a compromise between the accuracy of the replay (markers tracking) and the balance preservation. Such a compromise is achieved with the proposed balance weight (smaller than the weight of the distal extremities markers tasks). This solution enables the dynamic replay of most motions in which the feet do not move, as long as the motions are not too unstable. However, the classic ZMP preview control used in the balance task is not sufficient to enable the dynamic replay of walking motions (this issue is discussed in section 4.4.2.3). Therefore only motions in which the feet do not move are dynamically replayed in this work.

### 3.2.4   Cobot simulation

The purpose of the simulation tool presented in this chapter is to enable the simulation of co-manipulation activities with the virtual manikin. The manikin animation being described in the previous sections, this section focuses on the simulation of collaborative robots. This work focuses on collaborative robots which provide strength amplification, and which are manipulated by the end-effector only (parallel co-manipulation). The method presented here is therefore dedicated to such systems specifically. The different components needed to simulate a cobot in interaction with both the autonomous manikin and the environment are detailed hereafter.

**Manikin grasp:**  In parallel co-manipulation, the cobot is manipulated by the worker via its end-effector. On real cobots, the worker usually grasps a user handle mounted on the end-effector. In the simulation however, the manikin does not have any joints in its fingers, so simulating grasping is impossible[7]. Instead, the human grasp is represented by a 6D spring-damper system between the manikin hand and the robot handle. The values of the stiffness and damping coefficients are experimentally tuned according to the two following requirements:

- The distance between the manikin hand and the robot handle must remain very small even in fast motions. Indeed, when grasping an object, the hand and the object remain in contact all the time. So the spring-damper must be stiff enough to simulate the resistance of opposite fingers in human grasp.

---

[7]Even if the manikin fingers were articulated, grasping requires a complex control of the fingers, which is beyond the scope of this work.

- The grasp interaction must remain stable in all phases of the activity: free space motions as well as force exertion phases. Due to this constraint, the upper value of the stiffness is limited, especially when force amplification is provided.

The stiffness and damping coefficients are not modified during a simulation. So in order to respect both constraints, the upper value of the strength amplification coefficient is limited. It should be noted that for real strength amplification cobots, the problem of stability for all kinds of grasps is generally addressed with the passivity concept [Lamy 2011].

Before activating the manikin grasp (*i.e.* turning on the spring-damper system), the robot handle must be placed close to the manikin hand. Otherwise the restoring force at the time of the activation is very high, leading to the fall of the manikin, or unstable behavior of the simulated grasp. An initialization phase is therefore added at the beginning of the simulation, in order to correctly position the robot end-effector. During this phase, the robot is controlled with a LQP controller, similar to the one used for the manikin. An operational space acceleration task associated with the robot end-effector is defined, and a reference trajectory between the end-effector initial position and the manikin hand is created. However this trajectory does not take potential obstacles (environment or manikin segments) into account. Therefore it is preferable to initially position the manikin close to the robot end-effector to limit the chances of collisions. Once the end-effector is correctly positioned, the LQP controller is turned off, and the robot is controlled according to the strength amplification control law detailed hereafter.

**Strength amplification control law:** Strength amplification consists in controlling the robot so that the force it exerts on the manipulated tool (or environment) is an amplified image of the force applied by the worker onto the robot. The robot joint torques are therefore computed from the measure of the force exerted by the worker on the robot handle. On real cobots, a force sensor is embedded on the user handle. In the simulation, the spring-damper system representing the human grasp enables the measurement of the interaction force between the manikin hand and the robot end-effector.

Additionally to strength amplification, the weight of the robot and the viscous friction effects are compensated. However, the inertial effects are not compensated, because such compensation is hard to implement on real robots. Indeed, the compensation of inertial effects requires the estimation of the robot joint accelerations. On real robots, the joint accelerations can either be numerically estimated, or they can be measured with accelerometers placed on the robot, but none of these solutions are used in practice. The data obtained with the first solution are likely to be noisy, hence non usable to properly control the robot, while the second solution requires costly instrumentation. The global strength amplification control law is:

$$\boldsymbol{\tau_r} = \alpha \, J_{ee,r}^T \, \mathbf{F_{vh}} + \mathbf{g_r}(\mathbf{q_r}) + B \, \dot{\mathbf{q}}_{\mathbf{r}} \tag{3.19}$$

where $\boldsymbol{\tau_r}$ is the robot joint torques, $\mathbf{q_r}$ the vector of robot joint angles and $\dot{\mathbf{q}}_{\mathbf{r}}$ the vector of joint velocities, $\mathbf{g_r}$ the vector of gravity forces, $B$ the matrix of viscous friction coefficients, $J_{ee,r}$ the Jacobian matrix of the robot end effector, $\mathbf{F_{vh}}$ the force applied by the manikin onto the robot end-effector, and $\alpha$ the amplification coefficient.

Strength amplification can be provided either throughout the whole activity (free space and contact phases), or only when significant contact forces must be exerted on the environment (contact phases). In all examples presented in this work, strength amplification is activated only during contact phases. During the manipulation of the robot in free space, strength amplification is deactivated ($\alpha = 0$).

**Contact force simulation:** The simulation in XDE only includes rigid bodies, so the measurement of the interaction force between two bodies requires the simulation of a force sensor, *e.g.* with a spring-damper system. Many manual activities require the exertion of a given force on the environment. In such cases, the simulated robot end-effector or tool must be equipped with a virtual force sensor. Though possible, this solution increases the complexity of the simulation. Besides, rigid bodies interaction is not sufficient when certain motions are associated with the force exertion. For instance, in the drilling task simulated in chapter 4, drilling requires the deformation of the drilled material. So the drilling force cannot be simulated by the physical interaction with a rigid environment.

Therefore, instead of using physical contact, the interaction force with the environment is simulated by a virtual wrench acting on the tool or the robot end-effector. The value of this wrench is set equal to the desired interaction force. Thus the required interaction force is necessarily respected.

## 3.3 Conclusion

This chapter addresses the problem of measuring biomechanical solicitations during co-manipulation activities, through simulation. To this purpose, two complementary tools are developed, around a macroscopic representation of the human body (no muscles).

The first tool addresses the problem of what to measure. It consists in a list of ergonomic indicators, defined to match the requirements of collaborative robots evaluation. The proposed indicators are based on ergonomic considerations, human motion performance criteria, and robotics performance criteria.

In this work, an ergonomic indicator is an instantaneous scalar quantity which value represents a relative level of biomechanical solicitation. Each indicator represents only one kind of solicitation. Contrarily to what is done in most ergonomic assessment methods, the different kinds of solicitations are considered in separate indicators, so that the formulation of the indicators is not task-dependent. The proposed list therefore contains eleven indicators (some divided in several sub-

indicators), in order to account, as exhaustively and concisely as possible, for all the biomechanical solicitations to which a worker can be exposed during all kinds of manual activities. The repetitiveness factor is however omitted.

The proposed ergonomic indicators are divided into two families: constraint oriented indicators, and goal oriented indicators. The constraint oriented indicators are local quantities which directly represent the relative level of joint solicitations (in terms of position, effort, dynamics...), in different body-parts (both arms, legs, back). The goal oriented indicators are global (whole-body) quantities which quantify the ability to comfortably perform certain actions (in terms of balance, force exertion...). They are indirect images of the biomechanical solicitations experienced by the worker.

For each indicator, its instantaneous values can be time-integrated over the whole considered activity, in order to represent the whole activity with only one value (one per indicator). The numerical value of an indicator thus enables to identify, between several situations, the most demanding one (in regard to the considered solicitation), however it does not represent an absolute level of risk of developing MSDs.

The second tool addresses the problem of how to measure the proposed ergonomic indicators. It consists in a framework for simulating co-manipulation activities, *i.e.* a virtual manikin and a robot performing tasks together.

The simulation is implemented in a dynamic simulation framework based on a physic engine, which guarantees the physical consistency of the motion and forces. The virtual manikin is animated through a LQP optimization technique, which enables multiple tasks definition and ensures constraints enforcement. A list of tasks which must be included in the LQP controller in order to simulate manual activities is established.

A representation of the interaction between the manikin and the simulated robot is proposed. The manikin grasp is represented by a spring-damper system. A strength amplification control law is used to control the robot from the measurement of the interaction force with the manikin. Thus, realistic co-manipulation scenarii can be easily created and automatically simulated, with only very limited input data (*e.g.* no need for a real robot, or for motion capture data to animate the manikin).

Besides, a method for dynamically replaying motions recorded on human subjects is proposed, based on the use of the LQP controller. Motion capture data are not needed in the proposed simulation framework, since the manikin can be autonomously animated. However, within the design process of a cobot, such data are useful to establish a ground truth of the reference situation (*i.e.* workers performing the considered activity without assistance). Motion capture data can also be used for validation purposes. The proposed dynamic replay method has the advantage of providing estimations of the forces associated with the motion, contrarily to kinematic replay methods.

Thanks to the proposed tools, ergonomic indicators can be measured on the virtual manikin autonomously performing a task with the assistance of a collaborative robot. However, if the physical consistency of the measurements is guaranteed, it is not the case of their biomechanical consistency. All the components of the proposed framework may affect the consistency of the evaluation: manikin model, control, indicators formulae... The reliability of the measurements provided by the proposed framework therefore needs to be validated. This validation is the subject of the next chapter.

# Chapter 4

# Experimental validation of the measurement framework

## Contents

In the previous chapter, a framework for evaluating biomechanical solicitations during co-manipulation activities without the need for a human subject, is presented. Before using it for various applications (chapters 5 and 6), the reliability of the measurements provided by the proposed framework needs to be validated. Indeed, several factors may affect the biomechanical consistency of the results. Firstly, the model used for representing the human body is only an approximation of the

human body, especially regarding its kinematic, dynamic and actuation properties. These differences may physically prevent the manikin from accurately reproducing a human motion, and/or modify the effort required to perform a motion. Secondly, the animation technique used for automatically generating the manikin motions may not produce human-like motions. A motion is considered *human-like* if, when performing the same activity (*e.g.* reaching, walking, carrying an object), the joint trajectories and forces of the autonomous manikin are similar to those of a human subject. Such lack of realism in the generated motions may lead to unrealistic postures and consequently forces. Thirdly, beyond the realism of the human simulation, the consistency of the proposed ergonomic indicators is also questionable. Given the high-level representation of the human body (rigid bodies, no muscles) and the indicators formulae, the proposed indicators are indirect images - instead of exact measurements - of the real biomechanical solicitations. This raises the question of how well such indicators account for the relative exposure level to MSD risks.

In order to address the above-mentioned criticisms, this chapter presents a validation of the proposed evaluation framework. The validation consists in three steps. The first step addresses the realism of the manikin model. The second step addresses the consistency of the proposed ergonomic indicators. These two components are evaluated through comparisons with real data. Motion capture based experiments are carried out in order to establish a ground truth on real subjects. No collaborative robot is used in those two steps. Indeed, before introducing another potential source of error (the robot), one has first to ensure that the proposed framework correctly enables the evaluation of non-assisted manual activities. Then, the collaborative robot is introduced, in order to validate the reliability and usefulness of the manikin-robot simulation. In this third step, no motion capture data are used, however a simple task is considered so that the interpretation of the results is straightforward.

## 4.1 Validation of the human model realism

A first step towards the validation of the proposed framework is to evaluate the representation of the human body used for simulating the worker. The realism of this representation concerns both the motions and the forces: are the generated motions human-like (similar joint trajectories), and do the computed forces match the forces exerted by a human subject. The motions and forces of the manikin are affected by the body model (*i.e.* its physical properties) and by the animation technique (*i.e.* the manikin LQP controller). However, the influence of these two components are not independent, so they need to be evaluated together.

This section focuses on the evaluation of the forces consistency. The realism of the automatically generated motion is not addressed. The whole body motion is therefore assumed to be given as an input, so as to be sure that it is truly human-like. When assessing the forces realism, the main concern is the reliability of the force-related biomechanical solicitations measured on the manikin. Given the cho-

sen representation of the human body, such solicitations correspond to the manikin joint torques, computed with the LQP controller. In order to assess the consistency of the manikin joint torques, the joint torques generated by a human subject (via the muscle forces) could be measured, and compared with those calculated by the manikin controller, when performing an identical motion. However, such measurement on a real subject is hardly possible in practice. On the contrary, the contact forces exerted by a human subject on its environment (*e.g.* the ground) can easily be measured. The contact forces being linked to the joint torques through the equation of motion 3.1, they provide some information on these torques. The experimental validation proposed in this section therefore focuses on the comparison between experimental and simulated (*i.e.* computed with the manikin controller) ground contact forces.

A good match between the contact forces measured experimentally and those computed by the manikin controller do not guarantee the realism of the proposed human representation. Different combinations of joint torques and motions can result in similar contact forces, due to the redundancy of the human/manikin kinematics. However, though not sufficient, such a match is a necessary condition to ensure the validity of the human representation.

## 4.1.1 Experimental protocol

The proposed validation requires the manikin and the human subject to perform a similar motion. To this purpose, full-body motion capture data are used to animate the manikin. Several human subjects perform a manual task which includes postural changes and force exertion. Their motions as well as the interaction forces with the ground and the work surface are recorded. The recorded motions are dynamically replayed with the virtual manikin, animated by the LQP controller. The contact forces with the work surface are given as an input of the simulation as well. On the contrary, no reference value is specified for the ground contact forces: they result from the optimization in the manikin controller. These computed ground contact forces are compared with those measured experimentally. The quality of the replayed motion is also evaluated, to ensure the similarity between the manikin motion and the human subject's motion. Otherwise the force comparison is meaningless. Besides the quality of the replay gives an insight on the consistency of the model kinematics and of the proposed replay technique.

#### 4.1.1.1 Task description

The task considered in this experiment is an example of manual task which requires significant efforts. It consists in drilling six holes consecutively in a vertical slab of autoclaved aerated concrete, with a portable electric drill. The locations of the holes are imposed, and depicted on Fig. 4.1. They are chosen so that the task demands significant changes in the subjects' posture, yet remains feasible without feet motion. Indeed dynamically replaying walking motion is still an issue (see

section 4.4.2.3 for details).

The drill weights $2.1\,kg$. The average normal force needed to drill a hole in these conditions is about $40\,N$. There is no constraint on the task duration, however it takes about $1\,min$ to perform the whole task: take the drill, drill the six holes, and put the drill down.

Each subject performs the task ten times, with a resting period between each performance. The subjects choose their feet positions, and are allowed to change them between each performance. However, they are instructed not to move their feet during one performance. The drill is held with the right hand only. Before starting the experiment, the subjects train several times in order to find a comfortable feet position, and to limit the learning effect during the recording.
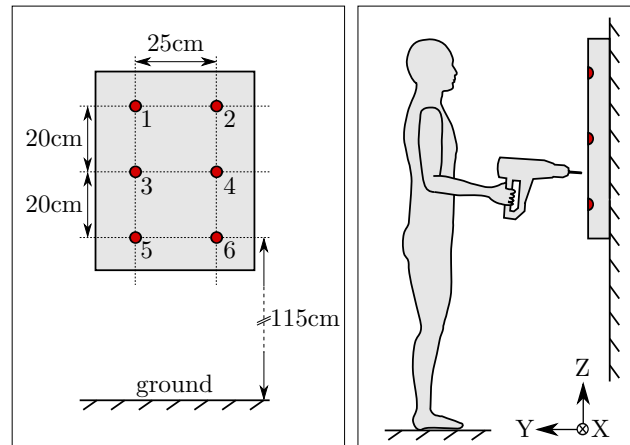


Figure 4.1: Geometric dimensions of the experimental set-up for the drilling activity. The red circles represent the drilling points.

### 4.1.1.2 Subjects and instrumentation

Five right-handed healthy subjects (3 males and 2 females) ranging from 25 to 30 years old take part in the experiment. Their average height is $1.72\,m$ (SD 0.1, min 1.53, max 1.82), and their average body mass index is $22.6\,kg.m^{-2}$ (SD 0.8, min 21.7, max 23.8).

The subjects' motions are recorded with the CodaMotion system (see section 3.2.3 for details) . The subjects are equipped with 25 markers spread all over their body (both legs, both arms, back and head). They stand on a force plate while performing the task, in order to measure the contact forces with the ground. A 6 axes ATI force sensor[1] is embedded in the drill handle, in order to measure the drilling forces. The drill is equipped with 3 CodaMotion markers so that the force sensor position and orientation is known. The instrumentation used to record the forces and motions is displayed in Fig. 4.2.

---

[1]http://www.ati-ia.com/products/ft/ft_models.aspx?id=Gamma
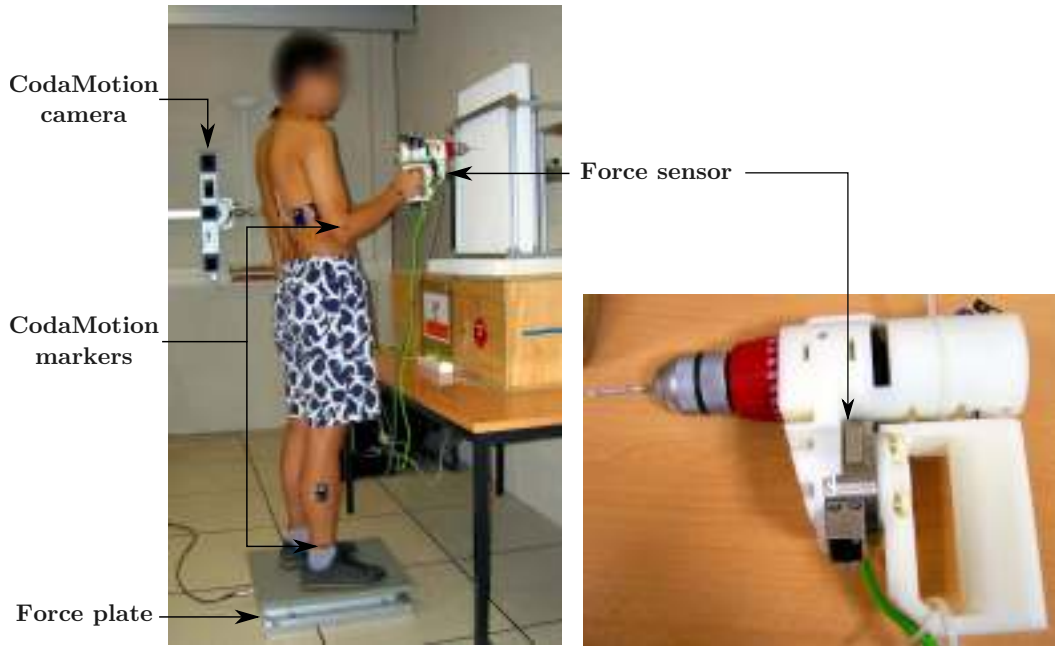
Figure 4.2: Motion and force capture instrumentation for the drilling task. A commercial drill has been modified in order to embed a force sensor.
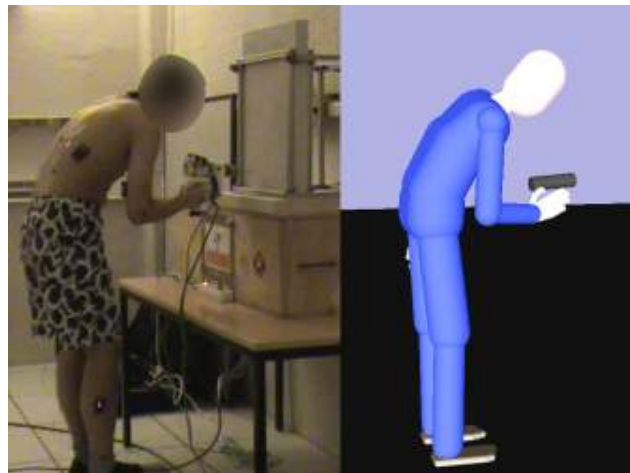


Figure 4.3: Left: A human subject performs the task while his motions are recorded. Right: The motion is dynamically replayed with the virtual manikin and the LQP controller.

### 4.1.1.3 Dynamic motion replay

The motions recorded on the human subjects are replayed with the XDE manikin and the LQP controller, according to the dynamic replay method detailed in section 3.2.3 (Fig. 4.3). The following tasks are included in the controller, in decreasing order of importance: markers tracking tasks (task weight depends on the marker),

right hand force task, balance task, postural task, and joint torque minimization task. The right hand force task corresponds to the drilling force: its reference value is provided by the measures from the force sensor. On the contrary, the ground contact forces measured with the force plate are not used in the simulation, since they are automatically computed by the manikin controller. The experimental values are needed for validation purpose only.

### 4.1.2   Results

The consistency of the replay is evaluated regarding both the motion and the contact forces. The comparison between the experimental data (recorded with the CodaMotion and force plate) and the simulated data (manikin motion and forces generated with the LQP controller) are presented and discussed hereafter.

**Motion:**   The 3D positions of the virtual markers in the simulation (*i.e.* spots on the manikin body for which tracking tasks have been created) are compared with the positions of the real markers recorded with the CodaMotion. The RMS errors between the experimental and simulated positions are presented in table 4.1, for each subject. The error is approximately the same for all markers placed on a same joint, therefore the results are presented for each joint rather than for each marker.

| | **Position RMS error (cm)** | | | | | | |
|---|---|---|---|---|---|---|---|
| | Sbj. 1 | Sbj. 2 | Sbj. 3 | Sbj. 4 | Sbj. 5 | Average | SD |
| Ankle | 1.5 | 1.0 | 0.9 | 1.1 | 1.3 | **1.2** | 0.2 |
| Knee | 4.6 | 4.9 | 3.7 | 3.8 | 4.8 | **4.4** | 0.5 |
| Back | 2.9 | 3.2 | 1.7 | 2.5 | 3.1 | **2.7** | 0.5 |
| Head | 1.6 | 1.6 | 0.6 | 1.5 | 1.0 | **1.3** | 0.4 |
| Right Shoulder | 7.8 | 6.9 | 2.0 | 6.8 | 7.0 | **6.1** | 2.1 |
| Left Shoulder | 3.9 | 2.7 | 1.9 | 2.2 | 3.5 | **2.8** | 0.8 |
| Right Elbow | 2.9 | 3.0 | 2.7 | 2.9 | 3.1 | **2.9** | 0.1 |
| Left Elbow | 0.8 | 0.5 | 0.3 | 0.8 | 0.7 | **0.6** | 0.2 |
| Right Wrist/Hand | 0.8 | 1.0 | 1.5 | 0.7 | 1.3 | **1.1** | 0.3 |
| Left Wrist/Hand | 0.5 | 0.4 | 0.2 | 0.3 | 0.2 | **0.3** | 0.1 |

Table 4.1: RMS errors between the experimental and simulated 3D positions of the markers, for each joint and each subject (*Sbj* stands for *subject*). For each subject, the value displayed is the average value of the ten trials. For each joint, the value displayed corresponds to the biggest error of all markers placed on the joint.

The tracking error is globally small - less that $3\,\mathrm{cm}$ for almost all joints - and there is no significant differences between the subjects. The morphology (at least the height) does not seem to affect the quality of the motion replay. The tracking error is the smallest for the distal parts of the body (ankle, hand and head). This result is

in accordance with the tasks weights distribution which is used in the LQP controller for the dynamic replay (see section 3.2.3). The tracking tasks associated with the distal parts of the body are given higher weights, so they are more likely to be achieved. Beyond the tasks weights distribution, the small value of the error for the ankle markers is expected since the feet do not move during the considered activity. Therefore a significant error on these markers would mean either a wrong initial placement of the manikin in the environment, or a wrong fitting of the markers on the manikin body. The non-zero error that is nevertheless observed for the ankle markers is due to the placement of the markers: they are positioned not on the feet but slightly above the ankle for visibility reasons. Contrarily to the feet, the bottom of the leg does move a little during the drilling activity.

The tracking of the left arm is better (for each joint) than the tracking of the right arm. This is due to the fact that the left arm does not move much, whereas the motion of the right arm is significant: the overall length of the right hand trajectory is about 1 m. A tracking error around 1 cm (for the right hand) is therefore satisfying. On the contrary, the tracking error of the right shoulder is not insignificant. One reason to this error is the deformation of the human skin - on which the markers are set - during gestures including a wide range of joint motions. This deformation results in a variation of inter-markers distances which can reach several centimeters. This phenomenon exists for all markers, however it it especially important for the right shoulder given the wide range of shoulder and elbow motions during the drilling activity. The distance between the elbow and shoulder markers therefore varies all along the recording. Since the tracking tasks of the elbow markers are given higher weights than the shoulder marker task, the variation of the inter-marker distance is almost entirely transmitted to the shoulder position. This phenomenon is reinforced by the fact that two markers are set on the elbow, but only one on the shoulder: regarding the LQP controller, the position of the elbow is all the more important. Another reason to the significant shoulder tracking error may be the complexity of the human shoulder joint. This complexity is only roughly modeled in the manikin kinematics, so some human shoulder motions cannot be accurately reproduced.

The tracking error of the knee markers is particularly big, given the small overall displacement of these markers during the drilling activity. This might be due to the balance task that is added in the LQP controller. The balance task is needed to prevent a fall of the manikin (the markers tracking tasks are generally not sufficient to ensure the balance), however it affects the other tasks, among which the markers tracking tasks. The knee markers and, to a lesser extent, the back markers are the most affected because the feet and arms Cartesian positions are either fixed or strongly constrained by high weight tasks. Therefore the balance regulation is mainly carried out with the pelvis, which Cartesian position affects the knee and back position.

**Forces and Moments:** In the simulation, the contact surface between the manikin foot and the ground is approximated by several contact points distributed under the foot. However the force plate only measures the global contact wrench. Therefore all the contact forces from the simulation (*i.e.* computed in the LQP controller) are gathered to form the global equivalent contact wrench. All six components of this contact wrench resulting on one hand from the simulation and on the other hand from the force plate measurement are compared. It should be noted that, though the value of the foot/ground friction coefficient in the simulation is only an approximation of the real value, it has no consequences on the force values. Indeed, the ratio between the tangential and normal forces is always far smaller (max 0.06) than the sliding limit (between 0.6 and 0.9 given the materials considered).

The linear correlation between the experimental and simulated data is calculated in order to quantify their similitude. The Pearson's correlation coefficients are summarized, for each subject, in Table 4.2 [Saporta 2011]. A good correlation is observed for each component of the contact wrench, since the correlation coefficient is always bigger than 0.70 (0.90 for four of the components). Among the force components, $F_Y$ (direction of drilling) shows a far better correlation than $F_X$ and $F_Z$, because the amplitude of its variations is much bigger (see Fig. 4.4 for typical ranges of variation of the forces and moments in the drilling task). Besides, except for the vertical force $F_z$, there is no significant differences between the subjects: the morphology (at least the height) does not seem to influence the quality of the results. The disparity of the $F_z$ results is probably caused by a lower precision of the force plate in this direction, because of the higher load. Indeed for each axis of the force plate, the measurement precision is about $\pm 0.1\,\%$ of the applied load. The ratio between the average measurement precision (computed from the average loading) and the range of variation of the force/moment is smaller than $10^{-3}$ for $F_X$, $F_Y$, $M_X$, $M_Y$ and $M_Z$, whereas is it around 0.15 for $F_Z$.

|  | Force | | | Moment | | |
|---|---|---|---|---|---|---|
|  | **F$_X$** | **F$_Y$** | **F$_Z$** | **M$_X$** | **M$_Y$** | **M$_Z$** |
| Subject No.1 | 0.82 | 0.98 | 0.70 | 0.78 | 0.98 | 0.96 |
| Subject No.2 | 0.82 | 0.98 | 0.62 | 0.95 | 0.98 | 0.95 |
| Subject No.3 | 0.62 | 0.98 | 0.57 | 0.96 | 0.98 | 0.96 |
| Subject No.4 | 0.78 | 0.98 | 0.91 | 0.96 | 0.98 | 0.98 |
| Subject No.5 | 0.77 | 0.98 | 0.82 | 0.96 | 0.98 | 0.97 |
| Average | **0.76** | **0.98** | **0.72** | **0.92** | **0.98** | **0.97** |
| SD | 0.07 | 0 | 0.13 | 0.07 | 0 | 0.01 |

Table 4.2: Pearson's correlation coefficient between the ground contact forces computed by the manikin controller and those measured experimentally. F stands for the force, and M for the moment. The X, Y and Z directions are defined in Fig. 4.1. For each subject, the value displayed is the average value of the ten trials.

Table 4.3 displays the root mean square (RMS) error for all six components of the contact wrench. These errors are not insignificant since they represent about 5 to 10 % of the maximal amplitude of variation (expect for $F_Z$ where the error is much bigger, for the reason explained above). However, these errors are partly due to a small temporal offset between the simulated and experimental data, which leads to significant differences in the force values during fast force changes (Fig. 4.5). Indeed, as depicted in Fig. 4.4, no significant permanent force or moment offset (*i.e.* vertical offset on the graphs) that could entirely explain the computed RMS errors is observed.

|  | **Force (N)** | | | **Moment (N.m)** | | |
|---|---|---|---|---|---|---|
|  | **$F_X$** | **$F_Y$** | **$F_Z$** | **$M_X$** | **$M_Y$** | **$M_Z$** |
| Subject No.1 | 3.1 | 5.3 | 4.7 | 6.0 | 6.5 | 1.2 |
| Subject No.2 | 3.6 | 4.2 | 6.1 | 6.8 | 6.7 | 1.4 |
| Subject No.3 | 3.0 | 2.6 | 5.1 | 5.8 | 6.2 | 1.6 |
| Subject No.4 | 2.3 | 3.1 | 3.3 | 4.8 | 3.9 | 0.9 |
| Subject No.5 | 2.7 | 3.9 | 3.2 | 5.9 | 4.4 | 1.7 |
| Average | **2.8** | **3.8** | **4.5** | **6.9** | **5.9** | **1.4** |
| SD | 0.4 | 0.9 | 1.1 | 0.6 | 1.2 | 0.3 |

Table 4.3: Root mean square error between the ground contact forces computed by the manikin controller and those measured experimentally. Typical ranges of variations of all six components of the ground contact wrench are given in Fig. 4.4. F stands for the force, and M for the moment. The X, Y and Z directions are defined in Fig. 4.1. For each subject, the value displayed is the average value of the ten trials.

**Center of pressure:** The center of pressure (CoP) is directly computed from the ground contact wrench (the CoP considered here corresponds to the contact forces of both feet together). Therefore, given the forces and moments consistent results, the CoP simulated position is expected to be quite consistent with the experimental one. Nevertheless, the CoP position error is computed because it gives an overview of the consistency of the virtual manikin model.

The average distance between the experimental and simulated CoP position is 1.1 cm (SD 0.6 cm, maximum 3.6 cm). The CoP position error is therefore smaller than 2.3 cm 95 % of the time, including dynamic phases. As a comparison, the amplitude of variation of the CoP position during the whole activity is about 15 cm in both X and Y directions. Table 4.4 summarizes the X and Y position errors between the experimental and the simulated CoP. There is not much difference between the X and Y directions, except that the maximal error - reached during fast force or postural changes - is always bigger in the drilling (Y) direction. As for the forces and moments, the maximal CoP error is reached during fast force or postural changes.

(a) Force $F_X$

(b) Force $F_Y$

(c) Force $F_Z$

(d) Moment $M_Z$

(e) Moment $M_X$

(f) Moment $M_Y$
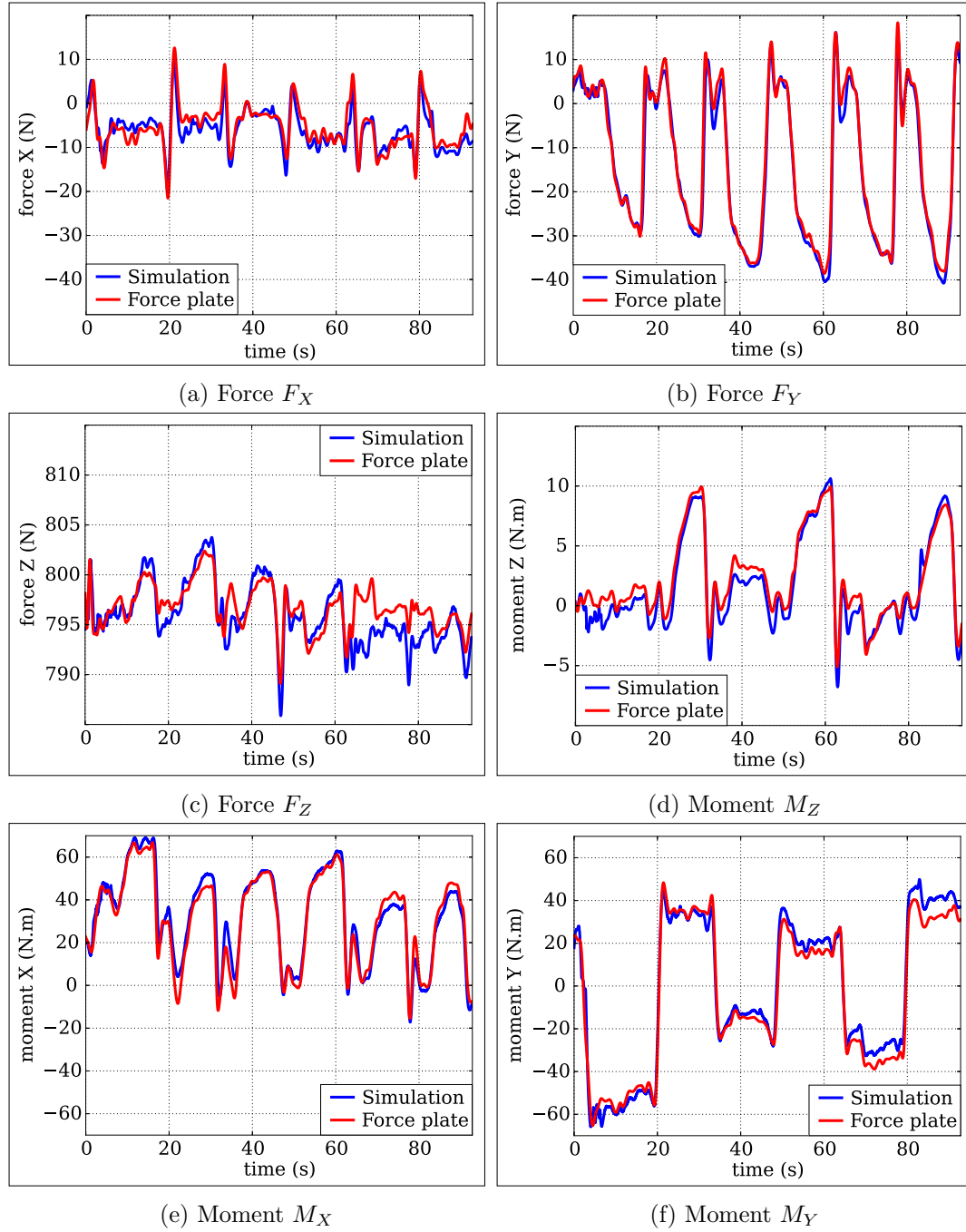
Figure 4.4: Time evolution of experimental and simulated components of the ground contact wrench, for one trial of subject No.5. The moments are expressed at the center of both feet. The subject and trial are chosen so that the errors (force, moment and CoP) are representative of their average values.
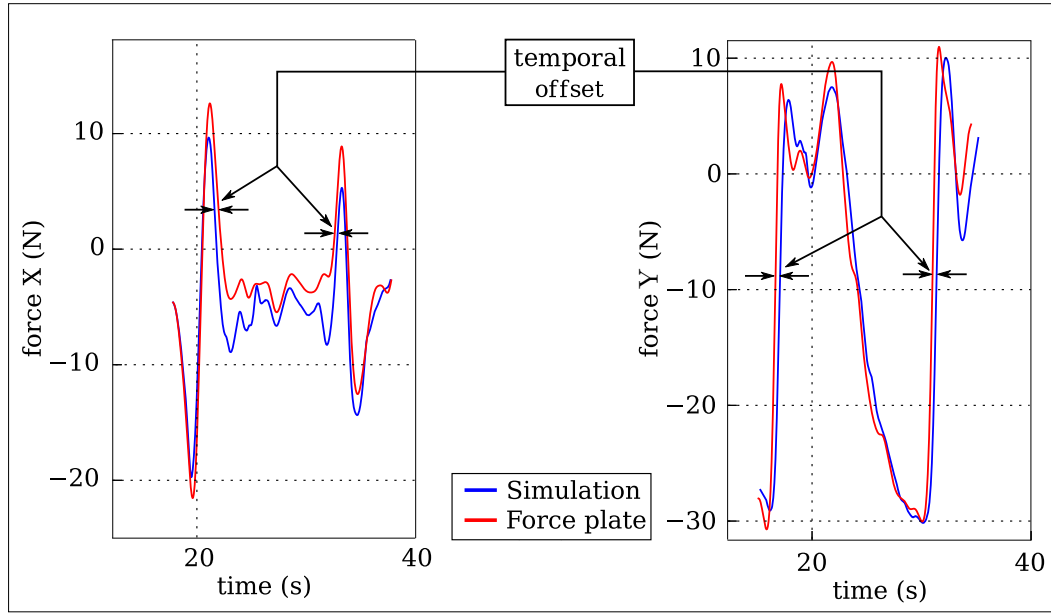
Figure 4.5: Zoom on the time evolution of experimental and simulated components $F_X$ (left) and $F_Y$ (right) of the ground contact wrench, for one trial of subject No.5. A temporal offset between the experimental and simulated graphs is observed during fast force changes. This offset leads to a significant error between the experimental and simulated force values during fast force changes.

| | Error CoP X (cm) | | | Error CoP Y (cm) | | |
|---|---|---|---|---|---|---|
| | average | SD | max | average | SD | max |
| Subject No.1 | 0.9 | 0.6 | 2.7 | 1.2 | 0.9 | 3.8 |
| Subject No.2 | 0.9 | 0.5 | 3.1 | 0.7 | 0.5 | 3.7 |
| Subject No.3 | 0.7 | 0.4 | 2.1 | 0.5 | 0.4 | 2.5 |
| Subject No.4 | 0.6 | 0.4 | 2.5 | 0.7 | 0.4 | 2.7 |
| Subject No.5 | 0.5 | 0.5 | 2.7 | 0.6 | 0.5 | 3.1 |
| Average | **0.7** | **0.5** | **2.6** | **0.7** | **0.5** | **3.2** |

Table 4.4: Position error between the experimental CoP and the simulated CoP. The X and Y directions are defined in Fig. 4.1. For each subject, the value displayed is the average value of the ten trials.

During the quasi-static drilling phases, the maximal position error is smaller: about 1 cm. However, its value on the Y direction increases when the subject drills the lowest holes (see Fig. 4.6, the lowest holes are No. 5 and 6 in Fig. 4.1). To reach theses holes with a correct orientation of the drill, the subject tends to bend his upper-body and moves his pelvis backwards, as in Fig. 4.3 left. This motion, especially the one of the pelvis, is not completely achieved in the simulation, because of the balance task which affects the markers tracking tasks.

(a) X CoP position

(b) Y CoP position
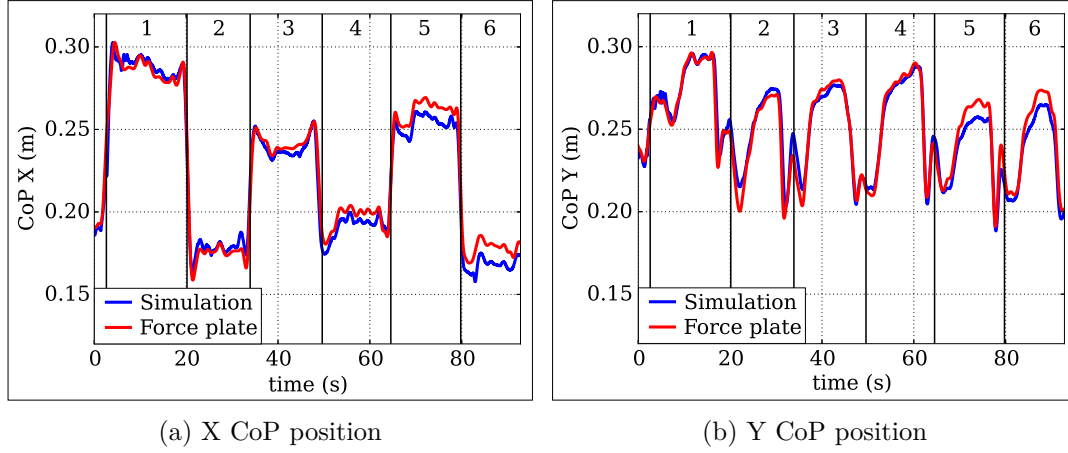
Figure 4.6: Time evolution of the experimental and simulated position of the CoP, for one trial of subject No.5. The subject and trial are chosen so that the errors (force, moment and CoP) are representative of their average values. The numbers at the top of the graph refers to the holes numbers, defined in Fig. 4.1.

### 4.1.3 Discussion

In the light of the results presented above, the consistency of the motion-related and force-related biomechanical quantities measured on the manikin are discussed hereafter.

**Motion consistency:** The manikin motion, generated with the LQP controller from motion capture data, is overall very similar to the original motion of the human subject. The similarity between the experimental and replayed motions is evaluated through Cartesian position errors. Nevertheless, given the high number of markers that are positioned all over the human body, the Cartesian motions of the markers strongly constrain the joint motions. In other words, there is not much redundancy left in the kinematic structure of the manikin body, given all the tasks that are included in the controller. Therefore, the similarity between the human and manikin motions is also valid at the joint level. The joint positions measured on the manikin animated through full-body motion capture are good approximations of the reality. Since the position errors remain quite small even during dynamic motions, the joint velocities and accelerations are also likely to be quite similar to those of the human subjects. Nevertheless, all these quantities remain approximations of the reality, since the manikin kinematics is a simplified version of the human kinematics. Therefore, the virtual manikin simulation does not enable very fine comparison: the small differences between two situations may as well come from inaccuracies due to the model or the controller - which does not ensure that the tasks are entirely fulfilled - as from real ergonomic differences.

However, the reliability of the replay is limited to motions in which the balance is not strongly solicited. Indeed, the open-loop control of the manikin balance

through the markers tracking tasks is not sufficient to maintain balance, because of the imprecisions in the markers positions and human model. Therefore, a balance task is added in the manikin controller, in order to perform close-loop control of the balance. Due to the lack of decision skills of the manikin regarding how to recover balance, the ZMP preview control scheme in the balance task is tuned to be quite conservative. Most unstable situations are thus avoided, as long as the original motion itself is not too unstable. However, the balance improvement is achieved only at the cost of a modified motion, hence of a less accurate replay. As observed in the results, the balance task interferes with the tracking of some markers, resulting in a less accurate tracking of some markers positions. This interference is all the more important that the original motion is unstable.

It should be noted that all the afore-mentioned conclusions only address the realism of replayed motions (*i.e.* based on motion capture data). However, the case of automatically generated trajectories is important, since the purpose of the tool developed in this work is to enable fully digital evaluation of co-manipulation activities. Therefore no motion capture data can be used to animate the manikin. Though not assessed in this work, the realism of automatically generated motions is discussed in section 4.4.2.

**Force consistency:** The ground contact forces and moments, and the CoP position, resulting from the simulation are close to those measured experimentally. It should be noted that, besides the error due to inaccuracies in the model and/or motion, a part of the difference between the experimental and simulated data comes from inaccuracies in the simulated drilling force. The error in the value of the drilling force used in the simulation is caused by inaccuracies in the estimation of the sensor position and orientation (the forces measurement accuracy being very high). Indeed, the drilling force is measured with a force sensor that is not fixed during the task. The 6D pose of the sensor frame is estimated from the positions of the CodaMotion markers on the drill. The markers positions are therefore subjected to measurement inaccuracy of the CodaMotion system. Given that the markers are placed quite close from one another, a small position error may lead to a significant error on the orientation of the force sensor (the markers are necessarily positioned on the drill handle: if placed on the drill body, the vibrations of the drill cause high measurement error). Moreover, there is no calibration of the markers positions relative to the force sensor origin. The offsets between the sensor origin and the drill markers are only measured, and are therefore subjected to inaccuracies. Due to the error in the force sensor position and mostly orientation, the distribution of the drilling force along the X, Y and Z axes in the simulation is not exactly similar to the real distribution. This error in the drilling force necessarily affects the simulated ground contact forces, through the equation of equation 3.1 (dynamic forces equilibrium). However, despite this non-negligible source of error, the simulated contact wrench is still very similar to the experimental one.

Thanks to this experiment, the consistency of the manikin joint torques can be estimated - though not accurately. The joint torques result from the dynamic motion equation 3.1, so they are affected by the external forces, the kinematic and dynamic properties of the manikin model (coefficients of the $M$ matrix and the $\mathbf{C}$ and $\mathbf{g}$ vectors), and the joint motions. The length and mass distributions of the manikin model coming from standard values, the coefficients of $M$, $\mathbf{C}$ and $\mathbf{g}$ can be assumed quite consistent. Then, according to the motion-related results, the replayed joint motion (position, velocity and acceleration) is quite similar to the original one. Finally, the simulated external forces are mostly consistent with the experimental ones. Therefore, the manikin joint torques computed with the LQP controller are likely to be consistent with the human joint torques.

It should however be noted that, even if the manikin joint torques were exactly equal to the human joint torques, they do not fully represent the physical effort exerted by the worker. Indeed, due to the redundancy of the human muscle actuation, different combinations of muscle forces can result in a same joint torque. But they do not correspond to the same physical effort. This issue is discussed in section 4.4.1.

## 4.2   Validation of the ergonomic indicators

A second step towards the validation of the evaluation tool proposed in this work is to ensure the consistency of the ergonomic indicators measured on the virtual manikin. The validity of the joint biomechanical quantities measured on the dynamically animated manikin has been partly addressed in the previous section. However, this is not sufficient to guarantee that the proposed ergonomic indicators correctly account for the exposure level to MSDs risks. Both the indicators mathematical formulae, and the fact that the quantities on which they are based are already a high level representation of real biomechanical solicitations (deformation of muscles, tendons...) may affect the ergonomic relevance of the indicators. An experimental validation is therefore carried out on some of the indicators defined in chapter 3, in order to ensure that they correctly account for the relative exposure level to MSDs risks. The proposed indicators are only defined for relative evaluation of the risk, *i.e.* for identifying, between two situations, which one is more dangerous. They do not aim at quantifying the absolute level of risk. Therefore, the proposed validation focuses on the variations of the ergonomic indicators, rather than on their values.

The reliability of the indicators is assessed based both on general ergonomic considerations, and on the feeling of human subjects. To this purpose, a manual task is performed by human subjects in different conditions, and the ergonomic indicators are computed for each situation. The variations of the indicators values are investigated to highlight their dependence on the task conditions. Firstly the indicators must not remain constant, otherwise they are useless regarding the ergonomic comparison of different situations. Secondly, for very typical situations in

which the worst ergonomic case can easily be identified, their variation must be in accordance with general ergonomic guidelines. Therefore some situations considered in this experiment are voluntarily extreme. For a finest evaluation of the indicators ability to discriminate different situations, the correlation of the indicators values with the strenuousness perceived by human subjects performing a task in different conditions is studied.

## 4.2.1 Experimental protocol

The proposed validation requires the computation of several ergonomic indicators in different situations. In order to measure the indicators values, the considered activity must be simulated with the virtual manikin. Since the purpose here is not to assess the realism of automatically generated motion, full-body motion capture data are used to animate the manikin. Thus the manikin motion is guaranteed to be very similar to the human subject's motion. Several human subjects therefore perform a manual activity under various time, load and geometric constraints, while their motions and interaction forces with the work surface are recorded. Each situation is then dynamically replayed with the virtual manikin, in order to compute the corresponding ergonomic indicators.

### 4.2.1.1 Task description

A generic manual task associating trajectory tracking and force exertion is performed. The subjects move a portable tool along a displayed path while pushing on the work surface with the tool. Performing the task means following the entire path once.

The tool is a 200 g and 15 cm long handle held with a power grasp of the right hand. The path is a 50 cm side square. Two sides are replaced respectively with a sinusoidal line and a sawtooth line, to accentuate the dynamics of the motion (see Fig. 4.7 and 4.9). The path dimension is chosen such that the task requires a wide range of joint motions yet remains feasible by a seated subject. Indeed, in the previous experiment (ground contact forces comparison), it is observed that when the balance of the subject is close to unstable, the replay of the motion lacks accuracy (because of the conservative balance task in the controller). The purpose of this experiment is to explore different situations, regarding, among other aspects, the posture. Therefore some situations correspond to extreme postures associated with unstable balance. In order to overcome the balance problem and still accurately replay the motion, the subjects are seated. The subjects are instructed to keep their whole buttocks in contact with the seat, and to use neither their left arm nor their legs during the task execution.

### 4.2.1.2 Parameters

Four parameters vary throughout the experiment:

- the orientation of the work surface (horizontal or vertical, Fig 4.7);

- the position of the seat relative to the work area (height, distance and orientation);

- the allotted time;

- the magnitude of the force to be applied.

The various positions of the worker's seat are described in Fig. 4.7 and table 4.5. The *close* and *medium* values are chosen to match ergonomic guidelines for seated work [Chaffin 2006]. All combinations are tested except *horizontal - close - high* because the legs do not fit under or in front of the table, and *45° right* is only done for *close - medium* for reachability reasons.
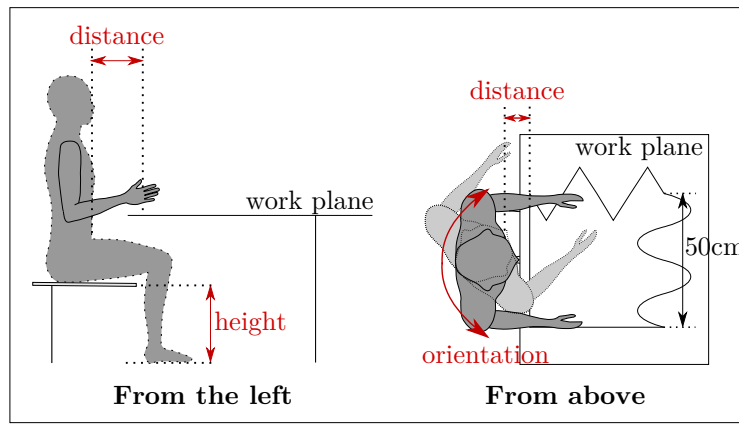


(a) Horizontal work plane
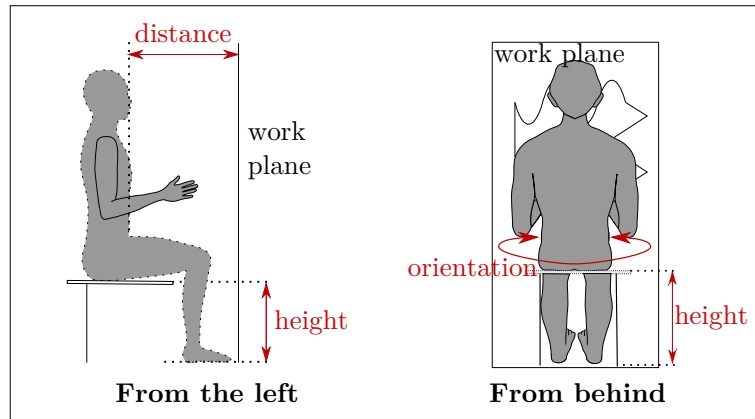


(b) Vertical work plane

Figure 4.7: Definition of the parameters describing the position of the worker's seat for both horizontal and vertical work planes. The seat position is defined with three parameters: the horizontal *distance* between the center of the seat and the closest border of the path, the *height* of the seat (which affects the vertical distance between the seat and the path), and the *orientation*, in the horizontal plane, of the worker on the seat.

| **Distance** | **Height** | **Orientation** |
|---|---|---|
| (H) close: 20 cm <br> (V) close: 45 cm | low: 38 cm | 45° right |
| (H) far: 45 cm <br> (V) far: 75 cm | medium: 52 cm | 45° left |
| | high: 66 cm | 0° (face on) |

Table 4.5: Values of the parameters describing the position of the seat (defined in Fig. 4.7). H stands for horizontal and V for vertical: they refer to the orientation of the work plane.

The allotted time and the magnitude of the force define three varieties of the original task, described in table 4.6 as *neutral*, *force* and *velocity* tasks. The force magnitude in the *force* task is slightly lower that the average maximal force capacity, calculated for this particular gesture according to [AFNOR 2008a]. The subject is provided with an audio feedback of the exerted force: low-pitched, high-pitched or no sound when the force is respectively too weak, too strong or within the imposed range. The allotted time is displayed through a progress bar on a screen, and the subjects are instructed to move the tool as regularly as possible along the path.

All three tasks - *neutral*, *force* and *velocity* - are performed in random order for both orientations of the work plane and for each seat position. Breaks are regularly allowed to prevent fatigue.

| **Task kind** | **Allotted time** | **Mean hand velocity** | **Force magnitude** |
|---|---|---|---|
| *neutral* | 30 s | $0.085\,\mathrm{m.s^{-1}}$ | none |
| *velocity* | 5 s | $0.5\,\mathrm{m.s^{-1}}$ | none |
| *force* | 30 s | $0.085\,\mathrm{m.s^{-1}}$ | $18\,\mathrm{N} \pm 2\,\mathrm{N}$ |

Table 4.6: Values of the time and force constraints for the *neutral*, *force* and *velocity* tasks.

### 4.2.1.3 Subjects and instrumentation

Seven healthy subjects (four males and two females) ranging from 23 to 28 years old perform the experiment for the horizontal work plane, and three of them also for the vertical work plane. Table 4.7 describes their physical features.

The subjects' motions are recorded with the CodaMotion system (see section 3.2.3 for details). The subjects are equipped with 16 markers on their torso, right arm and right hand. The motions of the left arm and the legs are not recorded since they are not used to perform the task and do not move. The contact forces with the work surface are measured through a 6 axes ATI force sensor[2] embedded in the

---

[2] http://www.ati-ia.com/products/ft/ft_models.aspx?id=Nano43

CodaMotion camera    Display of remaining allotted time    CodaMotion markers    Headphone for auditive force feedback
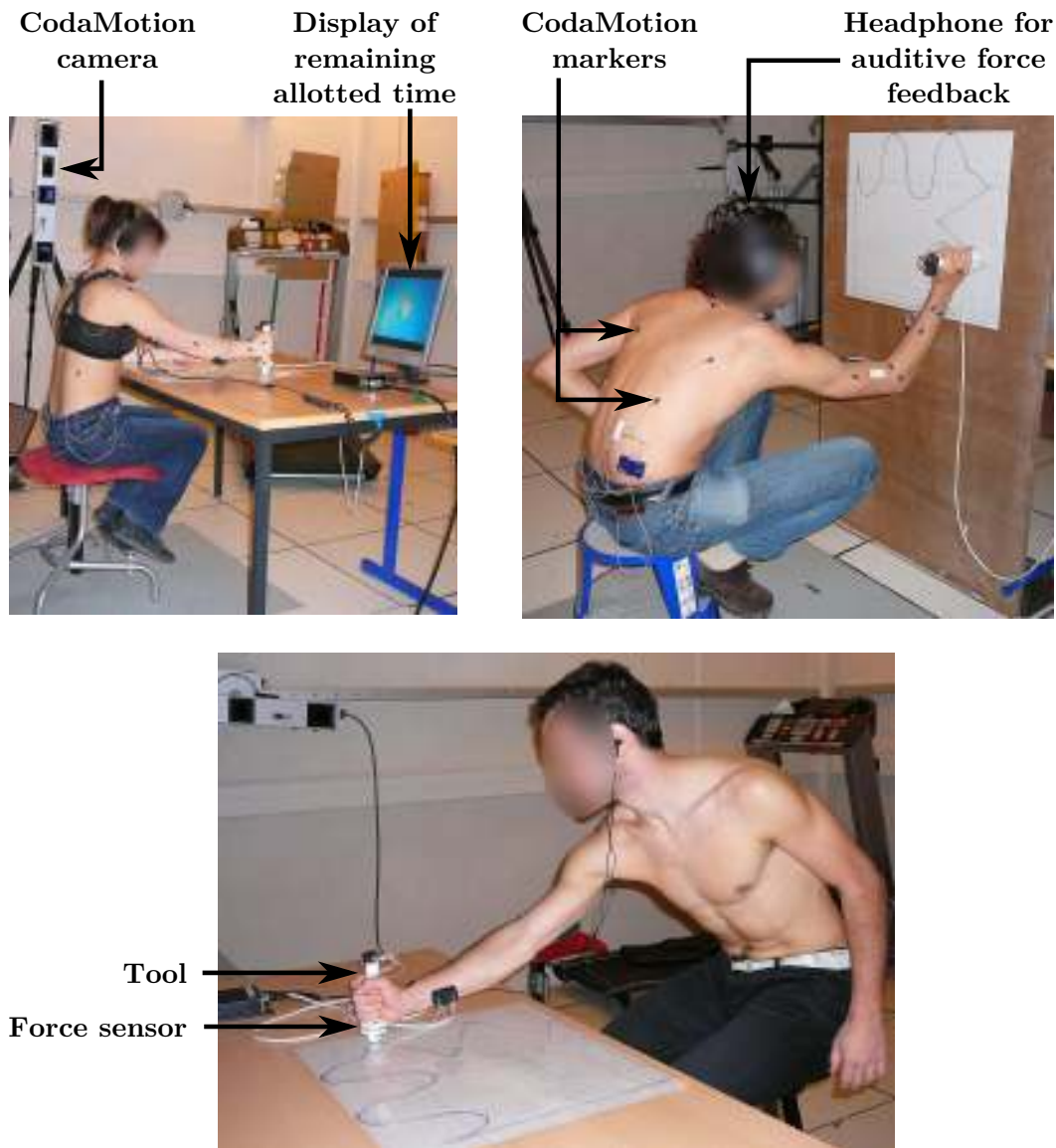
Tool

Force sensor

Figure 4.8: Motion and force capture instrumentation for the path tracking activity.

tool. The tool is equipped with 3 CodaMotion markers, so that the 6D pose of the force sensor is known. The instrumentation used to record the forces and motions is displayed in Fig. 4.8

After each performance, the subjects are asked to give the task a mark between 0 and 10, depending on how hard (physically) the task is perceived. 0 means that the task is very easy, whereas 10 means that the task is physically very demanding. This number between 0 and 10 is used to represent the strenuousness perceived by the subject.

| | Height (m) | | | |
|---|---|---|---|---|
| | Min | Max | Mean | SD |
| Horizontal plane | 1.53 | 1.83 | 1.71 | 0.11 |
| Vertical plane | 1.53 | 1.79 | 1.63 | 0.12 |

| | BMI (kg.m$^{-2}$) | | | |
|---|---|---|---|---|
| | Min | Max | Mean | SD |
| Horizontal plane | 20.9 | 33.3 | 24.5 | 3.9 |
| Vertical plane | 21.8 | 33.3 | 25.6 | 5.4 |

Table 4.7: Physical features of the human subjects: height and body mass index (bmi).

#### 4.2.1.4 Dynamic motion replay

The motions recorded on the human subjects are dynamically replayed with the XDE manikin and the LQP controller, according to the method detailed in section 3.2.3 (Fig. 4.9). The following tasks are included in the controller, in decreasing order of importance: markers tracking tasks (task weight depends on the marker), right hand force task, postural task, and joint torques minimization task. The right hand force task corresponds to the interaction force via the portable tool: its reference value is provided by the measures from the embedded force sensor. Contrarily to the previous experiment, no balance task is used here. The subjects being seated, the base of support is wide enough so that the markers tasks are sufficient to maintain the manikin balance. The contact surface between the manikin and the seat is modeled by several contact points distributed under the manikin thighs. The associated contact forces are computed by the manikin controller, and are therefore not experimentally measured.



Figure 4.9: Left: A human subject performs the task while his motion and interaction forces are recorded. Right: The motion is replayed with the virtual manikin and the LQP controller.

### 4.2.2 Results

Among all the ergonomic indicators defined in section 3.1, this experiment focuses on three constraint related indicators: the joint position indicator, the joint torque indicator, and the joint power indicator.

In order to summarize the whole task situation with just one value, each indicator is represented by its time integral value on the whole task. No time normalization is performed so as to take into account the variation of the task duration (the *velocity* task being six times faster than the *neutral* and *force* tasks). Since the subjects only use their right arm and their back to perform the task, only these body parts are considered in the indicators. Besides, since the back and right arm are both used to perform a same task, their contributions are summed up in a single *upper-body* indicator. The general formula for the upper-body (back and right arm) indicator $I_X^{B-RA}$ is therefore

$$I_X^{B-RA} = \int_0^T \frac{1}{N_B + N_{RA}} \left( N_B \, I_X^B(t) + N_{RA} \, I_X^{RA}(t) \right) \, dt \qquad (4.1)$$

where $B$ and $RA$ stand respectively for *back* and *right arm*. $N_B$ and $N_{RA}$ are the numbers of joints in the back and in the right arm respectively, and $T$ is the overall duration of the task. $I_X$ can stand for

- $I_q$: joint position indicator eq. 3.4;

- $I_\tau$: joint torque indicator eq. 3.5 (including fatigue);

- $I_p$: joint power indicator eq. 3.9.

The ergonomic indicators are defined to estimate the biomechanical solicitations experienced by the worker. In order to check whether they are in accordance with the physical demand associated with the task, the linear correlation between the indicators values and the strenuousness perceived by the subjects is computed. The Pearson's correlation coefficients are summarized in table 4.8 [Saporta 2011]. The correlation coefficients are computed for each task (*neutral*, *force* and *velocity*) separately, and for several tasks (two or three) together. Considering several tasks together means that all the situations corresponding to the two (or three) tasks considered are taken into account for the calculation of the correlation coefficient.

Besides, the variations of the indicators depending on the task features are displayed in Fig. 4.10 to 4.14, and interpreted hereafter. For each indicator, the average values on all subjects are used for studying the indicator variations. Indeed the indicators are not meant to be subject specific. For the sake of clarity, and since only variations are of interest, the values in each figure are normalized by the minimum and maximum values of the addressed case.

#### 4.2.2.1 Position indicator

A good linear correlation (Pearson's coefficient $> 0.84$) is observed between the values of the position indicator $I_q^{B-RA}$ and the strenuousness perceived by the

| Indicator Task | Position $I_q^{B-RA}$ | Torque $I_\tau^{B-RA}$ | Power $I_p^{B-RA}$ |
|---|---|---|---|
| *Neutral* | **0.86** | **0.81** | **0.71** |
| *Force* | **0.89** | **0.84** | **0.86** |
| *Velocity* | **0.87** | **0.85** | **0.70** |
| *Neutral - Force* | **0.84** | **0.84** | **0.76** |
| *Neutral - Force - Velocity* | **0.54** | **0.59** | **0.75** |

Table 4.8: Pearson's correlation coefficient between the strenuousness perceived by the subjects and respectively the position indicator $I_q^{B-RA}$, the torque indicator $I_\tau^{B-RA}$, and the power indicator $I_p^{B-RA}$. The correlation coefficients are computed firstly for the three tasks separately, then for the *neutral* and *force* tasks together, and finally for all three tasks together. For each case, the value displayed is the average value of the correlation coefficient for all subjects.

subjects when considering tasks of the same duration (Fig. 4.8). That is, when the three tasks are considered separately, and when the *neutral* and *force* tasks are considered together. However the correlation is much weaker (Pearson coefficient's = 0.54) when the *velocity* task, which is 6 times shorter than the others, is added. This may suggest that the proposed position indicator is only relevant to compare tasks of similar duration.

**Comparison within a same task**

**Seat distance and orientation:** The position indicator $I_q^{B-RA}$ is higher (p = 0.003 for Student's t-test computed on all the seat positions and all the subjects) when the subject seats further away from the work area (Fig. 4.10), because he has to deviate much from the neutral ergonomic posture (standing upright, arms along the body, elbows flexed at 80°) to reach the path. What actually matters is the average distance from the whole path to the right hand, which handles the tool. This explains why the *left* orientation seems better than the *face* one, and why the *right* orientation, though associated with a *close* position, is roughly equivalent to the *far* cases.

**Seat height:** In *close* position, the best seat height according to the position indicator $I_q^{B-RA}$ is the *medium* one when the work plane is horizontal, and the *high* one when it is vertical. Though not necessarily in accordance with the strenuousness value (vertical work plane), these results are ergonomically consistent. In the horizontal case, the *medium* height is chosen in accordance with ergonomic guidelines. In the vertical case, the higher the seat height, the less the subject needs to raise his arm to follow the path, and working with the arm raised is discouraged by ergonomic guidelines.

**Work plane orientation:** For a same position of the seat, the values of the position indicator $I_q^{B-RA}$ are significantly higher (Student's t-test, p < 0.01) in the vertical case than in the horizontal one (Fig. 4.10). The center of the path is higher

in the vertical case, so it requires the subject to work with the arm raised. Besides the imposed tool orientation (axis normal to the work plane) and power grasp lead to unusual arm angles when the work plane is vertical (elbow upper than shoulder).
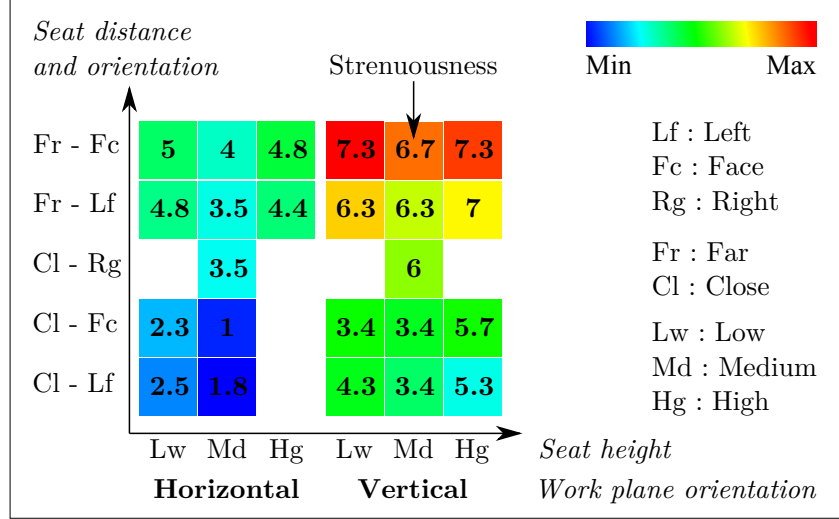


Figure 4.10: Variations of the upper-body position indicator $I_q^{B-RA}$ depending on the position of the subject's seat and the work plane orientation (*neutral* task). The value of the indicator is represented by a color on the hue scale: from blue (minimum) to red (maximum). The numbers in the squares correspond to the strenuousness perceived (between 0 and 10) by the subjects (average value on all the subjects). Only the *neutral* task is displayed, but the variations are similar for the other tasks.

**Comparison between different tasks**

As mentioned above, the position indicator $I_q^{B-RA}$ might not be suitable to compare tasks of different durations. Therefore, in order to compare the results of the *velocity* task with those of the *neutral* and *force* tasks, an *artificial velocity* task of the same duration as the *neutral* and *force* tasks is created. To create this *artificial velocity* task, for all the corresponding cases, the manikin replays the whole gesture not once but six times consecutively. Even after equalling the tasks durations, the *artificial velocity* task results in the smallest values of the position indicator $I_q^{B-RA}$ (Fig. 4.11). The allotted time for following the path once is so short that the path has to be smoothed, thus requiring less extreme joints angles. On the other hand the difference between the *neutral* and *force* tasks is not statistically significant. Despite the force exertion, the subjects do not modify their posture much, either because it is already strongly constrained by the imposed hand trajectory and seat position, or because the demanded external force is small enough not to require any change in the posture.
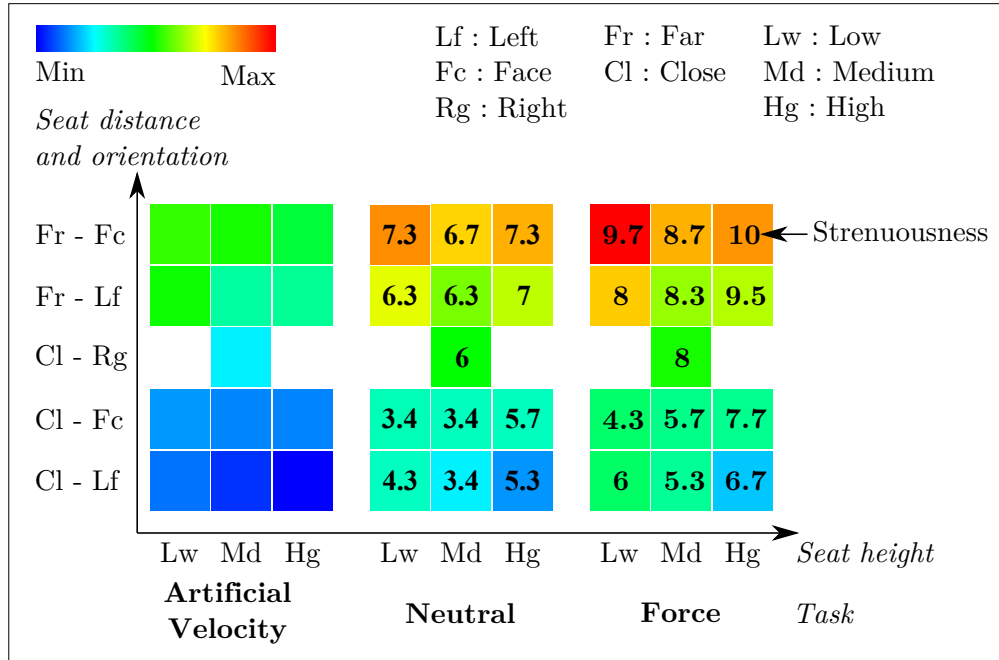
Figure 4.11: Variations of the upper-body position indicator $I_q^{B-RA}$ depending on the position of the subject's seat and the kind of task: *neutral*, *force* or *artificial velocity* task (vertical work plane). The value of the indicator is represented by a color on the hue scale: from blue (minimum) to red (maximum). The numbers in the squares correspond to the perceived strenuousness (average value on all the subjects). The strenuousness is not displayed for the *artificial velocity* task since this artificially created task (the manikin replays six times consecutively the original motion) has not been performed by human subjects, therefore its strenuousness has not been evaluated.

### 4.2.2.2 Torque indicator

Regarding the correlation with the strenuousness, the results for the torque indicator $I_\tau^{B-RA}$ are similar to those of the position indicator $I_q^{B-RA}$. The correlation is good (Pearson's coefficient $> 0.81$) when tasks of the same duration are considered, whereas it is much weaker (Pearson's coefficient $= 0.59$) when the shorter *velocity* task is added (Fig. 4.8). Therefore the torque indicator $I_\tau^{B-RA}$ might be suitable only to compare tasks of similar durations.

**Comparison within a same task**

The torque indicator $I_\tau^{B-RA}$ is highly affected by the position of the subjects relative to the work area, because of the effect of gravity on their body segments (Fig. 4.12). The further away the seat is from the work plane, the more the subjects must deviate from an upright position, needing higher joint torques to maintain the posture.
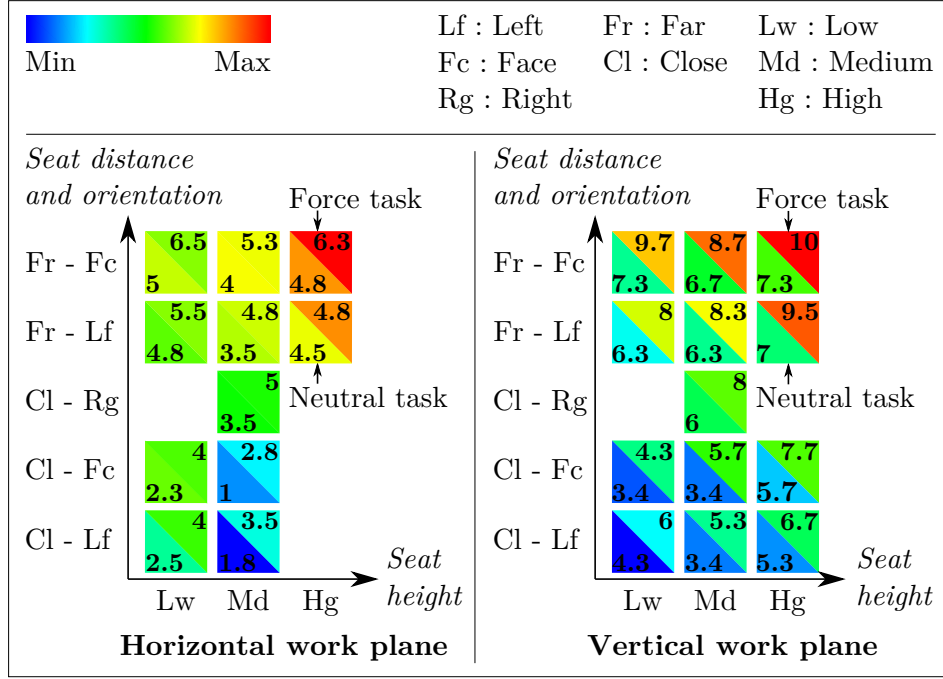
Figure 4.12: Variations of the upper-body torque indicator $I_\tau^{B-RA}$ depending on the external force and the seat position. Left: horizontal work plane. Right: vertical work plane. For each colored square, the right-up half corresponds to the *force* task whereas the left-bottom half corresponds to the *neutral* task. The value of the indicator is represented by a color on the hue scale: from blue (minimum) to red (maximum). The numbers in the squares correspond to the perceived strenuousness (average value on all the subjects).

**Comparison between different tasks**

**External force:** When the work plane is vertical the torque indicator $I_\tau^{B-RA}$ of the *force* task is significantly higher (Student's t-test, $p = 2.\,10^{-3}$) than the one of the *neutral* task, whereas they are not significantly different (Student's t-test, $p = 0.28$) in the horizontal case. Given the direction of the external force, the gravity torques and the external load torques are of opposite signs. So the absolute value of the joint torques does not increase much (and can even decrease) with the force exertion: pushing on the work plane helps maintaining balance. This phenomenon is more noticeable when the work plane is horizontal since the direction of gravity is directly opposed to the one of the external force.

**Speed of motion:** As mentioned above, the torque indicator $I_\tau^{B-RA}$ might not be suitable to compare tasks of different durations. Therefore, similarly to the position indicator $I_q^{B-RA}$, the *artificial velocity* task (the manikin replays the motion six times consecutively) is considered here instead of the raw *velocity* task (six times shorter than the *force* and *neutral* tasks). The torque indicator $I_\tau^{B-RA}$ of the *artificial velocity* task is significantly higher (Student's t-test, $p = 0.019$) than the one of the *neutral* task, because the faster dynamics of the movement induces

higher joint torques (Fig. 4.13). However, the increase in the joint torques of the *artificial velocity* task due to the faster dynamics is not as important as the one due to the external load in the *force* task.
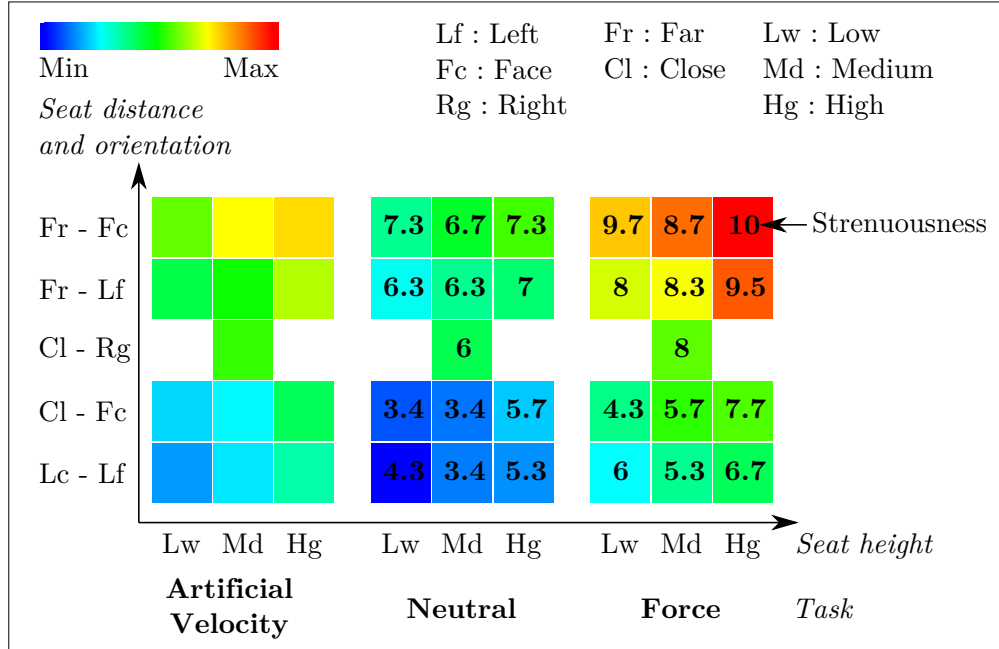


Figure 4.13: Variations of the upper-body torque indicator $I_\tau^{B-RA}$ depending on the seat position for all three tasks *velocity*, *neutral* and *force* (vertical work plane). The value of the indicator is represented by a color on the hue scale: from blue (minimum) to red (maximum). The numbers in the squares correspond to the perceived strenuousness (average value on all the subjects). The strenuousness is not displayed for the *artificial velocity* task since this artificially created task (the manikin replays six times consecutively the original motion) has not been performed by human subjects, therefore its strenuousness has not been evaluated.

#### 4.2.2.3 Power indicator

Contrarily to the position and torque indicators, the correlation between the power indicator $I_p^{B-RA}$ and the strenuousness is fairly good when all three tasks are considered together (Pearson's coefficient = 0.75). It does not improve when each task is considered separately (Fig. 4.8). This suggests that the power indicator $I_p^{B-RA}$ might be suitable to compare tasks of different duration, as well as tasks of the same duration.

#### Comparison between different tasks

**Speed of motion:** Though the *velocity* task lasts much less than the two others, the values of the power indicator $I_p^{B-RA}$ in the *velocity* task are only slightly lower (see Fig. 4.14 where the original *velocity* task is used). The motion being much

faster, the total energy spent (which corresponds to the time-integral of the power indicator, *i.e.* $I_p^{B-RA}$ considered in this experiment) is about the same.

**External force:** Contrarily to the torque indicator $I_\tau^{B-RA}$ (Fig. 4.12 left), the power indicator $I_p^{B-RA}$ of the *force* task is often lower than the one of the *neutral* task, especially when the seat is far. The fact that the torque and power indicators do not have similar variations is not surprising, since they have different biomechanical meanings (*e.g.* the power indicator is zero in static tasks, whereas the torque indicator is not). However, this difference could also be enhanced by the fact that the allotted time is not strictly respected. The subjects tend to move slightly more slowly in the *force* task to better control the force magnitude. This phenomenon is especially noticeable when the posture of the subject makes the exerted force hard to control, *e.g.* when the balance is unstable, or when the arm is outstretched.
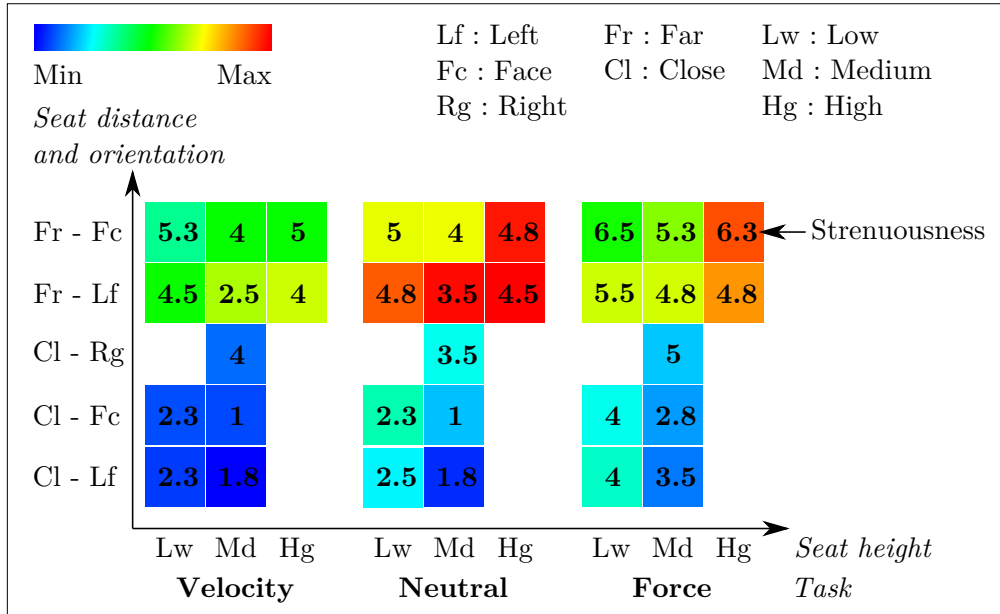


Figure 4.14: Variations of the upper-body power indicator $I_p^{B-RA}$ depending on the seat position for all three tasks *velocity*, *neutral* and *force* (horizontal work plane only). The value of the indicator is represented by a color on the hue scale: from blue (minimum) to red (maximum). The numbers in the squares correspond to the perceived strenuousness (average value on all the subjects).

### 4.2.3 Discussion

According to the previous results, the position indicator $I_q^{B-RA}$, the torque indicator $I_\tau^{B-RA}$ and the power indicator $I_p^{B-RA}$ measured with the dynamically animated manikin seem to account quite correctly for the way a task is performed. Their main variations are ergonomically, or at least physically, consistent, and the few unexpected results seem to come from ill-adapted choices in the task definition

(external force magnitude and direction, display of the time constraint) rather than from the indicators themselves.

However, all the indicators are not equivalent depending on the task features (*i.e.* on what is compared). According to the correlation with the strenuousness, the proposed position and torque indicators do not seem suitable to compare tasks of different durations. On the contrary, this remark does not apply to the power indicator. On the other hand, when considering tasks of the same duration, the position and the torque indicators generally account more accurately for the strenuousness perceived by the worker than the power indicator. The duration factor being taken into account through the time integral value of the indicator (for all indicators), it is aggregated with another factor of risk (posture, effort...). In the position and torque indicators, the duration factor represents the time spent in different "danger zones" (the danger coefficient being equal to the normalized position or torque). However, the relation between the time spent in a zone and the risk is very likely not linear: spending 10 s at half the maximal joint capacity (position or torque) is probably not equivalent to spending 20 s at a quarter of the maximal joint capacity. On the contrary, the duration factor in the power indicator is much more physically meaningful. Indeed, the time-integrated power indicator represent the overall energy spent while performing the task. Nevertheless, the correlation with the strenuousness cannot be the only criterion to judge the relevance of an indicator. Indeed, the strenuousness summarizes different kinds of solicitations (posture, static effort, dynamic effort...) in one value and is therefore an "aggregated" indicator. Whereas the ergonomic indicators proposed in this work consider different kinds of solicitations - except the duration - separately. However, in the absence of further validation, it seems wiser to use the proposed ergonomic indicators only to compare tasks of similar durations. This restriction is not very limiting regarding the purpose of this work. Indeed, this work focuses on strength amplification collaborative robots, which are not supposed to significantly modify the work rate. Therefore, the compared situations are supposed to have quite similar durations.

The duration factor issue aside, all indicators are still not equivalent regarding the information they provide. When addressing the position of the seat, the variations of the position and the torque indicators are mainly similar (the closer, the better), so one could be tempted to keep only one of them for their study. However these indicators are not redundant and sometimes bring antagonistic conclusions: for the best seat distance (*close - left*), the best seat height is the *high* one according to the position indicator whereas it is the *low* one according to the effort indicator (Fig. 4.10 and 4.12 right). More generally, the design of a workstation - or a collaborative robot - usually results from trade-offs. So this work does not mix several kinds of solicitations within a sole indicator, because considering antagonistic effects within a same task is easier if they are represented by different indicators. Nevertheless, multiple ergonomic indicators make the interpretation of the results harder for the user, especially when several indicators lead to antagonistic conclusions. To overcome, or at least simplify, this problem, the relevance of each indicator regarding the task of interest needs to be evaluated. This problem

is addressed in chapter 5.

Finally, it should be noted that the indicators proposed in this work leave out some important phenomena related to MSD. In particular, the co-contraction of antagonistic muscles, which occurs especially in tasks requiring high accuracy (in terms of position or force), is not modeled. This omission, due to the single actuator per joint representation of the human body, leads to an underestimation of the effort solicitation. Consequences of this omission can be observed in the linear relation between the strenuousness and the torque indicator: the y-intercept is bigger in the *force* task (2.8) than in the *neutral* task (1.8). The increase in the joint torques during the *force* task is underestimated in the simulation because it only takes into account the external load (the manikin is not preoccupied with accuracy). Whereas the human subjects must accurately control the force they apply on the work plane, which requires an additional effort due to co-contraction. The co-contraction issue is further discussed in section 4.4.1.

## 4.3   Validation of the manikin-robot simulation

The evaluation framework presented in this work aims at performing ergonomic comparisons of different robots for co-manipulation activities, without the need for the real robots. The relevance of the proposed ergonomic indicators measured with the virtual manikin has been partly validated for manual activities without any collaborative robot. The present section aims at demonstrating the reliability and usefulness of the ergonomic indicators measured through a manikin-robot simulation, regarding the evaluation of the ergonomic benefit provided by a cobot. To this purpose, a co-manipulation activity is simulated, with different designs of a collaborative robot: kinematic, dynamic, and control-related parameters of the robot are varied. The values of the ergonomic indicators are compared for each situation, in order to ensure their physical consistency, and to check whether they enable to distinguish the different designs from an ergonomic point of view.

In this experiment, the motions of the manikin are generated fully automatically, *i.e.* they are not based on motion capture data. Indeed, there is no physical mock-up of the robot for each design which is tested. Therefore motion capture data are not reliable, since a human subject cannot perform the activity with the robot design that is evaluated. Besides, the proposed framework is intended for ergonomic evaluations without the need for a human subject. That means no motion capture based animation, and therefore a fully autonomous manikin. By using a fully autonomous manikin, the present experiment also aims at - qualitatively - assessing the reliability of such a simulation.

### 4.3.1   Simulation set-up

The purpose of this experiment is not to evaluate a specific activity but to demonstrate the usefulness and consistency of ergonomic measurements through a manikin-cobot simulation. A simple case-study (activity as well as robot parameters) is

therefore considered, so that the interpretation of the results is quite straightforward. Otherwise, the consistency of the results can hardly be assessed.

A manual task including upper-body motions and force exertion is simulated with the autonomous manikin, either with or without the assistance of a strength amplification collaborative robot. Three parameters of different nature are varied: the kinematic structure of the robot (kinematic parameter), its mass (dynamic parameter), and the strength amplification coefficient (control parameter). The five constraint oriented ergonomic indicators defined in section 3.1.2 - joint position, torque, velocity, acceleration and power - are computed for each situation.

#### 4.3.1.1 Collaborative robot

The collaborative robot studied in this example is the strength amplification robot *Cobot 7A.15* (Fig. 1.6). This robot has been designed for manual tasks which require the application of significant efforts via a portable tool, *e.g.* machining jobs. Two structures (A and B) were considered during the design of this robot (see Fig. 4.15) and both are simulated. Both are 6 revolute joints serial chains, but the joint distribution is slightly different between robots A and B.



(a) Robot A                              (b) Robot B
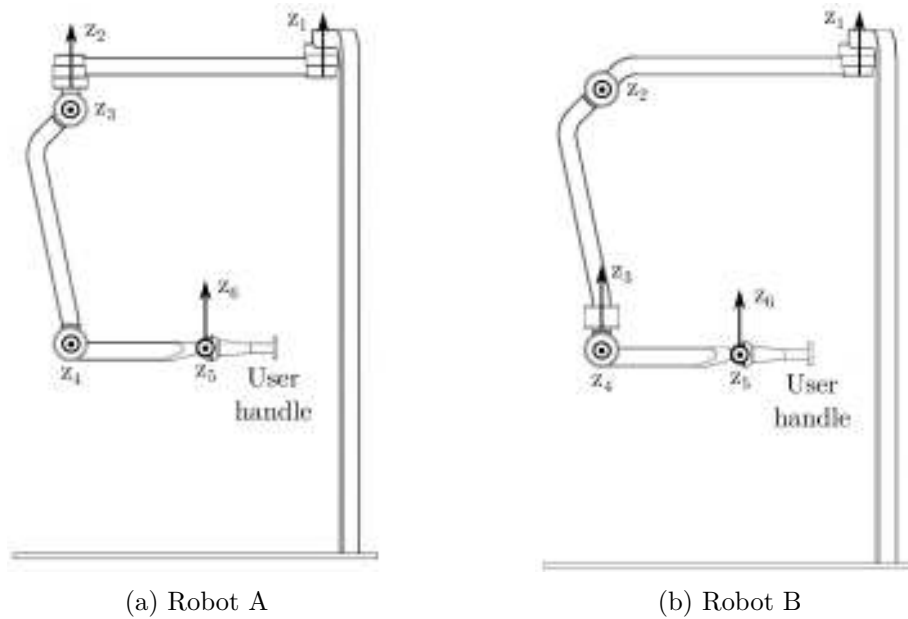
Figure 4.15: Kinematic structure of both simulated cobots. The configuration depicted correspond to zero joint angles. Left: robot A. Right: Robot B

The robot is controlled according to the strength amplification control law presented in section 3.2.4. The robot joint torques are computed to provide strength amplification, and to compensate the robot weight and the viscous friction effects. However the inertial effects are not compensated. Strength amplification is provided only when a significant contact force must be exerted on the environment, *i.e.* on

points $P_1$ and $P_2$ (Fig. 4.16). During the manipulation of the robot in free space (moving from one point to another), the strength amplification is not activated.
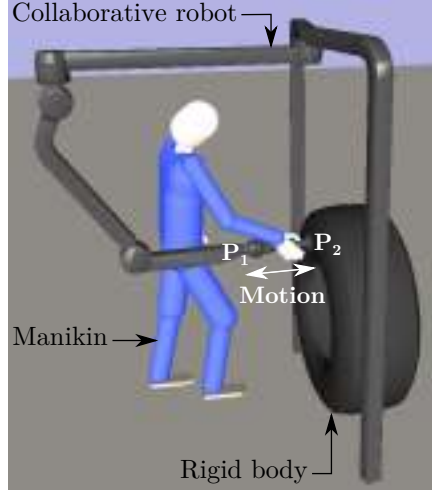


Figure 4.16: Simulation of the autonomous manikin performing a task with the assistance of a collaborative robot.

### 4.3.1.2 Task simulation

The manual tasks considered in this experiment consists in two different phases: a force exertion phase (contact phase) during which the end-effector of the robot does not move, and a free space phase during which the end-effector of the robot is displaced along a straight line trajectory while no contact force with the environment is required. The manikin moves a tool attached to the robot end-effector back and forth between point $P_1$ and point $P_2$, and stays 4 s on each point (Fig. 4.16). The displacement from one point to the other takes 2 s. Point $P_2$ is located on the surface of a fixed rigid body, on which a normal contact force of 80 N is exerted. Point $P_1$ is 20 cm backwards. One work cycle consists in: starting in $P_1$, going to $P_2$, exerting the required contact force, going back to $P_1$, waiting there for the next cycle. The overall duration of one work cycle is therefore 12 s.

The motions of the manikin are automatically generated with the LQP controller, according to the method described in section 3.2.2. The following tasks are included in the controller, in decreasing order of importance: balance task, right hand manipulation tasks (trajectory and force), gazing task, postural task, and joint torques minimization task. All these tasks are active throughout the whole simulation, except the right hand force task which is activated only when the exertion of a contact force with the environment is required (on point $P_2$). The right hand reference trajectory is generated automatically: it consists in a straight line between the origin and target points, with a bell-shape velocity profile. The manikin does not move its feet during the task [3].

---

[3] That is, the manikin is not asked to move its feet during the simulation. However, the manikin

### 4.3.1.3 Parameters

The task is performed with and without the assistance of the collaborative robot. The case without any robot represents the reference situation. In the case where the robot is used, three parameters of the robot are varied:

- The kinematic structure: robot A or B. The position of the robots bases are defined so that the end-effectors of both robots are at the same Cartesian position when their joint angles are zero (the corresponding configuration is depicted in Fig. 4.15).

- The mass of the robot, defined as a percentage of the original robot mass (from 60 to 140 % of the original mass).

- The value of the strength amplification coefficient $\alpha$ (from 0 to 3). The value of the amplification coefficient is limited for stability reasons [Lamy 2011]. However, the question of stability is not addressed in this work: it is assumed that the stability of the system has been studied beforehand and that acceptable values of $\alpha$ are provided.

The influence of the kinematic structure of the robot is studied for different values of the amplification coefficient, but for only one value of the robot mass (original mass). Besides, the masses of robots A and B are set equal, so that only the kinematic structures differs between both robots. The influence of the robot mass is studied only for robot A, and for one value of the amplification coefficient ($\alpha = 1$). The influence of the amplification coefficient is studied in more details for robot A (*i.e.* more values of $\alpha$ are tested).

### 4.3.2 Results

All the five constraints-oriented ergonomic indicators defined in section 3.1.2 are computed: joint position, torque, velocity, acceleration and power indicators. However, the indicators corresponding to the legs, the left arm and the back are not (or very little) affected by the changes in the robot structure, mass, and amplification coefficient. Therefore only the results for the right arm are presented. The proposed ergonomic indicators provide a relative assessment, but not an evaluation of the absolute level of MSDs risk. Therefore, the results are presented as a comparison with the reference situation, *i.e.* the case without any assistance.

Since the repetitiveness factor is not taken into account in this work (see section 3.1), only one work cycle is considered for the evaluation: $P_1 \rightarrow P_2 \rightarrow P_1$. A work cycle consists in phases of very different natures: contact phases (force exertion) and free space phases (motion). The prevailing physical phenomena are not the same during both phases, therefore the effects expected from the robot are very different from one phase to the other. During the contact phase (on $P_2$), the robot

---

feet are not mechanically attached to the ground: the ground-feet contact remains an unilateral contact, which can be broken if, for instance, the manikin falls.

is expected to decrease the worker's effort thanks to strength amplification. On the contrary, during the free space phase (from $P_1$ to $P_2$ and back), the robot is expected to be as transparent as possible, *i.e.* as if there was no robot [Jarrassé 2008]. Due to these differences, the free space phase and the contact phase are studied separately.

The results for the kinematic parameter (robot structure) are presented in tables 4.9 and 4.10. The results for the dynamic parameter (robot mass) are presented in table 4.11. The results for the control parameter (strength amplification coefficient) are presented in table 4.12. These results are analyzed hereafter, for each one of the five constraint-oriented ergonomic indicators.

| | Robot / No robot (%) | | | |
|---|---|---|---|---|
| | Robot A | | Robot B | |
| | $\alpha = 0$ | $\alpha = 3$ | $\alpha = 0$ | $\alpha = 3$ |
| Position | **117** | **116** | **140** | **135** |
| Torque | **106** | **21** | **110** | **24** |

Table 4.9: Influence of the kinematic structure of the robot on the position and torque indicators during the contact phase, for two different amplification coefficients. The velocity, acceleration and power indicators are not displayed, because there is no motion during the contact phase, so these indicators are always zero. For each case, the displayed value is the percentage of the reference value, *i.e.* the value of the indicator when the task is executed without any assistance.

| | Robot / No robot (%) | |
|---|---|---|
| | Robot A | Robot B |
| Position | **138** | **145** |
| Torque | **126** | **174** |
| Power | **144** | **160** |
| Velocity | **129** | **411** |
| Acceleration | **247** | **512** |

Table 4.10: Influence of the kinematic structure of the robot on the position, torque, power, velocity and acceleration indicators during the free space phase (no strength amplification is provided). For each case, the displayed value is the percentage of the reference value, *i.e.* the value of the indicator when the task is executed without any assistance.

### 4.3.2.1   Position indicator

In all the tested cases, the presence of the robot worsens the ergonomic situation, regarding the joint position indicator. However, the position indicator is barely affected by the mass of the robot (in free space), and by the strength amplification coefficient (during force exertion). The modification of the manikin posture is therefore mainly due to the geometric volume of the robot, which hinders the manikin

| | Robot A / No robot (%) | | | | |
|---|---|---|---|---|---|
| | $0.6\,m_0$ | $0.8\,m_0$ | $1.0\,m_0$ | $1.2\,m_0$ | $1.4\,m_0$ |
| Position | **138** | **138** | **138** | **139** | **139** |
| Torque | **113** | **118** | **126** | **136** | **148** |
| Power | **120** | **132** | **144** | **156** | **172** |
| Velocity | **106** | **112** | **129** | **176** | **250** |
| Acceleration | **137** | **178** | **247** | **397** | **821** |

Table 4.11: Influence of the robot mass on the position, torque, velocity, acceleration and power indicators during the free space phase, for robot A (no strength amplification is provided during free space phases). The influence of the robot mass is not studied for the contact phase, because there is no motion of the robot in this phase, hence no inertial effects. In the absence of any gravity effects (the robot weight is fully compensated by the robot control), all mass-related effects are null during the contact phase. For each case, the displayed value is the percentage of the reference value, *i.e.* the value of the indicator when the task is executed without any assistance.

| | Robot A / No robot (%) | | | |
|---|---|---|---|---|
| | $\alpha = 0$ | $\alpha = 1$ | $\alpha = 2$ | $\alpha = 3$ |
| Position | **117** | **117** | **116** | **116** |
| Torque | **106** | **42** | **28** | **21** |

Table 4.12: Influence of strength amplification coefficient on the position and torque indicators during the contact phase, for robot A. The free space phase is not studied, since no strength amplification is provided during the free space motions. The velocity, acceleration and power indicators are not displayed, because there is no motion during the contact phase, so these indicators are zero. For each case, the displayed value is the percentage of the reference value, *i.e.* the value of the indicator when the task is executed without any assistance.

gesture. This phenomenon is more important with robot B than with robot A. An ill-adapted robot kinematics could also prevent the manikin from correctly following the reference hand trajectory, thus modifying the manikin posture. However, given the reference trajectory and the robots kinematics used in this experiment, such a phenomenon probably does not happen.

### 4.3.2.2 Torque indicator

The joint torque indicator is affected by the robot structure, both during contact and free space phases. During contact phases, both robots are roughly equivalent regarding this indicator. The slight differences between robot A with $\alpha = 0$, robot B with $\alpha = 0$, and the case without assistance may come from the posture modification. Indeed, the manikin posture is affected by the robot presence (see

the position indicator results), and a change in the posture results in a change in the joint torques needed to maintain the posture. During free space motions, both robots induce higher efforts than without robot. This is due to the lack of transparency of the robot. The inertial effects are not compensated by the robot control, therefore setting the robot in motion and stopping it requires additional efforts. Robot B is much worse than robot A, because of the direction of the motion, and the distribution of its joint axes. With robot A, moving the end-effector from $P_1$ to $P_2$ can be done without moving axes $z_1$ and $z_2$ (see Fig. 4.15 for the axes definition). Whereas with robot B the motion of $z_2$ is needed. Therefore more segments of the robot are displaced with robot B, hence higher inertial effects.

The inertial effects also explain why the torque indicator is affected by the robot mass. The results regarding this parameter are physically consistent, since during free space motions, the torque indicator increases with the robot mass.

As expected, the torque indicator is strongly affected by the strength amplification coefficient during contact phases: the bigger $\alpha$, the smaller the external force required from the manikin, hence the smaller joint torques. However, the relation between the torque indicator values and $\alpha$ is not inversely proportional, because of the consideration of fatigue in the indicator calculation which modifies the joint torque capacity (eq. 3.6). When $\alpha$ increases, less joint torque is required therefore the decrease of the torque capacity over time is slower. So, at time $t$, the level of torque solicitation (ratio between the joint torque and the joint capacity) is reduced because less torque is required, but also because the past solicitations are smaller, inducing less fatigue hence a higher torque capacity (see Fig. 4.17). Therefore, the value of the torque indicator over the whole task (represented by its time-integral value) is reduced by a factor greater than $\alpha$.

### 4.3.2.3 Velocity, acceleration and power indicators

The joint velocity indicator is affected by the robot structure (A better than B), and by the robot mass. For the mass parameter, the variation in the velocity indicator is only due to inertial effects, since the manikin posture is not affected by the robot mass. The robot tends to drag the manikin arm during fast motions, thus increasing the joint velocities. This effect is all the more important that the mass of the robot is bigger.

The effect of the robot structure on the joint velocities is double. First the posture modification is different with both robots (see position indicator), which leads to different joint velocities. The second cause of variations is, as for the mass parameter, the inertial effect: robot B is more inertial than robot A for the motion considered (see torque indicator).

The results and interpretation of the acceleration and power indicators are qualitatively similar to those of the velocity indicator.
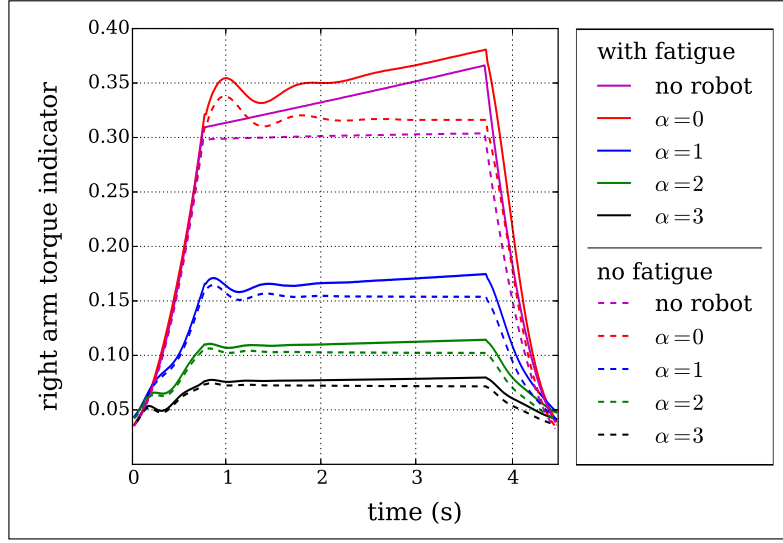
Figure 4.17: Time evolution of the right arm torque indicator during the contact phase, with and without fatigue consideration, and for different values of the strength amplification coefficient $\alpha$. When fatigue is not taken into account (dashed line), the joint torque capacities remain constant, therefore the torque indicator remains constant as long as the same force is exerted. When fatigue is taken into account (solid line), the joint torque capacities decrease over time due to the fatigue generated by force exertion. Therefore the torque indicator increases over time, even when the same force is exerted.

#### 4.3.2.4   Whole cycle

The influence of the robot on the manikin is not similar during free space and contact phases, because different physical phenomena are at play. The robot can have a positive effect in one phase, but a negative effect in the other phase. However, the same robot will be used for the whole task. Therefore the whole task must be considered when tuning the values of the parameters.

Robot B is not considered here, since robot A is better for all indicators, both in free space and during contact phases. The results of the velocity, the acceleration and the power indicators are similar whether the whole cycle or just the free space phase is considered. Indeed, these indicators equal zero during the contact phase. The position indicator is negatively affected in both phases, and besides it remains constant whatever the robot mass and amplification coefficient. Therefore only the torque indicator is studied on the whole task. Its variations (comparatively to the case without assistance) are displayed in tables 4.13 for the amplification coefficient parameter and 4.14 for the mass parameter.

Despite the increase in joint torques during free space motions, the use of the robot globally improves the worker situation regarding the torque indicator. The positive effect of the strength amplification overtakes the negative effects of the additional inertia and posture modification. This is due to the fact that the efforts

during the free space phase are much smaller (by about a factor 6, even with the additional inertia of the robot) than those in the contact phase. Furthermore, the free space phase is shorter. For similar reasons, the effect of the strength amplification coefficient is much more significant than the effect of the robot mass.

| Robot A $m = m_0$ / No robot (%) | | | |
|---|---|---|---|
| $\alpha = 0$ | $\alpha = 1$ | $\alpha = 2$ | $\alpha = 3$ |
| Torque    **107** | **45** | **33** | **29** |

Table 4.13: Influence of the strength amplification coefficient on the torque indicators during the whole task, for robot A, with a robot mass equals to $m_0$. For each case, the displayed value is the percentage of the reference value, *i.e.* the value of the indicator when the task is executed without any assistance.

| Robot A $\alpha = 1$ / No robot (%) | | | | |
|---|---|---|---|---|
| $0.6\,m_0$ | $0.8\,m_0$ | $1.0\,m_0$ | $1.2\,m_0$ | $1.4\,m_0$ |
| Torque    **44** | **45** | **46** | **47** | **48** |

Table 4.14: Influence of the robot mass on the torque indicators during the whole task, for robot A, with $\alpha = 1$. For each case, the displayed value is the percentage of the reference value, *i.e.* the value of the indicator when the task is executed without any assistance.

### 4.3.3   Discussion

This experiment demonstrates that the evaluation framework proposed in this work is useful to quantify the ergonomic effects of various parameters of a collaborative robot (another example of cobots comparison with this evaluation framework is presented in appendix C). The effects of kinematic, dynamic, and control parameters can be compared. Being able to quantify the respective ergonomic effects of different parameters is of great interest for the design of collaborative robots. Indeed, the tuning of the parameters of a cobot usually results from compromises. For instance, a high strength amplification is desirable because it reduces the joint torque solicitations during force exertion. However, it requires powerful actuators which are generally heavy. Therefore the robot mass increases, and moving it requires higher effort.

This evaluation framework also enables to quantify the effect of one parameter regarding different kinds of solicitations (positions, torque, velocity...). However, in this case the interpretation of the results is not always as straightforward, because the indicators cannot be numerically compared with one another. Choosing between robot A and robot B is easy here, because robot A is better for all indicators, and both phases. But different indicators may as well point out antagonistic results. For instance, the use of robot A is beneficial regarding the torque solicitations, whereas

it has negative effects on the other indicators. A similar phenomenon has already been observed without a robot in section 4.2 for the seat height parameter (torque *vs.* position indicators). Such cases correspond to a multi-objective problem: different values of a parameter are optimal regarding different objectives. The user must then compromise and choose the parameter value which best matches his priorities. Nevertheless, depending on the task that is considered, some indicators are more relevant than others. Identifying the most relevant indicators would therefore simplify the interpretation of the results by decreasing the number of potentially antagonistic ergonomic objectives. A method for analyzing the relevance of the ergonomic indicators depending on the task features is presented in chapter 5.

## 4.4 Limitations

The results obtained with the evaluation framework seem promising regarding the comparison of the ergonomic benefit provided by various collaborative robots. The variations of the ergonomic indicators observed in the two experiments (sections 4.2 and 4.3) are physically consistent. However, as mentioned in the introduction of this chapter, the global validity and accuracy of such measurements strongly depends on the realism of the human, and robot, models and behaviors.

The model of the robot that is used in section 4.3 is not entirely realistic. For instance, the dry friction in the robot joints, or the flexibilities in the joints and segments are not modeled. However, the main limitations which question the validity of the ergonomic assessment are related to the human model. Several experiments are carried out in this chapter, in order to validate different parts of the evaluation framework. Their results highlight several limitations, which are discussed thereafter.

### 4.4.1 Co-contraction phenomenon

The co-contraction phenomenon corresponds to the simultaneous contraction of antagonistic muscles in order to increase the joint impedance. The contraction of antagonistic muscles does not result in any operational force, but is needed to resist perturbations arising from limb dynamics or due to external loads. Co-contraction occurs in all motions, in order to stabilize the joint, thus protecting joint structures. Beyond this self-preservation purpose, co-contraction plays an important role in motion accuracy, since it increases the limb stiffness. Therefore co-contraction is especially important during activities which require high accuracy, in terms of position or force [Gribble 2003].

As mentioned in section 4.2.3, the co-contraction phenomenon is not taken into account in the evaluation process. The omission of the co-contraction phenomenon is not due to the ergonomic indicators formula, but to the representation of the human body. Contrarily to the muscle actuation of the human body, which is redundant, each joint of the manikin is controlled by a unique actuator. Because of the redundancy of the human muscle actuation, internal forces (*i.e.* forces which do

not generate any operational force) can be generated by a human subject. However, these internal forces do not have any equivalent in the manikin model. Therefore the manikin joint torques do not fully represent the physical effort of the worker. Nevertheless, the effect of co-contraction related to motion accuracy could be indirectly modeled without changing the body model, by using a variable impedance in the manikin control. This means varying the stiffness and damping of the operational hand tasks, *i.e.* adapting the gains $K_p$ and $K_d$ in equation 3.18. A higher stiffness thus increases the motion accuracy and corresponds to a higher joint torque, hence a higher value of the force-related ergonomic indicator. The arm impedance (hence the values of $K_p$ and $K_d$) therefore results from a compromise between accuracy and effort.

However, the criterion ruling the effort *vs.* accuracy compromise is not clearly established yet in the literature. Therefore the impedance of arm is kept constant in this work. The additional effort due to co-contraction is then not taken into account, leading to an under-estimation of the global effort. Nevertheless, the ergonomic evaluation proposed in this work is not intended for medical purposes (estimating the real exposure level to MSDs risk factors) but for comparing different collaborative robots. It can be assumed that for a same task (same required accuracy), the smaller the effort required to perform the task (not including the co-contraction), the smaller the co-contraction. Indeed external efforts (forces to apply on the robot or environment) and gravity-induced efforts (efforts required to maintain a posture) represent a perturbation regarding the position or force accuracy. If this perturbation is smaller, the stiffness required to resist it is also smaller. So a robot that is better regarding the joint torque indicator without considering the co-contraction is very likely to be also better with it. Therefore, though incomplete, the proposed evaluation is still a first step towards the evaluation of the ergonomic benefit provided by a collaborative robot.

### 4.4.2   Human-like behaviors

Both experiments intended to estimate the reliability of the human model and ergonomic indicators (sections 4.1 and 4.2) are based on motion capture data. Therefore they do not address the realism of automatically generated motions and postures of the manikin.

#### 4.4.2.1   Arm motion

Simulating highly realistic human motions requires to understand the psychophysical principles that voluntary movements obey. In this work, the hands operational trajectories are defined as straight lines and such that the velocity follows an invariant bell-shape profile. This is in accordance with the kinematics invariance principle highlighted by Morasso for straight hand motions [Morasso 1981]. However, other principles also affect human motions. Many studies have been conducted in order to establish mathematical formulae of these principles, *e.g.* Fitt's law [Fitts 1954],

two-thirds power law [Viviani 1995], minimum jerk principle [Flash 1985]...). De Magistris *et al.* successfully implemented some of them within the XDE framework [De Magistris 2013]. They validate the manikin control by comparing the results of a standard ergonomic assessment (OCRA index) carried out on a real person and with the manikin. However these improvements are currently limited to certain motions, mainly reaching. Indeed, these driving principles are not yet known for all kinds of motions, especially when significant external forces are at play.

### 4.4.2.2 Feet placement

Most of the activities on which this work focuses are not performed only with arm motion, but require whole-body motion. In such cases, and especially when significant efforts are at play, the question of whole-body posture adaptation is essential. One conclusion of the cobot comparison experiment (section 4.3.2) is that the value of the strength amplification coefficient - therefore the effort exerted by the manikin - does not influence its posture. This could be because the variation in the requested force is not significant enough to make any difference. However, this is more likely due to a limitation of the manikin control. Given the LQP controller formulation that is used for generating the manikin motion, the manikin posture should be affected by the external force. Indeed the external force is included in the QP constraints and linked to the joint torques through the equation of motion 3.16, and the QP controller tends to minimize the joint torques. However the fact that the feet positions are imposed makes any significant adaptation of the posture impossible. Once the feet positions are given, the hand position task and the balance task (and to a lesser extent the postural task) strongly constrain the posture.

The feet positions are set by the user and are therefore not necessarily well-adapted to the task. Liu *et al.* propose an optimization-based method for choosing feet placement for a manipulation task with external force [Liu 2012]. The objective is to maximize the force exertion capability in a given direction, the joint comfort, and the ground contact stability, subjected to hands reachability constraints. Marler *et al.* also use an optimization-based method to determine feet placement and joint configuration, given hands position and external load [Marler 2011]. These methods seem promising, but are however limited to activities during which the feet do not move. Indeed, they are computationally expensive and cannot be run online to modify feet placement during the simulation. Besides, these methods require the external force direction (and magnitude in Marler *et al.*) as an input. Whereas in collaborative robotics, the force to exert on the environment is known in advance, but not the force required to displace the robot.

The problem of online adaptation of feet placement is addressed by Ibanez *et al.* [Ibanez 2014]. An optimization problem is solved to determine whether a step should be triggered, with which foot, and where. Walking motions, as well as adaptation steps for balance recovery can be handled. However, the algorithm requires the desired center of mass velocity as an input. It is therefore convenient for activities in which balancing is the only goal, but less for manipulation activities.

Nevertheless, the need to specify the center of mass velocity beforehand can be circumvented in manipulation activities. Even with a zero velocity reference for the center of mass, feet motions can be achieved. Indeed hand motions represent a perturbation regarding balance, so adaptation steps are triggered to maintain balance while "following" the hands. However such a strategy results in a delay of the stepping motion over the hand motion, whereas human beings usually anticipate such displacements.

### 4.4.2.3   Dynamic replay of walking motions

A related issue is the dynamic replay of walking motions from motion capture data. As mentioned previously, a balance task must be added in the controller in order to close the balance control loop and improve/maintain the manikin balance in dynamically replayed motions. The ZMP preview control scheme on which is based the balance task enables walking motions when there is no strong constraints on the upper-body motion. However, it cannot be used as such for accurately replaying walking motions. The main problem is the feet placement. Indeed, the manikin model being only an approximation of the human model, human steps cannot be exactly reproduced. In particular, the walking controller and the manikin kinematics are designed for flat feet: there is no toe off or heel strike phases in the manikin walk. The absence of these two phases shortens the possible step length (longer steps are highly unstable and lead to a fall of the manikin). Therefore, the manikin feet cannot be placed at the same positions as the human feet, except for very small steps. Even with articulated feet, the legs motions of a human subject could likely not be exactly reproduced.

A partial solution is to replay the upper-body motion only. That is, remove the leg markers tasks and use, for the legs motions, well-adapted steps for the manikin. However, most existing walking algorithms require the stepping moments and sometimes also the feet placements to be given as an input. Such a solution therefore requires to compute beforehand feet trajectories which are both feasible by the manikin and enable an accurate tracking of the upper-body motion. This could be achieved for certain motions by manual tunings, however this is highly time-consuming, and does not provide any general method. Instead, the work of Ibanez *et al.* on online adaptation of feet placement may provide a solution to this problem, by removing the need for the user to compute well-adapted feet trajectories [Ibanez 2014]. This solution has not been implemented in this work because it has only been recently published. However it seems to be an interesting perspective.

### 4.4.2.4   Collision avoidance

Beyond the balance problem, the posture and motion of the worker are also affected by the robot for geometric reasons. If a segment of the robot physically or visually prevents the worker to reach (or see) the task target, the workers modifies his posture and possibly feet placement. Visual collisions are not implemented in XDE

yet, but physical collisions are already detected, and collision avoidance constraints can be added in the manikin controller. However, such constraints only reactively prevent any contact between the manikin and an obstacle. They do not provide a solution for bypassing the obstacle, contrarily to what a human being would do. This results either in awkward and unrealistic postures, or in the task not being properly carried out. The only solution to solve this problem is to rely on online planning methods. Indeed the position of the robot (obstacle) is not known beforehand and changes along with the manikin motion.

### 4.4.3 Conclusion

The manikin used to perform ergonomic assessment of collaborative robots admittedly shows several limitations. At low level, its motions and internal forces omit some phenomena and motion principles. At high level, its adaptability is almost non-existent since its control is only reactive and there is no planning or anticipation. However, generating more realistic motions and behaviors of the manikin is a current and broad research topic, which is out of scope here.

Nevertheless, as stated in chapter 2, the realism of most common DHM software tools for ergonomic assessments is even more limited. The interaction forces with the environment are rarely taken into account when computing the motion, and balance is almost always ignored. Besides, in most cases, dynamic phenomena are considered neither in the motion computation nor in the ergonomic evaluation. Therefore, biomechanical quantities computed through virtual human simulation do not always match their equivalent measured directly on a human-being, which leads to wrong assessment of the risk [Lämkull 2009, Savin 2011]. Besides, except for IMMA (see section 2.2.2), these software do not include planning methods to automatically simulate complex activities, but focus on elementary motions.

In this work however, the manikin is animated with an optimization technique which takes into account the dynamics of the human body, the external force exertion and the balance problem. Therefore, though there is still much to improve, this is a first step towards a more human-like behavior of the manikin, and a more accurate ergonomic assessment.

## 4.5 Conclusion

In this chapter, a validation of the framework for evaluating biomechanical solicitations during co-manipulation activities proposed in chapter 3 is presented. The proposed validation consists in three steps.

In the first step, the consistency of the virtual manikin model and control is evaluated, through force and motion comparison. Motion and force data are recorded on human subjects performing a drilling task (without assistance). The motion is dynamically replayed with the virtual manikin animated by the LQP controller.

The manikin whole-body motion is very similar to the original motion, as long as the balance is not strongly solicited. This validates the proposed dynamic replay method. However, walking motions cannot be replayed with the proposed method.

The ground contact forces computed by the controller are then compared with those measured experimentally. Both are very similar, which indirectly validates the consistency of the manikin joint torques. The motion-related and force-related biomechanical quantities measured on the manikin are therefore consistent, as long as the input motion is given.

In the second step, the ergonomic consistency of some of the proposed ergonomic indicators is evaluated. To this purpose, the influence of several task features (geometric, force and time constraints) on the values of three indicators (joint position, joint torque and joint power) is studied. The motions of human subjects performing a path-tracking task with force exertion are recorded and dynamically replayed with the virtual manikin, in order to compute the indicators values (without assistance).

The indicators show a linear correlation with the strenuousness perceived by the subjects, and their variations are consistent with ergonomic guidelines and physical considerations. The three tested indicators therefore seem suitable to assess the relative level of exposure to MSDs risks, as long as the situations which are compared have similar durations. However, the consistency of the other indicators is not addressed in the proposed experiment.

The third step aims at demonstrating the consistency and usefulness of the ergonomic indicators measured through a manikin-robot simulation, regarding the evaluation of the ergonomic benefit provided by a collaborative robot. To this purpose, a co-manipulation activity is simulated with the fully autonomous manikin assisted by a collaborative robot. Kinematic, dynamic, and control-related parameters of the robot are varied, in order to study their influence on the five constraint oriented ergonomic indicators.

The results are for the most part physically consistent. Therefore, thanks to the proposed framework, the effects of various robot parameters on the worker can be quantified, for each kind of biomechanical solicitations.

However the three proposed experiments also highlight some limitations of the manikin model and control. At low level, the manikin motions and internal forces omit some phenomena and motion principles. At high level, its adaptability is almost non-existent since its control is only reactive and there is no planning or anticipation. Consequences of such omissions and potential solutions for improving the manikin realism are discussed.

Finally, the last two experiments highlight the fact that several indicators may lead to antagonistic conclusions, regarding which situation is better. This is due

to the fact that different biomechanical solicitations are considered in separate indicators, rather than being mixed together in a single score (so that the indicators formulation is not task-dependent). Evaluating the detailed effects of various parameters is thus easier. However, when such an evaluation is used for choosing between different cobots, multiple ergonomic indicators make the choice harder for the user. Especially in the case of antagonistic conclusions since the different indicators cannot be compared.

To overcome, or at least simplify, this problem, the most relevant indicators for a given task need to be identified. Thus the number of potentially antagonistic ergonomic objectives can be decreased. The problem of analyzing the relevance of ergonomic indicators is addressed in the next chapter.

# Chapter 5

# Sensitivity analysis of ergonomic indicators

## Contents

In the previous chapters, a framework for measuring biomechanical quantities during co-manipulation activities is presented and validated. Co-manipulation activities are simulated with an autonomous virtual manikin and a virtual prototype of the robot, and various ergonomic indicators are measured on the manikin during the simulation. However, the indicators listed in section 3.1.4 aim at accounting for the various kinds of physical solicitations as exhaustively as possible. Therefore each one of them represents a different body part and/or a different biomechanical quantity, resulting in a large number of indicators. Furthermore, because of their non-homogeneous meanings, different indicators may lead to different conclusions,

as highlighted in section 4.3.3. The interpretation of the simulation outputs is then not straightforward for the user, when it comes to selecting a suitable robot. In order to facilitate this interpretation, the number of indicators that are considered must be limited. Yet the remaining indicators must sufficiently account for the global ergonomic level of the activity. This chapter therefore presents a method for analyzing the relevance of ergonomic indicators, depending on the activity features. Based on this analysis, the user can easily select the most informative indicators for comparing different collaborative robots.

## 5.1    Sensitivity analysis of ergonomic indicators

The general purpose of the evaluation framework developed in this work is not to assess the absolute level of MSDs risks, but to compare different collaborative robots. In this context, the relevance of an indicator is not related to its value, but to its variations when the activity is performed with different cobots. Indeed, a high value of an indicator means that the current situation is ergonomically wrong (the ergonomic indicators should be minimized). However, if this value remains the same, whichever the cobot that is used, this indicator does not enable to decide between several cobots. Therefore, the most useful indicators are the ones that best explain the disparity of the results when the activity is performed in various ways (*i.e.* with different cobots).

### 5.1.1    Method overview

The features of the considered activity necessarily affect the relevance of each indicator, since they affects the kinds of solicitations that the worker undergoes. However establishing general selection guidelines based only on the activity description (*a priori* selection) may be quite challenging and lead to inaccurate conclusions. This is especially true when a collaborative robot is used because it can deeply modify the physical stress experienced by the worker and change the nature of the activity. Besides, there is no straightforward analytical relation between the activity features and the indicators mathematical formulae. Therefore the analysis of the relevance of ergonomic indicators is rather based on the simulation of the considered activity, with a virtual manikin.

   The purpose is to estimate how much each ergonomic indicator varies when the activity is executed in different situations, *i.e.* with different collaborative robots. In order to correctly estimate these variations, the activity should be simulated with as many cobots as possible. However, using real cobots designs in the simulation has several drawbacks. The number of existing cobots is very limited, therefore tests cobots should be designed. But the number of possible designs is infinite, and there is *a priori* no reason to choose one over another. Therefore, in order to be very generic, real designs are not used, but rather a cobot is modeled by its effects - positive and negative - on the worker. These effects are represented by a set of

parameters. Different values of the parameters correspond to different situations (*i.e.* different cobots).

The whole process for analyzing the relevance of ergonomic indicators regarding the comparison of collaborative robots can be summarized as follows (Fig. 5.1)

1. Define the parameters which represent the physical effects of a collaborative robot on a worker.

2. Select, among all the possible combinations of parameters values, those that should be tested.

3. Simulate the execution of the activity with the virtual manikin, for each selected combination of parameters values, and compute the ergonomic indicators (time-integral version).

4. Analyze the variations of each indicator, based on its values in all the tested cases.

Steps 1, 2 and 4 are detailed in the following sections. The simulation step 3 is performed with the autonomous virtual manikin (automatically generated gestures, no motion capture), according to the control method described in section 3.2.2. It should be noted that the duration of the simulated activity is similar in all situations (whichever the parameters values), therefore the issue of the duration factor in the ergonomic indicators mentioned in section 4.2.3 does not occur here.

## 5.1.2 Robot parametrization

The input parameters represent the diversity of potential collaborative robots. Since this work focuses on parallel comanipulation, the worker manipulates the robot only by its end effector. The robot is therefore simulated by a 6D mass-spring-damper system attached to the manikin hand (Fig. 5.2). External forces can be applied on this system, to simulate the robot actuation ($F_{robot}$ in Fig. 5.2). The mass ($M_r$), stiffness ($K_r$) and damping ($B_r$) parameters represent the equivalent dynamics of the robot at the end-effector. Aside from these dynamic effects, the robot can interfere with the worker because of its volume. Such interference can be simulated without making hypotheses on the robot design, by limiting the movements of the manikin (limiting the joints range of motion) and modifying its posture (*e.g.* pelvis position, feet positions, joint reference position...). All the aforementioned parameters represent the negative effects of the robot, which correspond to its lack of transparency. The positive effect of the robot is the assistance provided to the worker. This work focuses on strength amplification, which control law is given in eq. 3.19. Its only parameter is the strength amplification coefficient $\alpha$.

Parameters representing the diversity of workers are added, so as to ensure that the human features do not have a strong impact on the ergonomic indicators. Otherwise several morphologies must be considered when comparing the benefit provided by different cobots. Or the cobot should include some adjustable parts in order to adapt to each worker.
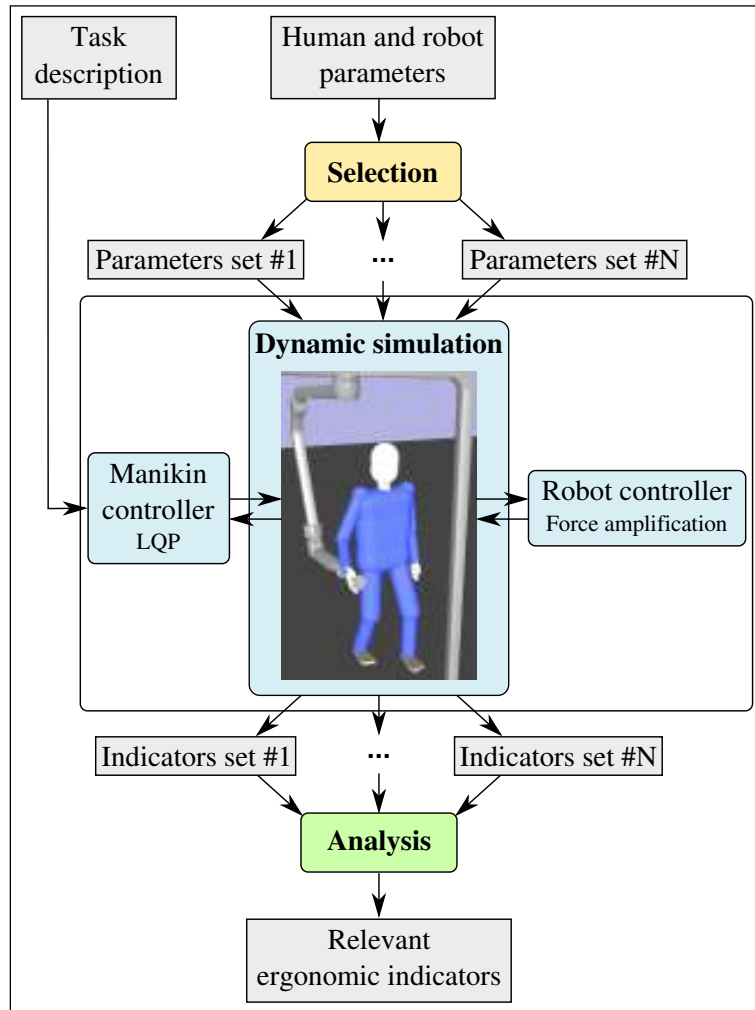
Figure 5.1: Flow chart of the method for analyzing the relevance of ergonomic indicators, regarding the comparison of collaborative robots.

### 5.1.3 Parameters selection

The parameters which represent the diversity of workers and cobots take continuous values, so they must be discretized to form the different combinations of parameters values to be tested. However, though it depends on the length and complexity of the activity that is simulated, the computational cost of a simulation is always quite expensive. The XDE simulation cannot run faster than real time, and in many cases (multiple contacts, many tasks in the manikin controller...), the simulation is slower than real time by a factor 1.5 to 2. Therefore the number of situations which are tested is limited and the values of the parameters must be carefully selected.

Optimizing the exploration of the parameters space comes under the theory of the design of experiments [Fisher 1935, Goupy 2006]. The choice of a design requires a compromise between the number of trials and the precision of the resulting
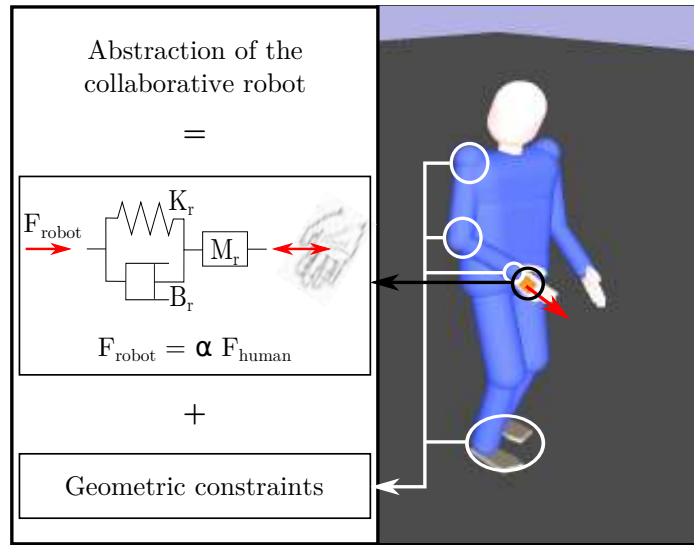
Figure 5.2: Abstraction of the collaborative robot by a mass-spring-damper system attached to the hand of the manikin, and geometric constraints on the manikin motions (only some examples of constraints are displayed here). $F_{robot}$ is an external force that simulates the actuation of the robot, according to a strength amplification control law.

information. This choice is therefore strongly influenced by the objective of the study. Here, the objective is double:

- Identifying the indicators which show the largest variations through the whole parameters space. This objective aims at selecting discriminating indicators, in order to reduce the number of criteria to facilitate the comparison of collaborative robots.

- Estimating the influence of each parameter on the ergonomic indicators. This second objective is not strictly necessary if the only purpose is the selection of discriminating indicators. However, quantifying the influence of the parameters is useful to orient the design or the choice of a well-adapted cobot.

These objectives come under the theory of global sensitivity analysis [Saltelli 2000]. The methods for analyzing the sensitivity of a numerical model are divided into three families [Iooss 2011]: screening, computation of sensitivity indices, and response surface methodology. They are detailed hereafter.

**Screening:** Screening aims at qualitatively analyzing the influence of the input parameters. It enables to coarsely distinguish the strongly influential parameters from the weakly influential ones. Non-linear effects or interactions between parameters can also be detected. The main advantage of screening methods is the small number of required trials (usually less that ten times the number of parameters). However, the resulting information is only qualitative. Therefore screening is often

used for a pre-analysis of models with a high number of inputs. The most influential parameters are thereby identified, and a quantitative analysis is then conducted on this reduced number of inputs only.

**Computation of sensitivity indices:** Sensitivity indices aim at quantifying the global influence of each input. Three different kinds of indices can be computed. The first family of indices gathers coefficients associated with linear regression [Saporta 2011]: linear correlation (Pearson correlation), partial correlation, and standard regression coefficients. If the model is not linear but monotonous, a linear rank regression (Spearman correlation) is applied instead, and provides similar indices. The second family of indices corresponds to statistical tests. Each input is divided in several classes and statistical tests (*e.g.* Fisher, $\chi^2$, Kruskal-Wallis...) are applied to evaluate the homogeneity of the different classes, regarding the model output (in the present case, the ergonomic indicators which are measured through the virtual manikin simulation). Contrarily to regression-based methods, statistical tests do not necessarily require hypotheses on the monotony of the model (though they may require other hypotheses on the data distribution). The third family corresponds to variance-based sensitivity indices, also called Sobol indices, which are computed through a variance-based analysis of the model output. All the methods for computing sensitivity indices require more trials than screening methods (usually between ten and more than ten thousand times the number of parameters, depending on the method that is chosen). However, sensitivity indices enable a precise ranking of the influence of the different inputs.

**Response surface methodology:** Response surfaces - or metamodels - aim at computing an approximation of a physical process or a complex numerical model [Box 1987]. Metamodels enable the estimation of the local effects of inputs all along their variation range, whereas sensitivity indices only give information on the global influence of an input. Metamodels are also used to estimate sensitivity indices when their computation on the original model (which corresponds here to the virtual human simulation) is too expensive (*e.g.* numerous inputs, computational cost of one trial). The number of trials of the original model that are needed to build a metamodel depends on the complexity of the original model, the number of inputs, and the desired accuracy of the approximation. However, the number of required trials is generally about a hundred times the number of input parameters.

In this work, the analysis aims at quantitatively estimating the sensitivity of ergonomic indicators to robot and human parameters. Such an analysis requires the computation of sensitivity indices. Since the number of input parameters is quite small (about a dozen), there is no need to eliminate parameters before a quantitative analysis. Screening methods are therefore out of scope. Though the computational cost of one simulation is quite expensive, the number of inputs is limited. Therefore sensitivity indices can be computed directly from virtual human simulations,

without the need for a metamodel. Especially as several trials can be simulated simultaneously, with multi-threading. Furthermore, the high number of outputs (*i.e.* ergonomic indicators), dramatically increases the complexity of the representation of the parameters-indicators relations. No assumptions can be made regarding the linearity or monotony of the relation between the parameters and the indicators. Besides the input-output relation is different for each parameter-indicator pair. Therefore building an accurate metamodel of the parameters-indicators relations requires a high number of trials. Eventually, since the knowledge of the local effects of the inputs is not an objective here, there is no reason for computing a metamodel.

Among the three kinds of sensitivity measures, the indices based on linear regression are excluded since no hypotheses can be made on the monotony of the ergonomic indicators. Sobol indices are preferred over statistical tests, because their interpretation is more straightforward: each index measures the percentage of the output variance that is explained by the corresponding input. The computation of Sobol indices relies on the decomposition of the output variance of the considered function (functional ANOVA decomposition) [Hoeffding 1948, Sobol 1993]. Given $X_i$ the $d$ random and mutually independent inputs (the human and robot parameters match these requirements), and $Y$ the output of the model (one of the ergonomic indicators), the variance of $Y$ is decomposed as follows:

$$\text{Var}[Y] = \sum_{i=1}^{d} V_i(Y) + \sum_i \sum_{\substack{j \\ j>i}} V_{ij}(Y) + \sum_i \sum_{\substack{j \\ j>i}} \sum_{\substack{k \\ k>j}} V_{ijk}(Y) + ... + V_{1...d}(Y) \quad (5.1)$$

where:

$$\begin{aligned}
V_i(Y) &= \text{Var}[\text{E}(Y|X_i)], \\
V_{ij}(Y) &= \text{Var}[\text{E}(Y|X_iX_j)] - V_i(Y) - V_j(Y), \\
V_{ijk}(Y) &= \text{Var}[\text{E}(Y|X_iX_jX_k)] \\
&\quad - \text{Var}[\text{E}(Y|X_iX_j)] - \text{Var}[\text{E}(Y|X_iX_k)] - \text{Var}[\text{E}(Y|X_kX_j)] \\
&\quad - V_i(Y) - V_j(Y) - V_k(Y),
\end{aligned} \quad (5.2)$$

and so on. The sensitivity indices are then defined by:

$$S_i = \frac{V_i(Y)}{\text{Var}[Y]}, \quad S_{ij} = \frac{V_{ij}(Y)}{\text{Var}[Y]}, \quad ... \quad (5.3)$$

Each index is between 0 and 1, and the sum of all indices is equal to 1. $S_i$ is a first order index which represents the sensitivity of the model to $X_i$ alone. A high $S_i$ means that $X_i$ alone strongly affects the output. $S_{ij}$ is a second order index which represents the sensitivity of the model to the interaction between $X_i$ and $X_j$, and so on. In order to simplify the interpretation of these indices when the model has numerous inputs, total sensitivity indices are defined as [Homma 1996]:

$$S_{T_i} = S_i + \sum_{\substack{j \\ j\neq i}} S_{ij} + \sum_{\substack{j \\ j\neq i}} \sum_{\substack{k \\ k\neq i \\ k>j}} S_{ijk} + ... \quad (5.4)$$

$S_{T_i}$ represents all the effects of $X_i$ on the model, including all interactions with other inputs. A small $S_{T_i}$ means that $X_i$ has very little influence on the output, even through interactions. The first order and total indices are of particular interest for ranking the inputs, since they give information about the *ith* parameter, independently from the influence of the other parameters. Only these indices are considered in the remaining of this work.

Sobol indices can be estimated with Monte-Carlo (or quasi Monte-Carlo) methods, however the number of trials is a major drawback. These methods often require about ten thousand trials (a little less for quasi Monte-Carlo) for each input in order to accurately estimate the sensitivity indices. Instead, Sobol indices can be estimated with the FAST (Fourier amplitude sensitivity testing) spectral method [Cukier 1978], which convergence is much faster. The FAST method only enables the calculation of the first order and total indices (with the extended FAST method [Saltelli 1999]), however this is sufficient for the current analysis. The exploration method used for the FAST analysis is a good compromise between the number of trials and the comprehensiveness of the space exploration (FAST uses space-filling paths). Therefore, in this work, the different parameters values that need to be tested are chosen according to the FAST exploration method.

### 5.1.4   Indicators analysis

Once the simulations are performed for all the selected combinations of parameters values, Sobol indices can be computed for each parameter, with the FAST method. However, these indices only address single-output models, whereas here each ergonomic indicator is an output of the model. A solution for multiple-output models is to perform a sensitivity analysis on each one of the outputs separately. Though informative, this solution quickly results in a very high number of indices (two indices - first order and total indices - for each parameter and for each indicator). Furthermore, computing Sobol indices separately for each indicator does not give any information about the global effect of a parameter on the overall ergonomy of the considered activity. No global sensitivity index can be computed for a parameter by aggregating Sobol indices relative to different indicators. Indeed, for each parameter, Sobol indices correspond to the percentage of contribution to the output variance of the ergonomic indicator they refer to. Therefore the comparison of Sobol indices referring to different indicators is meaningless. For instance, if parameter $i$ strongly influences indicator $A$, the corresponding Sobol index $S_i^A$ is high, even though the variance of indicator $A$ is very small. Whereas if parameter $j$ only moderately influences indicator $B$, $S_j^B$ is smaller than $S_i^A$, while the variance of indicator $B$ can be much bigger than the variance of indicator $A$. Parameter $j$ may have a more significant overall influence than parameter $i$, however it cannot be deducted from the comparison of $S_i^A$ and $S_j^B$. Computing Sobol indices for each one of all the ergonomic indicators is therefore not a suitable solution. Besides such an analysis does not enable the identification of discriminating indicators. Therefore, another solution is proposed and detailed hereafter.

### 5.1.4.1 Indicators ranking

The problem of sensitivity analysis for multiple-output models has been addressed by Campbell *et al.* [Campbell 2006], though they mainly focus on time-series outputs. They propose to decompose the model outputs in a well-chosen basis before applying sensitivity analysis to the most informative components individually. Choosing a well-adapted projection basis comes down to identifying the most interesting features in the model outputs, and is therefore a problem of dimensionality reduction. This problem is very similar to the problem of identifying discriminating ergonomic indicators, addressed in this work. Among the projection methods proposed by Campbell et *al.*, one of the most famous is the principal components analysis (PCA). This method is also recommended by Lamboni *et al.* [Lamboni 2011] for sensitivity analysis of multiple-output models.

However PCA, like most dimensionality reduction methods form composite variables, *i.e.* the resulting variables are combinations of the initial variables. Whereas here the resulting variables must remain the ergonomic indicators. Indeed meaningful ergonomic indicators cannot be formed by aggregating various indicators, because the latter potentially have very different physical meanings. Even for estimating the global influence of the different input parameters, using composite outputs is not physically meaningful, especially as the influence of a parameter is likely very different from an indicator to another. So standard dimensionality reduction methods cannot be used here. Instead the importance of each ergonomic indicator is represented directly by its variance. The indicators can thus be ordered, and the most discriminating ones (*i.e.* those with the highest variance) can easily be identified. A sensitivity analysis can then be performed separately for each one of the most discriminating indicators. The sensitivity indices relative to different indicators still cannot be compared, however the overall number of indices is reduced, making the interpretation of the results easier for the user. The main drawbacks of conducting sensitivity analyses separately on different outputs that are pointed out by Lamboni *et al.* (redundancy between the different responses, missing of important features of the response dynamics) do not apply here. Indeed, their work focuses on time-series outputs, for which strong relationship exists between the different responses. Whereas the relationships between the different ergonomic indicators are much lighter, or non-existent.

### 5.1.4.2 Scaling

Before ranking the ergonomic indicators based on their variance, the indicators must be scaled because they have non-homogeneous units. Therefore they do not have the same order of magnitude, so they cannot be compared as such. In standard dimensionality reduction methods, this is often done with the variables standard deviation, but then the scaled variables all have a unit variance. Since the variance is precisely what represents the indicators global sensitivity to the activity parameters, this scaling would result in the loss of relevant information. Therefore another option is to use the indicators physiological limit values for this scaling. Though

this is ergonomically very meaningful, some indicators do not have well-defined limits (*e.g.* kinetic energy), and even the existing ones are often hard to find, as stated in section 3.1.2.

Instead, the order of magnitude of an indicator can be roughly estimated by measuring the indicator in many different situations, and taking its average value. If activities of many different kinds are considered and performed in many different ways, it can be assumed that the range of values of each indicator is covered quite exhaustively. This last method is used in this work since it is the only way to estimate a reference value needed to scale the indicators. For each indicator $I$, the normalized indicator $I^{norm}$ is then:

$$I^{norm} = \frac{I}{I^{ref}} \tag{5.5}$$

where:

$$I^{ref} = \frac{\sum\limits_{a \in A} \sum\limits_{p \in P} I^{a,p}}{N_A \ N_P} \tag{5.6}$$

with $A$ the set of simulated activities, $P$ the set of all combinations of parameters values that are tested, $N_A$ and $N_P$ the number of elements respectively in $A$ and $P$, and $I^{a,p}$ the value of indicator $I$ for the activity $a$ and the parameters values $p$.

### 5.1.4.3   Number of discriminating indicators

One objective of the analysis performed here is to reduce the number of ergonomic indicators needed to compare different collaborative robots. The variance of the scaled indicators enables to rank them, from the most to the least discriminating. The number of indicators that are kept for the evaluation of cobots must then be decided. This problem is similar to selecting the number of dimensions in principal components analysis, therefore the same criteria can be applied.

The three main criteria used for selecting the dimension in PCA are: variance explained criterion, Kaiser criterion, and Scree criterion [Jolliffe 2002]. The variance explained criterion consists in fixing the percentage of variance that must be explained, and selecting as many components (or indicators here) as needed to reach this percentage. Once the desired percentage is reached, the following components are not considered, even if their percentage of variance is similar to the one of the last selected component. This criterion is therefore not well-adapted for selecting discriminating indicators, because indicators with similar variances are as informative, so they should either be both selected or both excluded. The Kaiser criterion consists in computing the average percentage of variance explained by a component, and keeping only the components which percentage of variance is greater than this average value. Let $\text{Var}[I_i^{norm}]$ be the variance (including all parameters) of the *ith* normalized ergonomic indicator $I_i^{norm}$, and $N_{ind}$ the total number of indicators.

The Kaiser criterion is:

$$\begin{cases} \text{select } I_i^{norm} & \text{if } \dfrac{\text{Var}[I_i^{norm}]}{\text{V}_{tot}} \geq 1 \\[3mm] \text{remove } I_i^{norm} & \text{if } \dfrac{\text{Var}[I_i^{norm}]}{\text{V}_{tot}} < 1 \end{cases} \tag{5.7}$$

where:

$$\text{V}_{tot} = \sum_{i=1}^{N_{ind}} \text{Var}[I_i^{norm}]. \tag{5.8}$$

For the Scree test, the percentage of variance associated with each component is plotted in decreasing order. The curves first drops, then makes an elbow toward less steep decline. The components after the elbow (usually including it) are not considered (Fig. 5.3). Both the Kaiser and the Scree criteria seem meaningful regarding the selection of discriminating indicators, therefore both are used and compared in this work.
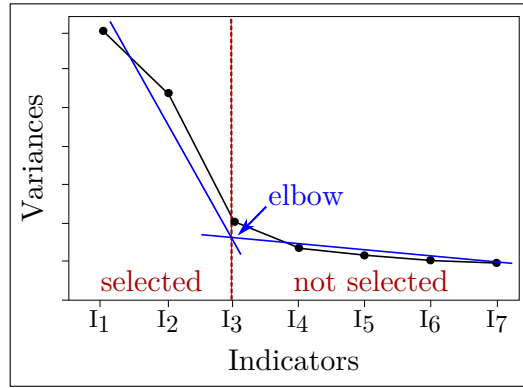


Figure 5.3: Scree plot for selecting relevant ergonomic indicators, based on their variance. The indicators are ranked in decreasing order of variance. The percentage of variance associated with each indicator is then plotted. Only the indicators before the curve elbow are considered.

## 5.2 Experiments

The method for analyzing the relevance of ergonomic indicators and their sensitivity to various parameters presented in the previous section is tested on several activities. The purpose of this experiment is to evaluate the consistency of the results on typical activities, and the usefulness of the method for identifying non-straightforward phenomena.

The work presented in this section has been carried out in collaboration with P. Schlehuber, during his master's internship. He contributed to the results, especially through the implementation of the simulation step (see section 5.1.1) of the sensitivity analysis method presented in the previous section.

### 5.2.1   Simulation set-up

In order to validate the method and ensure that the activity features do affect the selection of the ergonomic indicators, many case-study activities of different kinds are considered. This variety of activities is also needed for estimating the average order of magnitude of each indicator.

#### 5.2.1.1   Activities description

A total of 17 activities are simulated, which consists in

- walking one or several steps, forward, backward or sideways;

- reaching various targets, with both hands;

- exerting various forces (direction and magnitude) with and without motion of the hand (*e.g.* pushing or carrying objects);

- following trajectories with the hand, with various accuracies and at various speeds;

- bending while leaning with one hand.

Further details on theses activities are provided in Fig. 5.4. All these activities are performed with the abstraction of the collaborative robot, *i.e.* the mass-spring-damper system, attached to the manikin hand. Though such a robot is only useful when force exertion is required, it must nevertheless be manipulated by the worker to reach the target of the activity, hence the various displacement activities (walking, reaching...).

Each activity is simulated for all the selected combinations of parameters values (described in the next section), with the autonomous virtual manikin. The manikin is animated with the LQP controller, according to the method presented in section 3.2.2. The following tasks are included in the controller, in decreasing order of importance: balance task (center of mass, and feet acceleration task in walking motions), right hand manipulation task (trajectory and/or force, depending on the task), left hand trajectory task (only in the left hand reaching motion), gazing task, postural task and joint torques minimization task. The trajectories of the right and left hands are generated automatically (no motion capture data is used).

#### 5.2.1.2   Parameters

The input parameters represent the diversity of potential workers and collaborative robots. The worker is defined by his/her height and body mass index (BMI). The BMI is preferred over the mass because it is less dependent on the height than the mass (*e.g.* a BMI of $21\,kg.m^{-2}$ can be equally found among small people and among tall people, whereas a mass of $50\,kg$ is more frequent among small people than among tall people).

As explained in section 5.1.2, the robot is simulated by a mass-spring-damper system. To limit the number of parameters, only the robot mass varies whereas the stiffness and damping are currently kept constant. The amplification coefficient of the robot control law is also added to the parameters. The geometric interference of the robot with the worker is represented by the following parameters (see section 5.1.2 for further explanations): joint limits, joint reference position, and pelvis orientation. The robot is manipulated with the right hand, therefore only the right arm and back are affected by the restriction on the joint limits and the modification of the joint reference position. Eventually, the step length is added to the input parameters to represent either a preference of the worker or an interference with the robot. The numerical upper and lower bounds of the input parameters considered in this work are given in table. 5.1.

| Parameter | Minimum | Maximum |
|:---:|:---:|:---:|
| manikin height $(m)$ | 1.65 | 1.80 |
| manikin BMI $(kg.m^{-2})$ | 21.0 | 27.0 |
| step length $(m)$ | 0.2 | 0.4 |
| upper body joint limits | 0.3 | 1.0 |
| upper body reference positions $(°)$ | 0, 0, 0, 0 | 15, 45, 45, 135 |
| pelvis orientation $(°)$ | 0 | 30 |
| robot mass $(kg)$ | 2 | 10 |
| amplification coefficient | 1 | 3 |

Table 5.1: Parameters minimum and maximum values. The upper body joint limits are specified as ratio of the regular joint limits, and applied on each joint of the back and right arm. The reference positions of the upper body joint tasks are only modified for the following joints: back flexion, shoulder flexion, shoulder abduction, elbow flexion. They are given in this order and relative to the regular reference posture (upright, arms along the body). In order to limit the number of parameters, the reference positions of the four joints are not independent (they are functions of the back flexion parameter). The root orientation is given relative to facing the work area.

The design of experiments (*i.e.* the choice of the parameters values) for the extended FAST analysis is generated through the R software[1]. A uniform distribution is used for each parameter. In [Saltelli 1999], Saltelli *et al.* recommend a set of frequencies for different numbers of input parameters, and an associated sample size (given a set of frequencies, the sample size is constrained due to the Nyquist-Shannon theorem). The values recommended for 8 parameters[2] are used here, leading to a sample size $n = 1001$. Beyond the aliasing phenomenon, other biases occur in the estimation of Sobol indices by the FAST method when the sample

---

[1] http://www.r-project.org
[2] The reference positions of the upper body joints are all fixed by a same parameter.

size in not big enough [Tissot 2012]. These biases tend to vanish when the sample size increases, therefore a second sample size $n = 2000$ is tested, in order to check whether $n = 1001$ is sufficient to ensure the reliability of the results. Given that 8 input parameters are considered, this results in 8008 (resp. 16000) simulations for a sample size of 1001 (resp. 2000). One simulation of all the case-study activities one after the other takes approximately 2 minutes in total (the real activity lasts 70 s), on one core of a 2.4 GHz Intel® Core™ i7 laptop.

### 5.2.2 Results

The indicators which are included in this study are the ones summarized in table 3.1. However, the velocity and force transmission ratio of the left hand are excluded, because the left hand is not used for any manipulation or force task.

The ergonomic indicators that are identified as relevant for each activity, according to the Scree criterion, are summarized in Fig. 5.4. From 30 indicators in the global list, between 3 and 9 indicators are selected for each activity. The Kaiser criterion is also tested and the results are very similar. Out of the 17 activities that are simulated, the exact same number of indicators is selected in 12 cases. The selection differs from one indicator in 4 cases, and from 2 indicators in 1 case. Therefore both criteria can indifferently be used to determine the ergonomic indicators which should be used for cobots comparison. Since the computation of the Kaiser criterion is simpler, it is preferred over the Scree criterion. This reduction in the number of considered indicators results in the loss of less than 30 % of the total information about the variance. The Kaiser or Scree criteria are therefore sufficient to correctly represent the main variations regarding ergonomics. There is no need to set a fixed threshold on the total percentage of variance. Since many different activities are tested here, this conclusion can be generalized.

#### 5.2.2.1 General remarks

Many of the selected indicators are in accordance with what could be expected given the features of the corresponding activity. This is especially true for activities where force exertion is associated with slow dynamics, in which the biggest MSDs risk factor comes from the significant efforts (*e.g.* activities 12, 15 and 17, defined in Fig. 5.4). In such cases, the torque indicators of the upper body parts are among the most discriminating indicators (torque of right arm, back and left arm in activity 17 in which the left arm is used for supporting the body weight while bending).

In most walking and reaching activities, kinetic energy is selected as a relevant indicator, whereas it is not selected in other activities. This is consistent with the fact that walking and reaching generally involve whole-body motion, but no significant effort. Even if the aim of this work is not to provide general guidelines for indicators selection, kinetic energy seems to be a good indicator to summarize the global ergonomy of reaching and walking activities, independently from their detailed features.

| | 1 Walk forward 20cm | 2 Walk sideways 30cm | 3 Step forward | 4 Step backward | 5 Walk forward 50cm | 6 Reach RH 1 | 7 Reach RH 2 | 8 Reach RH 3 | 9 Reach RH 4 | 10 Reach RH 5 | 11 Reach LH | 12 Trajectory 1 RH[1] | 13 Trajectory 2 RH[2] | 14 Trajectory 3 RH[3] | 15 Push RH[4] | 16 Bend forward[5] | 17 Carry RH[6] |
|---|---|---|---|---|---|---|---|---|---|---|---|---|---|---|---|---|---|
| Head dexterity ● | | | | | | | | | | | | | | | | | |
| Kinetic energy ● | 0.28 | 0.91 | 0.20 | 0.15 | 0.18 | 0.75 | 0.08 | 0.34 | | 0.25 | | | | | | | |
| VTR RH Z ● | | | | | | | | | | | | | | | | | |
| VTR RH Y ● | | | | | | | | | | | | | | | | | |
| VTR RH X ● | | | | | | | | | | | | | | | | | |
| FTR RH Z ● | | | | | | | | | | | | 0.02 | | | | | |
| FTR RH Y ● | | | | | | | | | | | | | | | | | |
| FTR RH X ● | 0.39 | | | | | | | 0.07 | 0.23 | 0.38 | | | | | 0.7 | | |
| Dynamic balance ● | | | | | | | | 0.22 | | | | 0.09 | | 0.43 | | | |
| Balance stab. margin ● | | | | | | 0.09 | 0.22 | 0.14 | | | | 0.11 | | 0.15 | | | |
| Legs torque ● | 0.44 | 0.24 | 0.64 | 0.15 | 0.33 | | | | | | | | | | | | |
| Legs power ● | | 0.23 | 0.28 | 0.33 | 0.08 | | | | | | | | | | | | |
| Legs acceleration ● | 0.32 | 0.27 | 0.49 | | | | | | | | | | | | | | |
| Legs velocity ● | 0.17 | 0.45 | 1.25 | 0.74 | 0.09 | | | | | | | | | | | | |
| Legs position ● | | | | | | | | | | | | 0.14 | | 0.02 | | | 0.32 |
| LA torque ● | | | | | | | | | | | | | | | | 4.6 | 4.8 |
| LA power ● | | | | | | | | | | | | | | | | 2.1 | 0.40 |
| LA acceleration ● | 2.59 | 0.43 | 0.91 | | 0.16 | | | | 0.57 | | | | 8.9 | | 1.4 | | |
| LA velocity ● | 0.27 | | 0.22 | 0.59 | | | | | | | | 0.07 | 0.02 | | 0.99 | | |
| LA position ● | | | | | | | | | | | | | | | | | |
| RA torque ● | | | | | | 0.05 | | 0.11 | | | | 0.11 | | 0.06 | 0.83 | | 0.61 |
| RA power ● | | | | | | 0.40 | 0.13 | | | | | | | | | | |
| RA acceleration ● | | | | | | | 0.21 | | | | | | 16.7 | | | | |
| RA velocity ● | | | | | | 3.54 | 0.10 | 0.32 | 0.18 | 0.98 | | | | | 0.96 | | |
| RA position ● | | | | | | | | 0.15 | 0.20 | | | 0.05 | | 0.07 | 0.15 | | 1.1 |
| Back torque ● | | | | 0.15 | | | 0.08 | | | 0.12 | 0.65 | 0.07 | | 0.07 | 0.44 | | 1.3 |
| Back power ● | | 0.05 | | 0.14 | | 0.30 | 0.13 | 0.14 | 0.08 | 0.16 | 0.58 | | | | 0.84 | | |
| Back acceleration ● | | | | | | 0.27 | | 0.20 | | 0.12 | | | 6.9 | | 2.5 | | |
| Back velocity ● | | | | | | 0.49 | 0.15 | 0.17 | | 0.14 | | | | | 2.2 | | |
| Back position ● | | | | | | 0.05 | | 0.19 | 0.10 | 0.17 | | 0.05 | | 0.18 | 0.10 | | |
| % of total variance | 77 | 81 | 82 | 79 | 70 | 83 | 72 | 80 | 75 | 80 | 77 | 81 | 86 | 83 | 81 | 80 | 82 |

[1] Follow straight line roughly
 0.1m/s average velocity - 36N force down

[2] Follow straight line roughly
 0.5m/s average velocity - 5N force down

[3] Follow square path accurately
 0.065m/s average velocity - No force

[4] Push 100N RH along X axis - No RH movement

[5] Bend whole body forward - Lean on table LH

[6] Pick up 3kg object RH - Move it 60cm
 Lean on table LH

FTR: force transmission ratio
VTR: velocity transmission ratio

RH: right hand
LH: left hand
RA: right arm
LA: left arm

Figure 5.4: Ergonomic indicators identified as relevant based on their variance, for each activity. An indicator is relevant for a given activity when the corresponding square is colored. The number in the square is the value of the variance, computed on the scaled indicator. The number at the bottom of each column corresponds to the total percentage of variance explained by the selected indicators. The red-green-blue colors do not have any particular meaning, they only aim at helping the reading of the table.

| | Discriminating indicator | | Influential parameters | | |
|---|---|---|---|---|---|
| **Phase 2 Walk sideways** | Kinetic energy | | Step length | Manikin height | Manikin BMI |
| | min | 0.7 | 0.2 m | 1.65 m | 21 kg.m$^{-2}$ |
| | max | 3.4 | 0.4 m | 1.80 m | 27 kg.m$^{-2}$ |
| **Phase 13 Fast trajectory tracking** | RA acceleration | | Robot mass | Manikin BMI | |
| | min | 18 | 2 kg | 21 kg.m$^{-2}$ | |
| | max | 39 | 10 kg | 27 kg.m$^{-2}$ | |
| **Phase 15 Push 100N** | RA torque | | Pelvis orient. | Amplification | |
| | min | 1 | 0° | 3 | |
| | max | 9 | 30° | 1 | |
| **Phases 16-19 Bend forward with support** | LA torque | | Manikin height | Manikin BMI | |
| | min | 4 | 1.65 m | 21 kg.m$^{-2}$ | |
| | max | 12 | 1.80 m | 27 kg.m$^{-2}$ | |

Figure 5.5: Values of the most influential parameters associated with the extreme values of the most discriminating ergonomic indicator, in four typical phases. The indicators minimum and maximum values are displayed, with the corresponding parameters values. The indicators are scaled (see section 5.1.4.2), therefore there is no unit. RA (resp. LA) stands for right (resp. left) arm.

### 5.2.2.2   Analysis of parameters influences

Tables 5.2, 5.3, 5.4 and 5.5 display Sobol first order and total indices computed for the most discriminating indicator, in four different activities. These activities have been chosen because the most discriminating indicator can be clearly identified (*i.e.* its variance is distinctly superior to the others). The parameters values for which the most discriminating indicator takes extreme values are displayed in Fig. 5.5. Only the most influential parameters of each activity are considered. The lower and upper extreme values of an indicator are defined by its 5th and 95th percentiles values.

As an illustration, a snapshot of the simulation of activity 13 in four different situations (different values of the parameters) is displayed in Fig. 5.6, along with the evolution of the most discriminating indicator[3].

**Walking sideways:**   In activity 2, kinetic energy is mostly affected by the step length. Upper (resp. lower) values of the kinetic energy corresponds to a long (resp. short) step length. Indeed, the duration of one step is imposed, so the bigger the step length, the faster the leg trajectory. Besides, a faster step is more disturbing for the balance. Therefore it leads to more motion of the whole body, which also increases the kinetic energy. The manikin height and BMI also have a significant (though

---

[3]A video of the full simulation is available here: `http://pages.isir.upmc.fr/~padois/website/fichiers/videos/maurice_humanoids_2014.mp4`
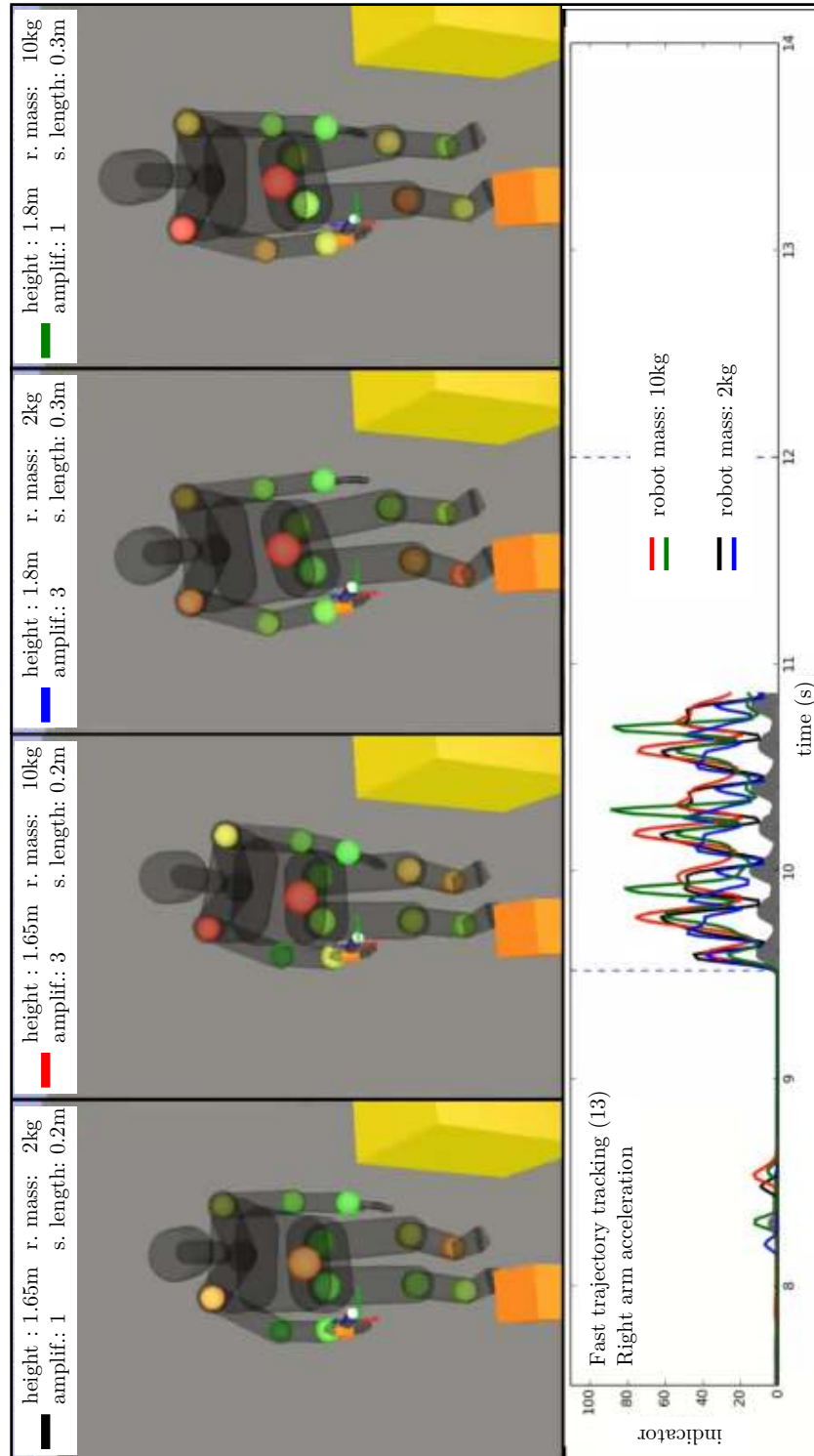
Figure 5.6: Simulation of the fast trajectory tracking activity 13 (defined in Fig. 5.4), in four different situations. The values of the parameters which differ from one situation to another are displayed in the picture (the other parameters are constant): the manikin height, the strength amplification coefficient $\alpha$, the mass of the robot abstraction $M_r$ and the step length. The colored spheres represent the level of torque solicitation in the manikin joints.

weaker) influence on the kinetic energy. Upper values of this indicator correspond to a tall/corpulent manikin. This is consistent with the indicator formula, since the mass of the manikin increases with its height and BMI.

|  | First order index | | Total index | |
|---|---|---|---|---|
| **Parameter** | $n = 2000$ | $n = 1001$ | $n = 2000$ | $n = 1001$ |
| manikin height | **0.17** | **0.14** | **0.23** | **0.26** |
| manikin BMI | **0.15** | **0.18** | **0.21** | **0.20** |
| step length | **0.52** | **0.51** | **0.59** | **0.59** |
| joint limits | $\mathbf{10^{-3}}$ | $\mathbf{10^{-3}}$ | **0.05** | **0.08** |
| reference positions | $\mathbf{10^{-4}}$ | $\mathbf{10^{-4}}$ | **0.04** | **0.06** |
| pelvis orientation | $\mathbf{10^{-3}}$ | $\mathbf{10^{-3}}$ | **0.08** | **0.10** |
| robot mass | $\mathbf{10^{-3}}$ | $\mathbf{10^{-3}}$ | **0.04** | **0.07** |
| amplification coefficient | $\mathbf{10^{-4}}$ | $\mathbf{10^{-3}}$ | **0.04** | **0.05** |

Table 5.2: Sobol indices for the kinetic energy indicator (most discriminating), during the walking sideways activity 2. The indices are computed with the extended FAST method, and two sample sizes are compared, $n = 1001$ and $n = 2000$. Numbers are colored from blue (minimum) to red (maximum), to facilitate the reading.

**Fast trajectory tracking:** In activity 13, the right arm acceleration is mostly influenced by the robot mass. Upper (resp. lower) values of this indicator corresponds to a heavy (resp. light) robot. This is due to the robot inertia driving the manikin arm when the direction of motion changes. The right arm acceleration indicator is also significantly affected by the manikin BMI, and upper values of this indicator correspond to a corpulent manikin. Contrarily to the robot mass, the influence of the manikin BMI on the arm acceleration is not obvious, and could not be figured out without the sensitivity analysis.

**Pushing:** In activity 15, the right arm torque indicator is mostly affected by the pelvis orientation. Upper values of the indicator correspond to a high angle between the manikin and the work area. This indicator is also affected - though to a lesser extent - by the force amplification coefficient, with upper values of the indicator corresponding to the strongest amplification. The effect of the amplification coefficient is simple, since the bigger the amplification provided by the robot, the smaller the force left to the manikin to exert. On the contrary, the effect of the pelvis orientation is much less obvious. In modifying the manikin posture, the pelvis orientation parameter necessarily affects the joint torques, both because of gravity effects and because of easiness of external force exertion. The latter phenomenon is probably dominant here, since the force transmission ratio along the pushing direction significantly varies (it is identified as the second most discriminating indicator). However, the importance of the pelvis orientation influence relatively to other parameters (such as force amplification) can hardly be *a priori* estimated.

| | First order index | | Total index | |
|---|---|---|---|---|
| **Parameter** | $n = 2000$ | $n = 1001$ | $n = 2000$ | $n = 1001$ |
| manikin height | 0.07 | 0.07 | 0.13 | 0.13 |
| manikin BMI | 0.17 | 0.13 | 0.25 | 0.24 |
| step length | $10^{-3}$ | $10^{-3}$ | 0.06 | 0.07 |
| joint limits | 0.03 | 0.04 | 0.11 | 0.12 |
| reference positions | 0.03 | 0.03 | 0.06 | 0.08 |
| pelvis orientation | 0.05 | 0.06 | 0.16 | 0.20 |
| robot mass | 0.25 | 0.28 | 0.44 | 0.47 |
| amplification coefficient | 0.03 | 0.03 | 0.14 | 0.15 |

Table 5.3: Sobol indices for the right arm joint acceleration indicator (most discriminating), during the fast trajectory tracking activity 13. The indices are computed with the extended FAST method, and two sample sizes are compared, $n = 1001$ and $n = 2000$. Numbers are colored from blue (minimum) to red (maximum), to facilitate the reading.

| | First order index | | Total index | |
|---|---|---|---|---|
| **Parameter** | $n = 2000$ | $n = 1001$ | $n = 2000$ | $n = 1001$ |
| manikin height | 0.11 | 0.11 | 0.12 | 0.13 |
| manikin BMI | 0.04 | 0.04 | 0.05 | 0.05 |
| step length | 0.03 | 0.02 | 0.04 | 0.04 |
| joint limits | $10^{-3}$ | $10^{-3}$ | 0.02 | 0.02 |
| reference positions | $10^{-4}$ | $10^{-3}$ | 0.01 | 0.01 |
| pelvis orientation | 0.53 | 0.51 | 0.59 | 0.58 |
| robot mass | $10^{-4}$ | $10^{-4}$ | $10^{-3}$ | $10^{-3}$ |
| amplification coefficient | 0.19 | 0.17 | 0.21 | 0.20 |

Table 5.4: Sobol indices for the right arm joint torque indicator (most discriminating), during the pushing activity 15. The indices are computed with the extended FAST method, and two sample sizes are compared, $n = 1001$ and $n = 2000$. Numbers are colored from blue (minimum) to red (maximum), to facilitate the reading.

**Bending:** In activities 16-17, the left arm torque indicator is significantly affected by the manikin height and BMI. Upper values of this indicator correspond to a tall/corpulent manikin. While bending, the manikin leans on a table with its left arm to help keep its balance. But the table height remains unchanged, so the taller the manikin, the more it has to bend to reach the table. This results in a more horizontal posture of its trunk, and therefore in more weight to support on its leaning arm. Besides, for a similar posture, a more corpulent manikin results in more weight supported by the left arm. Hence a higher left arm torque indicator, since the torque capacity remain constant whatever the manikin physical features.

|  | First order index | | Total index | |
|---|---|---|---|---|
| Parameter | $n = 2000$ | $n = 1001$ | $n = 2000$ | $n = 1001$ |
| manikin height | **0.30** | **0.29** | **0.36** | **0.36** |
| manikin BMI | **0.26** | **0.27** | **0.31** | **0.33** |
| step length | **0.10** | **0.10** | **0.15** | **0.17** |
| joint limits | **0.05** | **0.03** | **0.11** | **0.09** |
| reference positions | **0.02** | **0.03** | **0.10** | **0.12** |
| pelvis orientation | **0.04** | **0.04** | **0.09** | **0.09** |
| robot mass | $\mathbf{10^{-4}}$ | $\mathbf{10^{-4}}$ | **0.02** | **0.04** |
| amplification coefficient | $\mathbf{10^{-4}}$ | $\mathbf{10^{-4}}$ | **0.03** | **0.04** |

Table 5.5: Sobol indices for the left arm joint torque indicator (most discriminating), during the bending with left arm support activities 16-17. The indices are computed with the extended FAST method, and two sample sizes are compared, $n = 1001$ and $n = 2000$. Numbers are colored from blue (minimum) to red (maximum), to facilitate the reading.

The values of Sobol indices computed with the FAST method are quite similar whether a sample size of 1001 or 2000 is used. Only four activities are presented here but the results are similar for all the other simulated activities. The difference between the percentage of variance due to an input (first order or total) estimated with both sample sizes is always smaller than $5\,\%$. Therefore it seems that the recommended sample size (1001 for 8 parameters) is sufficient to ensure the convergence of the results and correctly estimate Sobol indices for the current application. Since the similarity of the results is verified for many different activities, this conclusion can probably be generalized to all co-manipulation power activities.

### 5.2.2.3   Analysis of specific phenomena

The results discussed in the previous section are mostly consistent with what could be expected. However Fig. 5.4 also displays some less straightforward results which require further explanation. They are detailed thereafter.

**Force/Velocity transmission ratio (FTR/VTR):**   As mentioned in section 3.1.3.2, the FTR is only ergonomically meaningful when a contact force is exerted in the considered direction (*e.g.* pushing activity 15). However it has no physical meaning when no contact force is exerted with the corresponding body part, *i.e.* the right hand in activities 1, 9, 10 and 11. The same remark applies to the velocity transmission ratio (VTR). Therefore, the fact that the VTR indicator is never selected as relevant could be due to the directions along which it is calculated. Most of the time, the hand motion is not solely along one of the 3 main directions (X,Y,Z). It would be more meaningful to compute the VTR along the hand direction of motion, and the FTR too since the right hand drags the robot.

**Arm indicators in walking activities:** The results of most walking/stepping activities are at first counter-intuitive. The left arm dynamic indicators are often very discriminating (large variance), sometimes more than the legs indicators. This actually highlights a balance problem. The stability of the stepping is strongly affected by the input parameters. So for some combination of their values, the manikin is very unstable and performs bracing motions to help regain balance. Since the feet positions and trajectories are imposed, the arm motions which are not constrained are in comparison much more diverse. The left arm is more affected because the robot inertia on the right arm slows the arm motions down. The balance-related indicators are not necessarily strongly affected by this phenomena, because the arms bracing can be sufficient to keep the ZMP trajectory quite unchanged between different situations. Therefore they do not appear in the discriminating indicators. However, though these results are physically meaningful, the balance loss might result more from a control problem (humanoid balance for dynamic movements), than from a truly unstable situation for a human being.

**Head dexterity:** This indicator is never selected as discriminating, but this is likely due to a limitation of the simulation framework. The potential visual occlusions due to the robot or the environment are not simulated in this work. Therefore the head position is not strongly affected by the various input parameters, so the vision is quite similar from one situation to another.

### 5.2.3 Discussion

The physically consistent results validate the analysis method proposed in this work. For very typical activities, some of the conclusions are qualitatively expected. However, this experiment also demonstrates that the proposed analysis highlights and, most importantly, ranks some non trivial phenomena (*e.g.* major influence of the pelvis orientation in the pushing activity). Such phenomena can be explained afterwards, but they cannot be quantified *a priori*. Besides, the results presented above focus on the ergonomic indicators which are identified as most discriminating when considering all the parameters, but Sobol indices can be estimated for all indicators. Such an analysis is particularly useful if the final purpose is the comparison of quite similar collaborative robots. For instance, if two cobots which differ only by their mass are to be compared, the most informative indicators are the ones which are significantly affected by the mass parameter.

However the application of the proposed method to the comparison of collaborative cobots for industrial activities should be considered carefully because of some current limitations which are discussed thereafter.

#### 5.2.3.1 Realism of the manikin behavior

Beyond the consistent results, this experiment also highlights some limitations of the current analysis, through several non-expected phenomena (*e.g.* arm dynamic

indicators in walking activities). Since the ergonomic indicators are analyzed based on a virtual human simulation, the ergonomic relevance of the results strongly depends on the realism of the manikin motions and forces. The limitations of the manikin discussed in section 4.4 therefore directly affect the current analysis. Nevertheless if the results of this analysis strongly depend on the realism of the manikin model and behavior, the methodology itself is independent from the manikin model and control. Thus, an improved manikin could be used (*e.g.* a control law generating more realistic motions, and/or a biomechanical model including muscles), while the indicators analysis method remains the same.

### 5.2.3.2 Segmentation of the activity

Another limitation of the current analysis is due to the time-integral form used for the ergonomic indicators. The method requires that, for a given situation, each ergonomic indicator is represented by a unique value (its time-integral value). This hypothesis makes sense here, because only elementary activities are considered. On the contrary industrial activities that could be addressed with collaborative robots are generally complex. They should not be regarded as one and only activity, but rather as a succession of elementary activities. The value of an ergonomic indicator may vary significantly from one elementary activity to another, so summarizing an indicator with its time-integral on the whole activity can result in a considerable loss of information. Instead, a complex activity could be segmented in several elementary phases, in order to select discriminating indicators separately for each phase.

If the rough identification of the main phases can be done manually by the user, defining the limit between two phases is more difficult. Indeed the first phase often affects the following one, therefore defining the limit between both phases when the second motion starts may not be optimal with respect to the selected indicators. This is especially true for post-walking phases. The end of the walking represents a strong change in the global dynamic of the body. This change, which happens at the end of the walking phase, can disturb the balance and therefore have consequences in the next phase because regaining balance is not immediate. To illustrate this phenomenon, activities 3 (step forward) and 9 (reach 4) of Fig. 5.4 are concatenated and simulated as one single activity. Fig. 5.7 displays the ergonomic indicators that are identified as discriminating for each time step of this two phases (the instantaneous values of the indicators are considered here, instead of their time-integral values). The limit between both phases is chosen as the moment when the objectives in the manikin controller change. No modification in terms of the selected indicators happens at the pre-defined limit (red line on Fig. 5.7). On the contrary, the fact that the same indicators are selected around the transition (pink zone in Fig. 5.7) suggests that the biomechanical solicitations during the transition are specific. Therefore the transition should be considered as a distinct phase. But the duration of the transition phase strongly depends on the features of the first phase and cannot be known beforehand. Therefore the segmentation

of the activity in phases should rather be automatic and based on the evolution of the indicators relevance. However, choosing a meaningful criterion to automatically identify different phases in a activity is not straightforward. As depicted in Fig. 5.7, a segmentation based only on a change in the set of discriminating indicators is not possible, because it leads to far too many phases.
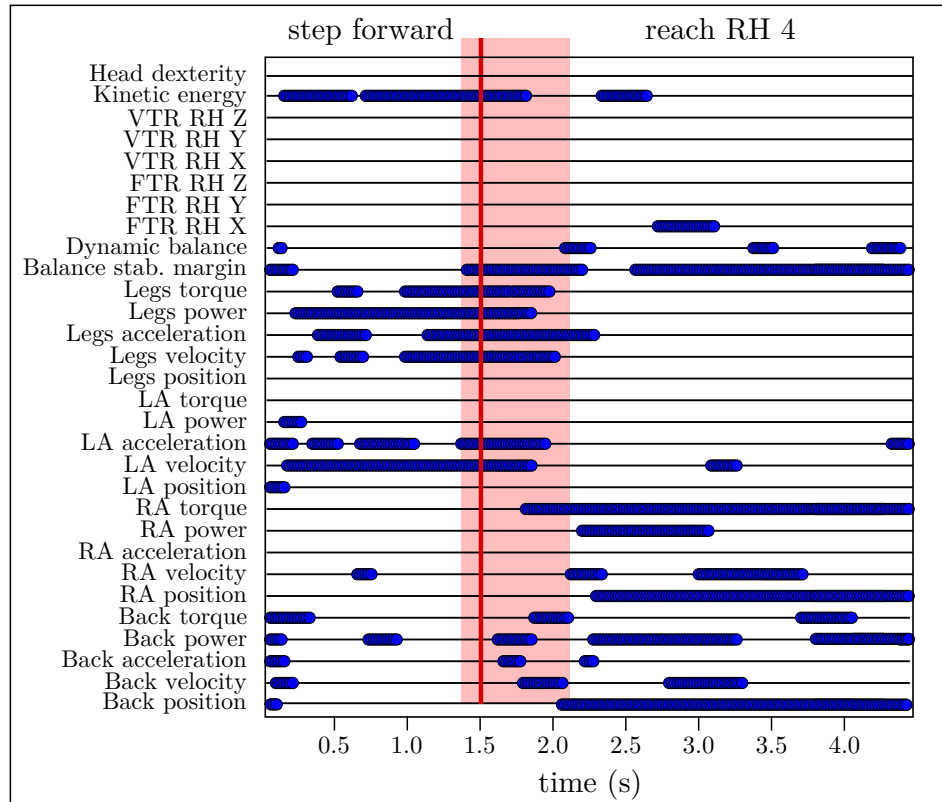


Figure 5.7: Ergonomic indicators identified as discriminating for each time step of tasks 3 and 9 played as a unique complex task (the instantaneous values of the indicators are considered). A blue dot on an indicator line means that this indicator is relevant for the corresponding time step. The red line is the limit between the tasks used in this work. The pink zone represents the transition phase in which the selected indicators remain quite the same.

Nonetheless, whether the activity should be segmented or not mainly depends on the goal of the analysis. If the purpose is to analyze some specific phenomena in details, segmenting the activity probably leads to more accurate results. However, if the purpose is to select relevant indicators to decide between different collaborative robots, the segmentation is not desirable. Indeed, the whole activity must be considered when choosing a cobot over another, because the cobot cannot be changed during the task execution. If the activity is divided into several phases, the global ergonomic situation is represented by all the relevant indicators in each phase, which dramatically increases the number of indicators. The advantage of

identifying a few relevant indicators to facilitate the user's interpretation of the results is therefore lost.

## 5.3   Application to an industrial activity

In the previous section, the method for analyzing the sensitivity of ergonomic indicators is applied to many elementary activities in order to validate it. The same method is now applied to an activity more representative of industrial jobs: the drilling task studied in section 4.1. The purpose of this application is double:

- Demonstrate the usefulness of the proposed method for real activities.

- Identify the most informative indicators for the drilling activity.  They are needed in chapter 6 for the optimization of a cobot for this activity.

### 5.3.1   Simulation set-up

The drilling activity studied in section 4.1 is considered in this experiment.  The main purpose of the present analysis is to identify discriminating indicators, which will then be used to select a well-adapted collaborative robot to help workers perform the considered activity.  Therefore, though the activity is clearly composed of different phases (mainly drilling and moving from one hole to the other), it is not segmented in different phases but considered as a whole, so as to limit the overall number of indicators.

#### 5.3.1.1   Activity simulation

The activity consists in drilling six holes consecutively in a vertical slab, with a portable drill.  The distribution of the six holes is the same as in section 4.1, but this time the order in which they are drilled is fixed.

The activity is simulated with the autonomous virtual manikin, animated according to the technique detailed in section 3.2.2.  The following tasks are included in the manikin controller, in decreasing order of importance:  balance, right hand manipulation (trajectory and force), gazing, posture and torques minimization.  The left hand is not used in this drilling activity, and the manikin feet are fixed all along the simulation[4].  The drilling itself is represented by a trajectory to follow (right hand operational acceleration task), and a force to exert (right hand operational force task).  An average hand trajectory (position and duration) as well as profile and magnitude of the drilling force is estimated from the data of the five human subjects.  The right hand acceleration task is active throughout the whole simulation, whereas the right hand force task is only active when a drilling force must be exerted.  The drilling force is introduced and removed gradually, instead of suddenly turning the force task on or off.  However, only the force in the drilling direction is

---

[4]The term *fixed feet* means that the manikin is not asked to move its feet during the simulation. However the ground-feet contact remains an unilateral contact.

simulated. The weight of the drill is supposed to be supported by the collaborative robot, and the other forces normal to the drilling direction are neglected.

The kind of collaborative robots that are considered for such an activity provide strength amplification. However, the amplification is active only during the drilling phases. It is deactivated during the free space phases. The robot weight is always compensated, but not the inertial effects.

### 5.3.1.2 Parameters

The parameters which represent the diversity of cobots and workers are almost similar to those used for the validation of the analysis method. The step length is removed from the parameters list, since there is no walking phase in the drilling activity. The pelvis orientation ranges here from $-30°$ (instead of $0°$) to $30°$. The position of the pelvis parallel to the drilling area (X direction on Fig. 4.1) is modified depending on the pelvis orientation, so that whatever this orientation, the manikin is always approximately facing the drilling area. Eventually, a second parameter is added for the pelvis pose. It represents the horizontal distance between the pelvis and the center of the drilling area. However, rather than a metric distance, it is defined as a percentage of the manikin arm length. A *far* position is therefore far whatever the height of the manikin. The other parameters (and their upper and lower bounds) remain unchanged. The total number of parameters is therefore 8, as in the validation activities. Since a sample size of 1001 (minimal value requested to prevent aliasing) was found to be sufficient for correctly estimating Sobol indices in the case of 8 inputs (see section 5.2.2.2), this value is also used here.

### 5.3.2 Results

All the ergonomic indicators presented in table 3.1 are included in this study. However, as in the previous experiment, the velocity and force transmission ratio of the left hand are excluded, because the left hand is not used for any manipulation or force task. The force transmission ratio of the right hand is computed along the direction of drilling, and along the direction of motion, since they are the two directions in which a force must be exerted (drilling force and force for dragging the robot).

Five ergonomic indicators are identified as discriminating according to the Kaiser criterion, out of 27 indicators in the initial list (table 5.6). These five indicators together represent $80\%$ of the total variance information, therefore only little information is lost by not considering the other indicators. The five relevant indicators are, in decreasing order of variance: the legs joint position indicator, the right arm joint torque indicator, the back joint torque indicator, the force transmission ratio of the right hand along the drilling direction, and the right arm joint position indicator. The absence of any velocity or acceleration indicators seems consistent, given the fact that the drilling activity does not require fast motions. The selection of upper-body (right arm, back) force and position related indicators is not surprising.

However, the presence of the legs joint position indicator as the most discriminating indicator is less expected.

| | | Relevant ergonomic indicators | | | | |
| --- | --- | --- | --- | --- | --- | --- |
| | | 1 | 2 | 3 | 4 | 5 |
| | | Legs position | Right Arm torque | Back torque | FTR RH drilling | Right Arm position |
| **Parameters** | Manikin height | $10^{-3}$ | 0.13 | 0.19 | 0.42 | 0.07 |
| | | 0.03 | 0.15 | 0.29 | 0.52 | 0.12 |
| | Manikin bmi | $10^{-3}$ | 0.05 | 0.02 | 0.21 | $10^{-5}$ |
| | | 0.02 | 0.06 | 0.03 | 0.23 | 0.02 |
| | Pelvis orientation | $10^{-4}$ | 0.10 | 0.01 | 0.15 | 0.15 |
| | | 0.01 | 0.14 | 0.03 | 0.23 | 0.28 |
| | Pelvis distance | $10^{-3}$ | $10^{-4}$ | 0.01 | 0.02 | 0.03 |
| | | 0.01 | 0.02 | 0.02 | 0.03 | 0.12 |
| | Upper body ref. position | 0.60 | 0.20 | 0.56 | 0.08 | 0.23 |
| | | 0.73 | 0.22 | 0.69 | 0.10 | 0.42 |
| | Upper body joint limits | 0.26 | 0.01 | 0.06 | $10^{-3}$ | 0.28 |
| | | 0.37 | 0.03 | 0.10 | 0.02 | 0.43 |
| | Robot mass | $10^{-4}$ | $10^{-6}$ | $10^{-5}$ | $10^{-6}$ | $10^{-5}$ |
| | | $10^{-3}$ | $10^{-3}$ | $10^{-3}$ | $10^{-3}$ | 0.02 |
| | Amplification coefficient | $10^{-4}$ | 0.46 | $10^{-5}$ | $10^{-4}$ | $10^{-5}$ |
| | | $10^{-3}$ | 0.49 | $10^{-3}$ | $10^{-3}$ | 0.02 |

Table 5.6: Sobol indices for all five ergonomic indicators identified as relevant (according to the Kaiser criterion), for the drilling activity. For each parameter and indicator, the upper value is the first order index, the lower value is the total index. The ergonomic indicators are presented in decreasing order of importance (decreasing variance) from left to right: the numbers above their names correspond to their ranks. FTR stands for force transmission ratio, and RH for right hand. Numbers are colored from blue (minimum) to red (maximum), to facilitate the reading.

In order to analyze the relevant indicators in more details, Sobol first order and total indices are computed for all parameters and for each one of the five relevant indicators. Their values are displayed in table 5.6. Among the results presented in this table, some are strongly expected, which confirms the consistency of the proposed analysis. For instance, the right arm joint torque indicator is significantly affected by the strength amplification coefficient, because this coefficient modifies the required drilling force exerted with the right hand. Another straightforward example is the influence of the upper-body geometric parameters (reference position and joint limits) on the right arm joint position indicator. However, the sensitivity analysis also highlights some less straightforward effects. Quite unexpectedly, the legs position indicator is not affected by the pelvis position and orientation relative to the drilling area. However, it is strongly affected by the two other parameters

which represent the potential geometric interference of the robot with the worker: upper body reference position and joint limits (this phenomenon might be due to the fact that the manikin cannot move its feet during the activity, see section 4.4.2). The fact that the strength amplification coefficient does not affect the back torque indicator is also unexpected. Another example of non-straightforward effect is the non-negligible influence of the manikin body mass index on the force transmission ratio.

### 5.3.3  Discussion

The previous results demonstrate the consistency (on typical cases) and the usefulness (for less straightforward effects) of the proposed analysis. Beyond the analysis of detailed phenomena enabled by the proposed sensitivity analysis, the previous results also highlight two global trends.

Firstly, the robot mass has no influence on any of the discriminating indicators. Given that these indicators represent $80\,\%$ of the total variance information, the robot mass seems to be an insignificant parameter regarding the ergonomy of the drilling activity. This phenomenon is probably due to the fact that the motions in the drilling activity are quite slow. Given the fact that the robot weight is fully compensated, the robot mass affects the worker only through inertial effects. The inertial effects of the robot depend on its mass, but also on the velocity and acceleration of the motion. So slow motions lead to very limited inertial effects, even when the robot is heavy. When designing a collaborative robot for the drilling activity, the mass of the robot is therefore not a critical parameter, from an ergonomic point of view. This conclusion should however be considered cautiously, since some phenomena are not modeled in the simulation. In particular, dry friction in the robot joints, which increases with the robot mass, is not included in the robot representation. Yet, dry friction increases the effort required from the worker to set the robot in motion (or the energy consumption, if the dry friction is partly compensated). Besides, the robot mass could also be a constraint for the robot designer for non ergonomic reasons, *e.g.* the energy consumption (the heavier the robot, the more torque is required from the actuators to compensate the robot weight).

Secondly, all the discriminating indicators (except the force transmission ratio) are significantly affected by at least one of the parameters representing the geometric interference of the robot with the worker (especially the upper-body reference position and joint limits). This shows that, for the drilling task, the morphology of the robot is critical regarding the ergonomic benefit provided by a collaborative robot.

## 5.4  Conclusion

In this chapter, a method for analyzing the relevance of ergonomic indicators in regard to any given co-manipulation activity is presented. The analysis must be independent from the robot design, therefore many different cobots must be tested.

To this purpose, a collaborative robot is represented by a set of parameters corresponding to its effects on the user. The theory of the design of experiments is used to explore the parameters space efficiently. For each situation (*i.e.* each combination of the parameters values), the activity is simulated with the fully autonomous virtual manikin, in order to compute the values of all ergonomic indicators. The ergonomic indicators are then ranked according to their variance, so that the most discriminating indicators (biggest variance) are easily identified. A sensitivity analysis is performed on the most discriminating indicators: Sobol indices are computed for all the robot parameters, thus providing quantitative informations on the influence of each parameter.

The proposed method is validated on various elementary activities, such as reaching, walking, exerting forces, following a trajectory... Between 3 and 9 indicators are selected in each activity, out of a list of 30 indicators. The selected indicators and influential parameters are for the most part in accordance with intuitive ergonomic considerations. Results also highlight some less straightforward phenomena.
    When a more complex activity is considered, a more accurate analysis can be achieved by segmenting the activity into several phases. However, it is demonstrated that finding an optimal segmentation with respect to the relevance of the ergonomic indicators is not straightforward, and should probably be done automatically.

The method is then applied to a drilling activity. The results highlights the significant influence of the robot morphology on the ergonomic benefit provided by the cobot. Therefore the morphology of the robot should be optimized with respect to this ergonomic objective. This is the subject of the next chapter.

Thanks to the proposed analysis method and to the previously developed simulation framework, the relevance of ergonomic indicators can be evaluated with only very few external data. For instance, there is no need for many subjects to perform the task, since all the situations are created and simulated automatically. Furthermore, though it is applied here to co-manipulation activities, the same method can apply to a wider class of manual activities. It only requires the modification of some input parameters. Finally, beyond the analysis of ergonomic indicators, the proposed framework could be used for other applications which require to perform a task in many different ways. Indeed, the association of designs of experiments with a framework for automatic virtual human simulation enables the generation of a huge amount of data from a very limited input.

# Chapter 6

# Evolutionary design of a cobot morphology

## Contents

In the previous chapters, a methodology for comparing the ergonomic benefit provided by different collaborative robots is presented. One possible application of this method is the optimal design of a collaborative robot. As stated in chapter 1 the efficiency of a particular cobot is highly task-dependent. Non task-specific cobots do exist, in particular exoskeletons which enable many different gestures thanks to their anthropomorphic structure. However, generic systems are complex and expensive, and not necessarily well-adapted to the task of interest. Therefore it is often preferable to design a dedicated cobot specifically for the considered task.

Contrarily to classic robot design, a collaborative robot must be optimized not only with respect to the task, but also with respect to the worker. That is, a cobot

should be designed to decrease at best the risk of developing MSDs. The evaluation framework developed in this work provides a solution to rank different robot candidates in regard to this ergonomic objective. However, designing and modifying test candidates is left to the robot designer, which has to rely on his/her experience and preliminary studies. This process is both time and resource intensive. Besides, the final design is partly limited to the experience of the designer, and might therefore be suboptimal. This is all the more true in collaborative robotics, because it is a rather new approach. So experience in this field is limited, especially regarding the ergonomic aspect. To circumvent these problems, optimization techniques can be used for the evolution of the robot design. This chapter therefore presents a method for automatically generating optimal cobot designs for a specific task. This method is based on genetic algorithms, and on the cobots evaluation framework detailed in the previous chapters.

Generally the word *design* represents both the structure (or morphology) of the robot, and its control law. Mechanical and control parameters all affect the ergonomic benefit provided by a cobot, as highlighted in sections 4.3 and 5.3. Therefore both the morphology and the control law should be optimized, preferably together since their effects on the worker are not independent. However, co-evolution of structure and control leads to a high number of variables in the optimization problem, especially if complex control laws are considered. In order to limit the complexity of the problem - hence the convergence time - only the optimization of the robot morphology is addressed in this work. It should be noted that the purpose of such an optimization is not to replace the designer, but rather to provide a preliminary design of an optimal cobot: the output of the optimization constitutes a starting point for the designer's work.

The work presented in this chapter is extensively based on the work of P. Schlehuber during his master's project [Schlehuber 2015]. He developed a genome, genetic operators and a genotype to phenotype translation suitable for representing collaborative robots (section 6.2). He also implemented the coupling between Sferes$_{v2}$ (genetic algorithms software) and XDE (simulation software).

## 6.1 Genetic algorithm for cobot optimization

Genetic algorithms (GA) are part of Evolutionary algorithms (EA) which gather all population-based optimization techniques inspired from biological evolution. Genetic algorithms were first introduced by Holland [Holland 1975], and later popularized by Goldberg [Goldberg 1989]. The general scheme of GAs is described in Fig. 6.1. It is based on natural evolution mechanisms such as inheritance, mutation, crossover, and selection.

GAs are used to approximate the solution to an optimization problem for which no exact method can provide a solution, at all or in a reasonable time. Indeed, GAs are well adapted for optimization over vast and non-continuous search spaces. They are therefore particularly interesting to address the problem of optimal robot

design [Doncieux 2011], especially as some GAs handle multi-objectives problems. GAs have already been applied to determine whole robot structure designs, *e.g.* [Chocron 1997, Leger 1999, Rubrecht 2011], however they have never been used for collaborative robot design.
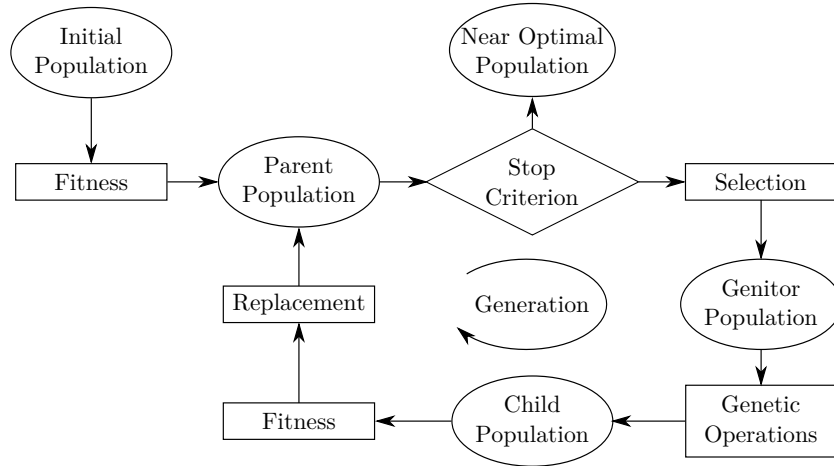


Figure 6.1: Genetic algorithm general scheme (image taken from [Rubrecht 2011]). A genitor population is created from the parent population through selection process. Genetic operations (mutation and crossover) are carried out on the genitor population to form the child population. The fitness function (*i.e.* objective to optimize) is evaluated on each individual of the child population. Then a replacement process is applied to create the next parent population, and a new generation loop begins. This loop is interrupted when a stop criterion is reached (optimality criterion or maximal number of generations).

## 6.1.1  Overview of the framework

The main concept of GAs is to select the best individuals in regard to some chosen features. Therefore, as depicted in Fig. 6.1, the replacement and selection processes are based on a fitness function which needs to be evaluated for each individual of the population. The fitness function represents the performance of the individual regarding the objective(s) to optimize. In this work (collaborative robotics for MSDs reduction), an important component of this performance corresponds to the ergonomic benefit provided by the robot. In order to measure this performance, a GA framework is therefore linked to the XDE simulation framework, as depicted in Fig. 6.2. For each robot individual, the task execution is simulated with the autonomous virtual manikin assisted by the robot, so that various ergonomic and task-oriented indicators can be evaluated. The evolutionary calculation part is performed with Sferes$_{v2}$ [Mouret 2010], a framework providing a lightweight C++ implementation of many common genetic algorithms. The different components of the whole optimization framework (Sferes$_{v2}$ linked with XDE) are detailed thereafter.
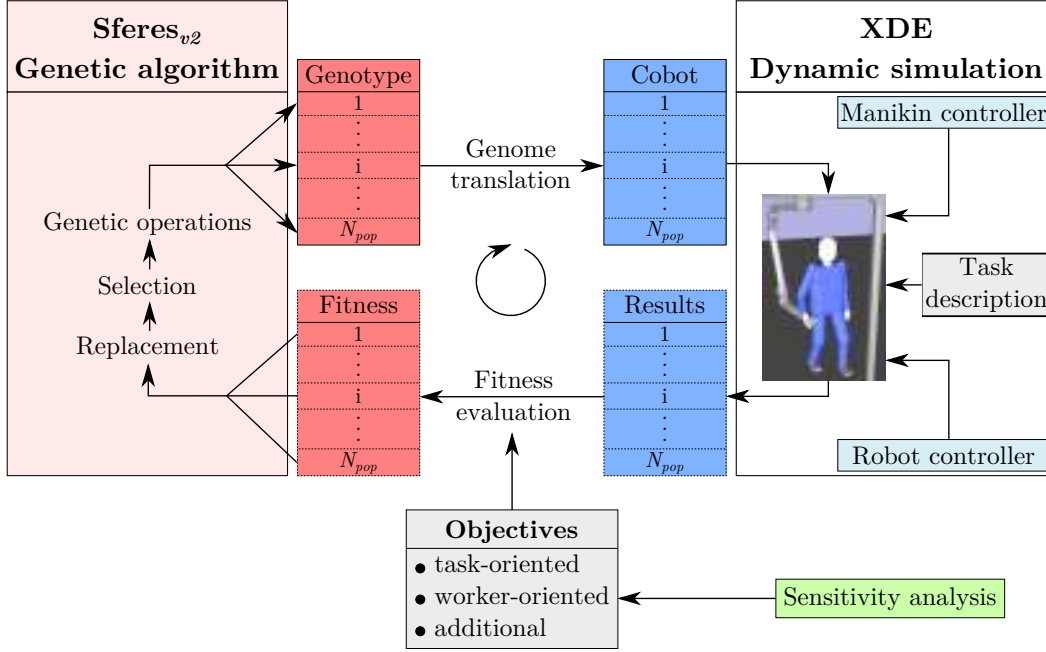
Figure 6.2: Framework for the optimization of cobots design: XDE-Sferes$_{v2}$ coupling (only one generation loop is represented). The genetic operations are performed by the Sferes$_{v2}$ software, which provides a population of robot candidates to evaluate. For each candidate, the objectives are measured through an XDE simulation. The objectives include worker-oriented objectives (*i.e.* the ergonomic benefit provided by the collaborative robot), task-oriented objectives (*i.e.* quality of task execution) and additional objectives (*e.g.* cost, complexity...). In order to reduce the overall number of objectives, only the most discriminating ergonomic indicators are included in the worker-oriented objectives (according to the analysis method describes in chapter 5).

### 6.1.2   Multi-objective genetic algorithm

Optimal cobot design is a multi-objective problem, since the robot must be optimized regarding both the task and the worker, and potentially other aspects such as the cost or the complexity of the structure. Moreover, each one of these general objectives can be divided in several specific objectives. For instance the ergonomic benefit provided to the worker can be evaluated through multiple indicators (see section 3.1.4). The fitness function of multi-objective optimization can therefore be written as a vector:

$$\mathbf{f} = \begin{pmatrix} f_1 \\ \vdots \\ f_{N_{obj}} \end{pmatrix} \tag{6.1}$$

where each component $f_i$ corresponds to a single objective, with $N_{obj}$ the total number of objectives. However a multi-variate fitness function raises the question of the comparison between individuals. A weighted sum approach can be applied to

form a single fitness value, but it forces the user to prioritize the different and possibly conflicting objectives. Besides it results in a single optimal solution, whereas multiple objectives naturally lead to a set of optimal solutions. To overcome these limitations, the notion of Pareto optimality is commonly used. A solution $x$ to the optimization problem dominates another solution $x'$ if (assuming the objectives must be maximized):

$$\exists i \text{ such as } f_i(x) > f_i(x') \tag{6.2}$$

and:

$$\forall j \neq i, \ f_j(x) \geq f_j(x'). \tag{6.3}$$

Based on this principle, the individuals are sorted in different non-dominant groups, called Pareto fronts. Within a group, no individual dominates another, and in the absence of any further information, no individual can be said to be better than another. The set of individuals that are not dominated at all form the solutions to the optimization problem (Pareto-optimal solutions). The user can then choose one solution over the others, depending on his main concern.

In order to approach the Pareto-optimal front at best, two aspects must be considered: convergence (minimizing the distance between the final Pareto front, and the optimal front), and diversity (maximizing the difference in terms of objectives or parameters between the generated solutions). Among the various multi-objective GAs, the Non-dominated Sorting Genetic Algorithm-II (NSGA-II) addresses these two features efficiently, while limiting the input needed from the user [Deb 2002]. NSGA-II is therefore chosen in this work. This algorithm especially presents the following features: low computational cost, elitist approach, and parameter-less selection.

Elitism is the process of selecting the best solutions out of the combined parent and child populations. It guarantees that the solution quality obtained by the GA does not decrease from one generation to the next, and speeds up the performance of the algorithm. Let $N_{pop}$ be the population size (user-defined). To form the parent population of iteration $k+1$ (*Replacement* step in Fig. 6.1), NSGA-II first sorts all the $2N_{pop}$ individuals of the parent and child populations of iteration $k$ considered together, with respect to the Pareto dominance principle. The best Pareto fronts are entirely assigned to the next parent generation, until the number of individuals gets superior to the population size $N_{pop}$, as illustrated in Fig. 6.3. The extra individuals are then removed according to the crowding distance criterion, until exactly $N_{pop}$ individuals remain. The crowding distance criterion consists in preferring, within a same Pareto front, the most isolated individuals in the objectives space, so as to support exploration. This criterion leads to a widely spread population, therefore maintaining diversity. Besides, it has the advantage of not requiring any user-tuned parameter, contrarily to most other diversity criteria [Deb 2002].
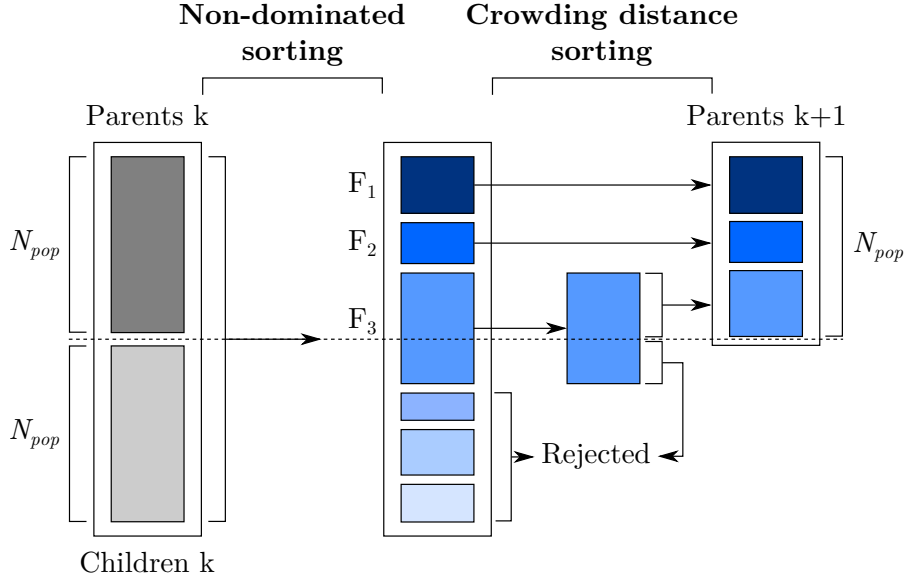
Figure 6.3: Formation of the next parent population according to the elitist approach (image adapted from [Deb 2002]). In NSGA-II, individuals are sorted first according to the Pareto dominance principle, and then, within a same Pareto front $F_i$, according to the crowding distance.

### 6.1.3 Number of objectives

NSGA-II, and multi-objective GAs in general, are designed to solve problems with multiple objectives. However, the number and properties of the objectives directly affect the convergence of the optimization. If $N_{obj}$ objectives are considered, the Pareto front can roughly be approximated by an hyper-surface of dimension $N_{obj}-1$. Therefore in order to maintain a similar resolution for the Pareto front approximation when the number of objectives increases, a number of individuals exponential in $N_{obj}$ is required. Besides, the relationships between the objectives affect the shape of the Pareto front and thus the complexity of the problem. Two objectives can be either independent (absence of influence between them), conflicting (impossibility to satisfy both of them simultaneously), or in harmony (both objectives have similar variations) [Purshouse 2003]. Independence and harmony only slightly affect the algorithm convergence, whereas conflict significantly worsens it. Therefore the number of objectives, and particularly of conflicting objectives, should be kept quite low, especially when the evaluation of one individual is computationally expensive. A general recommendation is to limit the number of conflicting objectives to three [Deb 2001].

As stated in section 6.1.2, when addressing collaborative robots design, the objectives can be classified into three families: worker-oriented (ergonomic benefit), task-oriented (quality of task execution) and additional objectives (*e.g.* complexity, cost, environment-related...). The relationships between these objectives are

complex and probably not constant over the whole search space. For instance, minimizing the complexity of the robot leads to a smaller and therefore less inertial robot, so it is likely to decrease the effort required from the worker. But a robot with fewer degrees of freedom is more likely to cause awkward postures and decrease the job quality.

The quality of task execution can be summarized with only one or two objectives: position error, and if needed, force error. Additional objectives can be used if necessary, but their number should remain small (one or two). The main problem is the high number of worker-oriented objectives: the full list of ergonomic indicators contains 30 different (and sometimes conflicting) indicators. Therefore, the analysis method presented in chapter 5 is first applied to the task of interest in order to identify the most informative ergonomic indicators. Only these discriminating indicators are used as objectives in the optimization of the cobot morphology.

If the number of objectives is still too high, a solution can be to turn some objectives into constraints. The objective to remove is still evaluated (*i.e.* measured in the simulation here), but it is not included in the fitness function. Instead, the measured value is compared with a user-defined threshold value and affects the values of the other objectives according to the output of the comparison. Generally, the other objectives are not modified while the measured value is higher than the threshold (assuming the objectives must be maximized). On the contrary, if the measured value is smaller than the threshold, the candidate is considered unsuitable for the task and should therefore be eliminated. To this purpose, very bad values are assigned to all the other objectives, so that the candidate is naturally excluded at the next selection step.

## 6.2 Genetic description of collaborative robots

Even though GAs are in general well suited for optimization over vast and non-continuous search spaces, the search space topology still significantly affects the convergence of the optimization and the final result [Rothlauf 2006]. The search space is defined by the genome which represents the optimization variables (the value of the genome for a particular individual is its genotype). The search space is then linked to the objective space via the phenotype, which is the physical expression of the genotype. Therefore, an inadequate genome definition or expression causes more discontinuities and higher gradients in the objective space, thus degrading the algorithm overall performance. So the genome, and everything that is related to it (genetic operations, translation to phenotype), must be carefully adapted to the considered problem.

### 6.2.1 Genome definition

In GAs, the genome is usually formulated as an array of numbers, with the items of this array (the genes) corresponding to the optimization variables. This work focuses on the optimization of cobots morphology, and more specifically kinematic

structure. Therefore the genome only contains mechanical parameters: no control parameters are included[1]. The optimization variables are the following:

- number of joints;

- type of joints;

- position and orientation of joints;

- position and orientation of the robot base.

**Position and orientation of joints:**   The position and orientation of each joint relative to its parent joint are described with the four Denavit-Hartenberg (DH) parameters $\alpha_i$, $d_i$, $r_i$, and $\theta_i$. Besides being a common way to define robot manipulators, the DH convention guarantees locality, *i.e.* small changes in the genotype result in small changes in the phenotype. The locality feature is recommended, since it prevents certain discontinuities in the objective space.

**Type of joints:**   A fifth gene $j_i$ is added to the joint description, for specifying the type of joint: fixed, revolute ($\theta_i$ is the actuation variable), prismatic ($r_i$ is the actuation variable), or screw ($\theta_i$ and $r_i$ are coupled). Fixed joints are included in this description, since they allow to consider non rectilinear segments without the need for further parameters. If needed, joints with more than one degree of freedom are represented by two elementary joints. The five parameters describing a joint $(j_i, \alpha_i, d_i, r_i, \theta_i)$ are gathered in a set, called a *functional group* in this work.

**Number of joints:**   The number of joints in the robot could be defined by the number of functional groups defining the joints features in the genome. However such a representation is not suitable for GAs. Each feature must appear explicitly in the genome, so that it can be affected by genetic operations such as crossovers and mutations. Therefore the number of joints in the robot is defined by a gene $N_J$.

**Position and orientation of the robot base:**   The position and orientation of the robot base are represented by six genes $X_b$, $Y_b$, $Z_b$, $\alpha_b$, $\beta_b$ and $\gamma_b$. The first three genes correspond to the Cartesian positions, and the last three genes to the roll-pitch-yaw angles. These six parameters are gathered in a separate functional group.

**Scaling factor:**   An additional gene $\lambda$ is added to the genome. It corresponds to an overall scaling factor, which acts on the length DH parameters $d_i$ and $r_i$ of each segment. This scaling factor is added, because it introduces some redundancy in the genome (*i.e.* different genotypes correspond to the same phenotype), which is often profitable in GAs [Rothlauf 2006].

---

[1]Control parameters can be optimized with the same Sferes$_v$2/XDE framework, however the genome, its translation to phenotype and some genetic operations must be modified.

The proposed genome is summarized in Fig. 6.4. It should be noted that the formulation adopted in this work is only one (reasonable) choice among many possible. Some other genome formulations could yield better performance in terms of convergence and final results. However the comparison of the performances of different genome formulations is beyond the scope of this work.

| $\lambda$ | $N_J$ | $X_b$ | $Y_b$ | $Z_b$ | $\alpha_b$ | $\beta_b$ | $\gamma_b$ | $j_1$ | $\alpha_1$ | $d_1$ | $r_1$ | $\theta_1$ | $\ldots$ |
|---|---|---|---|---|---|---|---|---|---|---|---|---|---|

| $\ldots$ | $j_{N_J}$ | $\alpha_{N_J}$ | $d_{N_J}$ | $r_{N_J}$ | $\theta_{N_J}$ |
|---|---|---|---|---|---|

Figure 6.4: Structure of the genome used to represent the morphology of a collaborative robot. A single vertical line indicates the separation between two genes. A double vertical line indicates the separation between two groups of genes, called *functional groups* in this work. The genes defining a joint (type, position and orientation: $j_i$, $\alpha_i$, $d_i$, $r_i$ and $\theta_i$) are gathered in a functional group. So are the genes defining the position and orientation of the robot base ($X_b$, $Y_b$, $Z_b$, $\alpha_b$, $\beta_b$ and $\gamma_b$). The genes corresponding to the scaling factor $\lambda$ and to the number of joints $N_J$ do not belong to any functional group.

### 6.2.2 Genetic operations

Genetic operations define how the child population is formed out of the parent population.

The first step consists in selecting a part of the parent population - the genitor population - on which genetic changes will be applied (*Selection* step in Fig. 6.1). In NSGA-II, this selection process is carried out according to the binary tournament method. The parent population is randomly divided into pairs of individuals. The better individual of each pair is chosen according first to the Pareto dominance principle, and then to the crowding distance, to be included in the genitor population. The binary tournament is applied twice on the same parent population - the random pairing being different both times - in order to form a genitor population of the same size as the parent population.

Then each individual of the genitor population is either directly assigned to the child population, or, with a certain probability, it is mutated and/or crossed with another individual beforehand (*Genetic operations* step in Fig. 6.1). The mutation and crossover operators enable the apparition of new solutions, therefore they considerably influence the convergence and the results of the optimization. They are further detailed hereafter, because some specific features are introduced in their implementation, in order to remain consistent with the chosen genome formulation.

#### 6.2.2.1 Crossover

Generally, a crossover between two individuals means that their genes are exchanged from a certain randomly chosen index $i^*$, as depicted in Fig. 6.5. However this

straightforward method cannot directly be applied to the genome used for describing a robot, in particular because the separation index does not take functional groups into account. Two major changes are therefore carried out to adapt the crossover operator to the specificities of the genome. These changes are detailed below, and the resulting crossover operator is depicted in Fig. 6.6.
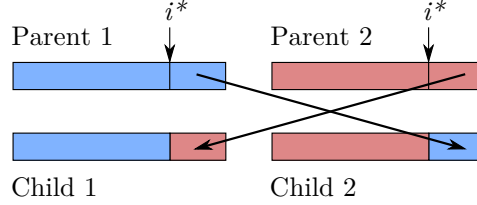


Figure 6.5: Regular crossover operator. The genes of both parents are exchanged from a randomly chosen index $i^*$.

**Functional groups segmentation:**   The separation index $i^*$ can only take values corresponding to the beginning of a group of genes describing a joint. This ensures that only entire segments of the robot are exchanged.

**Species-oriented approach:**   Crossover mimics the natural mechanism of reproduction, so the children resulting from a crossover are expected to quite resemble their parents. However, if for instance two robots with respectively a high and a low number of degrees of freedom are crossed, the resulting robots will very likely be totally different from both parents. In such cases, the purpose of crossover is lost and the operation is closer to a random transformation. Therefore a kind of species oriented approach is implemented. The individuals of the genitor population are divided in subgroups, called species, according to a compatibility function [Goldberg 1987]. Crossover can only happen between two individuals which belong to a same species. The compatibility function quantifies how much two individuals are alike, therefore the species approach prevents crossover between ill-matched genotypes. In this work, two individuals $A$ and $B$ belong to a same species if:

$$N_J^A = N_J^B \tag{6.4}$$

and:

$$\forall i \in [1, N_J^A], \quad |j_i^A - j_i^B| \leq \Delta_j^{max} \tag{6.5}$$

where $N_J^A$ (resp. $N_J^B$) is the number of joints of individual $A$ (resp. $B$), $j_i$ is a number representing the type of the *ith* joint (see section 6.2.3 for more details on the gene-to-joint mapping), and $\Delta_j^{max}$ is a user-defined parameter. So two parents are compatible if they have the same number of joints, and if the types of their joints are quite similar.
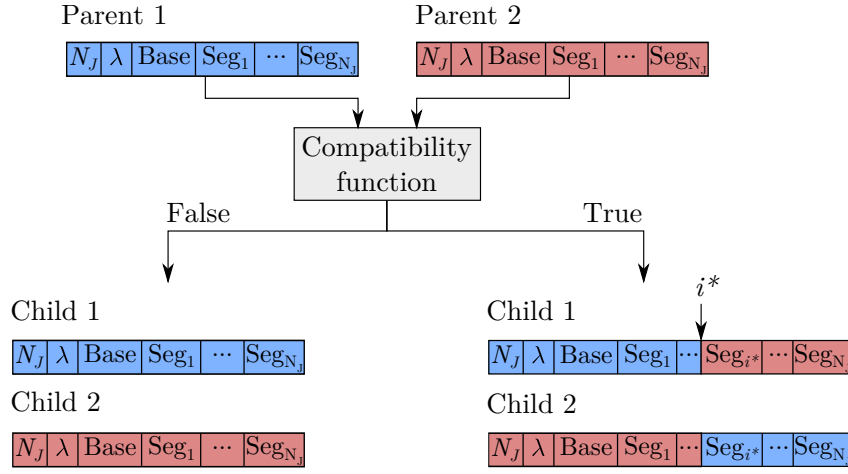
Figure 6.6: Modified crossover operator. Two parents can be crossed only if they belong to a same species, *i.e.* if their number and types of joints are close enough. Besides, only entire segments (*i.e.* functional groups of genes defining a joint) can be exchanged.

### 6.2.2.2 Mutation

The role of the mutation operator is to modify the genotype of an individual by a, generally small, perturbation in order to generate a new, hopefully better solution. Different functions can be used to generate this perturbation, most of which require hand-tuned parameters [Deb 2014]. The choice of the function and mostly of the parameters values affects the convergence rate: small perturbations tend to stick to local minima while large perturbations turn the GA into a random search algorithm (especially if associated with a high mutation rate).

In this work, a classic polynomial mutation scheme is initially chosen. A gene which is affected by a mutation is first scaled by its extreme values so that its normalized value $g_i$ lies in $[0, 1]$. An offset $\Delta g_i$ is calculated according to:

$$\Delta g_i = \begin{cases} (2u)^{\frac{1}{1+\eta_m}} - 1 & \text{if } u < 0.5 \\ 1 - (2 - 2u)^{\frac{1}{1+\eta_m}} & \text{if } u \geq 0.5 \end{cases} \tag{6.6}$$

where $u$ is a random number in $[0, 1]$, and $\eta_m$ is a used-defined parameter (general recommendations are $\eta_m \in [20, 200]$, depending on how sensitive the objectives are to the gene changes) [Deb 2014]. The offset $\Delta g_i$ is added to $g_i$, and the following function is applied to ensure that the mutated gene $g_i'$ lies in $[0, 1]$:

$$g_i' = f(g_i + \Delta g_i) = \begin{cases} 0 & \text{if } g_i + \Delta g_i < 0, \\ g_i + \Delta g_i & \text{if } 0 \leq g_i + \Delta g_i \leq 1, \\ 1 & \text{if } g_i + \Delta g_i > 1. \end{cases} \tag{6.7}$$

Finally $g_i'$ is scaled back according to the extreme values of the considered gene.

However, two modifications are performed on the polynomial mutation operator, in order to take the specificities of the genome into account.

**Mutation of cyclic genes:** This modification aims at resolving the discontinuity which arises when mapping a gene defined in $[0, 1]$ to an angle describing the robot structure defined on $\mathbb{R}/2\pi\mathbb{Z}$. Instead of using the threshold function defined in eq. 6.7 to fit $g_i'$ in $[0, 1]$, the following modulo function is used:

$$g_i' = f^*(g_i + \Delta g_i) = \text{mod}(g_i + \Delta g_i, 1). \tag{6.8}$$

This function is applied to all genes corresponding to cyclic values, *i.e.* the DH angular parameters $\alpha_i$ and $\theta_i$, and the roll-pitch-yaw angles defining the robot base orientation $\alpha_b$, $\beta_b$ and $\gamma_b$. Depending on the chosen genotype/phenotype mapping, it can also be applied to the gene $j_i$ defining the type of joint.

**Mutation of the number of joints:** The gene $N_J$ defining the number of joints in the robot is special in two ways. Firstly, a change in the number of joints significantly changes the overall robot morphology, so $N_J$ is somehow more important than the other genes. Secondly, contrarily to the other genes, $N_J$ does not have a continuous domain of definition: only positive integers are meaningful. Therefore, if this gene is selected for mutation, a different mutation scheme is applied. A random number $m \in [0, 1]$ is generated, and depending on its value, three actions are possible:

$$\begin{cases} \text{remove one joint} & \text{if } m < \eta_{cut} \\ \text{do nothing} & \text{if } \eta_{cut} \leq m \leq 1 - \eta_{add} \\ \text{add one joint} & \text{if } m > \eta_{add} \end{cases} \tag{6.9}$$

where $\eta_{cut}$ and $\eta_{add}$ are two user-defined parameters. If the action of removing a joint (resp. adding a joint) is selected, a random integer $i^*$ between 1 and $N_J$ (resp. 1 and $N_J + 1$) is generated. This number indicates the position in the kinematic chain where the joint should be removed or added. In case a joint is added, the values of the corresponding genes ($j_i$, $\alpha_i$, $d_i$, $r_i$ and $\theta_i$) are randomly initialized. This mutation scheme ensures that only one joint is removed or added, thereby avoiding too big differences between parent and child genotypes. Besides, the chance of mutating $N_J$ (compared to other genes) can be reduced by choosing $\eta_{cut} + \eta_{add} < 1$, thus translating the higher importance of this gene.

### 6.2.3 Genome translation

Each robot candidate is defined by its genotype, which is an array of numbers. In order to evaluate the values of the different objectives, the task of interest is simulated with the virtual manikin assisted by the robot to assess. Therefore the genotype of each individual must be translated into its phenotype, *i.e.* into a physical representation of the robot. The genotype/phenotype mapping is not necessarily unique, and it must be carefully chosen since it can affect the algorithm performance.

The entire robot morphology is defined by geometric, kinematic and inertial parameters. These parameters are generated, partly from the genotype of the individual, and partly from general considerations, as described hereafter.

**Geometric parameters:** The purpose of the present optimization is to provide a preliminary design of the general robot morphology, but not to fix all the details of the robot shape. Therefore, a simple representation is chosen for the segments of the robot: each segment is modeled by a cuboid. This choice does not prevent the emergence of more complex geometries, since non-straight segments can be obtained by the combination of two segments linked together by a fixed joint.

The length of a segment is given by the positions of its parent and child joints, defined by the corresponding DH parameters. The side-length $l$ is defined according to a heuristic proposed in [Rubrecht 2011], and obtained by comparing the data of existing robots:

$$l = l_0 \left(1 + \frac{1}{i}\right) \tag{6.10}$$

where $i$ is the position of the segment in the kinematic chain, and $l_0$ is a pre-defined parameter which depends on the average dimension of the workspace (in this work $l_0 = 0.1\,m$ is used). It means that the width of a segment decreases when it is placed closer to the end-effector in the kinematic chain.

The position and orientation of the robot base in the work environment are directly defined by the parameters $X_b$, $Y_b$, $Z_b$, $\alpha_b$, $\beta_b$, and $\gamma_b$.

**Kinematic parameters:** The position and orientation of each joint $i$ relatively to its parent joint are directly defined by the four DH parameters $\alpha_i$, $d_i$, $r_i$, $\theta_i$. However the mapping between the parameter $j_i \in [0,1]$ and the nature of the joint is not as straightforward. A mapping with threshold values such as:

$$\text{joint}_i = \begin{cases} \text{fixed} & \text{if } 0 \leq j_i < 0.25 \\ \text{revolute} & \text{if } 0.25 \leq j_i < 0.5 \\ \text{screw} & \text{if } 0.5 \leq j_i < 0.75 \\ \text{prismatic} & \text{if } 0.75 \leq j_i \leq 1 \end{cases} \tag{6.11}$$

causes large discontinuities because an infinitesimal change in the genome can drastically modify the robot morphology, hence performance. Instead, a continuous mapping is introduced, and described in Fig. 6.7. The joint limits gradually change with the value of $j_i$, so that the transition from one type of joint to another is smooth. In this work, only fixed and revolute joints are considered. The following continuous mapping is therefore used:

$$\text{joint}_i = \begin{cases} \text{fixed} & \text{if } 0 \leq j_i < \frac{1}{3} \\ \text{revolute with } \theta_i^{lim} = \pm\pi(3j_i - 1) & \text{if } \frac{1}{3} \leq j_i < \frac{2}{3} \\ \text{revolute with } \theta_i^{lim} = \pm\pi & \text{if } \frac{2}{3} \leq j_i < 1 \end{cases} \tag{6.12}$$

where $\theta_i^{lim}$ is the value of the joint limits (assumed symmetrical).
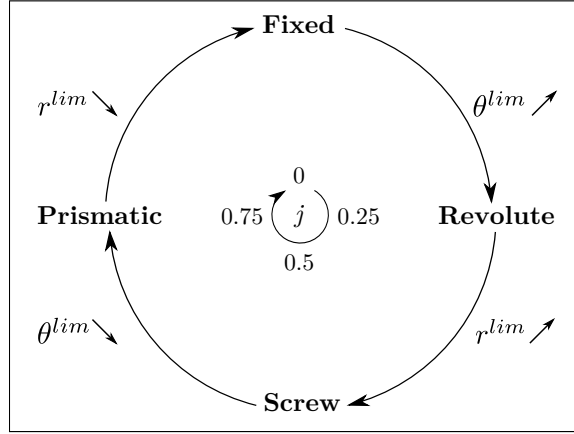
Figure 6.7: Continuous mapping of the joint type. The limit values of the two possible actuation variables $r$ and $\theta$ are gradually increased or decreased to provide smooth transition from one type of joint to another.

**Inertial parameters:**  The mass of each segment is calculated based on the segment volume and a pre-defined density (same density for all segments). This density is estimated from the data of different robots. It includes not only the segment structure, but also all embedded items, such as actuators etc... The moments of inertia are calculated based on the segment mass and geometry, assuming an homogeneous mass distribution.

All the physical parameters described above are written in a URDF file defining the phenotype of an individual. Thus robots can be automatically loaded in XDE, without any user input.

## 6.3   Application

The optimization framework presented in the previous sections is applied to a real activity. The purpose here is not to answer a specific industrial demand, but to make a proof of concept by studying the resulting optimal cobot morphologies. Indeed the coupling between Sferes$_{v2}$ and XDE has already been tested for a purely robotic task [Schlehuber 2015], but not for co-manipulation activities.

### 6.3.1   Simulation set-up

The drilling activity studied in sections 4.1 and 5.3 is chosen for a first validation of the optimization framework. Indeed, according to the sensitivity analysis conducted in section 5.3, the geometric parameters of the cobot significantly affect the ergonomy of the task execution. This activity is therefore particularly interesting regarding the optimization of the cobot morphology.

#### 6.3.1.1 Task simulation

For each robot candidate, the execution of the drilling activity is simulated with the autonomous virtual manikin assisted by the robot, according to the method described in section 3.2.2. The manikin controller includes the exact same tasks as in the sensitivity analysis of the drilling activity (section 5.3): balance, right hand manipulation (trajectory and force), gazing, posture and torques minimization, in decreasing order of importance. The only difference lies in the reference position for the postural task, which does not vary. The reference position here is always the resting posture (standing upright arms along the body). The manikin cannot move its feet on purpose during the simulation, therefore their initial positions must be chosen sensibly. They are set accordingly to what most human subjects did when performing the same drilling activity. However this solution does not take into account the effects (positive and negative) of the collaborative robot.

According to the sensitivity analysis conducted in section 5.3, the physical features of the worker (height and body mass index) significantly affect the ergonomy of the task execution. Therefore the optimal cobot morphology is probably worker-dependent. However given that the purpose here is to make a proof of concept and not to design a real robot, the worker diversity is not considered. The manikin used for the optimization is therefore assigned average values for its height and body mass index.

Contrarily to the sensitivity analysis where an abstraction of the collaborative robot is used, the drilling activity is performed here with full cobots. The morphology of each robot candidate is entirely defined by its genotype and by the genotype/phenotype mapping detailed in section 6.2. The robot control law, on the contrary, is not addressed by the optimization. The strength amplification control law (defined in eq. 3.19) is therefore used for all candidates. The amplification coefficient is set to $\alpha = 3$ (higher values lead to non stable robot behaviors, due to the spring-damper simulating the manikin grasp: see section 3.2.4). As in the sensitivity analysis, the strength amplification is activated only during the drilling phases, whereas the robot and tool weight compensation is always active.

#### 6.3.1.2 Objectives

As stated in section 6.1, when optimizing a collaborative robot dedicated to MSDs reduction, the objectives concern the worker, the task, and external constraints. The specific objectives used for the present application are detailed hereafter.

**Worker-oriented objectives:** Relevant worker-oriented objectives are identified through the sensitivity analysis of all ergonomic indicators, conducted in section 5.3. Five ergonomic indicators are selected for the drilling task: right arm joint position indicator, legs joint position indicator, right arm joint torque indicator, back joint torque indicator, and right hand force transmission ratio (FTR) in the drilling direction (its inverse actually, so that the indicator should be minimized).

As stated previously, the number of objectives should ideally be limited to three. This limit can be exceeded if not all indicators are conflicting, however, given that task-oriented and external objectives must still be added, five worker-oriented objectives are too many. To decrease the number of worker-oriented objectives, the right hand FTR is removed. Indeed, according to the results of the sensitivity analysis (Fig. 5.6), the FTR is mainly affected by parameters which are not varied in the present experiment (the manikin height, body mass index, and the initial pelvis orientation which is set through the feet positions). Therefore, the FTR is probably not very informative for the comparison of cobots morphologies.

Besides, the right arm and the back torque indicators are gathered into one single indicator, called upper-body torque indicator (though it excludes the left arm), as in section 4.2. Except for the strength amplification coefficient which is constant here[2], the most influential parameters are roughly the same for both indicators. Moreover, for the parameters related to the robot morphology, the global trends of the indicator *vs.* parameter relation are quite similar for both indicators.

Contrarily to the right arm and the back torque indicators, the right arm and the legs position indicators are still considered separately. Indeed, for the parameters related to the robot morphology, the global trends of the indicator *vs.* parameter relation are different for both indicators. Consequently, a total of three worker-oriented objectives are considered here.

**Task-oriented objectives:**   The quality of the drilling task execution depends on two things: the accuracy of the reference trajectory tracking during the drilling phases, and the respect of the reference value for the drilling force. These two quantities can be estimated by the position and force errors of the corresponding tasks (right hand operational acceleration and force tasks) during the drilling phases. However, as mentioned in section 5.3, the resistive force is simulated by a virtual wrench which value is the opposite of the desired drilling force. Therefore if the error of the hand force task is not zero, the external forces equilibrium is not satisfied, resulting in a displacement of the manikin hand. So the force error leads to a position error (which tends to be corrected by the hand position task). The quality of the task execution is therefore evaluated only through the right hand position error in the drilling phases.

In order to limit the overall number of objectives, the quality of the task execution is however not included in the fitness function, but it is turned into a constraint (see section 6.1.3). A threshold value is defined for the maximal right hand position error (2 cm). If the measured error is smaller than this threshold, the task is properly executed, and the fitness function is not modified. On the contrary, if the measured error is bigger than the threshold, the task is not correctly performed and bad fitness values are assigned to all the objectives, so that the candidate is eliminated during the selection process.

---

[2]The right arm torque indicator is not removed from the list of objectives, even though the strength amplification coefficient (most influential parameter) is constant in this experiment, because it is also significantly affected by geometric parameters of the robot.

**External objectives:** Another objective is added, which concerns the overall length of the robot structure. Indeed, a short robot is preferable, because it is easier to integrate in a workstation. Besides, a shorter robot is generally lighter (this is definitely the case here given the geometry and the mass distribution that are used for the robot segments, but such length-mass relation is more general). And as stated in section 5.3, the robot mass should be minimized, in order to limit the energy consumption due to weight (and possibly dry friction) compensation. Despite the length-mass relation, the ergonomic objectives are not sufficient to ensure the minimization of the robot length (for this specific task), because the mass parameter does not have a significant effect on any of the discriminating ergonomic indicators (section 5.3). Therefore the minimization of the robot length is directly added to the objectives.

Finally, four objectives are considered for the optimization of the cobot morphology for the drilling task:

- right arm joint positions indicator $I_q^{RA}$;

- legs joint positions indicator $I_q^{L}$;

- upper-body joint torques indicator $I_\tau^{B-RA}$;

- overall length of the robot.

Four objectives is superior to the recommended limit (three conflicting objectives at most), however these objectives are probably not all conflicting, in particular among the ergonomic objectives.

All the considered objectives must be minimized. Besides, for the GA, each objective must be represented by only one value. So the three ergonomic objectives are summarized by their average value on the whole task execution. However, some robots do not enable the task execution at all, and lead to the fall of the manikin. In such cases, the simulation is interrupted before the end and the fitness function cannot be evaluated. Nevertheless, for the selection the next parent population, the GA requires a numerical value for the fitness function of each robot candidate. So in order to account for the bad candidates without modifying the GA framework, the robots which make the manikin fall are assigned very bad fitness values (each objective is assigned a value around -100 when the manikin falls, whereas the objectives usually ranges between -10 and 0 when the task is fully performed). Thus such candidates are naturally eliminated by the algorithm.

Due to the relatively high number of objectives, the probability of an individual not being dominated (*i.e.* belonging to the Pareto front) is quite high, except if a very large population size is used. However, the population size is constrained by the computation time. Having most of the population in the Pareto front - at least early in the optimization - is not desirable, because it turns the GA into a random

search algorithm. A way to limit the number of individuals in the Pareto front is to discretize the fitness values.

All four objectives are discretized here. For the robot length objective, a threshold is first set. If the robot is longer than the threshold, it is considered unsuitable: bad fitness values are assigned to all the objectives so that the robot is eliminated during the selection process. The discretization step is then chosen so that the suitable range of robot lengths is divided into ten classes. For each worker-oriented objective, the discretization step is chosen so that 95 % of the values reached during the sensitivity analysis are contained in ten classes (the values reached during the sensitivity analysis are supposed to be representative of the global distribution of the values). Such a discretization is obviously arbitrary, however trials show that it is useful to significantly decrease the number of individuals in the Pareto front.

### 6.3.1.3 Algorithm and genome parameters

Both the genome parameters (limit values of each gene) and the GA parameters (values related to the population and to the genetic operators) significantly affect the convergence rate and the final result. The values chosen for these parameters are summarized in tables 6.1 and 6.2, and discussed hereafter.

**GA parameters:** The population size and the number of generations should be as big as possible in order to approach the real optimal Pareto front at best. However the values of these parameters are limited by calculation time. For a population size of 100 individuals, 1 generation is entirely evaluated in about 1 hour when using a four core, 2.4 GHz Intel® Core™i7 laptop[3]. The time needed for performing all genetic operations (replacement, selection, crossover and mutation) is negligible compared to the evaluation time of a generation. Here, the optimization is stopped after 220 generations, because the results suggest that a convergence is reached.

In general, a mutation rate that is too high may lead to loss of good solutions. It must not be too small either, otherwise the solutions stick to local optima. A general recommendation is to take a mutation rate equal to $1/n_{genes}$ where $n_{genes}$ is the number of genes in the genome [Deb 2014]. Thus in average, one gene of each individual is mutated per generation. However, when elitist selection is employed, the risk of loosing good solutions through mutation disappears. Therefore the mutation rate used here is higher than standard recommendations, since NSGA-II provides elitism.

The values of the other parameters are chosen according to general considerations. Other values could yield better performance, however the tuning of the GA parameters is beyond the scope of this work.

---

[3]The overall optimization time could however be significantly reduced if a computer with more cores were used. Indeed, the optimization framework is implemented so that several XDE simulations can be run simultaneously.

| Parameter | Definition | Value |
|:---:|:---:|:---:|
| $N_{pop}$ | Population size | 100 |
| $N_g$ | Number of generations | 220 |
| $\mu_c$ | Crossover rate | 0.4 |
| $\Delta j^{max}$ | Compatibility function parameter for species-oriented approach | 2/3 |
| $\mu_m$ | Mutation rate | 0.1 |
| $\eta_m$ | Polynomial mutation parameter | 25 |
| $\eta_{cut}$ | Probability of removing a joint if $N_J$ is mutated | 0.3 |
| $\eta_{add}$ | Probability of adding a joint if $N_J$ is mutated | 0.3 |

Table 6.1: Values of the GA parameters used for the optimization of the cobot morphology for the drilling task.

**Genome parameters:**   The ranges of variation of the genes values determine the extent of the search space. Therefore their bounds must be reasonably chosen, so that no time is lost in the exploration of obviously ill-adapted solutions. To this purpose, the possible values for the number of joints are strongly limited. Four degrees of freedom (DoFs) are required to correctly execute the considered task (drilling several holes in a vertical slab): two translational DoFs for the displacement in the slab plane, and two rotational DoFs for the drill orientation, which must remain normal to the slab plane. Therefore, the robot must at least have four DoFs. The upper bound for the number of joints is set to seven, in order to limit the complexity of the robot structure, hence its cost.

The other bounds presented in table 6.2 mostly come from general considerations on reasonable dimensions for a collaborative robot. Very small segment lengths are nevertheless allowed, since they enable the quasi co-localization of two elementary joints to represent a multiple degrees of freedom joint.

The limit values of the robot base horizontal position (genes $X_b$ and $Y_b$) are set to zero: these two genes are in fact removed from the variables. This choice is made, because instead of positioning the robot relatively to the work environment (with the robot base genes), the drilling area and the manikin are positioned relatively to the robot end-effector. The horizontal distance between the robot initial end-effector position and the drilling area is fixed (besides, the position of the manikin relatively to the drilling area is constant). Given that the robot initial configuration is also an optimization variable (genes $\theta_i$), removing the genes $X_b$ and $Y_b$ does not cause much loss of generality. However, this solution significantly decreases the number of failures in the task execution (not reachable drilling area leading to the fall of the manikin). The robot end-effector being already positioned quite close to the drilling area, the chances of not being able to reach it are much smaller.

| Parameter | Min value | Max value | Definition and Remarks |
|:---:|:---:|:---:|:---:|
| $\lambda$ | 0.8 | 1.2 | Overall scaling factor<br>Adds redundancy in the genome |
| $N_J$ | 4 | 7 | Number of joints<br>Specific mutation scheme |
| $X_b, Y_b$ | $0\,m$ | $0\,m$ | Horizontal base position |
| $Z_b$ | $0\,m$ | $3\,m$ | Vertical base position |
| $\alpha_b, \beta_b, \gamma_b$ | $-\pi$ | $\pi$ | Base orientation<br>Cyclic genes |
| $j_i$ | 0 | 1 | Joint type<br>Fixed or Revolute |
| $\alpha_i$ | $-\pi$ | $\pi$ | DH angular parameter<br>Cyclic gene |
| $d_i$ | $0.05\,m$ | $1.2\,m$ | DH length parameter |
| $r_i$ | $0.05\,m$ | $1.2\,m$ | DH length parameter |
| $\theta_i$ | $-\pi$ | $\pi$ | DH angular parameter<br>Cyclic gene |

Table 6.2: Limit values of the genome parameters used for the optimization of the cobot morphology for the drilling task.  Double horizontal lines indicate the beginning/end of a functional group of genes.

## 6.3.2   Results

In order to evaluate the capability of the proposed optimization method to find suitable cobot morphologies, the evolution of the four objectives are first studied. The cobots resulting from the optimization are then compared with the situation without assistance, to estimate the overall ergonomic benefit - or loss - caused by the cobot.

**Evolution of the objectives:**   The evolution of the four objectives is displayed in Fig. 6.8 for the individuals in the Pareto front, and in Fig. 6.9 for the whole population (each indicator must be minimized in order to improve the situation). The mean value of each objective globally decreases over generations (in the Pareto front and in the whole population), showing that the individuals in the population in general, and in the Pareto front in particular, do improve.  After about 150 generations, the evolution of the objectives is almost null, suggesting that some convergence is reached.

The minimal values of the legs position indicator $I_q^L$ and of the upper-body torque indicator $I_\tau^{B-RA}$ stop evolving almost immediately (after the second generation): the best achievable value for these objectives is found quite easily.  The same remark applies to the right arm position indicator $I_q^{RA}$, though to a lesser extent (best value found after 15 generations).  This phenomenon might indicate that the

(a) Right arm position indicator $I_q^{RA}$

(b) Legs position indicator $I_q^L$

(c) Upper-body torque indicator $I_\tau^{B-RA}$

(d) Robot length
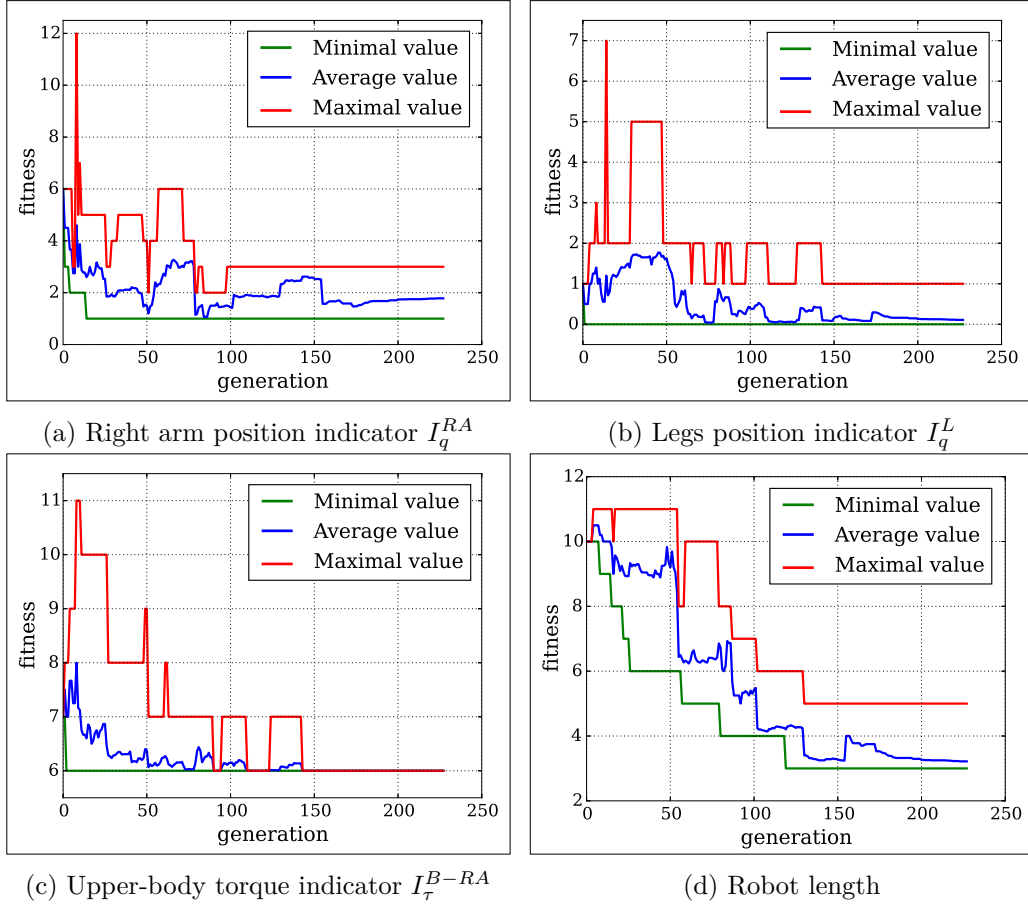
Figure 6.8: Evolution of the values of the four objectives within the Pareo front, over generations (only the individuals belonging to the Pareto front are considered). The graphs represent the evolution of the fitness values (*i.e.* discretized values, no units), and not directly of the ergonomic indicators/robot length values. The maximal (red), minimal (green) and average (blue) values of each objective are plotted (each objective should be minimized). The average value depends on the number of individuals in the Pareto front. This number can change from one generation to another, which explains why the average value sometimes changes even though the minimal and maximal values remain constant.

proposed discretization (for these indicators) is not well-adapted. A finer discretization could probably be used, especially for the upper-body torque indicator $I_\tau^{B-RA}$ since at the end, all individuals in the Pareto front are equivalent regarding this objective (equality of the minimal and maximal values). However, for all three ergonomic indicators, the convergence of the maximal value is much slower (between 100 and 150 generations). It is therefore quite easy to find a robot which performs well on one objective, but finding a robot which matches all objectives quite well is much harder. The difficulty to improve all objectives is even more noticeable on the evolution of the robot length. The convergence of this objective (and especially

(a) Right arm position indicator $I_q^{RA}$



(b) Legs position indicator $I_q^L$



(c) Upper-body torque indicator $I_\tau^{B-RA}$



(d) Robot length
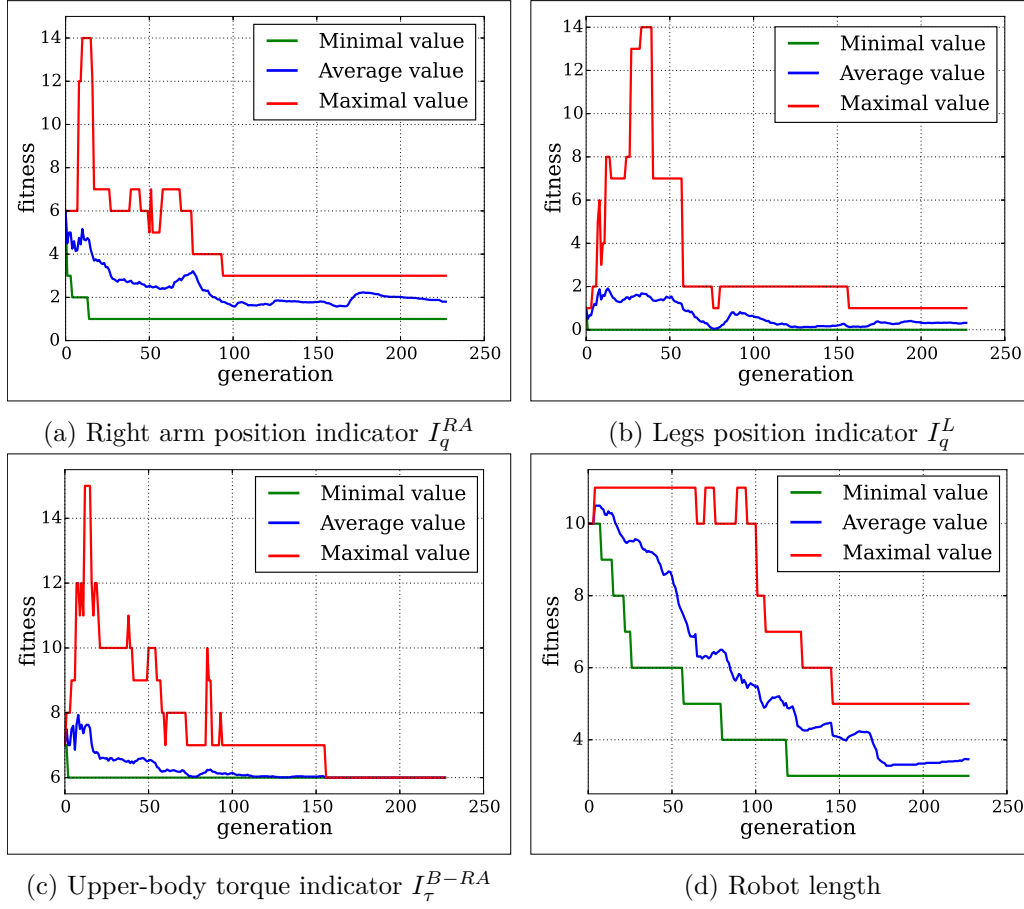
Figure 6.9: Global evolution of the values of the four objectives, over generations (all the individuals of the population are considered). The graphs represent the evolution of the fitness values (*i.e.* discretized values, no units), and not directly of the ergonomic indicators/robot length values. The maximal (red), minimal (green) and average (blue) values of each objective are plotted (each objective should be minimized).

of its minimal value) is very slow compared to the ergonomic objectives.

In order to illustrate these phenomena, table 6.3 displays the values of the four objectives for several individuals of the Pareto front, at the beginning of the optimization ($10^{th}$ generation), and at the end of the optimization ($220^{th}$ generation). In generation 10, some individuals perform not too badly regarding one of the ergonomic objectives, in comparison with the results of generation 220 (*e.g.* $R_2^{10}$ for the arm position indicator $I_q^{RA}$, or $R_3^{10}$ for the legs position indicator $I_q^L$). However, the values of the other objectives are much worse than those of generation 220 (*e.g.* the legs position indicator $I_q^L$ for $R_2^{10}$, or the arm position indicator $I_q^{RA}$ for $R_3^{10}$). Furthermore, the robot is always much longer - about twice as long in average - in generation 10 than in generation 220. The shortest robot of generation 10 ($R_1^{10}$), is 40 % longer than the longest robot of generation 220 ($R_3^{220}$), whereas its ergonomic

performances are much worse. To illustrate the decrease in the robot length and complexity, the shortest robots of the Pareto front of generations 10 and 220 are displayed in Fig. 6.10.

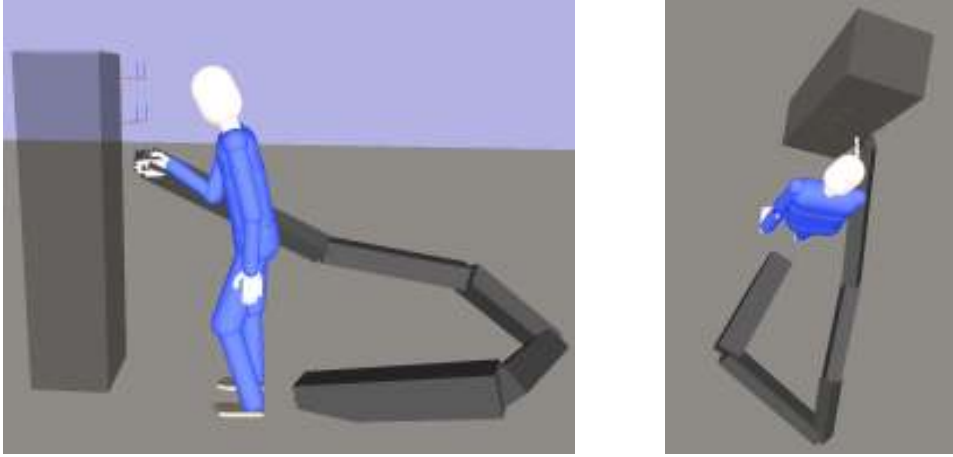| | | Generation 10 | | | Generation 220 | | |
|---|---|---|---|---|---|---|---|
| | | $R_1^{10}$ | $R_2^{10}$ | $R_3^{10}$ | $R_1^{220}$ | $R_2^{220}$ | $R_3^{220}$ |
| Right arm position indicator | $I_q^{RA}$ | 3.0 | 1.39 | 1.65 | 1.49 | 1.01 | 1.18 |
| Legs position indicator | $I_q^L$ | 0.49 | 0.34 | 0.13 | 0.13 | 0.12 | 0.16 |
| Upper-body torque indicator | $I_\tau^{B-RA}$ | 0.79 | 0.63 | 0.55 | 0.45 | 0.48 | 0.40 |
| Robot length (m) | | 4.72 | 5.49 | 5.95 | 1.74 | 2.37 | 3.37 |
| Number of joints | | 5 | 6 | 6 | 4 | 4 | 5 |

Table 6.3: Values of the four objectives for three individuals of the Pareto front of the $10^{th}$ and $220^{th}$ generations. The individuals $R_i^j$ are selected according to the crowding distance criterion, so that they represent a diversity of solutions. For each ergonomic objective, the values are scaled by the reference value of the indicator defined in eq. 5.6 (*i.e.* a value representing the average order of magnitude of the indicator, estimated on many different trials), so that the comparison between two cases is more understandable. The objectives are not discretized here, for the sake of clarity. Though not optimized here, the number of joints in the robot structure is displayed, as an indicator of the robot complexity.

The evolution of the number of joints in the robots is also worth noticing. Indeed, even though the number of joints is not optimized here, it tends to decrease over generations. This might be due to the fact that reducing the number of joints is as easy way to reduce the robot length. The decrease in the number of joints is interesting, because a simpler robot (with less joints) is generally less expensive to produce and maintain.

**Comparison with the reference situation:** Thanks to the optimization, the performances of the cobot, regarding its length and the three ergonomic indicators $I_q^{RA}$, $I_q^L$, and $I_\tau^{B-RA}$, are improved. However, during the optimization, the situation with the cobot is never compared with the situation without assistance. There is therefore no certainty that the use of the cobot is indeed beneficial. Furthermore, the cobot is optimized regarding only a small number of ergonomic indicators (the most discriminating ones, according to the sensitivity analysis). Though the other ergonomic indicators have been beforehand identified as little discriminating for

(a) Generation 10
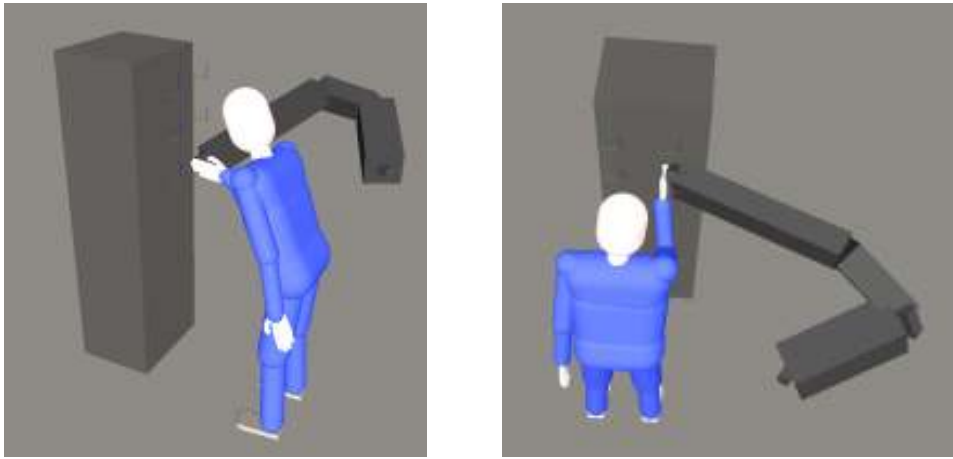


(b) Generation 220

Figure 6.10: Shortest robot of the Pareto front for the $10^{th}$ and $220^{th}$ generations. Over generations, the overall length of the robot decreases, while the biomechanical solicitations experienced by the worker are kept constant or decreased. The gray cuboid represents the wall where the slab to drill is set (the robot cannot go through this wall).

the drilling activity, it is safer to ensure that these indicators are not significantly worsened by the use of the cobot (which would mean that the cobot delocalizes the MSDs risk). Table 6.4 therefore displays the values of all the ergonomic indicators defined in section 3.1, measured during the reference situation (no cobot) and with the assistance of three near-optimal cobots.

The three cobots in table 6.4 (same as in table 6.3) are selected within the Pareto front of the last generation, according to the crowding distance criterion, so that they represent a diversity of solutions. For the reference situation, two kinds of simulations are considered: a fully automatic simulation (no motion capture data, case *Autom.*), and a dynamic replay of data recorded on human subjects (cases

| | No assistance (% ref. value) | | | With robot (% ref. value) | | |
|---|---|---|---|---|---|---|
| | Autom. | Sbj. A | Sbj. B | $R_1^{220}$ | $R_2^{220}$ | $R_3^{220}$ |
| **Right arm pos.** | 90 | 143 | 133 | 149 | 101 | 118 |
| Left arm pos. | 7.4 | 6.7 | 6.5 | 7.5 | 7.5 | 7.9 |
| **Back pos.** | 46 | 40 | 32 | 66 | 56 | 46 |
| Legs pos. | 15 | 19 | 23 | 13 | 12 | 16 |
| **Right arm vel.** | 19 | 36 | 25 | 47 | 55 | 40 |
| Left arm vel. | 3.1 | 3.5 | 4.7 | 4.4 | 6.6 | 2.5 |
| Back vel. | 10.2 | 28 | 27 | 21 | 29 | 19 |
| Legs vel. | 1.7 | 2.5 | 4.2 | 1.6 | 4.1 | 1.0 |
| **Right arm acc.** | 5.4 | 12 | 8.3 | 16 | 25 | 13 |
| Left arm acc. | 0.3 | 1.2 | 2.5 | 1.7 | 4.7 | 1.7 |
| Back acc. | 0.2 | 4.7 | 3.4 | 1.8 | 3.8 | 1.3 |
| Legs acc. | 0.2 | 2.7 | 2.4 | 0.3 | 0.9 | 0.2 |
| **Right arm power** | 54 | 84 | 95 | 48 | 59 | 40 |
| Left arm power | 3.9 | 8.0 | 7.0 | 5.8 | 9.6 | 4.8 |
| Back power | 40 | 69 | 57 | 52 | 74 | 42 |
| Legs power | 16 | 12 | 18 | 13 | 17 | 11 |
| **Right arm torque** | 125 | 148 | 155 | 39 | 46 | 49 |
| Left arm torque | 4.0 | 4.5 | 3.4 | 5.7 | 5.2 | 5.6 |
| **Back torque** | 75 | 88 | 81 | 53 | 53 | 49 |
| **Legs torque** | 34 | 29 | 30 | 17 | 21 | 20 |
| Kinetic energy | 9.8 | 20 | 25 | 15 | 32 | 12 |
| FTR RH drilling | 130 | 92 | 102 | 134 | 131 | 108 |
| VTR RH drilling | 98 | 102 | 98 | 99 | 90 | 98 |
| **Balance stab. margin** | 89 | 83 | 91 | 77 | 83 | 76 |
| **Dynamic balance** | 45 | 44 | 39 | 63 | 64 | 67 |
| Head dexterity | 66 | 70 | 73 | 66 | 66 | 67 |

Table 6.4: Values of the ergonomic indicators measured without assistance (cases *Autom.*, *Sbj. A*, and *Sbj. B*), and with the assistance of three near-optimal cobots (cases $R_1^{220}$, $R_2^{220}$, $R_3^{220}$). The case *Autom.* corresponds to a fully automatic simulation, whereas the cases *Sbj. A* and *Sbj. B* correspond to the dynamic replays of motion-capture data. For each indicator, the value displayed is the percentage of the indicator reference value (defined in eq. 5.6), so that the comparison between two cases is more understandable (the reference value gives an insight of the average order of magnitude of the indicator, however it does not provide any indication of the absolute level of risk). The indicators in red are overall worsens by the cobot, whereas the indicators in green are improved by the cobot. The force and velocity transmission ratio are only computed when they are meaningful, *i.e.* for the right hand, in the drilling direction, during the drilling phases.

*Sbj. A* and *Sbj. B*). Indeed, when answering an industrial demand, the reference situation should be established by recording the motions of real workers. Among the five subject who performed the drilling experiment (section 4.1), two subjects are selected for the dynamic replay, because their height and body mass index are very similar to those of the manikin used in the optimization. However, in fully automatic simulations, the realism of the manikin motions and behavior is currently limited (see section 4.4). So when comparing a replay without assistance and a fully automatic simulation with a cobot, the differences may come from the manikin limitations as well as from the robot presence. To limit this effect, a fully automatic reference situation is added to the comparison.

Significant differences are observed between the three non-assisted situations, especially for the most solicited body parts (back and right arm). The differences between subject A and subject B show the inter-individual variability: different persons, even with similar morphologies, may use different strategies to perform a same task. The even more significant differences between the automatic simulation and the replays underline the current lack of realism of some fully automatic manikin motions.

Nevertheless, general trends can still be observed when comparing the situations with and without cobots. The position, velocity and acceleration indicators of the right arm and the back are degraded by the use of a cobot. As stated in section 4.3, this is due to the lack of transparency of the robot (geometric volume, additional inertia...). The lack of transparency is not similar for every robot. $R_1^{220}$ especially worsens the position indicator, whereas $R_2^{220}$ mostly worsens the dynamic (velocity and acceleration) indicators. The effects of the lack of transparency are smaller for $R_3^{220}$, but at the detriment of the robot length (see table 6.3). On the contrary, the force-related indicators (power, and especially torque indicators) are significantly improved by the use of the cobot. This is expected since the robot provides strength amplification, and also supports the drill weight. Here again the three robots are not equivalent: for instance, $R_3^{220}$ is the most demanding for the arm, but the least demanding for the back (regarding the torque indicator). Finally, the two balance-related indicators are affected in different ways. The balance stability margin is improved by the use of a cobot, possibly because it reduces the force required for the drilling, hence removing the need to bend forward to resist this perturbation. On the contrary, the dynamic balance indicator is degraded by the cobot. This might be due to the perturbations caused by the robot lack of transparency during its displacement, which are not foreseen by the manikin (especially the additional inertia in the starting and stopping phases).

### 6.3.3   Discussion

The results of the optimization of the cobot morphology are overall encouraging. Compared to randomly selected robots, the optimization provides much more compact robots, with better ergonomic performances. Furthermore, the use of a near-

optimal cobot significantly decreases the force-related biomechanical solicitations, compared with the situation without assistance. However, even after the optimization, some solicitations are increased by the robot presence, because of its lack of transparency (though the degradation of some performances might be overestimated because of the manikin actual limitations). Due to these antagonistic performances, and since the ergonomic indicators do not provide an estimation of the absolute level of risk, it is hard to say which robot is overall the best, or if the use of a robot is indeed beneficial. Using only the most discriminating indicators simplifies but does not solve this issue. The choice between the different near-optimal robots is then left to the user, according to his/her main concerns. At this stage, the intervention of an ergonomist may be useful, to decide between the various options. The optimization remains nevertheless useful, since it performs a pre-selection of the better performing robots.

The main question regarding the usefulness of the optimization is whether it outperforms the results a robot designer could achieve (*i.e.* provides cobots with best or similar performances, in less or comparable time). The answer to this question is not straightforward, though for the drilling job, a designer might have performed at least as well. However, several elements must be underlined. Firstly, the activity that is considered here is not very complex, especially regarding the task-related and environment-related constraints. For instance, a good solution would probably be much less intuitive in a cluttered environment: the optimization would then be more useful [Rubrecht 2011]. However, the success of the optimization in a complex environment is strongly dependent on the manikin autonomy for solving complex problems (*e.g.* anticipating and avoiding collisions while still reaching the task target). Secondly, the performances of the optimization could probably be improved by tuning some parameters (*e.g.* genetic operator parameters, or even genome definition). Indeed, the choices proposed in this work are based on general recommendations and considerations, but no comparative studies have been carried out. One interesting approach could be the time-triggered mutation because it has positive effects when optimizing long genomes, as it is the case here [Deb 2014]. Comparative studies could be interesting to achieve better results, however, the tuning should not be task-dependent, since the purpose is to provide a generic tool, and not to address one specific task. Finally, it should be reminded that the purpose of the optimization is not to replace the designer, but to provide him/her with preliminary designs to be worked on.

One limitation of the current optimization is the small number of objectives that can be considered. Indeed, as stated previously, the number of conflicting objectives in multi-objective evolutionary algorithms (EA) must generally be limited to three, in order to ensure the convergence of the optimization. This is a consequence of the Pareto dominance relation: the proportion of non-dominated individuals in the population rises quickly with the number of objectives. Even when the objectives are not strictly conflicting, their number is still limited: that is why the right arm

and the back torque indicators are considered together here. However, the aggregation of different objectives is not always possible (indicators of different nature) nor desirable (loss of information). One potential solution is to use many-objective EAs, instead of multi-objective EAs. Contrarily to multi-objective EAs such as NSGA-II, many-objective EAs are not (or not only) based on the Pareto dominance relation, and yield better performances when the number of objectives rises [He 2013]. Nonetheless, even with many-objectives EAs, the number of objectives cannot be too high (*e.g.* considering several dozens of objectives is unrealistic). The sensitivity analysis proposed in chapter 5 remains therefore useful to identify discriminating indicators, and thereby limit the number of objectives. Besides, since many-objectives EAs are also based on evolutionary principles, their use does not require the modification of the entire optimization framework proposed here (*e.g.* the genome definition and translation could probably be kept unchanged).

Finally, since the whole optimization is based on the evaluation of the robot candidates with a simulation tool, it is subjected to what is called the reality gap. That is, some phenomena are not or not perfectly modeled in the simulation, hence affecting the reliability of the results (*i.e.* if the same measurements were performed on real robots, some results might be different). In particular, the dynamic simulation of contacts is not yet a hundred percent deterministic: the resolution of a same situation sometimes slightly differs. This problem is not due to the specific simulation framework used in this work, but this is a wider issue due to the difficulty of properly simulating contacts. Such a lack of determinism in the resolution may lead to variations of the values of the ergonomic indicators (or other quantities) measured in the simulation: if a same robot is evaluated twice, the output might be a little different. The measurements can then be considered noisy. This phenomenon is not specific to the robot optimization: it exists for all kinds of evaluations. However, it is more likely to happen during the evaluation of randomly generated robots because the probability of generating unstable situations (unstable contacts) is higher. And the lack of determinism is enhanced in unstable situations. In order to reduce the effects of this lack of determinism, techniques for robust evolutionary computations could be used instead of the NSGA-II algorithm. In particular, the Covariance Matrix Adaptation Evolution Strategy (CMA-ES) [Hansen 1996] (or [Igel 2007] for a mutli-objective version) enables to account for noise or uncertainties in the fitness evaluation. Nevertheless, such a solution only partially answers the problem, since it requires the variations in the output to be quite small (in order to be considered as noise). In some cases however, small variations in the resolution may lead to entirely different situations: for instance the manikin may or may not fall.

## 6.4　Conclusion

In this chapter, a method for optimizing the morphology of a collaborative robot for a given activity is proposed. A cobot must be designed so that it optimizes

the quality of the task execution, but also the ergonomic situation of the worker. The objectives of the optimization are therefore multiple. The number of objectives must nevertheless be limited, otherwise no convergence can generally be reached. To this purpose, the ergonomic indicators analysis method presented in chapter 5 is used to select relevant worker-oriented optimization criteria (objectives).

The optimization method then relies on genetic algorithms for exploring the space of robot morphologies and selecting candidates to evaluate. Indeed, genetic algorithms (and evolutionary algorithms in general) are well adapted for optimizing non-analytic functions over vast and non-continuous search spaces. The fitness of each robot candidate is numerically evaluated thanks to the simulation framework presented in chapter 3. To this purpose, a multi-objective genetic algorithm software is linked with the cobots simulation framework.

A genome suited to describe the structure of collaborative robots (and more generally of serial robots) is defined. Several modifications are made to classic genetic operators in order to avoid discontinuities and enhance the regularity between genes and objectives, hence facilitating the optimization.

The proposed optimization method is applied to a cobot for a drilling job, with encouraging results. The optimization enables a significant reduction in the robot length while ensuring satisfying ergonomic performances. The results could further be improved through the tuning of some optimization parameters. Nevertheless, the results demonstrate the interest of the approach proposed in this work, as a tool for providing well-performing preliminary cobot designs to be worked on.

# Chapter 7

# Conclusion

The main contributions presented in this work are summarized hereafter. Then, perspectives for improvements and potential applications of the developed evaluation framework are proposed.

## 7.1 Contributions

More and more industrial sectors are interested in collaborative robotics, as a solution to address the growing problem of work-related musculoskeletal disorders. In this context, the main purpose of collaborative robots is to reduce the biomechanical solicitations to which the workers are exposed, by physically assisting them during the execution of demanding tasks. However, the ergonomic benefit provided by a cobot is hardly ever quantitatively evaluated, because of the lack of relevant assessment tools. Therefore, the work presented in this thesis focuses on the development of a methodology to quantitatively compare the ergonomic benefit provided by different collaborative robots, when performing a given task.

The proposed methodology relies on an evaluation carried out within a digital world, using a virtual manikin to simulate the worker. Indeed, using a virtual manikin is advantageous because it enables easy access to many detailed biomechanical quantities, without the need for a real human or a physical mock-up of the robot. Such an evaluation can therefore easily be integrated within the design process.

The existing software tools for ergonomic evaluations are reviewed, however none of them fully match the requirements of collaborative robots evaluation. The tools used for workstation design provide simple human models and return a sole (or a few) indicator representing the global level of exposure. However, these indicators are very rough and/or task-specific, and do not cover all kinds of manual activities. On the contrary, the tools used for biomechanical studies provide a high number of detailed measurements, but their interpretation - both in terms of reliability and task-related relevance - requires specific biomechanical knowledge. Besides none of

these software (macroscopic or biomechanical models) enable the simulation of a virtual manikin interacting with a controlled collaborative robot.

In this work, a novel approach is proposed, which aims at associating the advantages of both the macroscopic and the biomechanical DHM (digital human model) tools. The proposed approach combines a framework for measuring numerous ergonomic indicators during co-manipulation activities, with an analysis method to identify the most relevant indicators for a given task.

Ergonomic indicators which match the requirements of collaborative robotics are first defined. Such indicators account as exhaustively and concisely as possible for the different biomechanical solicitations which occur during all kinds of manual activities. The proposed indicators aim at comparing different situations, but not at providing an absolute level of risk. Contrarily to what is done in most ergonomic assessment methods, the different kinds of solicitations are considered in separate indicators, so that the formulation of the indicators is not task-dependent.

The measurement of the proposed ergonomic indicators requires the simulation of the activity to evaluate. To this purpose, an implementation of a generic simulation for co-manipulation activities is proposed. The simulation is implemented in a dynamic simulation framework which guarantees the physical consistency of motions and forces. The virtual manikin is animated through a LQP optimization technique, while a strength amplification control law is used for the cobot. A method for dynamically replaying motions recorded on human subjects is also proposed, so that a reference situation (without any assistance) can be established. The dynamic replay has the advantage of providing estimations of the forces associated with the motion, contrarily to kinematic replay methods. The replay method can also be used to evaluate existing cobots.

The reliability of the proposed measurement framework is then evaluated. Two motion capture based experiments are carried out - without any cobot - in order to estimate the realism of the manikin model and control, and the consistency of some of the proposed ergonomic indicators. Then, a fully automatic simulation is implemented, in order to validate the reliability and usefulness of the manikin-robot simulation. The results obtained in all three experiments are mostly satisfying, and partly validate the framework proposed for biomechanical measurements during co-manipulation activities. The manikin-cobot simulation also demonstrates that, thanks to the proposed framework, the effects of various robot parameters on the worker can be quantified, for each kind of biomechanical solicitations. However the proposed experiments also highlight some limitations of the manikin model and control. At low level, the manikin motions and internal forces omit some phenomena and motion principles. At high level, its adaptability is almost non-existent since its control is only reactive and there is no planning or anticipation.

The proposed simulation framework allows to estimate a variety of ergonomic indicators while performing a given task. However the high number of indicators makes any kind of conclusion difficult for the user. Hence, a methodology for analyzing the sensitivity of the various indicators to the robot and task parameters is proposed. The goal of such an analysis is to reduce the number of ergonomic indicators which are considered in an evaluation, while sufficiently accounting for the global ergonomic level of the considered activity. The proposed method associates a standard sensitivity analysis method, with the previously described framework for measuring ergonomic indicators through simulation. The proposed method is validated on various simple activities, and on a more complex drilling job, with promising results. However, when a complex activity is considered, it seems that segmenting the activity into several phases would lead to a more accurate analysis. Finding an optimal segmentation criterion nevertheless remains an open problem.

Finally, an application of the proposed methodology is presented. It aims at optimizing the morphology of a collaborative robot for a given activity. The ergonomic indicators analysis method enables the selection of relevant optimization criteria (objectives). Then, the simulation framework is linked to a multi-objective genetic algorithm software for the optimization. The genetic algorithm is used for exploring the space of robot morphologies, *i.e.* providing robot candidates to be evaluated. The simulation tool is used for numerically estimating the various objectives for each robot candidate. The proposed optimization is applied to a cobot for a drilling job. The results demonstrate the interest of the evaluation tool developed in this work, though better results could probably be achieved, through the tuning of some optimization parameters.

Beyond the specific application to the evaluation of collaborative robots, presented here, the tool developed in this work partly answers a more general problem. It provides a generic tool for performing accurate ergonomic assessments of dynamic situations, with the need for only very little input data.

## 7.2 Perspectives

In the future, some interesting points should be investigated to improve and extend the ergonomic evaluation framework proposed in this work.

### 7.2.1 Improvements

The ergonomic indicators proposed in chapter 3 aim at accounting as precisely as possible for the different biomechanical solicitations to which workers are exposed during manual jobs. However, some phenomena are not properly taken into account, which may lead to a wrong estimation of the risk. Some indicators (mainly the joint velocity and joint acceleration indicators) do not take joint capacities into account. Therefore, when summing the contributions of several joints, much information

is lost (all joints are then virtually equivalent in terms of capacities). Besides, even when joint capacities are included in the indicator, the couplings which exist between adjacent joints, and also between different biomechanical quantities, are not considered. Yet such couplings affect the joint capacities, and thereby the level of solicitation. Mathematical relations for some couplings can be found in [Chaffin 2006]. Integrating these relations within the indicators formulae could significantly improve the reliability of the proposed indicators.

Such couplings could also be included in the manikin model and controller, in order to improve the realism of the manikin motions. However, the feasibility of their integration in the current controller depends on the nature of the relations. Indeed, the LQP controller requires linear constraints. Therefore, if the couplings are not linear, the controller must be modified, or the couplings must be linearized. For instance, some torque capacities *vs.* joint angle relations are quadratic [Chaffin 2006]: the LQP controller could be changed for a quadratically constrained quadratic program (QCQP) to account for such constraints (to the detriment of the computation time however) [Boyd 2004].

The realism of the manikin could also be improved by taking the effect of fatigue into account in the controller. Indeed, fatigue is currently considered in the joint torque indicator, but it is not included in the controller. So the manikin torque capacities - and hence motions - are not affected by fatigue, which is unrealistic. Integrating the decrease of the joint torque capacities (eq. 3.6) in the controller is straightforward. However, a recovering law should also be implemented, otherwise the simulations are limited to very short activities.

Finally, as mentioned in section 4.4, the co-contraction phenomenon is not simulated, and therefore not taken into account in the ergonomic evaluation. Simulating the varying impedance of the human limbs (and in particular the human arm) would allow for a more accurate evaluation. Moreover, it would enable the evaluation of a wider class of activities, especially precision tasks. Indeed, contrarily to power tasks, in precision tasks, the co-contraction phenomenon may be the dominant cause of effort. Therefore this phenomenon cannot be excluded from an ergonomic evaluation.

Another point which needs to be addressed in order to provide reliable evaluations is the improvement of the manikin motions (low level) and behaviors (high level). One solution which seems promising is the integration of the controller for online adaptation of feet placement developed by Ibanez *et al.* [Ibanez 2014] (see section 4.4). Such a controller would remove the constraint of non-moving feet or pre-defined steps during the activities that are evaluated, thus leading to more natural postures. However, achieving realistic behaviors during complex activities probably requires not only the use of reactive techniques, but also of higher level planning methods.

### 7.2.2  Applications

A first potential application is directly related to the improvement of the manikin realism. Indeed, as stated in section 4.4, the generation of human-like motions requires to understand the underlying principles which determine human motions. Transposed to the manikin, it requires to establish which mathematical quantities are minimized when human-like motions are performed. If some criteria already exist for some kinds of motions (*e.g.* reaching), it is not the case for all kinds of activities. The framework proposed in this work might be useful to help establishing such criteria. Indeed, thanks to the dynamic replay method (see section 3.2.3), many biomechanical quantities can be measured on human-like motions, forming a ground truth. The analysis method presented in chapter 5 could then be adapted to simulate multiple ways of performing the same activities (*e.g.* parameters of the controller could be varied). By comparing the values of numerous quantities measured on the human-like motion (motion capture data) and on the fully automatic simulations, it may be possible to identify some quantities which are minimized during the human-like motion. By carrying out the same process on many other similar activities, some generic pattern may be identified.

The possibility - offered by the proposed framework - to easily introduce variability into the execution of an activity could also be used to perform more exhaustive evaluations. Indeed, when a workstation is designed or evaluated, the ergonomic assessment is usually carried out on a single execution of the activity. More and more, various morphologies of workers are considered, however, the intra-worker variability is never considered. Yet, when a worker performs a task, he/she does not always perform it the same way. His/her level of fatigue, but also numerous other factors may significantly affect the way the task is performed (*i.e.* the motions and postures). Accounting for such variability with commercial DHM software is not straightforward, because it is highly time-consuming, and also because automatic motions are generally not parametrizable. On the contrary, such variability can easily and quickly be added with the framework which has been developed for sensitivity analysis of ergonomic indicators.

Another application concerns the optimization of some parameters of the robot. In chapter 6, a method for optimizing the robot morphology has been proposed. However, other parameters, such as control parameters could be optimized with the same method (only the genome needs to be modified). An interesting application is the optimization of the position of the robot-worker interaction point (*i.e.* the user handle), the structure of the cobot being known. Such an optimization can have two advantages. On one hand, and as highlighted by the sensitivity analysis in chapter 5, the worker's morphology does influence the ergonomic indicators. Therefore, a robot which is optimal for a worker might not be for another. It is not possible (for cost reasons), to design a different robot for each worker. However, adding adjustable parts, such as the user handle, to the robot in order to adapt to each worker seems

a good compromise. The optimization can then be used to define acceptable limits for the range of variation of the handle position, or to provide recommendations regarding which position should be used for different workers' morphologies. On the other hand, modifying the robot-worker interaction point can also enable to adapt a generic platform to various activities. Indeed, designing a dedicated cobot from scratch is very costly, and therefore not accessible to small companies. Adapting existing structures is a way to reduce the development cost, through economy of scale. The modification of the interaction point could be the first level of such an adaptation.

Finally, the framework developed in this work addresses specifically the collaborative robots providing strength amplification. Nevertheless, with only slight modifications, other kinds of collaborative robots, or assistive devices, could be compared. The modifications concern mainly the robot control law, the modeling of the human-robot physical interaction, and the representation of the robot effects on the worker (for the sensitivity analysis). For instance, appendix C details an application of the simulation framework for the evaluation of a co-worker robot (*i.e.* a robot which occasionally interact with a worker, but while performing a task autonomously). Workstations could also be evaluated with the proposed framework. This would be of particular interest for dynamic activities, since most existing DHM software do not include dynamic phases and phenomena in the ergonomic evaluation. Nevertheless, if the temporal organisation of the work is significantly modified by the robot or workstation, the proposed ergonomic indicators need to be completed in order to take into account the duration and the repetitiveness risk factors.

# Appendix A
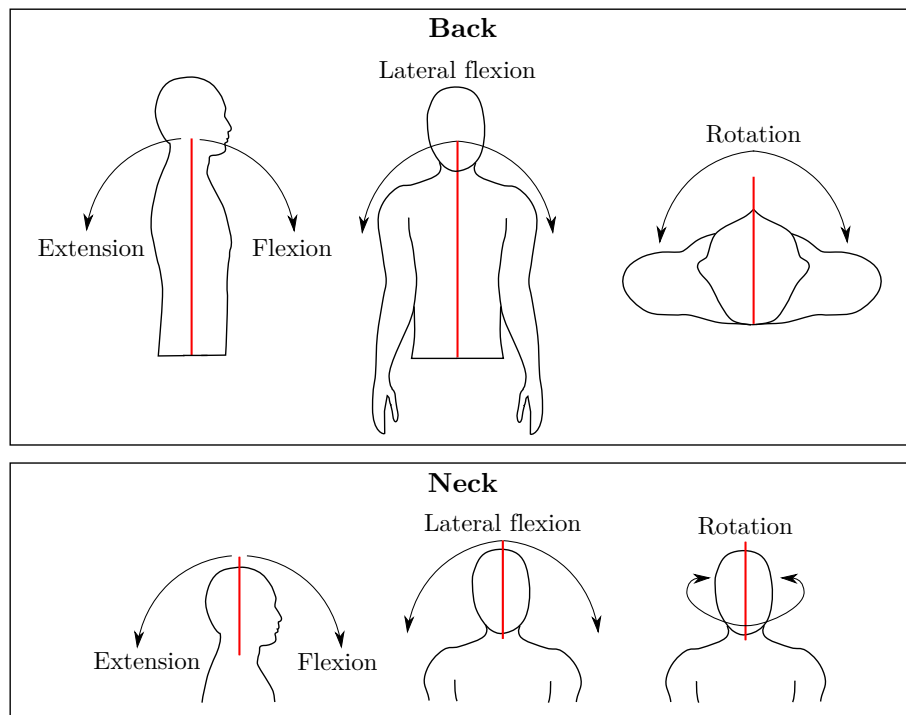
# Human joint motion



Figure A.1: Definition of back and neck motion. Neutral position is depicted by the red line.
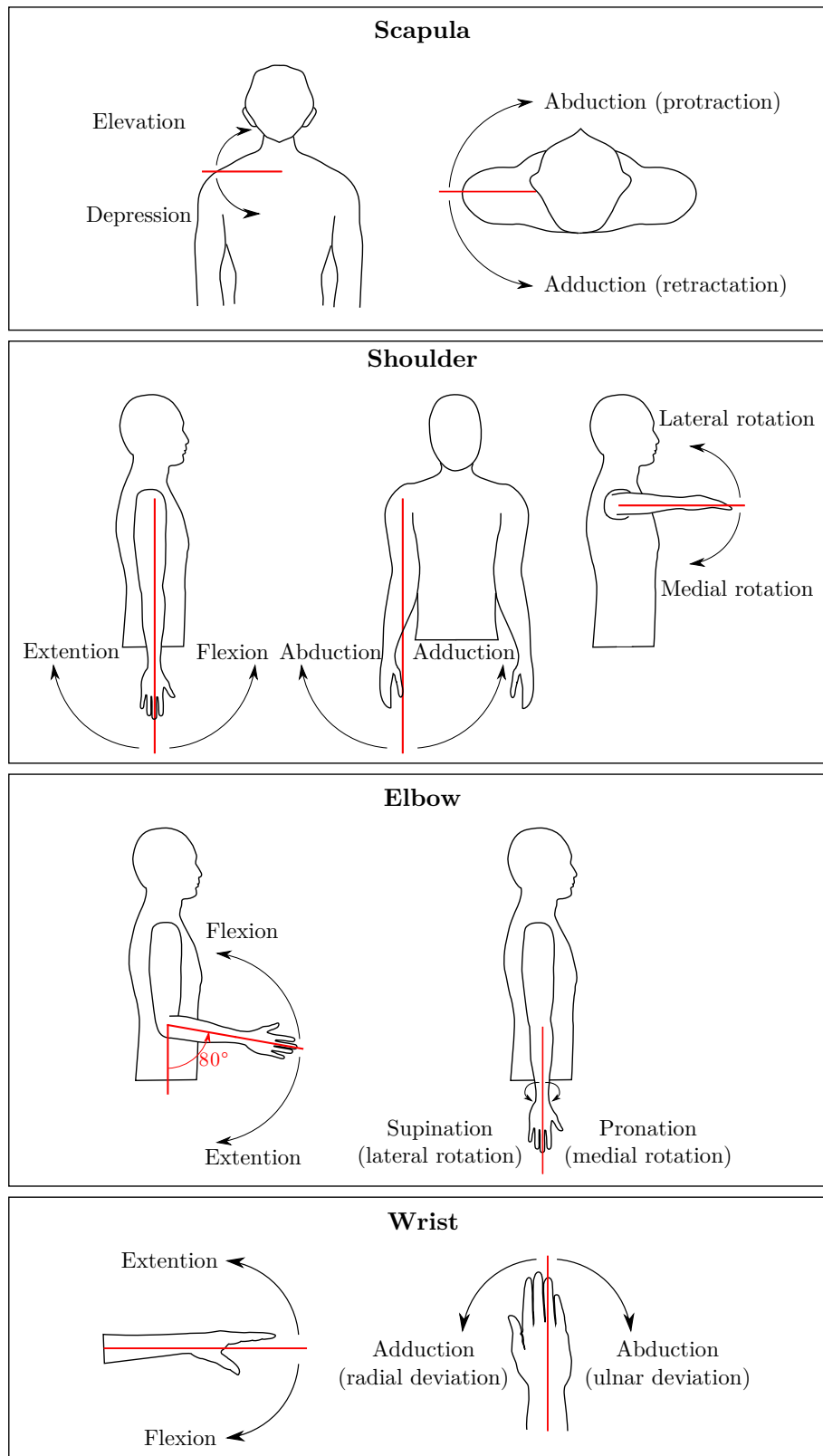
Figure A.2: Definition of upper limb motion. Neutral position is depicted by the red line.
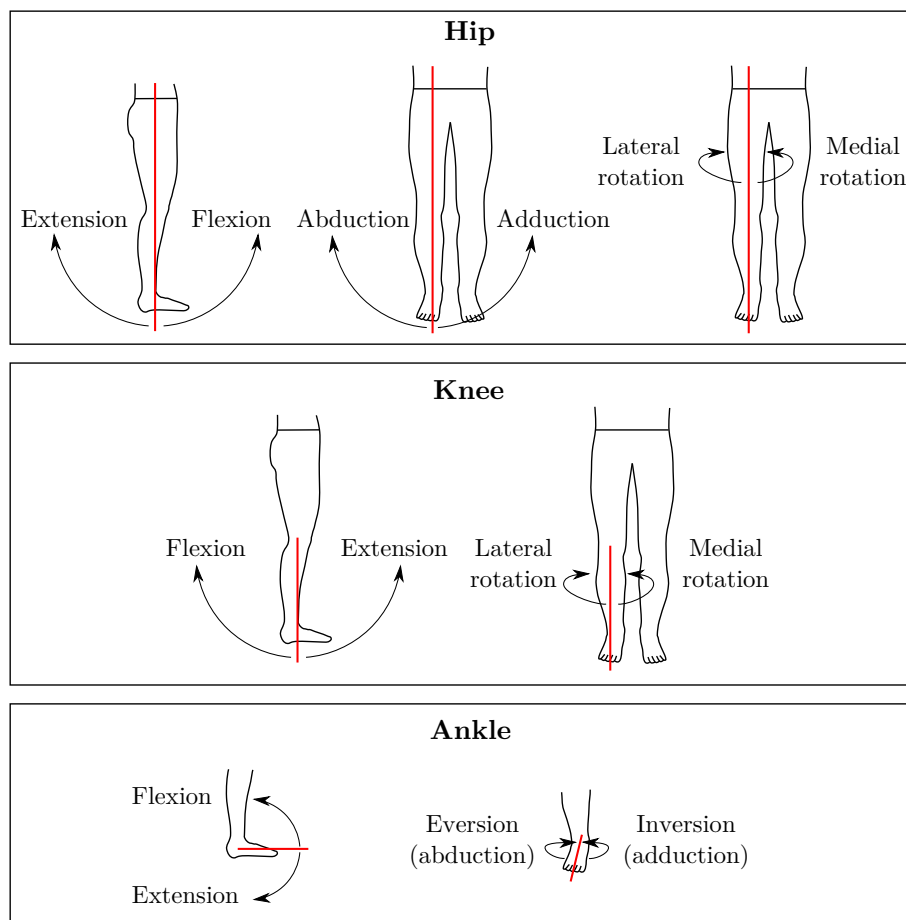
Figure A.3: Definition of lower limb motion. Neutral position is depicted by the red line.

| | Flexion | Extension | Abduction | Adduction | Medial rotation | Lateral rotation |
|---|---|---|---|---|---|---|
| Wrist | 90 | 99 | 47 | 27 | - | - |
| Elbow | 142 | 0 | - | - | 77 | 113 |
| Shoulder | 188 | 61 | 134 | 48 | 97 | 34 |
| Scapula | 40 | 10 | 20 | 15 | - | - |
| Neck | 85 | 50 | 50 | 50 | 85 | 85 |
| Back | 50 | 20 | 30 | 30 | 35 | 35 |
| Hip | 113 | 15 | 53 | 31 | 39 | 34 |
| Knee | 140 | 5 | - | - | 35 | 43 |
| Ankle | 35 | 38 | 23 | 24 | - | - |

Table A.1: Human average joint range of motion (in degree) [Chaffin 2006]. No coupling between adjacent joints is considered. The reference posture for setting the zero of joint angles is similar to the neutral position depicted on Fig. 3.1, except the elbow is stretched (upright, straight legs, arms along the body).

| | Flexion | Extension | Abduction | Adduction | Medial rotation | Lateral rotation |
|---|---|---|---|---|---|---|
| Wrist | 10 | 7 | 11 | 9 | - | - |
| Elbow | 75 | 45 | - | - | 8 | 13 |
| Shoulder | 90 | 65 | 69 | 65 | 51 | 32 |
| Scapula | 105 | 78 | 107 | 88 | - | - |
| Neck | | | | | | |
| Back | 140 | 228 | 155 | 155 | 65 | 65 |
| Hip | 180 | 186 | 97 | 108 | 67 | 28 |
| Knee | 97 | 164 | - | - | 17 | 22 |
| Ankle | 44 | 123 | 22 | 29 | - | - |

Table A.2:  Human average joint torque capacities (in N.m) [Holzbaur 2005, Chaffin 2006]. The influence of joint position and velocity is not considered. These values correspond to the joint maximal capacities, which are usually reached when the joints are close to the center of their range of motion

# Appendix B

# Description of the XDE manikin

The XDE-manikin consists of 21 rigid bodies linked together by 20 joints with a total of 45 degrees of freedom (DoF), plus 6 DoFs for the free floating base. The manikin DoFs are listed in table B.1. However, the toes DoF is not used in this work, so its range of motion, as well as its torque capacity are set to zero.

Each DoF is a revolute joint controlled by a sole actuator. The DoFs which in the human body are distributed along a segment (*e.g.* pronosupination, or knee medial/lateral rotation) are localized in the parent adjacent joint.

The kinematic structure of the manikin and the volume of its body segments are automatically scaled given the desired mass[1] and height[2], according to average scaling coefficients.

| Limb | Joint | DoFs | Axes |
|------|-------|------|------|
| Torso | Lower back | 3 | X Y Z |
| | Upper back | 3 | X Y Z |
| | Neck | 3 | X Y Z |
| | Head | 2 | X Y |
| Arm | Clavicle | 2 | X Z |
| | Shoulder | 3 | X Y Z |
| | Elbow | 2 | Y Z |
| | Wrist | 2 | X Z |
| Leg | Hip | 3 | X Y Z |
| | Knee | 2 | Y Z |
| | Ankle | 2 | X Y |
| | Toes | 1 | Y |

Table B.1: Kinematic structure of the XDE-manikin. The bodies and axes are defined in Fig. B.1.

---

[1] http://biomech.ftvs.cuni.cz/pbpk/kompendium/biomechanika/geometrie_hmotnost_vypocet_en
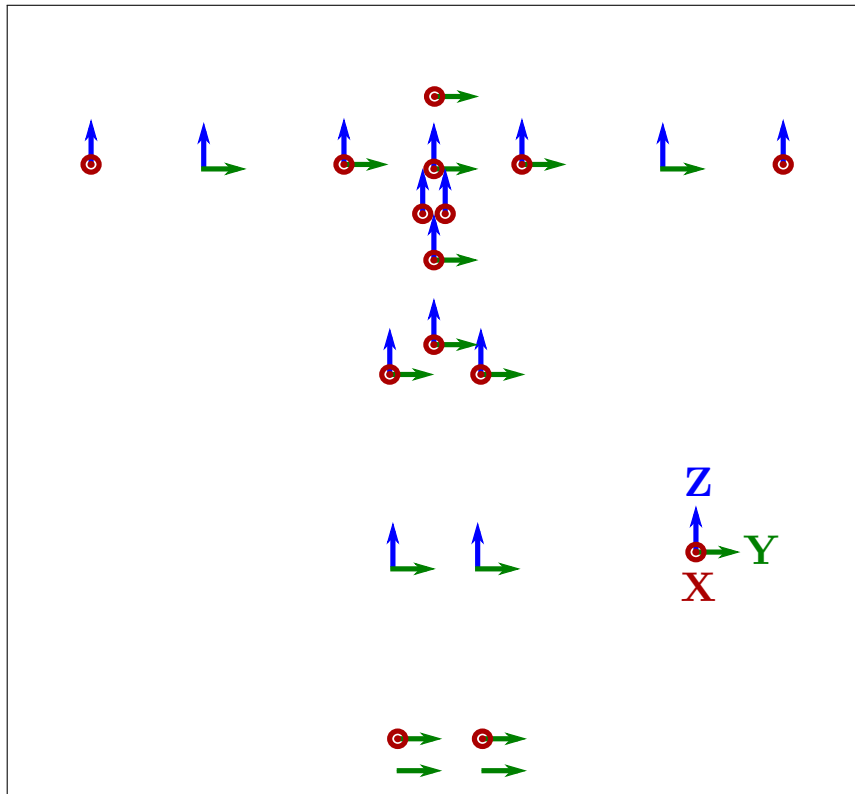[2] http://www.openlab.psu.edu/tools/calculators/proportionalityConstant

Figure B.1: Kinematic structure of the manikin (front view). The colored arrows represent the axes of the DoFs. X is red, Y is green, and Z is blue.

# Application of the evaluation framework to the comparison of collaborative robots

This section presents an application of the evaluation framework described in chapters 3. The ergonomic indicators tested in section 4.2 and the XDE virtual manikin are used to highlight and compare the benefit provided by two kinds of collaborative robots. The purpose of this experiment is not to choose a robot for a specific task, but rather to demonstrate the usefulness of different kinds of robotic assistance, and what they can be used for. Indeed this experiment was designed as a demonstration for industrial exhibitions[1].

## C.1   Experimental protocol

Two scenarii are presented in this experiment, which correspond to two different kinds of collaborative robot. Contrarily to the human-cobot simulation in section 4.3, none of these robots provide strength amplification.

In the first scenario, a manual manipulation task is performed by a human subject, with and without an exoskeleton providing weight compensation. His motions are recorded in both cases and then replayed with the virtual manikin, in order to compute the corresponding values of the ergonomic indicators.

In the second scenario, the execution of the different phases of the tasks is divided between the worker and the robot. The robot occasionally interacts with the worker and safely shares his/her workspace, but meanwhile, it autonomously performs certain tasks. Such a collaborative robot is generally called a *co-worker robot.* The co-worker robot considered here only exists as a prototype, so the task is not performed by a real subject (no motion capture), but it is simulated with the

---

[1]A video of the experiment is available here: http://pages.isir.upmc.fr/~padois/website/fichiers/videos/maurice_INNOROBO2014.mp4

autonomous virtual manikin.

The values of the ergonomic indicators are compared for the three cases (without assistance, with weight compensation, and with the co-worker robot).

### C.1.1   Task description

The task considered here consists in manually manipulating an object, in order to control its quality. The object is a 2 kg metal disk with four holes in it. The disk is initially located on point A (Fig. C.1). The worker takes the disk with his/her right hand, puts it on a table in front of him/her and checks the depth of each one of the four holes with a rod held in his/her left hand. Once the control is performed, he/she takes again the disk with his/her right hand, and moves it to its final destination on point B. The control area is located in between point A and point B, which are separated from 80 cm. The worker does not move his/her feet during the task.

There is no time constraint for this task, however it takes about 20 s for a human subject to perform it. The control phase takes about 8 s and the manipulation phases about 6 s each. The only added value in this task lies in the control phase; the manipulation phases only aim at bringing the object to and from the control area.

### C.1.2   Collaborative robot

Two different collaborative robots are used to help the worker perform the manipulation task. The first one is an arm exoskeleton providing weight compensation, whereas the second one is a serial manipulator co-worker robot, which performs some parts of the task in place of the worker.

**Exoskeleton for weight compensation:**   The first collaborative robot that is tested is the ABLE exoskeleton, a 7 degrees of freedom arm exoskeleton designed by CEA-LIST [Garrec 2008]. It is used to compensate the weight of the manipulated object (the mass and center of mass position must be known beforehand). However, the weight of the human arm is not compensated here. Only the right arm of the subject is equipped with the exoskeleton, since the left arm does not execute any strenuous tasks. The exoskeleton is fixed on a support, so that the subject does not have to carry its weight.

As a first approach, the exoskeleton is not integrated in the XDE simulation, for complexity reasons. The assistive effect is represented by setting the mass of the simulated object to zero. This solution however also cancels (in the simulation) some effects which are not compensated with the real robot: the inertial effects due to the object mass, and the moments associated with the weight. However, the inertial effects of the object are negligible anyway during the considered task, and the subject is told to hold the object horizontal and at its center of mass, so that the moments of the weight are null. The proposed simplification therefore mainly comes

down to considering that the exoskeleton is fully transparent: the efforts needed to manipulate it are not taken into account in the ergonomic evaluation. However, the considered exoskeleton has been mechanically designed to be very backdrivable, therefore, this additional effort is not significant.
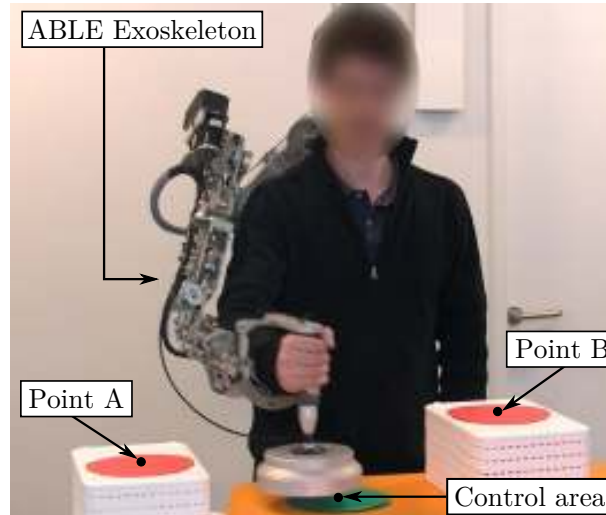


Figure C.1: A subject performing the task (manipulation phase) with the ABLE arm exoskeleton.

**Co-worker robot:** The second robot (Fig. C.2) is not designed for permanent physical interaction with the worker, contrarily to weight compensation or strength amplification robot. It is an autonomous 6 degrees of freedom serial manipulator, which is designed to ensure the safety of the physical interaction with a human being. Therefore the robot can share the workspace of the worker, without needing any fences or further securities. Meanwhile, the robot can carry out certain tasks autonomously.

With the co-worker robot, the scenario is slightly modified. The worker only performs the control task which requires the human perception skills, whereas the simple manipulation tasks are performed by the robot. The robot brings the object to the worker, holds it during the control phase, and then takes it back when the control is over. The robot is autonomous, in that during its displacement, its trajectory is not controlled by the worker. However, the worker remains in control of the work pace: he/she triggers a new work cycle (taking back the object and bringing a new one) by pushing the robot away.

In order to reduce the time of the manipulation phases in which there is no added value, two identical co-worker robots are used. While the first robot waits for the control of a first piece to be over, the second robot brings the next piece close to the control area. Therefore the control of the second piece can start almost immediately after the departure of the first piece. Regarding the output of the task, the manipulation phase is then a background task.
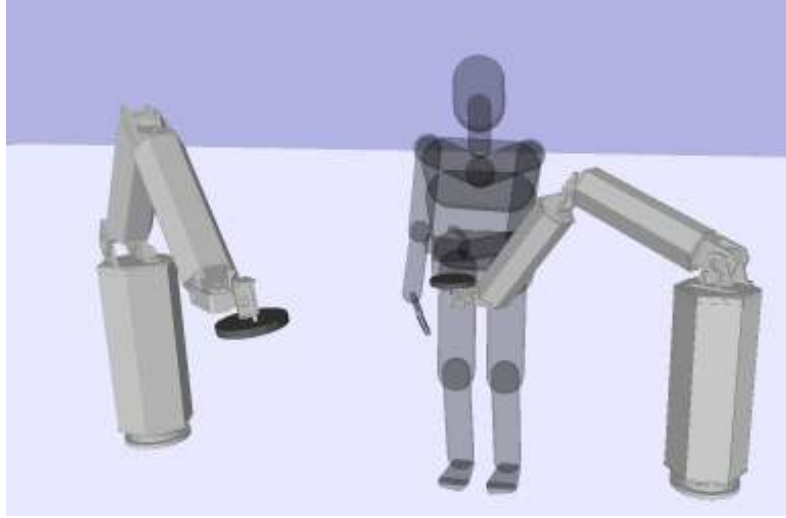
Figure C.2: Simulation with a task performed with a co-worker robot. The robot shares the worker's workspace and occasionally interacts with him/her, but it also performs tasks autonomously. Two co-worker robots are used here in order to increase the productiveness. The worker however remains in control of the work pace.

### C.1.3 Subjects and instrumentation

Data are recorded on real subjects only for the cases without assistance and with weight compensation. Since this experiment is initially designed for a demonstration, and not for a scientific validation, proper data are only recorded for one subject. The subject performs the task six times (with resting periods in between), both with and without assistance, while his/her motions are recorded.

**No assistance:** The conditions of the exhibition impose some constraints on the instrumentation. Standard motion capture systems cannot be used to track the subject's motions, because the required instrumentation cannot be installed on the exhibition site. Non-invasive systems, such as Kinect sensors could be used instead, but they are not sufficiently reliable in such open environment. Instead, the motions of the subject's right arm are recorded thanks to the ABLE exoskeleton (which joint positions as well as geometry are known). The subject is therefore equipped with the exoskeleton, even when weight compensation is not provided. The case without assistance is then slightly biased, since the presence of the exoskeleton might affect the subject's motion.

The other parts of the body are not tracked. The exoskeleton being mounted on a fixed base, the subject is asked to keep his/her back in contact with this base, and not to move his/her feet. So the motions of the back and legs are almost non-existent. The left arm is used for the control phase, but its motion is not recorded.

The motion is then replayed with the virtual manikin, according to the technique described in section 3.2.3. The following tasks are included in the manikin controller, in decreasing order of importance: markers tracking tasks for the right wrist (position and orientation), the right elbow (position only) and the right shoulder (position only), balance task, gazing task, postural task, and joint torques minimization task. What is called "marker" here is in fact the Cartesian position of a joint, given by the exoskeleton geometric model.

Since the motion of the left arm is not recorded here, it is generated automatically, based on the average time needed to execute the control task. To this purpose, a manipulation task (trajectory only) is added in the manikin controller for the left hand (see section 3.2.2). This task is active only during the control phase. The weight of the left hand manipulation task is similar to the weight of the right wrist tracking task. This solution leads to a motion of the left arm that is not strictly similar to the original motion of the human subject. However, this is not limiting for the comparison of the different situations, since the left arm is not affected by any of the robotic assistance. Therefore the motion of the left arm can reasonably be considered the same in all three cases.

**Exoskeleton with weight compensation:** The case with weight compensation is exactly similar - both in the acquisition and in the replay - to the case without assistance, except here, the weight compensation is activated. Therefore, as explained in section C.1.2, the weight of the simulated object is set to zero in the simulation.

**Co-corker robot:** In the case of the co-worker robot, this task is not performed by a human subject, but only simulated with the autonomous manikin. Indeed, the robot is still under development and no physical prototype was available for the demonstration.

The manikin is autonomously animated according to the technique described in section 3.2.2. The following tasks are included in the controller, in decreasing order of importance: balance task, right hand manipulation tasks (trajectory and force), left hand manipulation task (trajectory only, same weight as the right hand manipulation tasks), gazing task, postural task, and joint torques minimization task.

Contrarily to the cases with the exoskeleton, the right arm is not used here to manipulate the object, but to push the robot away when the control phase is over, in order to trigger a new cycle. The right hand manipulation tasks therefore correspond to this motion, and are active only during this phase (the force task is active only when the hand is in contact with the robot). The left hand manipulation task is exactly similar to the cases with the exoskeleton. It is active only during the control phase.

## C.2    Results and Discussion

For each case - without assistance, with weight compensation and with the co-worker robot - three ergonomic indicators are computed (the back and the right arm are considered in one single indicator):

- joint position indicator of the back and right arm $I_q^{B-RA}$;

- joint torque indicator of the back and right arm $I_\tau^{B-RA}$;

- joint power indicator of the back and right arm $I_p^{B-RA}$.

The left arm is not included in the evaluation, because its motion is quite similar in the three situations. Each indicator is time-integrated so that only one value (for each indicator) represents the whole task. The effect of the robots on the productiveness of the worker (*i.e.* how many pieces can be treated in a given time) is also investigated.

When considering only the situations without assistance and with the exoskeleton providing weight compensation, the average time needed to perform the whole task (*i.e.* one work cycle) is very similar in both cases. Therefore, all three indicators can directly be used to compare the two situations (see section 4.2). On the contrary, when the co-worker robot is used, the duration of a work cycle is about twice as short as without assistance. Indeed, the manipulation phases are carried out by a robot while the subject performs the control task. The situation with the co-worker robot can therefore not be compared with the other cases, at least not with the position and the torque indicators (see section 4.2). In order to be able to compare the ergonomic benefit provided by the different robots, the durations of the three situations are artificially equalled. To this purpose, two work cycles are simulated consecutively with the co-worker robot, whereas only one is replayed for the exoskeleton and without assistance. The values of the three ergonomic indicators for the corresponding situations are displayed in table C.1.

### C.2.1    Position indicator

**No assistance *vs.* weight compensation:**    The position indicator $I_q^{B-RA}$ without assistance or with weight compensation is very similar in both cases. The slight difference comes from the fact that the subject does not reproduce exactly the same motion at each trial. The manipulated object is probably not sufficiently heavy to induce a change in the posture when the manipulation time is short. Indeed, the subject only performs the task a few times, and with resting periods in between, so there is no influence of fatigue on the posture. However, if the task was performed repetitively during several hours, it is likely that the posture would differ more between the two cases (the situation without assistance causing more fatigue).

The similarity of the posture is also - and perhaps mainly - due to the presence of the exoskeleton in both cases. During a real industrial task, if no assistance is

| | Position $I_q^{B-RA}$ | Torque $I_\tau^{B-RA}$ | Power $I_p^{B-RA}$ | Number of work cycles |
|---|---|---|---|---|
| **No assistance** | 100 | 100 | 100 | 1 |
| **Exoskeleton with weight compensation** | 104 | 52 | 75 | 1 |
| **Co-worker robot** | 68 | 30 | 38 | 2 |

Table C.1: Comparison of the three ergonomic indicators for the situations without assistance, with the exoskeleton providing weight compensation, and with the co-worker robot. 20 s of work are considered for computing the indicators. This duration approximately corresponds to one work cycle without assistance and with the exoskeleton, and to two work cycles with the co-worker robot. For each case, the displayed value is the percentage of the reference value, *i.e.* the value of the indicator when the task is executed without any assistance. The values of the cases where motion capture is used (no assistance and weight compensation) are the averages over all the trials.

provided, the subject is not equipped with any instrumentation. Here on the contrary the exoskeleton is needed to record the subject's motions. Therefore his/her motions in the reference situation are not entirely unconstrained, especially as the exoskeleton imposes to keep the back fixed.

**Weight compensation *vs.* co-worker robot:** Compared to the cases with the exoskeleton, the position indicator $I_q^{B-RA}$ is significantly improved with the co-worker robot. Indeed, with the co-worker robot, the manipulation phases are removed: the only motion of the right arm consists in pushing on the robot to trigger a new cycle. The robot being quite close to the worker, this motion does not require a large motion of the arm. On the contrary, with the exoskeleton, the locations of points A and B force the subject to horizontally straighten his/her arm to reach the object.

### C.2.2 Torque and power indicators

**No assistance *vs.* weight compensation:** As expected, the torque indicator $I_\tau^{B-RA}$ and the power indicator $I_p^{B-RA}$ decrease when weight compensation is provided. The subject does not support the weight of the manipulated object any more, so the corresponding efforts disappear. The power indicator $I_p^{B-RA}$ is mainly affected through the torque modifications, since the joint velocities remain similar (similar posture, similar duration).

**Weight compensation *vs.* co-worker robot:** Compared to what is achieved with weight compensation, the co-worker robot leads to a much more significant

reduction in the torque indicator $I_\tau^{B-RA}$ and the power indicator $I_p^{B-RA}$. Indeed, the exoskeleton removes the weight of the object to carry, but not the weight of the arm. The initial and final positions of the manipulated object (points A and B) being quite far from the subject, he/she must straighten his/her arm to reach them. The gravity effects on the arm are therefore significant during the manipulation phases, so important joint torques are required to maintain the arm posture. On the contrary, since the manipulation phases are removed with the co-worker robot, the associated efforts disappear.

Though the co-worker robot requires the worker to push on it to trigger a new cycle, this additional gesture does not cause much effort. Indeed, the robot being quite close to the worker, he/she does not need to extend his/her arm to touch the robot, so the gravity effects on the arm remain small. And a light push on the robot is sufficient to trigger a new cycle, so no significant force is required in this phase.

### C.2.3   Productiveness

**No assistance *vs.* weight compensation:**   The duration of one work cycle is very similar with and without weight compensation. However this result should be considered cautiously here, because some phenomena are neglected. On one hand, the use of the exoskeleton during the situation without assistance (to record the subject's motions) may affect the way the task is performed, hence its duration. Most likely, the exoskeleton slightly hinders some motions, thus slowing down the task execution. The use of the exoskeleton would therefore reduce the productiveness, though this tendency might decrease after a learning period. On the other hand, the effect of fatigue on the motions are not considered. Fatigue generally causes a decrease in the work rate. Therefore, by reducing the force-related solicitations, thus the fatigue, the use of the exoskeleton could improve the productiveness.

**Weight compensation *vs.* co-worker robot:**   Compared to the exoskeleton, the co-worker robot approximately doubles the productiveness (a work cycle is twice as short with the co-worker robot). This is mostly due to the use of two robots, which transform the manipulation task in a background task (executed simultaneously with the control task). Despite this increased productiveness, the biomechanical solicitations experienced by the worker are significantly reduced (see the results for the ergonomic indicators). Therefore, it seems that the co-worker robot is more adapted to the task considered here than the exoskeleton, in regard to both the ergonomy and the productiveness.

However this conclusion should be considered cautiously, because some MSDs risk factors are not considered. In particular, the repetitiveness factor is not taken into account. The global ergonomic benefit provided of the co-worker robot may therefore be over-estimated, since this robot doubles the repetitiveness of the gestures.

## C.3 Conclusion

Thanks to the evaluation framework proposed in chapter 3, different kinds of collaborative robots can be quantitatively compared, in order to identify the one with the best performances for the considered activity. In the present experiment, the use of the exoskeleton supporting the weight of the manipulated object enables the reduction of the force-related biomechanical solicitations. However, the benefit provided by the co-worker robot is significantly more important, regarding both the ergonomic situation of the worker, and his/her productiveness.

Such a result is not general, but specific to the activity that is considered. Indeed, the phase of the activity in which the robotic assistance is used is very simple here. No perception or decision skills are needed to move the object to and from the control area, especially as the worker remains in charge of triggering the robot displacement. Therefore the manipulation task can easily be fully automated. For more complex tasks however (especially tasks in which the gesture cannot be modified), the automation would be much more difficult, and the exoskeleton could be a good solution. For instance, in [Sylla 2014], the ABLE exoskeleton is used in a car assembly line, to assist workers while they work with a screw gun. For such a task, the exoskeleton is proved particularly useful, since it supports the weight of the tool (and of the human arm in this case), while leaving the worker relatively free of his/her motions.

# Bibliography

[Abdel-Malek 2005] K. Abdel-Malek, J. Yang, W. Yu and J. Duncan. *Human Performance Measures: Mathematics*. Technical report, Department of Mechanical Engineering, The University of Iowa, 2005. (Cited on page 38.)

[Abdel-Malek 2006] K. Abdel-Malek, J. Arora, J. Yang, T. Marler, S. Beck, C. Swan, L. Frey-Law, A. Mathai, C. Murphy and S. Rahmatallah. *Santos: A physics-based digital human simulation environment*. Proceedings of the Human Factors and Ergonomics Society Annual Meeting, vol. 50, no. 20, pages 2279–2283, 2006. (Cited on page 25.)

[Abe 2007] Y. Abe, M. da Silva and J. Popović. *Multiobjective control with frictional contacts*. Proceedings of the ACM SIGGRAPH/Eurographics symposium on Computer animation, pages 249–258, 2007. (Cited on page 43.)

[AFNOR 2008a] AFNOR. *NF EN 1005 Sécurité des Machines - Performance physique humaine*. Association française de normalisation (AFNOR), 2008. (Cited on pages 15 and 73.)

[AFNOR 2008b] AFNOR. *NF EN ISO 15536 Ergonomics - Computer manikins and body templates*. Association française de normalisation (AFNOR), 2008. (Cited on page 19.)

[Aptel 2011] M. Aptel, F. Cail and A. Aublet-Cuvelier. *Les troubles musculosquelettiques du membre supérieur (TMS-MS). Guide pour les préventeurs.* Institut national de recherche et de sécurité (INRS), 2nd edition, 2011. (Cited on page 2.)

[Blanchonette 2010] P. Blanchonette. *Jack human modelling tool: A review*. Technical report, DTIC Document, 2010. (Cited on page 19.)

[Bogue 2009] R. Bogue. *Exoskeletons and robotic prosthetics: a review of recent developments*. Industrial Robot: An International Journal, vol. 36, no. 5, pages 421–427, 2009. (Cited on page 7.)

[Bohlin 2014] R. Bohlin, N. Delfs, P. Mardberg and J.S. Carlson. *A Framework for Combing Digital Human Simulations with Robots and Other Objects.*

Proceeedings of the 3rd International Digital Human Modeling Symposium, 2014. (Cited on page 28.)

[Book 1996] W.J. Book, R. Charles, H.T. Davis and M.W. Gomes. *The concept and implementation of a passive trajectory enhancing robot.* Proceedings of the International Mechanical Engineering Congress and Exposition (IMECE), pages 633–638, 1996. (Cited on page 8.)

[Bossomaier 2010] T. Bossomaier, A. Bruzzone, A. Cimino, F. Longo and G. Mirabelli. *Scientific Approaches for the Industrial Workstations Ergonomic Design: A Review.* Proceedings of the 24th European Conference on Modelling and Simulation, 2010. (Cited on page 19.)

[Box 1987] G.E.P. Box and N.R. Draper. Empirical model-building and response surfaces. John Wiley & Sons, 1987. (Cited on page 106.)

[Boyd 2004] S. Boyd and L. Vandenberghe. Convex optimization. Cambridge University Press, 2004. (Cited on page 162.)

[Busch 2013] F. Busch, S. Wischniewski and J. Deuse. *Application of a character animation SDK to design ergonomic human-robot-collaboration.* Proceedings of the 2nd International Digital Human Modeling Symposium, 2013. (Cited on page 28.)

[Campbell 2006] K. Campbell, M.D. McKay and B.J. Williams. *Sensitivity analysis when model outputs are functions.* Reliability Engineering & System Safety, vol. 91, no. 10, pages 1468–1472, 2006. (Cited on page 109.)

[Chaffin 1997] Don B Chaffin. *Development of computerized human static strength simulation model for job design.* Human Factors and Ergonomics in Manufacturing & Service Industries, vol. 7, no. 4, pages 305–322, 1997. (Cited on page 20.)

[Chaffin 2006] D.B. Chaffin, G.B.J. Andersson and B.J. Martin. Occupational biomechanics. Wiley, 4th edition, 2006. (Cited on pages 27, 35, 36, 72, 162 and 168.)

[Chaffin 2007] D.B. Chaffin. *Human motion simulation for vehicle and workplace design.* Human Factors and Ergonomics in Manufacturing & Service Industries, vol. 17, no. 5, pages 475–484, 2007. (Cited on page 19.)

[Chedmail 2002] P. Chedmail, B. Maille and E. Ramstein. *Etat de l'art sur l'accessibilité et l'étude de l'ergonomie en réalite virtuelle.* Mécanique & Industries, vol. 3, no. 2, pages 147–152, 2002. (Cited on page 19.)

[Chiaacchio 1998] P. Chiaacchio and M. Concilio. *The dynamic manipulability ellipsoid for redundant manipulators.* Proceedings of the IEEE International Conference on Robotics and Automation, vol. 1, pages 95–100, 1998. (Cited on page 39.)

[Chiu 1987] S.L. Chiu. *Control of redundant manipulators for task compatibility.* Proceedings of the IEEE International Conference on Robotics and Automation, vol. 4, pages 1718–1724, 1987. (Cited on pages 38 and 39.)

[Chocron 1997] Olivier Chocron and Philippe Bidaud. *Genetic design of 3D modular manipulators.* Proceedings of the IEEE International Conference on Robotics and Automation, vol. 1, pages 223–228, 1997. (Cited on page 131.)

[Claudon 2008] L. Claudon, B. Daille-Lefèvre and J. Marsot. *La révolution du numérique: un atout pour concevoir des postes de travail plus sûrs.* Hygiène et sécurité du travail, vol. 210, pages 5–13, 2008. (Cited on page 18.)

[Colgate 1996] J.E. Colgate, M.A. Peshkin and W. Wannasuphoprasit. *Cobots: Robots for collaboration with human operators.* Proceedings of the ASME Dynamic Systems and Control Conference, vol. 58, pages 433–440, 1996. (Cited on page 5.)

[Colgate 2003] J.E. Colgate, M. Peshkin and S.H. Klostermeyer. *Intelligent assist devices in industrial applications: a review.* Proceedings of the IEEE/RSJ International Conference on Intelligent Robots and Systems, vol. 3, pages 2516–2521, 2003. (Cited on page 5.)

[Collette 2007] C. Collette, A. Micaelli, C. Andriot and P. Lemerle. *Dynamic balance control of humanoids for multiple grasps and non coplanar frictional contacts.* Proceedings of the 7th IEEE/RAS International Conference on Humanoid Robots, pages 81–88, 2007. (Cited on page 43.)

[Cukier 1978] R.I. Cukier, H.B. Levine and K.E. Shuler. *Nonlinear sensitivity analysis of multiparameter model systems.* Journal of computational physics, vol. 26, no. 1, pages 1–42, 1978. (Cited on page 108.)

[Damsgaard 2006] M. Damsgaard, J. Rasmussen, S. T. Christensen, E. Surma and M. de Zee. *Analysis of musculoskeletal systems in the AnyBody Modeling System.* Simulation Modelling Practice and Theory, vol. 14, no. 8, pages 1100–1111, 2006. (Cited on pages 25 and 27.)

[David 2005] G.C. David. *Ergonomic methods for assessing exposure to risk factors for work-related musculoskeletal disorders.* Occupational medicine, vol. 55, no. 3, pages 190–199, 2005. (Cited on pages 14 and 18.)

[De Magistris 2013] G. De Magistris, A. Micaelli, P. Evrard, C. Andriot, J. Savin, C. Gaudez and J. Marsot. *Dynamic control of DHM for ergonomic assessments.* International Journal of Industrial Ergonomics, vol. 43, no. 2, pages 170–180, 2013. (Cited on page 95.)

[Deb 2001] K. Deb. Multi-objective optimization using evolutionary algorithms. John Wiley & Sons, 2001. (Cited on page 134.)

[Deb 2002] K. Deb, A. Pratap, S. Agarwal and T. Meyarivan. *A fast and elitist multiobjective genetic algorithm: NSGA-II.* IEEE Transactions on Evolutionary Computation, vol. 6, no. 2, pages 182–197, 2002. (Cited on pages 133 and 134.)

[Deb 2014] K. Deb and D. Deb. *Analysing mutation schemes for real-parameter genetic algorithms.* International Journal of Artificial Intelligence and Soft Computing, vol. 4, no. 1, pages 1–28, 2014. (Cited on pages 139, 146 and 155.)

[Delp 2007] S.L. Delp, F.C. Anderson, A.S. Arnold, P. Loan, A. Habib, C.T. John, E. Guendelman and D.G. Thelen. *OpenSim: open-source software to create and analyze dynamic simulations of movement.* IEEE Transactions on Biomedical Engineering, vol. 54, no. 11, pages 1940–1950, 2007. (Cited on page 25.)

[Demircan 2010] E. Demircan, T. Besier, S. Menon and O. Khatib. *Human motion reconstruction and synthesis of human skills.* Advances in Robot Kinematics: Motion in Man and Machine, pages 283–292, 2010. (Cited on page 51.)

[Doncieux 2011] S. Doncieux, J.B. Mouret, N. Bredeche and V. Padois. *Evolutionary robotics: Exploring new horizons.* New Horizons in Evolutionary Robotics, pages 3–25, 2011. (Cited on page 131.)

[Erden 2011] M.S. Erden and B. Marić. *Assisting manual welding with robot.* Robotics and Computer-Integrated Manufacturing, vol. 27, no. 4, pages 818–828, 2011. (Cited on page 5.)

[Escande 2014] A. Escande, N. Mansard and P.B. Wieber. *Hierarchical quadratic programming: Fast online humanoid-robot motion generation.* The International Journal of Robotics Research, 2014. (Cited on page 43.)

[Feyen 2000] R. Feyen, Y. Liu, D. Chaffin, G. Jimmerson and B. Joseph. *Computer-aided ergonomics: a case study of incorporating ergonomics analyses into workplace design.* Applied Ergonomics, vol. 31, no. 3, pages 291–300, 2000. (Cited on page 19.)

[Fisher 1935] R.A. Fisher. The design of experiments. Oliver & Boyd, 1935. (Cited on page 104.)

[Fitts 1954] P.M. Fitts. *The information capacity of the human motor system in controlling the amplitude of movement.* Journal of experimental psychology, vol. 47, no. 6, page 381, 1954. (Cited on page 94.)

[Flash 1985] T. Flash and N. Hogan. *The coordination of arm movements: an experimentally confirmed mathematical model.* The journal of Neuroscience, vol. 5, no. 7, pages 1688–1703, 1985. (Cited on pages 37, 45 and 95.)

[Garcia 2002] E. Garcia, J. Estremera and P.G. de Santos. *A classification of stability margins for walking robots.* Proceedings of the International Symposyum on Climbing and Walking Robots, vol. 20, 2002. (Cited on page 40.)

[Garg 1978] A. Garg, D.B. Chaffin and G.D. Herrin. *Prediction of metabolic rates for manual materials handling jobs.* The American Industrial Hygiene Association Journal, vol. 39, no. 8, pages 661–674, 1978. (Cited on page 37.)

[Garrec 2008] P. Garrec, J.P. Friconneau, Y. Measson and Y. Perrot. *ABLE, an innovative transparent exoskeleton for the upper-limb.* Proceedings of the IEEE/RSJ International Conference on Intelligent Robots and Systems, pages 1483–1488, 2008. (Cited on page 172.)

[Goldberg 1987] D.E. Goldberg and J. Richardson. *Genetic algorithms with sharing for multimodal function optimization.* Proceedings of the 2nd International Conference on Genetic Algorithms, pages 41–49, 1987. (Cited on page 138.)

[Goldberg 1989] D.E. Goldberg. Genetic algorithms in search, optimization, and machine learning. Addison Wesley, 1989. (Cited on page 130.)

[Goswami 1999] A. Goswami. *Postural stability of biped robots and the foot-rotation indicator (FRI) point.* The International Journal of Robotics Research, vol. 18, no. 6, pages 523–533, 1999. (Cited on page 40.)

[Goupy 2006] J. Goupy. *Plans d'expériences.* Techniques de l'Ingénieur, 2006. (Cited on page 104.)

[Gribble 2003] P.L. Gribble, L.I. Mullin, N. Cothros and A. Mattar. *Role of cocontraction in arm movement accuracy.* Journal of Neurophysiology, vol. 89, no. 5, pages 2396–2405, 2003. (Cited on page 93.)

[Groshaw 1969] P.F. Groshaw. *Hardiman I arm test, Hardiman I prototype.* General Electric Report S-70-1019, General Electric Co., Schenectady, NY, 1969. (Cited on page 6.)

[Hansen 1996] N. Hansen and A. Ostermeier. *Adapting arbitrary normal mutation distributions in evolution strategies: The covariance matrix adaptation.* Proceedings of the IEEE International Conference on Evolutionary Computation, pages 312–317, 1996. (Cited on page 156.)

[Hanson 2011] L Hanson, Dan Högberg, R Bohlin and J Carlson. *IMMA–Intelligently Moving Manikins–Project Status 2011.* Proceedings of the 1st International Symposium on Digital Human Modeling, 2011. (Cited on page 22.)

[He 2013] Z. He and G.G. Yen. *Ranking many-objective evolutionary algorithms using performance metrics ensemble.* Proceedings of the IEEE Congress on Evolutionary Computation, pages 2480–2487, 2013. (Cited on page 156.)

[Hignett 2000] S. Hignett and L. McAtamney. *Rapid entire body assessment (REBA)*. Applied Ergonomics, vol. 31, no. 2, pages 201–206, 2000. (Cited on page 15.)

[Hoeffding 1948] W. Hoeffding. *A class of statistics with asymptotically normal distribution*. The annals of mathematical statistics, pages 293–325, 1948. (Cited on page 107.)

[Holland 1975] J.H. Holland. Adaptation in natural and artificial systems: an introductory analysis with applications to biology, control, and artificial intelligence. University of Michigan Press, 1975. (Cited on page 130.)

[Holzbaur 2005] K.R.S. Holzbaur, W.M. Murray and S.L. Delp. *A model of the upper extremity for simulating musculoskeletal surgery and analyzing neuromuscular control*. Annals of biomedical engineering, vol. 33, no. 6, pages 829–840, 2005. (Cited on pages 36 and 168.)

[Homma 1996] T. Homma and A. Saltelli. *Importance measures in global sensitivity analysis of nonlinear models*. Reliability Engineering & System Safety, vol. 52, no. 1, pages 1–17, 1996. (Cited on page 107.)

[Hoyet 2010] L. Hoyet. *Adaptation dynamique de mouvements humains*. PhD thesis, Insa de Rennes, 2010. (Cited on page 40.)

[Ibanez 2014] A. Ibanez, P. Bidaud and V. Padois. *Emergence of humanoid walking behaviors from Mixed-Integer Model Predictive Control*. Proceedings of the IEEE/RSJ International Conference on Intelligent Robots and Systems, 2014. (Cited on pages 95, 96 and 162.)

[Igel 2007] C. Igel, N. Hansen and S. Roth. *Covariance matrix adaptation for multiobjective optimization*. Evolutionary computation, vol. 15, no. 1, pages 1–28, 2007. (Cited on page 156.)

[Iooss 2011] B. Iooss. *Revue sur l'analyse de sensibilité globale de modèles numériques*. Journal de la Société Française de Statistique, vol. 152, no. 1, pages 3–25, 2011. (Cited on page 105.)

[Jacquier-Bret 2012] J. Jacquier-Bret, P. Gorce and N. Rezzoug. *The manipulability: a new index for quantifying movement capacities of upper extremity*. Ergonomics, vol. 55, no. 1, pages 69–77, 2012. (Cited on page 38.)

[Jarrassé 2008] N. Jarrassé, J. Paik, V. Pasqui and G. Morel. *How can human motion prediction increase transparency?* Proceedings of the IEEE International Conference on Robotics and Automation, pages 2134–2139, 2008. (Cited on page 88.)

[Jolliffe 2002] I. Jolliffe. Principal component analysis. Wiley Online Library, 2002. (Cited on page 110.)

[Kajita 2003] S. Kajita, F. Kanehiro, K. Kaneko, K. Fujiwara, K. Harada, K. Yokoi and H. Hirukawa. *Biped walking pattern generation by using preview control of zero-moment point.* Proceedings of the IEEE International Conference on Robotics and Automation, vol. 2, pages 1620–1626, 2003. (Cited on page 45.)

[Kang 2005] T. Kang, J. He and S.I.H. Tillery. *Determining natural arm configuration along a reaching trajectory.* Experimental Brain Research, vol. 167, no. 3, pages 352–361, 2005. (Cited on page 37.)

[Kanoun 2009] O. Kanoun, F. Lamiraux, P.B. Wieber, F. Kanehiro, E. Yoshida and J.P. Laumond. *Prioritizing linear equality and inequality systems: application to local motion planning for redundant robots.* Proceedings of the IEEE International Conference on Robotics and Automation, pages 2939–2944, 2009. (Cited on page 43.)

[Karhu 1981] O. Karhu, R. Härkönen, P. Sorvali and P. Vepsäläinen. *Observing working postures in industry: Examples of OWAS application.* Applied Ergonomics, vol. 12, no. 1, pages 13–17, 1981. (Cited on page 15.)

[Kazerooni 1993] H. Kazerooni. *Extender: a case study for human-robot interaction via transfer of power and information signals.* Proceedings of the 2nd IEEE International Workshop on Robot and Human Communication, pages 10–20, 1993. (Cited on page 7.)

[Khatib 2004] O. Khatib, J. Warren, V. De Sapio and L. Sentis. *Human-like motion from physiologically-based potential energies.* Advances in robot kinematics, pages 145–154, 2004. (Cited on page 36.)

[Khatib 2008] O. Khatib, L. Sentis and J.H. Park. *A unified framework for whole-body humanoid robot control with multiple constraints and contacts.* Proceedings of the European Robotics Symposium, pages 303–312, 2008. (Cited on page 43.)

[Lamboni 2011] M. Lamboni, H. Monod and D. Makowski. *Multivariate sensitivity analysis to measure global contribution of input factors in dynamic models.* Reliability Engineering & System Safety, vol. 96, no. 4, pages 450–459, 2011. (Cited on page 109.)

[Lämkull 2009] D. Lämkull, L. Hanson and R. Örtengren. *A comparative study of digital human modelling simulation results and their outcomes in reality: A case study within manual assembly of automobiles.* International Journal of Industrial Ergonomics, vol. 39, no. 2, pages 428–441, 2009. (Cited on pages 24 and 97.)

[Lamy 2011] X. Lamy. *Conception d'une Interface de Pilotage d'un Cobot.* PhD thesis, Université Pierre et Marie Curie-Paris VI, 2011. (Cited on pages 7, 53 and 87.)

[Leboeuf 2006] F. Leboeuf, G. Bessonnet, P. Seguin and P. Lacouture. *Energetic versus sthenic optimality criteria for gymnastic movement synthesis.* Multibody System Dynamics, vol. 16, no. 3, pages 213–236, 2006. (Cited on pages 36 and 37.)

[Lee 2006] K.Y. Lee, S.Y. Lee, J.H. Choi, S.H. Lee and C.S. Han. *The application of the human-robot cooperative system for construction robot manipulating and installing heavy materials.* Proceedings of the IEEE SICE-ICASE International Joint Conference, pages 4798–4802, 2006. (Cited on page 7.)

[Leger 1999] C. Leger. *Automated synthesis and optimization of robot configurations: an evolutionary approach.* PhD thesis, Carnegie Mellon University Pittsburgh, 1999. (Cited on page 131.)

[Li 1999] G. Li and P. Buckle. *Current techniques for assessing physical exposure to work-related musculoskeletal risks, with emphasis on posture-based methods.* Ergonomics, vol. 42, no. 5, pages 674–695, 1999. (Cited on pages 14, 17, 18 and 41.)

[Liu 2012] M. Liu, A. Micaelli, P. Evrard, A. Escande and C. Andriot. *Interactive virtual humans: A two-level prioritized control framework with wrench bounds.* IEEE Transactions on Robotics, vol. 28, no. 6, pages 1309–1322, 2012. (Cited on pages 43 and 95.)

[Luttmann 2003] A. Luttmann, M. Jäger, B. Griefahn, G. Caffier, F. Liebers and U. Steinberg. *Preventing musculoskeletal disorders in the workplace.* World Health Organization. Protecting Workers' Health Series, vol. 5, 2003. (Cited on page 2.)

[Ma 2009] L. Ma, W. Zhang, D. Chablat, F. Bennis and F. Guillaume. *Multi-objective optimisation method for posture prediction and analysis with consideration of fatigue effect and its application case.* Computers & Industrial Engineering, vol. 57, no. 4, pages 1235–1246, 2009. (Cited on page 36.)

[Marler 2006] T. Marler, K. Farrell, J. Kim, S. Rahmatalla and K. Abdel-Malek. *Vision performance measures for optimization-based posture prediction.* Technical report, SAE Technical Paper, 2006. (Cited on page 39.)

[Marler 2011] T. Marler, L. Knake and R. Johnson. *Optimization-based posture prediction for analysis of box lifting tasks.* Proceedings of the 3rd International Conference on Digital Human Modeling, pages 151–160, 2011. (Cited on page 95.)

[Marras 1993] W.S. Marras, S.A. Lavender, S.E. Leurgans, S.L. Rajulu, W.G. Allread, F.A. Fathallah and S.A. Ferguson. *The Role of Dynamic Three-Dimensional Trunk Motion in Occupationally-Related Low Back Disorders:*

*The Effects of Workplace Factors, Trunk Position, and Trunk Motion Characteristics on Risk of Injury.* Spine, vol. 18, no. 5, pages 617–628, 1993. (Cited on page 18.)

[McAtamney 1993] L. McAtamney and E.N. Corlett. *RULA: a survey method for the investigation of work-related upper limb disorders.* Applied Ergonomics, vol. 24, no. 2, pages 91–99, 1993. (Cited on page 15.)

[Merlhiot 2012] X. Merlhiot, J. Le Garrec, G. Saupin and C. Andriot. *The XDE mechanical kernel: Efficient and robust simulation of multibody dynamics with intermittent nonsmooth contacts.* Proceedings of the 2nd Joint International Conference on Multibody System Dynamics, 2012. (Cited on page 43.)

[Moore 1995] S.J. Moore and A. Garg. *The strain index: a proposed method to analyze jobs for risk of distal upper extremity disorders.* American Industrial Hygiene Association, vol. 56, no. 5, pages 443–458, 1995. (Cited on page 15.)

[Morasso 1981] P. Morasso. *Spatial control of arm movements.* Experimental brain research, vol. 42, no. 2, pages 223–227, 1981. (Cited on pages 45 and 94.)

[Mouret 2010] J.B. Mouret, S. Doncieux *et al. Sferesv2: Evolvin'in the multi-core world.* Proceedings of the IEEE Congress on Evolutionary Computation, 2010. (Cited on page 131.)

[Murray 1994] R. M. Murray, Z. Li and S.S. Sastry. A mathematical introduction to robotic manipulation. CRC press, 1994. (Cited on page 33.)

[NRC 2001] NRC. Musculoskeletal Disorders and the Workplace: Low Back and Upper Extremities. Institute of Medicine and National Research Council, National Academy Press, 2001. (Cited on page 3.)

[Occhipinti 1998] E. Occhipinti. *OCRA: a concise index for the assessment of exposure to repetitive movements of the upper limbs.* Ergonomics, vol. 41, no. 9, pages 1290–1311, 1998. (Cited on pages 15 and 41.)

[Ore 2014] F. Ore, L. Hanson, Delfs N. and Wiktorsson M. *Virtual evaluation of industrial human-robot cooperation: An automotive case study.* Proceedings of the 3rd International Digital Human Modeling Symposium, 2014. (Cited on page 28.)

[OSHA 1999] OSHA. *Ergonomics program, proposed rule.* Occupational Safety and Health Administration, vol. 64, no. 225, pages 65768–66078, 1999. (Cited on page 15.)

[Peshkin 2001] M.A. Peshkin, J.E. Colgate, W. Wannasuphoprasit, C.A. Moore, R.B. Gillespie and P. Akella. *Cobot architecture.* IEEE Transactions on Robotics and Automation, vol. 17, no. 4, pages 377–390, 2001. (Cited on page 6.)

[Pholsiri 2004] C. Pholsiri. *Task-based decision making and control of robotic manipulators.* PhD thesis, The University of Texas at Austin, 2004. (Cited on page 32.)

[Porter 2004] J.M. Porter, K. Case, R. Marshall and M. Freer. *SAMMIE: A Computer-Aided Ergonomics Design Tool.* In Working postures and movements – Tools for evaluation and engineering, pages 431–437. CRC Press, 2004. (Cited on page 20.)

[Powell 1969] E.R. Powell. *Tool Balancer*, 1969. US Patent 3,428,298. (Cited on page 6.)

[Pratt 2006] J.E. Pratt and R. Tedrake. *Velocity-based stability margins for fast bipedal walking.* Fast Motions in Biomechanics and Robotics, pages 299–324, 2006. (Cited on page 40.)

[Purshouse 2003] R.C. Purshouse and P.J. Fleming. *Conflict, harmony, and independence: Relationships in evolutionary multi-criterion optimisation.* Proceedings of the 2nd International Conference on Evolutionary Multi-Criterion Optimization, pages 16–30, 2003. (Cited on page 134.)

[Raschke 2004] U. Raschke. *The Jack human simulation tool.* In Working postures and movements – Tools for evaluation and engineering, pages 431–437. CRC Press, 2004. (Cited on page 19.)

[Reed 2006] M.P. Reed, J. Faraway, D.B. Chaffin and B.J. Martin. *The HUMOSIM Ergonomics Framework: A new approach to digital human simulation for ergonomic analysis.* Technical report, SAE Technical Paper, 2006. (Cited on page 24.)

[Regazzoni 2014] D. Regazzoni, G. De Vecchi, C. Rizzi and G. De Ponti. *DHM to investigate product ergonomics and visual representation of results.* Proceedings of the 3rd International Digital Human Modeling Symposium, 2014. (Cited on page 19.)

[Rice 2004] S. Rice. *Boeing Human Modeling System.* In Working postures and movements – Tools for evaluation and engineering, pages 462–465. CRC Press, 2004. (Cited on page 20.)

[Rosenbaum 1995] D.A. Rosenbaum, L.D. Loukopoulos, R.G.J. Meulenbroek, J. Vaughan and S.E. Engelbrecht. *Planning reaches by evaluating stored postures.* Psychological review, vol. 102, no. 1, page 28, 1995. (Cited on page 37.)

[Rothlauf 2006] F. Rothlauf. Representations for genetic and evolutionary algorithms. Springer, 2nd edition, 2006. (Cited on pages 135 and 136.)

[Rubrecht 2011] S. Rubrecht. *Contributions à la commande de robots sous contraintes.* PhD thesis, Université Pierre et Marie Curie-Paris VI, 2011. (Cited on pages 131, 141 and 155.)

[Saab 2011] L. Saab, N. Mansard, F. Keith, J.Y. Fourquet and P. Soueres. *Generation of dynamic motion for anthropomorphic systems under prioritized equality and inequality constraints.* Proceedings of the IEEE International Conference on Robotics and Automation, pages 1091–1096, 2011. (Cited on page 43.)

[Salini 2011] J. Salini, V. Padois and P. Bidaud. *Synthesis of complex humanoid whole-body behavior: a focus on sequencing and tasks transitions.* Proceedings of the IEEE International Conference on Robotics and Automation, pages 1283–1290, 2011. (Cited on page 43.)

[Saltelli 1999] A. Saltelli, S. Tarantola and K.P.S. Chan. *A quantitative model-independent method for global sensitivity analysis of model output.* Technometrics, vol. 41, no. 1, pages 39–56, 1999. (Cited on pages 108 and 113.)

[Saltelli 2000] A. Saltelli, K. Chan and E.M. Scott. Sensitivity analysis. Wiley, 2000. (Cited on page 105.)

[Santos-Munne 2010] J.J. Santos-Munne, M. Peshkin, E.L. Faulring, J.E. Colgate, A. Makhlin, T. Moyer, T. Hauptman and W. Hoffman. *An apparatus for use in breaking down an animal carcass*, 2010. WO Patent WO/2010/025,522. (Cited on page 7.)

[Saporta 2011] G. Saporta. Probabilités, analyse des données et statistique. Technip, 2011. (Cited on pages 64, 76 and 106.)

[Savin 2011] J. Savin. *Digital human manikins for work-task ergonomic assessment.* Journal of Engineering Manufacture, vol. 225, no. 8, pages 1401–1409, 2011. (Cited on page 97.)

[Schaub 1997] K.H. Schaub, K. Landau, R. Menges and K. Grossmann. *A computer-aided tool for ergonomic workplace design and preventive health care.* Human Factors and Ergonomics in Manufacturing & Service Industries, vol. 7, no. 4, pages 269–304, 1997. (Cited on page 20.)

[Schlehuber 2015] P. Schlehuber. *Robot morphology optimization using genetic algorithms.* Technical report, Université Pierre et Marie Curie-Paris VI, 2015. (Cited on pages 130 and 142.)

[Schneider 2010] E. Schneider and X. Irastorza. *OSH in figures: Work-related musculoskeletal disorders in the EU - Facts and figures.* European Agency for Safety and Health at Work, 2010. (Cited on page 3.)

[Seidl 2004] A. Seidl. *The RAMSIS and ANTHROPOS Human Simulation Tools.* In Working postures and movements – Tools for evaluation and engineering, pages 454–462. CRC Press, 2004. (Cited on page 20.)

[Sentis 2004] L. Sentis and O. Khatib. *Prioritized multi-objective dynamics and control of robots in human environments.* Proceedings of the 4th IEEE/RAS International Conference on Humanoid Robots, pages 764–780, 2004. (Cited on page 43.)

[Siciliano 1991] B. Siciliano and J.J.E. Slotine. *A general framework for managing multiple tasks in highly redundant robotic systems.* Proceedings of the 5th IEEE International Conference on Advanced Robotics, pages 1211–1216, 1991. (Cited on page 43.)

[Snook 1991] S.H. Snook and V.M. Ciriello. *The design of manual handling tasks: revised tables of maximum acceptable weights and forces.* Ergonomics, vol. 34, no. 9, pages 1197–1213, 1991. (Cited on page 15.)

[Sobol 1993] I.M. Sobol. *Sensitivity estimates for non linear mathematical models.* Mathematical Modelling and Computational Experiments, pages 407–414, 1993. (Cited on page 107.)

[Sylla 2014] N. Sylla, V. Bonnet, F. Colledani and P. Fraisse. *Ergonomic contribution of ABLE exoskeleton in automotive industry.* International Journal of Industrial Ergonomics, vol. 44, no. 4, pages 475–481, 2014. (Cited on page 179.)

[Tissot 2012] J.Y. Tissot and C. Prieur. *Bias correction for the estimation of sensitivity indices based on random balance designs.* Reliability Engineering & System Safety, vol. 107, pages 205–213, 2012. (Cited on page 114.)

[Viviani 1995] P. Viviani and T. Flash. *Minimum-jerk, two-thirds power law, and isochrony: converging approaches to movement planning.* Journal of Experimental Psychology: Human Perception and Performance, vol. 21, no. 1, page 32, 1995. (Cited on page 95.)

[Vukobratović 2004] M. Vukobratović and B. Borovac. *Zero-moment point - thirty five years of its life.* International Journal of Humanoid Robotics, vol. 1, no. 1, pages 157–173, 2004. (Cited on page 40.)

[Waters 1993] T.R. Waters, V. Putz-Anderson, A. Garg and L.J. Fine. *Revised NIOSH equation for the design and evaluation of manual lifting tasks.* Ergonomics, vol. 36, no. 7, pages 749–776, 1993. (Cited on page 15.)

[Xiang 2010a] Y. Xiang, J.S. Arora, S. Rahmatalla, T. Marler, R. Bhatt and K. Abdel-Malek. *Human lifting simulation using a multi-objective optimization approach.* Multibody System Dynamics, vol. 23, no. 4, pages 431–451, 2010. (Cited on pages 27, 36 and 41.)

[Xiang 2010b] Y. Xiang, H.J. Chung, J.H. Kim, R. Bhatt, S. Rahmatalla, J. Yang, T. Marler, J.S. Arora and K. Abdel-Malek. *Predictive dynamics: an optimization-based novel approach for human motion simulation.* Structural and Multidisciplinary Optimization, vol. 41, no. 3, pages 465–479, 2010. (Cited on page 27.)

[Yang 2004] J. Yang, R.T. Marler, H. Kim, J. Arora and K. Abdel-Malek. *Multi-objective optimization for upper body posture prediction.* Proceedings of the 10th AIAA/ISSMO multidisciplinary analysis and optimization conference, vol. 30, 2004. (Cited on page 35.)

[Yoshikawa 1985a] T. Yoshikawa. *Dynamic manipulability of robot manipulators.* Proceedings of the IEEE International Conference on Robotics and Automation, vol. 2, pages 1033–1038, 1985. (Cited on page 39.)

[Yoshikawa 1985b] T. Yoshikawa. *Manipulability of robotic mechanisms.* The International Journal of Robotics Research, vol. 4, no. 2, pages 3–9, 1985. (Cited on page 38.)